Design, Synthesis and Evaluation of Drought Stress Tolerance-inducing Compounds

DISSERTATION

zur Erlangung des Doktorgrades der Naturwissenschaften

(Dr. rer. nat.)

der

Naturwissenschaftlichen Fakultät II

Chemie, Physik und Mathematik

der Martin-Luther-Universität

Halle-Wittenberg

vorgelegt von

Herrn Robert Berger

Die vorliegende Arbeit wurde im Zeitraum Mai 2013 bis Februar 2017 am Leibniz-Institut für Pflanzenbiochemie in der Abteilung Natur- und Wirkstoffchemie unter der Anleitung von Prof. Dr. Ludger A. Wessjohann angefertigt.

Erstgutachter: Prof. Dr. Ludger A. Wessjohann

Zweitgutachter: Prof. Dr. Elżbieta Wojaczyńska

Tag der mündlichen Prüfung: 12. Okt. 2023

"Chicken fizz! O Lord, protect all of us who toil in the vineyards of experimental chemistry!"

Flavia de Luce

The Sweetness at the Bottom of the Pie

Danksagung

Ich bedanke mich herzlich bei meinem Betreuer und Gutachter Herrn **Prof. Dr. Ludger A. Wessjohann** für viele Jahre der Zusammenarbeit, einige zusätzliche Jahre der Geduld seinerseits und seine immerwährende Bereitschaft, Raum zur persönlichen Entwicklung zu bieten.

Frau Prof. Dr. Elżbieta Wojaczyńska gilt mein aufrichtiger Dank für die Anfertigung des Zweitgutachtens.

Für stets schnelle und kompetente Unterstützung und Zuarbeit von HPLC- und MS-Analysen bedanke ich mich zutiefst bei Frau **Anja Ehrlich**, Frau **Martina Lerbs**, Herrn **Dr. Jürgen Schmidt**, Frau **Gudrun Hahn** und Frau **Dr. Andrea Porzel**.

Der gesamten Abteilung NWC danke ich für die stets kollegiale und inspirierende Atmosphäre. Mein besonderer Dank gilt Herrn **Dr. Peter Paul Heym**, Herrn **Prof. Dr. Bernhard Westermann** und Herrn **Dr. Danilo Meyer** – die unzähligen Diskussionen und Brainstormings mit euch waren stets eine Quelle der Inspiration und Motivation, noch einen Blick mehr über den Tellerrand zu wagen.

Für eine unbeschreiblich schöne und vergnügsame Zeit vor, während und abseits, sowie nach der Promotionsforschung bedanke ich mich bei meinen lieben Ex-Kolleginnen und -Kollegen – zum Einen bei der '"alten Gang"' **Dr. Benjamin Genz**, **Dr. Anne-Katrin Dupont**, **Dr. Sebastian Stark**, **Dr. Julia Kufka**, **Dr. Rainer Kufka**, **Dr. Jeanette Ludwig** und **Dr. Steve Ludwig**, zum Anderen bei der '"neuen Gang"' **David Edeler**, **Dr. Annegret Laub**, **Dr. Pauline Stark**, **Dr. Michelle Kammel**, **Dr. Pia Schöne**, **Sarah Scharfenberg** und **Dr. Susann Herrmann**. Ihr wart stets zur Stelle, wenn es darum ging, Frustration mit Galgenhumor, Ratlosigkeit mit Ideen und Langeweile mit Geselligkeit beizukommen.

Abschließend möchte ich mich bei meinen Eltern **Jana** und **Maik Elste** für die vielen Jahre der Unterstützung in jeglicher Hinsicht bedanken, insbesondere jedoch für die sanften aber regelmäßigen Erinnerungen daran, den Abschluss der vorliegenden Arbeit nicht aus den Augen zu verlieren.

Contents

List of Abbreviations, Quantities, and Units

°C .... Degree Celsius

4-ANI 4-Amino-1,8-naphthalimide

A .... Plant frond area

ABA .... Abscisic acid

ADP .... Adenosine diphosphate

approx. .... Approximately

ART .... ADP-ribosyltransferase

Asp .... Aspartic acid

ATP .... Adenosine triphosphate

CI .... Confidence interval

CDF .... Cumulative distribution function

Δ .... Effect size measure according to GLASS

d .... Effect size measure according to COHEN

d .... Day

DMF .... N,N-Dimethylformamide

DMSO .... Dimethyl sulfoxide

DNA .... Desoxyribonucleic acid

EC_{50} .... Half maximal effective concentration

E .... Effect size

et al. .... And others (*et alii*)

e. g. .... For example (*exempli gratia*)

E.C. .... Enzyme commission

EDG .... Electron-donating group

PGR	....	Plant growth regulator
Pht	....	4-Substituted phthalazin-1(2*H*)-one
PS	....	Polystyrene
px	....	Pixel
Q-Q	....	Quantile-quantile (plot)
Qui	....	2-Substituted quinazolin-4(3*H*)-one
RG	....	Relative growth
R^2	....	Coefficient of determination
RE	....	Random-effects (model)
ROS	....	Reactive oxygen species
SD	....	Standard deviation
SE	....	Standard error
S	....	Sample of plant population
Ser	....	Serine
tbl.	....	Table
TFA	....	Trifluoroacetic acid
ThQui	....	2-Substituted 5,6,7,8-tetrahydroquinazolin-4(3*H*)-one
Tyr	....	Tyrosine

SI units (and derived) are not listed. Typefacing of quantities and units follows the rules of ISO 31-0:1992 to ISO 31-13:1992.

1 Introduction: Chemical Agents in Abiotic Stress Tolerance

1.1 Plant stress and its relevance for global food safety

"Plant stress" in general is understood to describe environmental conditions that hinder a plants' development – growth, productivity, reproduction and survival – through induction of adverse physiological reactions. Throughout their entire life cycle, plants are exposed to a variety of stressors, which can primarily be divided into two classes: organisms that infect or feed on a plant are regarded biotic stressors, while all climatic, physical and chemical influences in a broader sense are considered abiotic stressors [1]. Naturally, all plants are target to different stresses – however, a special interest in understanding, mitigating and even preventing plant stress exists in an agricultural environment. With the ever increasing demand for crop plants used as food and feed – despite diverse industrial applications, e. g. in bioethanol production – the humanitarian and economic impact of substantial crop losses steadily grows as well. While 38 % of the global land area are already used for crop production [2] and ever advancing agricultural technology and improved breeding enhance crop yields, the number of undernourished people is increasing anew since 2014, reaching an estimated 821 million in 2018 [3]. This counter-intuitive development is not least due to more extreme climatic variability and the substantial gain in global temperature, leading to severe droughts which rendered responsible for "$ 29 billion in losses to developing world agriculture between 2005 and 2015" [3, 4].

Drought as leading cause for crop losses is merely a facet of a set of environmental conditions that can be summarized as "water stress". This stress situation is characterized either by a limited availability of water or a restricted ability of the plant to uptake water that is present,

the latter known as "physiological drought" [5]. The main causes for such deficiencies include (a) insufficient water activity within the soil (which describes the availability of water rather than its concentration) due to drought, high salinity or frost, (b) increased transpiration of the plant due to elevated temperatures, or (c) floods. In the following discussion and throughout this work, the main focus will lie on drought as the main aspect of water stress. Nevertheless, most of the highlighted facts apply to all types of water stress in a similar manner. Therefore, "drought" and "water stress" are used as synonyms whenever no clear distinction between drought and e. g. high salinity is possible or necessary.

1.2 Physiological and molecular effects of drought and plant responses

Depending on its constitution, each plant has an individually preferred range of water activity in the soil – still, under sufficiently prolonged withdrawal of water, even the most specialized plant will dehydrate and eventually die. Dehydration and death are accompanied by different physiological signs of decay, which originate from complex changes in the most central molecular metabolic pathways including photosynthesis, protein synthesis and redox metabolism, as well as cell membrane integrity. The effects on the molecular level, including sophisticated signaling pathways, have been extensively investigated and reviewed [5, 6, 7, 1]. Here, only selected stress effects and responses will be discussed, which have been targeted by chemical tolerance-inducing treatment.

One of the first facultative responses to water stress is an osmotic adjustment through accumulation of compounds, that exhibit a strong osmotic activity but at the same time do not negatively affect cellular metabolism. Such compounds are known as osmolytes. In order to guarantee water supply, the plant needs to actively lower its intracellular water potential to a level below the water potential of the surrounding soil. Otherwise, water uptake from the soil and influx into the cell is physically impossible and the plant cannot maintain its turgor, which is the osmotic pressure that is created through physically bound water inside a cell in comparison to its extracellular matrix. Following a loss in turgor, the cell size decreases which results in an inhibition of plant growth and is accompanied by wilting of leaves. The degree to which an accumulation of osmolytes like proline or glycine betaine can mitigate

an unfavorable discrepancy in water potential strongly depends on the plant species, with so-called xerophytes being best adapted to arid conditions. Representative values for water potentials in soil and different compartments of plants are given in tbl. 1, highlighting the variability in environmental conditions as well as the plants' capability for adaptation.

The impact of water deficiency onto the photosynthesis – which constitutes the main anabolic pathway in plants – is especially strong. Water is of central importance as electron donor for the reduction of $NADP^+$ to NADPH in the course of oxygenic photosynthesis. As result of a deficiency in water, and consequently NADPH, the reduction of 1,3-bisphosphoglycerate is hindered, which ultimately inhibits the biosynthesis of glucose and leads to an inhibition in growth. Consequently, another early response to water stress is the rapid closure of leaf stomata as depicted in fig. 1, p. 4: The plants' plausible reaction to mitigate the effects of a deficiency in water uptake is the limitation of additional loss in water by evaporation. This evaporation takes place whenever the leaf stomata open to enable the assimilation of carbon dioxide, which is the second necessary substrate for carbohydrate synthesis, besides water. On the molecular level, regulation of the stomatal state, and thus transpiration, is controlled by the phytohormone abscisic acid (ABA). In case of a water deficiency, the signaling pathway leads to an increase in ABA concentration, which in turn triggers stomatal closure. Alas, with the stomata closed, exchange of both water vapour and carbon dioxide with the environment is practically impossible. Concludingly, uptake of one of the main substrate of photosynthesis is blocked, which afflicts the dark reaction and thus photosynthesis overall.

A third effect of water stress is the generation of reactive oxygen species (ROS). The described disturbance of photosynthesis leads to a misbalance between formation and depletion of redox equivalents in favor of oxidizing agents. These excess oxidants are responsible for the formation of ROS like singlet oxygen $^1O_2$, hyperoxide anions $O_2^{\ominus}$, hydrogen peroxide

Table 1: Representative values for water potentials ψ in soil and different plant compartments [8, 9]

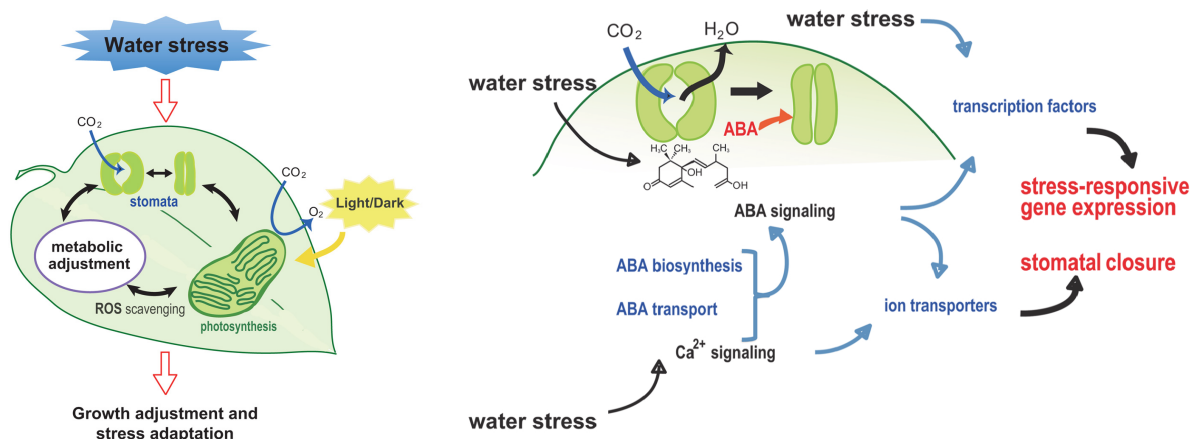| ψ [MPa]	Location
−0.01	Freshly irrigated soil
−0.30	Soil 0.1 m below ground and 10 mm from root
−0.50	Soil adjacent to root
−0.80	Leaf xylem 10 m above ground
−1.50	Soil water potential that causes permanent wilting in many crops
−3.50	Leaf of *Stipa borysthenica* (semiarid grass) at 22 % leaf water deficit

Figure 1: Schematic representation of the water stress response; left: Physiological adjustments; right: Activation of ABA-signaling pathway; modified from [6]

H_2O_2 and a variety of radicals such as the hydroxyl radical, which are well-known to pose a serious threat to biologically important structures like membranes and proteins. For this reason, upregulation of the plants' ROS detoxification mechanisms is part of the stress response: Enzymes such as catalases, peroxidases and superoxide dismutases allow direct chemical transformation of reactive species, while other compounds, namely ascorbic acid and glutathione, act as ROS scavengers, which are recycled from their oxidized state by specialized enzymes.

1.3 Stress tolerance-inducing agents and their modes of action

Plant growth regulators (PGRs) in general are understood as naturally occuring or synthetic compounds that influence the development of plants through stimulation or inhibition of parts of the growth regulatory system involving the main plant hormones auxins, gibberellins, cytokinins, abscisins and ethylene. Observable effects include the promotion, delay and prevention of growth, rooting, flowering, fruiting and aging. Thereby, PGRs mostly affect signaling pathways, which are also known to be important in plant stress response and tolerance. Thus, stress tolerance-inducing agents are hypothesized to exhibit plant growth-regulating effects in general, even in absence of abiotic stressors.

With first commercial applications dating back to the 1940's, the field of PGRs is well-investigated today. Before, yield improvements in crops have been achieved mainly by development of new cultivation techniques, as well as selection and breeding. Today, these "traditional" techniques are still an important tool in securing food supplies for a steadily

growing world population – however, PGRs aim to improve crop yields even beyond the limitations of natural growth regulation [10, 11]. In the near future, as traditional breeding will steadily lose relevance in yield improvement and stress tolerance induction, genetic engineering of plants will gain in importance and represent the only true competition to chemical agents [12, 13].

The class of PGRs shows considerable structural heterogeneity, as known from other classes of agrochemicals, e. g. pesticides or herbicides. The compounds known to induce tolerance towards different kinds of abiotic stresses can be roughly divided into three groups: inorganic agents, plant endogenous metabolites and synthetic compounds. The inorganic and organic endogenous compounds NO, H_2O_2, H_2S/NaHS and polyamines (e. g. spermine) are in some way involved in early stress responses. In fact, they were also found to be beneficial for plant stress tolerance when applied externally during different stages of development (germination, vegetation, reproduction). Although proof of their modes of action has not been achieved yet, a viable hypothesis connects the observed increase in stress tolerance to a "training effect" caused by the chemical pretreatment before the actual stress sets in [14]. Alongside polyamines, glycine betaine, proline and allantoin have been described to specifically milden water stress in plants, although evidence exists that stress tolerance induction in general is effective against multiple abiotic stressors due to the closely related physiological reactions and targeted regulatory networks [15, 16, 14].

Among the marketed synthetic compounds with stress-protecting effects, the class of imidazole- and triazole-based fungicides takes a central position and shall therefore be exemplified here: Originally designed and developed for treatment of fungal diseases in plants, several compounds exhibit additional growth-regulating and stress tolerance-inducing activity. Triadimefon (see fig. 2) for instance is not only an effective inhibitor of ergosterole biosynthesis in fungi but also interferes with the isoprenoid pathway in plants, thus affecting biosynthesis of gibberellins, cytokinins and abscisic acid. FLETCHER and HOFSTRA demonstrated
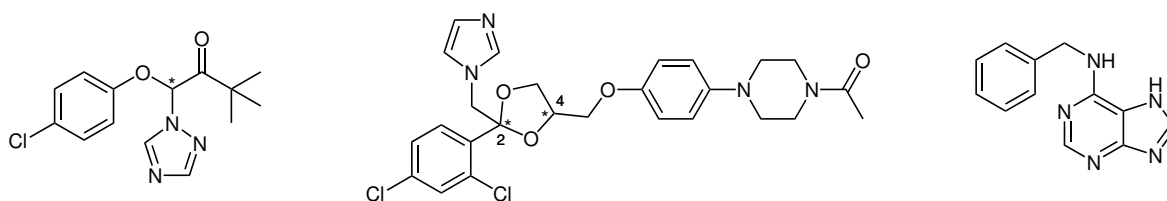
Figure 2: Chemical structures of synthetic water stress tolerance-inducing compounds
left: triadimefon (racemic mixture); middle: ketoconazole (racemic mixture of 2*S*,4*R*- and 2*R*,4*S*-isomers); right: 6-benzylaminopurine

that the triazole derivative effectively increases stomatal resistance in tomato plants, thus reducing transpiration under water stress, which led to an increase of 20 – 30 % in fruit fresh weight compared to the controls [17, 18]. JALEEL *et al.* could further show that the effect of salt stress on physiological markers in *Withania somnnifera* (winter cherry), namely germination rate and chlorophyll content, as well as molecular antioxidant markers (ascorbic acid, glutathione and the enzymes superoxide dismutase and peroxidase) could be mitigated by treatment with triadimefon [19]. Additional investigations conducted by JALEEL *et al.* revealed that the imidazole-based fungicide ketoconazole (see fig. 2) induces drought stress tolerance in *Catharanthus roseus* (rosy periwinkle) through promotion of the antioxidant potential, both on protein level (upregulation of e. g. superoxide dismutase and catalase) as well as on the level of small molecule ROS scavengers [20]. A most recent example of salt stress reduction in an agricultural important crop was reported by BAJWA, which achieved considerable stress tolerance in wheat (*Triticum aestivum L.*) by treatment of seeds ("priming") with 6-benzylaminopurine, a synthetic cytokinine [21].

Eventually, the class of neonicotinoids is worth mentioning due to their importance in industrial agriculture and the controversy linked to their application, among which imidacloprid is of central relevance. Released for industrial application as pest control in 1994 by the Bayer AG (Bayer CropScience), the agent rose to become the most widely sold and used insecticide in the world, before beneficial side effects in relation to stress tolerance and enhanced crop yield were reported. Initially to be considered an off-label use, the application as stress tolerance-inducing agent was commercialized in 2006 as "Confidor ® Stress Shield Inside", a product proclaiming both activity as pest control, as well as drought stress tolerance-enhancer. While the mode of action for the induction of stress tolerance has not been elucidated conclusively, 6-chloronicotinic acid as major degradation product of imidacloprid was proposed to be the active principle, effecting a reduction in plant poly(ADP-ribose) polymerase (PARP) activity [22, 23].

1.4 Objective of this thesis

The investigations presented herein sought to deepen the knowledge about drought stress tolerance-inducing effects and the underlying mode(s) of action(s) believed to be present in selected classes of synthetic chemical compounds different from the known ones described so

far. Previously conducted research based on the hypothesis of PARP enzymes being involved in plant stress response yielded a hypothetic mode of action and a selection of promising synthetic compounds found through *in silico* screening [24]. In order to provide experimental proof, an *in vivo* assay system was developed and first evidence of the desired activity being inherent to different compounds was documented [25, 26].

The first aim of the current work was to confirm the described effects and to expand the phenotypical screening onto additional structural classes, including diverse heterocyclic compounds. Therefore, the established assay system was to be improved in efficiency, allowing for shorter screening time, thus enabling faster and broader screening of compound libraries. Potentially active compound classes should then be investigated in depth by syntheses of various new derivatives and subsequent assessment of their activity. Thereby, special emphasis was put onto the development of a robust, cost-effective and upscalable synthetic access to the desired compounds in order to facilitate an industrial-scale application. Ultimately, this work was planned to conclude with the formulation of a sophisticated pharmacophore describing the structure-activity-relationship of identified drought stress tolerance inducers qualitatively and quantitatively as basis for further research concerning the identification of possible targets on a molecular level and transferability of beneficial effects onto economically valuable crops. The respective results are presented in the following chapters.

# 2 High-throughput Screening of Potential Drought Stress Tolerance-inducing Compounds

This chapter   is based on experimental work carried out by R. BERGER and includes results obtained and published by P. P. HEYM.

Abstract   Based on previous work, an improved high-throughput whole-plant bioassay employing *Lemna minor* has been developed, which allows for the identification of drought stress tolerance-inducing effects of small molecules. The assay aims at monitoring plant growth under stress conditions, as well as in a subsequent recovery phase with a high level of automatization and accuracy through software-based optical recognition of plant surfaces. Extensive statistical analysis was conducted to define reliable critical effect sizes for small, medium and large effects in plant growth acceleration. Based on the developed assay a compound library was screened containing 119 compounds previously found to be promising candidates for inhibition of plant PARP enzymes, thus assumed to positively affect plant energy homeostasis under abiotic stress conditions. A detailed analysis of screening results in relation to the compounds' structural features allowed for the identification of distinct chemical features connected to promising activity and the formulation of a sophisticated lead pharmacophore, partly agreeing with and partly extending the "classical" PARP pharmacophore known from inhibitors of *Hs*PARP-1. However, neither clear confirmation nor disproof of the "PARP hypothesis" were achieved.

2.1 Introduction

2.1.1 The role of PARP/ART proteins in plant abiotic stress tolerance

The enzymatic activity of poly(ADP-ribose) polymerases (E.C. 2.4.2.30) was first described in 1963 by CHAMBON *et al.*, based on their observation of a DNA-dependent depletion of NAD$^+$ in kidney nuclei, resulting in the formation of polyadenine [29]. Today it is known that genes encoding for this superfamily of enzymes can be found throughout organisms from bacteria to humans, in which these nuclear enzymes fulfill manifold and crucial functions in relation to cellular stress response, DNA repair and genomic stability, cell death, energy homeostasis as well as pathogen infection [30, 31, 32, 33]. The main catalytic activity of PARP enzymes consists in the transfer of negatively charged ADP-ribose units from the donor molecule NAD$^+$ onto a suitable acceptor molecule – a process known as mono(ADP-ribosyl)ation (MARylation). Besides other NAD$^+$-molecules acting as acceptor as depicted in fig. 3, the most prominent targets of MARylation are amino acids (e. g. Glu, Asp, Lys) of nuclear proteins, which are modified reversibly and post-translationally [34, 31]. These protein-bound ADP-ribose units can, in turn, serve as acceptor for further ADP-ribose transfer, leading to protein-associated poly(ADP-ribose) chains (PARylation). The fact that some members of the enzyme family are resticted to MARylation, while others are able to catalyze PARylation up to chain lengths of over 200 units [35], led to the suggestion of renaming the enzyme family ADP-ribosyltransferases (ARTs) [33, 34, 35].
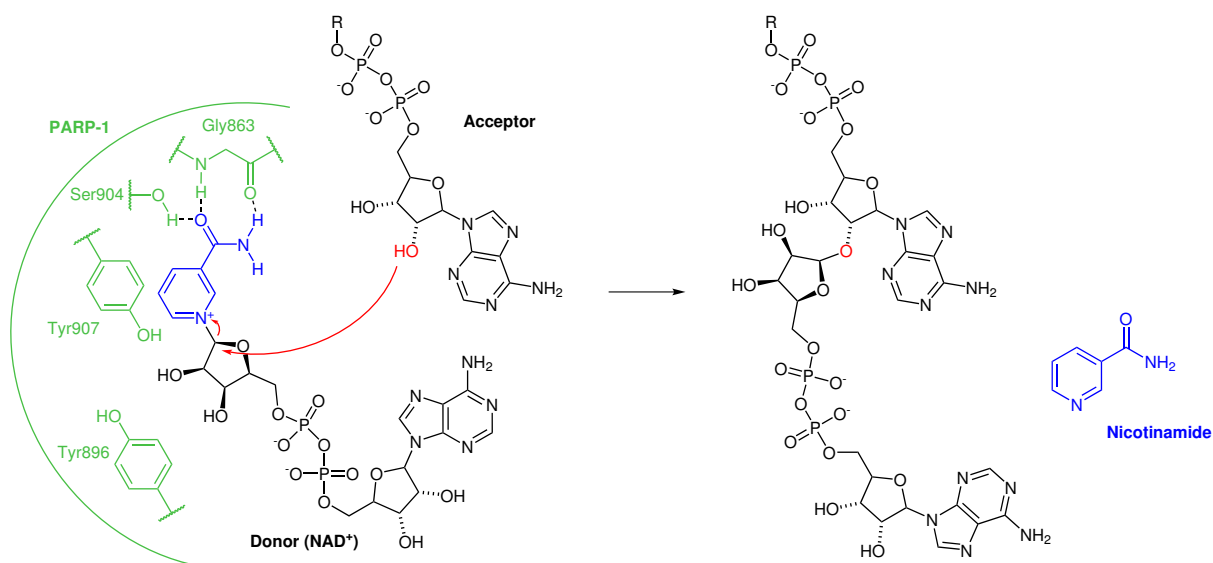
Figure 3: Schematic representation of the PARP-1 catalytic mechanism showing the binding of NAD$^+$ to chicken PARP-1 (based on [27] and reproduced with modifications from [28])

The by far best-studied member of the PARP/ART family is PARP-1, which is highly conserved among eukaryotes and accounts for over 90 % of the PARP activity within the cell. Its high abundance and key role in DNA repair made it a prominent target in human disease-related research, including cancer, stroke and diabetes (see [28, 36, 37] for extensive review). In 2005 DE BLOCK *et al.* made first attempts towards transferring this knowledge onto plants and proposed a possible enhancement in abiotic stress tolerance by inhibition of PARP enzymes: stress factors like drought (or water stress in general) and heat trigger PARP activation through formation of reactive oxygen species (ROS), which are well-known to cause DNA damage. In turn, an increased PARP activity causes consumption of both the cells' NAD^+ and ATP pools, thus affecting energy homeostasis, promoting cell death and hindering growth. The authors found a reduction of PARP activity accomplished by either inhibition of the enzyme with known small molecule inhibitors (nicotinamide and the structually related isonicotinamide and 3-methoxybenzamide) or silencing of PARP-1 and PARP-2 genes to be beneficial for abiotic stress tolerance in *Brassica napus* and *Arabidopsis thaliana* [38]. Follow-up studies confirmed and extended the obtained results [39, 40, 41].

The possibility of enhancing abiotic stress tolerance in plants through PARP inhibition motivated earlier research activities in the Department of Bioorganic Chemistry in the Leibniz-Institute of Plant Biochemistry (Halle, Germany), including comparative *in silico* studies between human *Hs*PARP-1 and *Arabidopsis thaliana* PARP enzymes. Based on the high structural conservation of PARP-1 in eukaryotes, known and proposed small molecule inhibitors of *Hs*PARP-1 were screened for their potency of inhibiting *At*PARP-1/*At*PARP-2 by means of homology modeling and docking studies [24]. Available compounds from the virtual hits of possible inhibitors were subjected to the *in vivo* screening within this work (see section 2.2.3, p. 33).

2.1.2 Structural features of PARP-1 inhibitors

The development and evolution of *Hs*PARP-1 inhibitors gives an outstanding example of the achievements in the field of medicinal chemistry research, accomplished both by academic researchers as well as pharmaceutical enterprises. Starting from the first generation of inhibitors analyzed in the light of cancer research to the approval of olaparib (Lynparza©, AstraZeneca) as treatment for advanced ovarian cancer in December 2014, over 30 years of
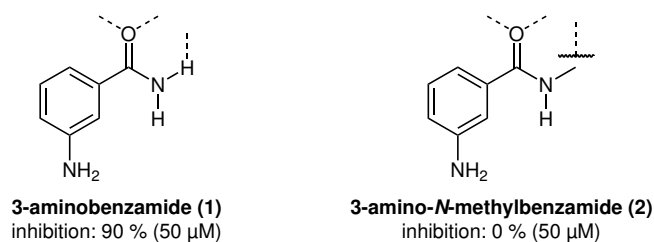
Figure 4: Influence of the *cis*-amide motif in PARP inhibitors reflected by *in vitro* activity data [42]

medicinal chemistry have yielded a plethora of diverse heterocyclic compounds – many of which were found to have nanomolar inhibitory activity towards *Hs*PARP-1. FERRARIS gives an excellent outline of the efforts made by the most prominent research groups towards the development of potent inhibitors [36]. Here, only key steps in this development will be highlighted, necessary for understanding the constitution of the pharmacophore shown in fig. 6, p. 12.

First attempts towards finding potent inhibitors focused on nicotinamide as by-product of the PARP-catalyzed reaction and the closely related benzamide, as well as 3-substituted benzamides. All of the benzamides were found to have a higher inhibitory activity than nicotinamide itself, while related compounds lacking the amide group (2-, 3- or 4-substituted benzoic acids and acetophenones) showed no significant inhibition at a concentration of 50 μM [42]. These findings already highlight the common structural motif of all PARP-1 inhibitors: an s-*cis*-amide group, available both as H-bond donor (N‒H) as well as acceptor (C=O) (fig. 6, red), required for coordination by Gly863 and Ser904 within the active site of PARP-1 (fig. 3). The importance of this structural feature becomes evident by comparison of two closely related compounds investigated by PURNELL *et al.* shown in fig. 4: the un-substituted amide group in 3-aminobenzamide **1** is a potent H-bond-donor, since there is no distinction possible between s-*cis*- and s-*trans*-configuration of the amide-bond. On the contrary, in 3-amino-*N*-methylbenzamide **2** the peptide bond is fixed in the thermodynami-cally favored s-*trans*-configuration due to mesomeric stabilization, thus hindering optimal coordination by the enzyme. This supposedly small structural change leads to an entire abolishment of inhibitory activity in this case [42].

Consequentially, higher inhibitory activities were found in compounds that comprise an at least bicyclic lactam system: a second ring (B, see fig. 6), fused to the aromatic system (A) of the basic nicotinamide structure, fixes the amide group in its s-*cis*-configuration, guaranteeing the availability of the N‒H-bond as H-bond donor. Among the first of these lactams, 4-amino-1,8-
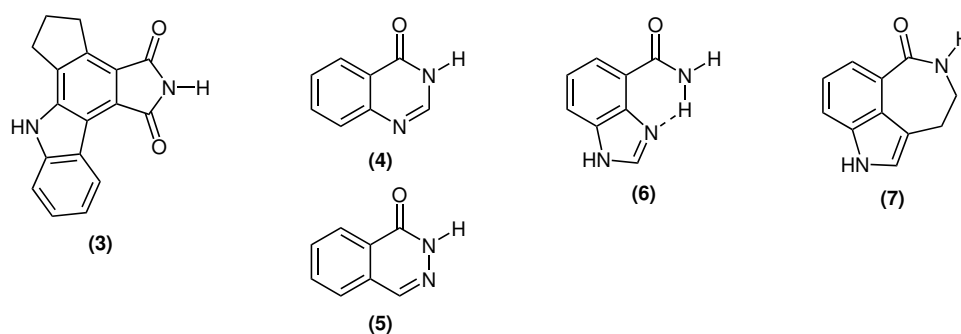
Figure 5: Variations of scaffolds fixing the *cis*-amide motif in PARP inhibitors
3 phthalimide-derived [43], **4** quinazolinones [44], **5** phthalazinones [44], **6** "pseudoring" in indole derivatives [45], **7** cycloheptane-derived [46]

naphthalimide (4-ANI), 6-(5H)-phenanthridinone, and 1,5-isoquinolinediol were found to be potent inhibitors with IC_{50}-values below 1 μM [44]. However, fixation of the amide group is not restricted to simple six-membered aromatic rings: structural variations include different types and positions of heteroatoms leading to quinazolinones **4** and phthalazinones **5**, or variations in ring size (e. g. five-membered phthalimide-like **3**, seven-membered cyloheptane-like **7**). Even fixation of the amide-NH$_2$ via an intramolecular H-bond to an adjacent imidazole nitrogen **6** proved to result in a highly active core structure for PARP-1 inhibitors (see fig. 5) [45, 47].

Based on the first resolved cocrystals of human PARP-1 inhibitors and chicken PARP-1 (87 % homology to the human enzyme), an understanding of the additional structural features of the pharmacophore could be acquired [27]. As depicted in fig. 3, the pyridine ring of the natural substrate is oriented towards the two tyrosine residues Tyr907 and Tyr896, forming a sandwich-like stack due to $\pi-\pi$ interactions. This fact gives an explanation of the experimen-
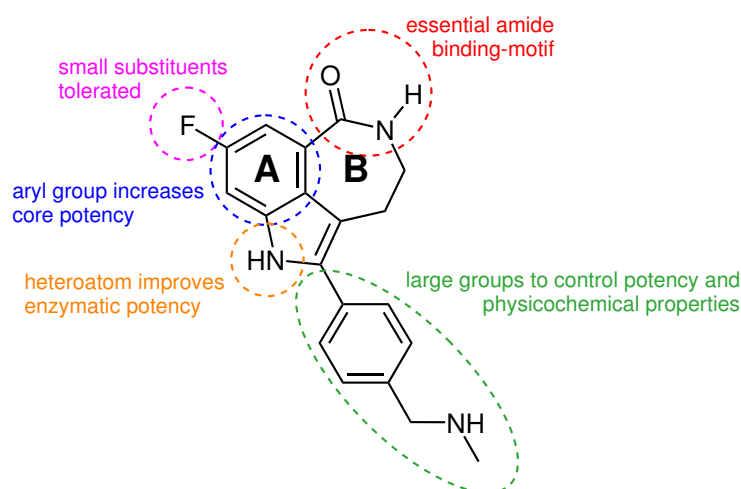
Figure 6: Pharmacophore of *Hs*PARP-1 inhibitors
Clinical candidate AG014699 (Newcastle University/Pfizer [48]) with highlighted structural features mandatory for activity or enhancing activity/physicochemical properties (reproduced with modifications from [36])

tally found superiority in activity of compounds bearing an aromatic A-ring over saturated derivatives [36]. KINOSHITA *et al.* eventually found that spacious hydrophobic substituents in opposition to the amide moiety (fig. 6, green) induce a conformational change in the active site, opening a new subsite wide enough to hold even such large, linear groups [49]. This insight further enlarged the design space for the finetuning of the inhibitors' physicochemical properties.

2.1.3 *Lemna minor* as model plant

As part of the aforementioned research project, a whole-plant *Lemna minor*-based bioassay was developed, designed to identify growth-accelerating effects of small molecules under drought stress conditions [25, 26].

Several duckweed species serve as model organisms in – mainly ecotoxicological – research with *L. minor* and *L. gibba* being the most widespread ones (see [50] for an overview). The utilization of *Lemna* species holds several advantages over model plants like *Arabidopsis thaliana* or *Nicotiana* species:

▷ As water plants, they can be cultivated in hydroculture, allowing for an easy and uniform supply of nutrients and stressors (chemicals, temperature etc.) of interest. Moreover, preservation of culture sterility is simplified [51, 52].

▷ Under continuous illumination they exclusively reproduce vegetatively by budding, which reduces the genetic and therefore the phenotypic variability – a major advantage with regard to the robustness of statistical evaluation of population growth [53, 54].

▷ Reproduction rates are extremely high – doubling times as low as 24 – 48 h are reported, which allow for short assay time and high number of replicates [50, 55].

▷ *Lemna* plants are small in size, consisting only of a floating frond and a thin root. Non-invasive assessment of population growth is easily achieved by counting the number of fronds or measuring the frond surface of plants using optical methods, offering a high level of accuracy and means of automatization.

These advantages promise a phenotypical screening to be operationally simple, as well as faster and more reliable in terms of statistical evaluation than *in vivo* assay systems based on more complex land plants.

2.2 Results and discussion

2.2.1 Assay development

The assay designed by GEISSLER aimed at monitoring growth of *L. minor* plants in 24-well microtiter plates, one plant per well. The utilized STEINBERG medium was equipped with PEG6000 to simulate drought stress over the whole assay period of seven days. Microtiter plates were placed inside an environmental test chamber and plants were grown under constant illumination with semi-automatic measurement of frond areas every 24 h [25].

Several parameters of the assay were modified to account for effects during recovery from stress and to increase robustness of the statistical model. The assay parameters, including the changes applied, are summarized in tbl. 2, p. 15 and will further be discussed in detail.

Assay duration, stress and recovery phase

The original assay design allowed for the identification of growth-enhancing effects of compounds under stress conditions only. Possible stabilization of the plants' physiological state under stress conditions, enabling a rapid recovery under non-stress conditions could not be assessed in this setup. To account for these protective effects – resulting in a faster recovery after the stress phase – the assay was split into a stress period of 48 h and a recovery period of 24 h. To ensure a sufficiently high plant growth rate in the shorter time span of the assay, incubation temperature and irradiance were elevated in a range that promotes growth without exposing the plants to additional stress besides the water stress [50].

Preparation of growth media

GEISSLER sought to impose two different levels of water stress onto the plants by adding PEG6000 to STEINBERG growth medium [25]. Referring to a publication investigating the relation between concentration of PEG6000 and osmotic potential of aqueous solutions, -0.2 MPa and -0.3 MPa were chosen as stress levels, corresponding to concentrations of PEG6000 of 180.0 g/l and 211.9 g/l, respectively. The relation found by the authors, alongside two other models, is given in tbl. 3, p. 15 and graphically in fig. 7, p. 16 [57,

Table 2: Comparison of *Lemna minor* assay parameters

Parameter	GEISSLER [25]	This work
Assay duration	7 d	3 d
Compound application	t_0	t_0
Stress period	7 d	48 h
Recovery period	–	24 h
Frond area measurement	every 24 h	0, 48 and 72 h
Measurement method/software	LemnaTec Scanalyser© w/ manual correction	ImageJ algorithm [56]
Groups	6 groups	4 groups
	4 wells each	6 wells each
	one plant per well	one plant per well
Growth parameter	relative growth rate	relative growth
	μ	RG_{st}, RG_{rec}, RG_{tot}
Temperature	24 °C	27 °C
Illumination	constant	constant
	$100\,\mu\text{mol} \cdot \text{m}^{-2} \cdot \text{s}^{-1}$	$120\,\mu\text{mol} \cdot \text{m}^{-2} \cdot \text{s}^{-1}$
Osmotic stressor	PEG6000	PEG6000
	211.9 g/l	150.0 g/l

58]. Investigation of the models shows discrepancies between the original publication and GEISSLERS application: Despite the fact that the relation found by MICHEL *et al.* is based on the concentration of PEG given in g/kg water – a molal rather than a molar quantity as stated by GEISSLER – application of given amounts of PEG6000 would have resulted in osmotic potentials of −0.44 MPa and −0.58 MPa, not −0.2 MPa and −0.3 MPa. The projection of actually applied PEG amounts onto a molar relation (fig. 7, dotted line) results in even lower osmotic potentials of −0.44 MPa and −0.62 MPa [58]. Thus, it needs to be assumed that the stress levels applied were substantially higher than intended, which calls the comparability to similar studies into question. Within the scope of this work amounts of PEG6000 were calculated based on the molar relation found by MONEY *et al.* for 21 °C,

Table 3: **Empirical models for solution water potential** depending on the concentration of PEG6000 at 21 °C (see fig. 7)

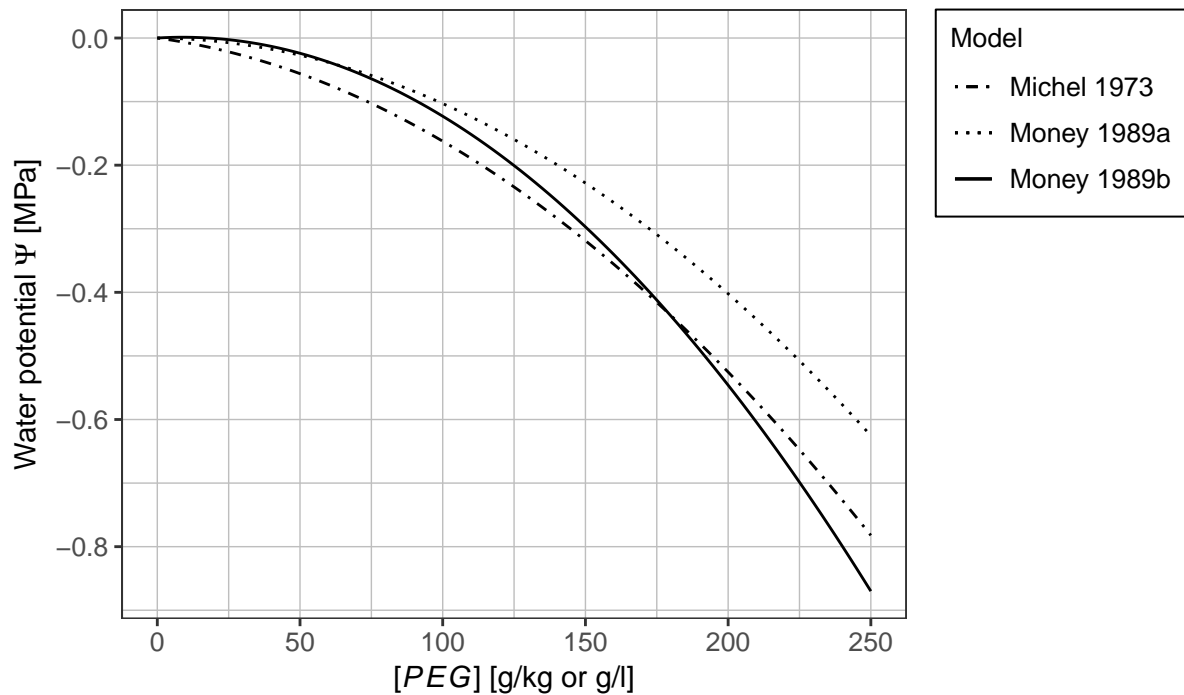| Reference	Unit of $[PEG]$	Model equation
Michel 1973 [57]	g/kg H$_2$O	$\psi = -1.0 \cdot 10^{-4}[PEG]^2 - 6.2 \cdot 10^{-3}[PEG]$
Money 1989a [58]	g/kg H$_2$O	$\psi = -9.8 \cdot 10^{-6}[PEG]^2 - 5.1 \cdot 10^{-5}[PEG]$
Money 1989b [58]	g/l solution	$\psi = -1.5 \cdot 10^{-5}[PEG]^2 + 2.7 \cdot 10^{-4}[PEG]$

Figure 7: Empirical models for solution water potential depending on the concentration of PEG6000 at 21 °C (see tbl. 3)

resulting in 150 g/l and approximately −0.25 to −0.30 MPa for the standard assay setup (the elevated temperature of 27 °C results in a higher – less stressful – osmotic potential than the calculated −0.30 MPa for 21 °C).

Assessment of frond areas

The possibility of estimating growth rates by software-based optical evaluation of frond areas makes *Lemna* species particularly valuable model plants. In contrast to more traditional methods of growth estimation in plants, three major advantages need to be highlighted: Firstly, an algorithm provides much more precise and unbiased, and therefore accurate, assessments of the parameter of interest, compared to manual measurements of plant dimensions, e. g. overall height, leaf diameter or root length. This maximizes interpretability of results while minimizing the number of individual plants required to make reliable statements, therefore optimizing statistical power. Secondly, a high level of automatization is usually achievable for software-based methods, which allows for a significantly higher gain in information in less time, compared to methods that require more manual operation, e. g. analysis of molecular markers in freeze-dried plant material. Lastly, a non-invasive measurement offers the possibility for continuous experimental evaluation even under varying conditions – a flexibility that is not achievable using destructive techniques of growth

estimation, which, consequently, are end-point methods, e.g. measurement of plant dry weight, chlorophyll content or molecular markers [59].

Assessment of plant frond areas was carried out using the open-source image analysis software ImageJ, which provides several state-of-the-art algorithms for the detection and measurement of objects fit for batch processing of image series [56]. *L. minor* plants could be identified with high accuracy, while the LemnaTec Scanalyser© software used by GEISSLER frequently required manual correction in plant recognition.

Grouping and choice of growth parameters

GEISSLER estimated growth rates in the exponential phase by linear regression of the relation between time t and log-transformed frond area $\ln A$ (eqn. 2.1b, p. 17), which after transformation gave the relative growth rate for each individual well μ (eqn. 2.1c, p. 17) [25]. The growth rates of the four wells belonging to one group were averaged to give the mean growth rate $\overline{\mu}$ (eqn. 2.1d), which was reported alongside its standard error (SE).

$$A = A_0 \cdot \mu^t \tag{2.1a}$$

$$\ln A = \ln A_0 + t \cdot \mu \tag{2.1b}$$

$$\mu = \frac{\ln A - \ln A_0}{t} \tag{2.1c}$$

$$\overline{\mu} = \frac{1}{4} \sum_{i=1}^{4} \mu_i \tag{2.1d}$$

This way of estimating the group parameter can clearly be improved. The growth rate μ is an estimate of the true, but unknown growth rate μ_{real}, which is connected with a certain error resulting from biological and experimental factors as well as the variance not explained by linear regression (expressed through the coefficient of determination R^2). It does not appear as if the individual errors of μ_i were taken into consideration in estimating the group parameter $\overline{\mu}$ and its standard error, which is supposed to allow statements on the goodness of estimation of μ_{real}. This goodness of estimation and therefore the reliability of the presented results ought to decrease considerably, taken error propagation into account.

The effect of error propagation and the low robustness of linear regression on such limited numbers of measurements made the growth rate μ appear a less useful parameter for assessing growth-accelerating effects. Moreover, in the revised assay setup, growth rates in stress and recovery phase were expected to differ, which is why the relative growth was deemed a more reliable parameter to assess. Starting from eqn. 2.1b the relation can be transformed to eqn. 2.2 which allows the definition of parameters RG for different intervals in time: both the two phases (stress and recovery) as well as the total assay time (eqns. 2.3a – 2.3c, p. 18).

$$\mu \cdot t = \ln A - \ln A_0 \tag{2.2}$$

$$RG_{st} = \mu_{st} \cdot (t_{48} - t_0) \quad = \ln A_{48} - \ln A_0 \tag{2.3a}$$

$$RG_{rec} = \mu_{rec} \cdot (t_{72} - t_{48}) = \ln A_{72} - \ln A_{48} \tag{2.3b}$$

$$RG_{tot} = \mu_{tot} \cdot (t_{72} - t_0) \quad = \ln A_{72} - \ln A_0 \tag{2.3c}$$

Treatment groups may then be described by the mean total relative growth

$$\overline{RG}_{tot} = \frac{1}{6} \sum_{i=1}^{6} RG_{tot,i} \tag{2.4}$$

and its standard deviation, respectively other, more robust measures describing the location (e. g. median) and variability of a distribution (e. g. median absolute deviation). Based on these descriptive measures, two questions have to be answered to decide on the effectiveness of a treatment:

1. Does the treatment (positively) affect the growth of *Lemna* plants during and/or after periods of water stress in comparison to non-treated plants?
2. How big is the effect of the treatment and is it of practical relevance?

The most wide-spread approach to answer the first question is a classical null hypothesis significance test (NHST), e. g. the two-sample t-test. Though widely accepted and used

throughout all scientific disciplines, basic misconceptions prevail about the information content of a (howsoever low) P-value. Serious criticism was voiced in the scientific community lately regarding the common practice in reporting statistical analysis results, at times resulting in the so-called "P-hacking" [60, 61, 62, 63]. In fact, P-values are often treated in a purely dichotomous – yes/no – fashion: results exhibiting $P < 0.05$ are reported as significant while test results with higher P-values are likely to be withheld or discarded as unimportant [61, 64]. This way, P-value-based statistics promote an enormous bias in research results. From a methodical point of view, P-values usually do not only lack reproducibility, but also – if treated as hard limits – fail to inform about the practical relevance of results, which is the size of the measured effect [61, 65]. A (usually) practically irrelevant growth enhancement in plants as low as 1 % in biomass can be proven to be statistically significant (at sufficiently low variability of the measurements), while a truly relevant growth enhancement by 50 % may be "insignificant" in terms of P-values. To avoid misinterpretations and to overcome the limitations of NHST, this work will focus on and present results exclusively in terms of effect sizes, which are the parameter of choice to address the second question.

Several different measures of effect sizes have been proposed (for an overview refer to [66, 67, 68]). In terms of estimating group differences, three measures can be regarded as the most prominent ones:

> ▷ **COHEN's d** [69]: standardizes the difference in means between the treated group (M_T) and the control group (M_C) by the pooled standard deviation of both groups:
>
> $$d = \frac{M_T - M_C}{\sqrt{\frac{SD_T^2 + SD_C^2}{2}}} \tag{2.5}$$

> ▷ **GLASS's Δ** [70]: standardizes the difference in means by the control groups' standard deviation (SD_C); useful if group sizes are large and treatment is expected to affect the standard deviation of the treated group or if the standard deviations of both groups differ significantly [68]:
>
> $$\Delta = \frac{M_T - M_C}{SD_C} \tag{2.6}$$

> ▷ **HEDGES' g** [71]: similar to Cohen's d, but employing a corrected pooled standard deviation to account for differing group sizes [68]

Depending on the experimental setup and the effect of interest, one or another measure may

promise more robustness in statistical evaluation. All considered effect size measures are point estimates in the same way an arithmetic mean of a group is. To attribute a measure of precision or reliability, several confidence intervals on different effect sizes have been proposed (for an extensive overview see [72]). The derivation of a robust effect size measure to be employed in this work is described in the following section.

2.2.2 Statistical analysis

The foundation of any robust and reliable statistical model lies in resilient assumptions about the underlying population and the effect of interest, its type and size. To make reasonable assumptions, one has to define the basic characteristics of the system of interest first: In terms of the developed phenotypic assay, the sum of all *L. minor* plants growing under given conditions can be regarded as the basic population, which shall be called P_0. In absence of outside influences, a plants' life in this population is characterized by the following four states:

1. A new plant grows as bud, attached to the mother plant until it reaches a critical size A_{min} and is disconnected. At the time of disconnection, when the young plant is recognizable as individual, it has a frond area equal to or higher than the critical size A_{min}.
2. The plant grows towards adulthood, steadily gaining in biomass, increasing in size.
3. The adult plant starts forming a fresh bud, growing towards its maximum size A_{max} before eventually releasing a new plant into the population. The mother plant itself repeats this cycle of growing and forming daughter plants several times [55].
4. At the end of its lifespan (about 31 d for *L. minor* [55]) the plant ends its metabolic activity, becomes chlorotic and exits the population.

Based on this definition of a life cycle, two assumptions could be made:

Assumption 1: The distribution of frond areas in the population P_0 follows a normal distribution within the limits A_{min} and A_{max}. This also holds true for any random sample S – given the sampling is representative.

To avoid interference by dead plants, the time span for renewal of plant cultures using young plants was chosen sufficiently short (7 d) to ensure that the population P_0 only consists

of plants in the states 1 – 3. Therefore, the plant size – respectively the frond area A – should follow the same distribution at any given point in time. Since the lower limit of the distribution is given by A_{min} and the upper limit by the maximum size A_{max} (a single plant cannot steadily grow bigger without releasing a daughter plant) a normal distribution of A is assumed for the population P_0. Thus, a representative sample S should also follow this distribution.

> **Assumption 2:** The relative growth RG in the population P_0 under constant experimental conditions is normally distributed. This also holds true for any random sample S – given the sampling is representative.

Experimental evidence first communicated by ASHBY suggests a cycle of senescence and rejuvenation in *L. minor* cultures grown under static environmental conditions [73]. These observations were later reassessed by BARKS in greater depth [74]. Both studies report a decline in plant fitness within ageing *Lemna* cultures, observable by a decrease in survival rate (share of plants surviving on a given day), decrease in reproduction rate (share of plants producing offspring on a given day) and offspring fitness. At the same time, a dimnishment in mean frond area in a (sub-)population of plants could not be observed due to a simultaneous rejuvenation process, suggesting that while the growth rate of a single plant may be affected by ageing, the mean absolute growth rate of a (sub-)population may be considered stable over time. However, since the possible impact of such global effects onto analysis results can hardly be eliminated with certainty, the experimental design presented in this work includes a control group on each plate as reference for "normal" growth under stress conditions, independent from the state of ageing of the population in order to ensure maximal reliability of the obtained data.

In an ideal experiment, each plant's reaction to a certain treatment – its phenotype – would be determined exclusively by the type of treatment (application of a certain compound) and not be influenced by the genotype (biological rhythms or variability in a wider sense) or experimental parameters, in particular. This ideal experiment would yield an exact value or factor for the acceleration/deceleration of a plant's growth, expressed by the growth rate μ, the slope of the linearized growth curve (eqn. 2.1b). In reality, even in a population of plants with the same genetic background – as it is the case with *L. minor* – the observed slope of this linear function is individual for each plant and results from many different factors apart from the treatment, e. g. the biological preconditions, slight variations in irradiation, temperature,

humidity or air circulation, measurement error etc. However, the basic requirement for the experiment to give reasonable results is the superior influence of the treatment on the growth rate, while all other influencing factors can be summarized as "random noise", expressed through the error term ε (eqn. 2.7a). Due to its random nature, neither size nor sign of this error term ε can be determined and it becomes part of the parameter of interest – it adds variability onto the growth rate $\overline{\mu}$, which can be assumed to be normally distributed (eqn. 2.7b). Because of the proportionality between growth rate $\overline{\mu}$ and relative growth $\overline{RG}$ (see eqns. 2.3a – 2.3c), the latter is also afflicted with this random error as expressed in eqn. 2.7c. Therefore, in a well-designed experimental setup it is reasonable to assume that the parameters $\overline{RG}$ follow a normal distribution.

$$\ln A = \ln A_0 + t \cdot \mu + \varepsilon \tag{2.7a}$$

$$\mu \cdot t + \varepsilon = \ln A - \ln A_0 \tag{2.7b}$$

$$\overline{RG} = \frac{1}{6} \sum_{i=1}^{6} RG_i + \varepsilon \tag{2.7c}$$

Experimental setup

To check the validity of the aforementioned assumptions, the following experiment was carried out: Twelve 500 ml Erlenmeyer flasks were filled with STEINBERG medium and inoculated with approx. ten *Lemna minor* plants each. After a seven-day growth period each flask hosted 50 – 100 *L. minor* plants belonging to P_0, divided into twelve subpopulations $P_{\text{sub},1...12}$. From each subpopulation a sample $S_{1...12}$ of 24 plants was randomly chosen and transferred to a 24-well microtiter plate containing 2 ml STEINBERG stress medium and 2 μl DMSO per well – according to the assay design equivalent to 4 control groups with 6 plants each (see tbl. 2). Let these groups be called $G_{1...12,1...4}$. The plates were incubated according to the assays' setup for 48 h, followed by removal of the stress medium and addition of PEG-free medium. The plates were then incubated for further 24 h, which constituted the recovery phase. Eventually, relative growth parameters were obtained for $12 \cdot 4 \cdot 6 = 288$ plants.

Normal distribution of plant size

The 288 plants originating from P_0 are assumed to constitute a representative sample of the population P_0, which is a basic requirement for the experimental setup to not suffer from bias. To validate this assumption, the initial frond areas (measured in px) of the complete set of plants were projected onto a normal distribution, as shown in fig. 8, p. 24. The histogram in fig. 8a shows a distribution of frond areas in the range of approx. $4000 - 8000$ px, centering around 6000 px, following the typical bell-shaped curve of a normal distribution. Descriptive measures of the distribution are summarized in tbl. 4, p. 24: The similarity between mean and median as well as the low skewness value – a measure of a distribution's symmetry – confirm the agreement-by-eye between the sample and a normal distribution. The "classical" goodness-of-fit plot in fig. 8b, the cumulative distribution function (CDF), shows a slight shift to higher frond areas at the upper end, which is also indicated by the positive skewness value. The quantile-quantile (Q-Q) plot (fig. 8c) highlights the lack-of-fit at the distribution tails [75] where few extreme values can be observed on both sides. Nevertheless, the normal distribution gives a good approximation of the sample and confirms a representative sampling according to assumption 1.

Normal distribution of relative growth

For each of the 288 plants in the experiment, the individual RG values were calculated according to eqns. 2.3a – 2.3c. In analogy to the evaluation of the frond area distribution, each of the three parameters was projected onto a normal distribution to check for the validity of assumption 2. The results shall be exemplified here using the total relative growth RG_{tot}: fig. 9, p. 25, shows the diagnostic plots for the fit – the histogram and CDF plot are again in agreement with a normal distribution, while the Q-Q plot shows a higher dispersion in the data set than expected from the theoretical distribution, indicated by the extreme values below and above the line $y = x$ at both ends. This could possibly lead to observations of unexpectedly high or low relative growth in single plants, while the whole set of samples, and therefore the population P_0, is well described by a normal distribution. This is also true for the stress phase and recovery phase relative growth parameters RG_{st} and RG_{rec}, respectively.
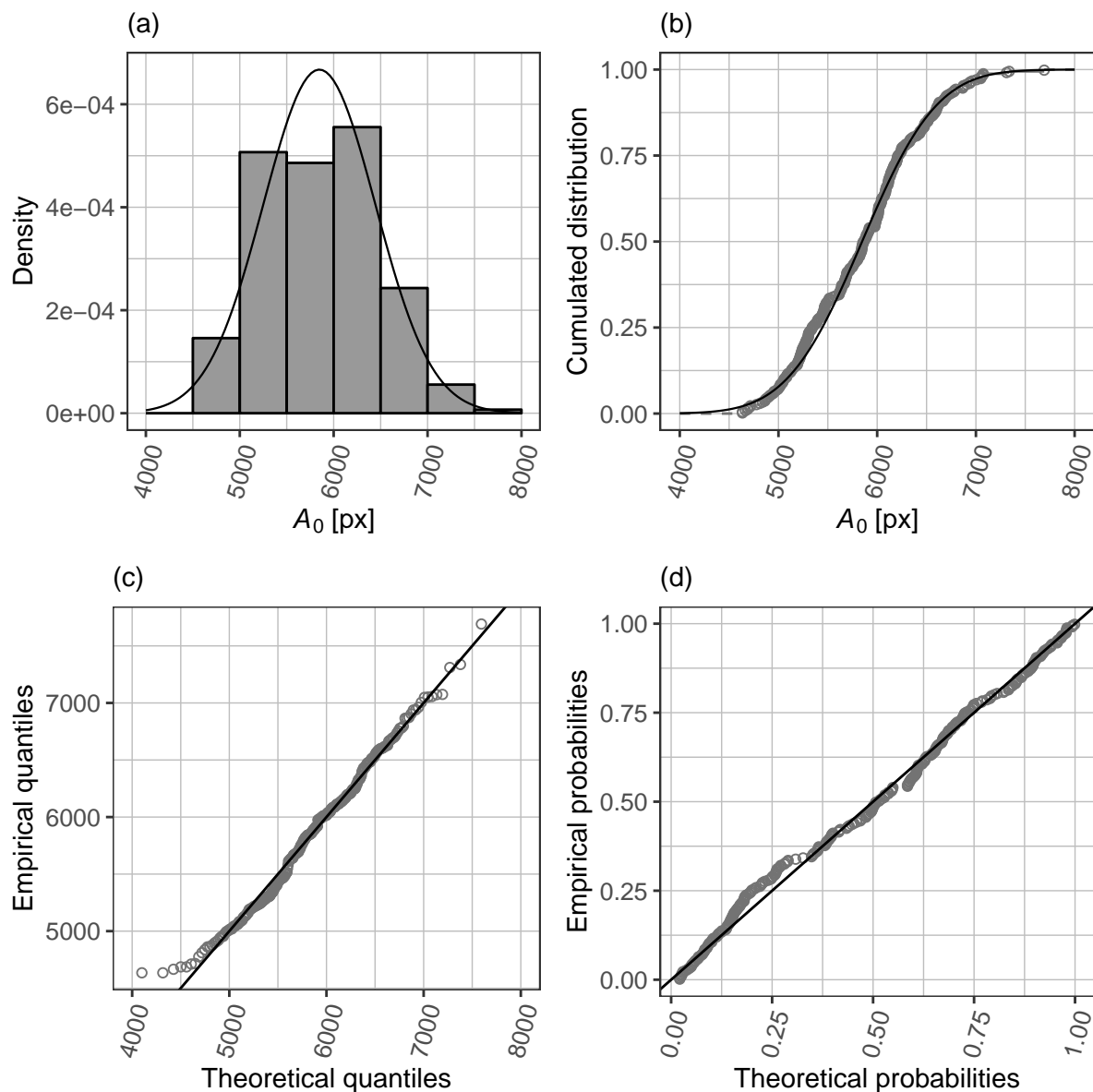
Figure 8: Distribution of initial frond areas
Comparison between empirical distribution of A_0 (gray) and theoretical normal distribution (black); (a) Histogram and density curve, (b) Cumulative distribution function, (c) Quantile-quantile plot, (d) Probability-probability plot

Table 4: Parameters describing the distribution of initial frond areas (see fig. 8a)

Parameter class	Parameter	Value [px]
Location	Mean $\overline{A}_0$	5847
	Median $\widetilde{A}_0$	5863
Variability	Standard deviation SD	599
	Median absolute deviation MAD	631
Range	Minimum area A_{min}	4635
	Maximum area A_{max}	7692
Symmetry	Skewness	0.164
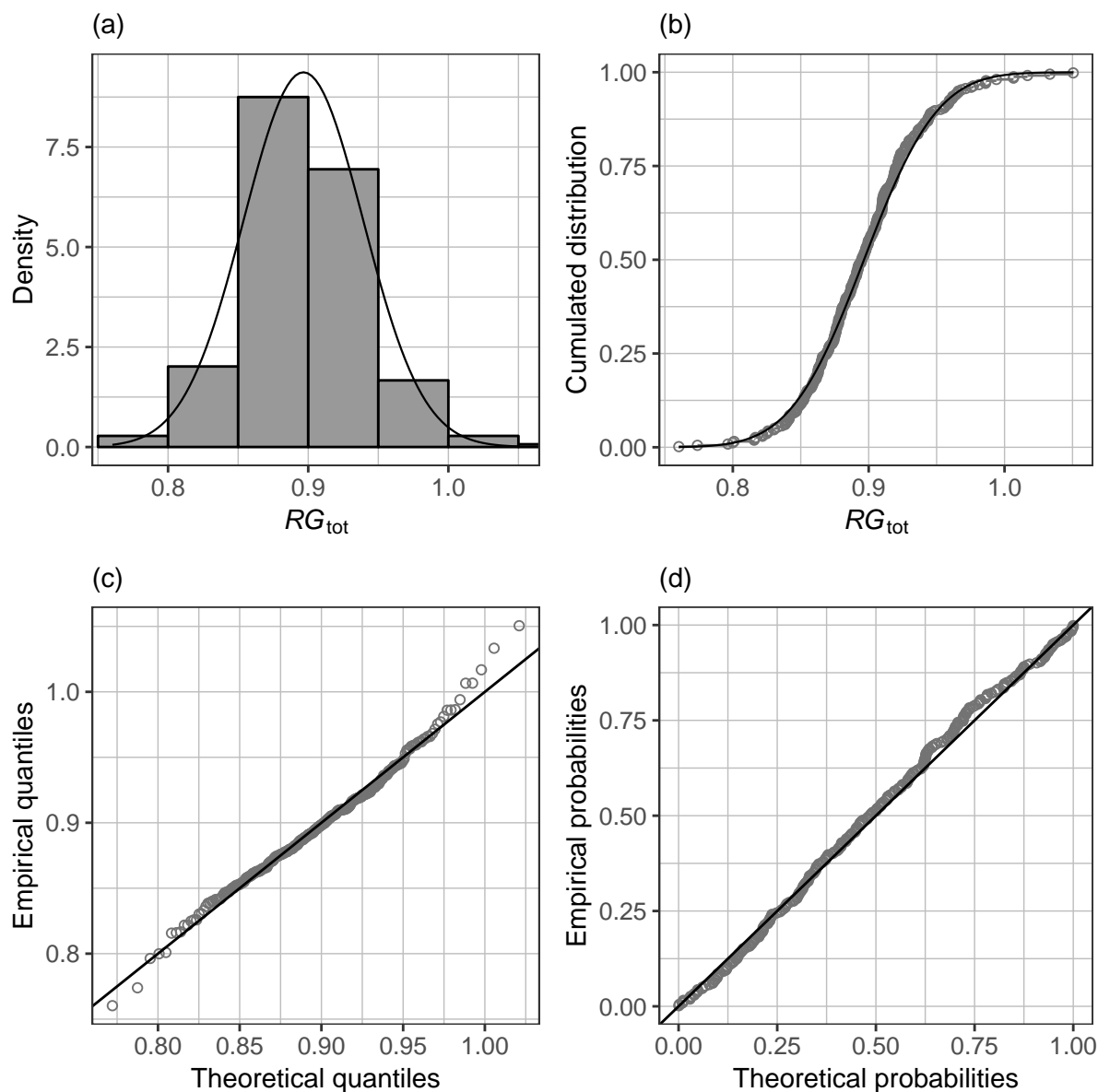
Figure 9: Distribution of total relative growth
Comparison between empirical distribution of RG_{tot} (gray) and theoretical normal distribution (black); (a) Histogram and density curve, (b) Cumulative distribution function (CDF), (c) Quantile-quantile (Q-Q) plot, (d) Probability-probability plot

Table 5: Parameters describing the distribution of relative growth parameters (see fig. 9a)

Parameter class	Parameter	RG_{st}	RG_{rec}	RG_{tot}
Location	Mean	0.426	0.470	0.897
	Median	0.424	0.470	0.895
Variability	Standard deviation	0.049	0.037	0.043
	Median absolute deviation	0.053	0.043	0.039
Range	Minimum	0.309	0.369	0.760
	Maximum	0.572	0.559	1.051
Symmetry	Skewness	0.125	−0.127	0.277

A summary of the distribution of the three RG parameters is given in tbl. 5, p. 25. The effectiveness of the stress application becomes evident by comparison of the mean relative growth in stress and recovery phase: during 24 h of recovery the plants show a slightly higher relative growth than in 48 h of stress – a deceleration of growth by more than 50 % through application of PEG6000.

Group analysis

So far, the whole set of 288 plants was regarded as a single sample – ideally, each compound would have to be tested on such high numbers of plants, which is usually not feasible and not suitable for high-throughput assays. Therefore, with regard to experimental feasability, the question of interest is whether the control groups $G_{1...12,1...4}$ consisting of only 6 plants will still reflect the nature of the population's relative growth. If this was the case, each of these groups would have means and standard deviations for each growth parameter in agreement with the ones reflecting the population (see tbl. 5). Fig. 10, p. 27, shows the distribution of RG_{tot} throughout all 48 groups spread over the twelve microtiter plates used in the experiment.

In most cases, the group means (black points) scatter within a range of ± 0.05 around the population mean of 0.897 and the standard deviations show a high uniformity. Nevertheless, several groups show a higher dispersion (e. g. $G_{11,1}$) or skewness because of single extreme values (e. g. $G_{6,4}$). Moreover, the plates containing samples S_6 and S_{12} show a systematically enhanced relative growth in comparison to the other plates – this could be due to chance or variability within the experimental conditions, e. g. better exposition of the plates to the light source. However, since each plate in the screening contains a control group, only the within-plate variation is of interest, e. g. the differences between groups $G_{1,1}$ and $G_{1,4}$.

A different presentation of the data is given in fig. 11, p. 27, for all three growth parameters: in the upper plot the distribution of observed means and medians (as central value measures of a distribution) is shown for all 48 groups alongside the estimated population mean, the "target" value (see tbl. 5). The following conclusions can be drawn from the plot:

> ▷ Both mean and median as estimators for the population mean show a distribution around the target value. This effect is likely due to sampling variation and differing experimental conditions between plates.
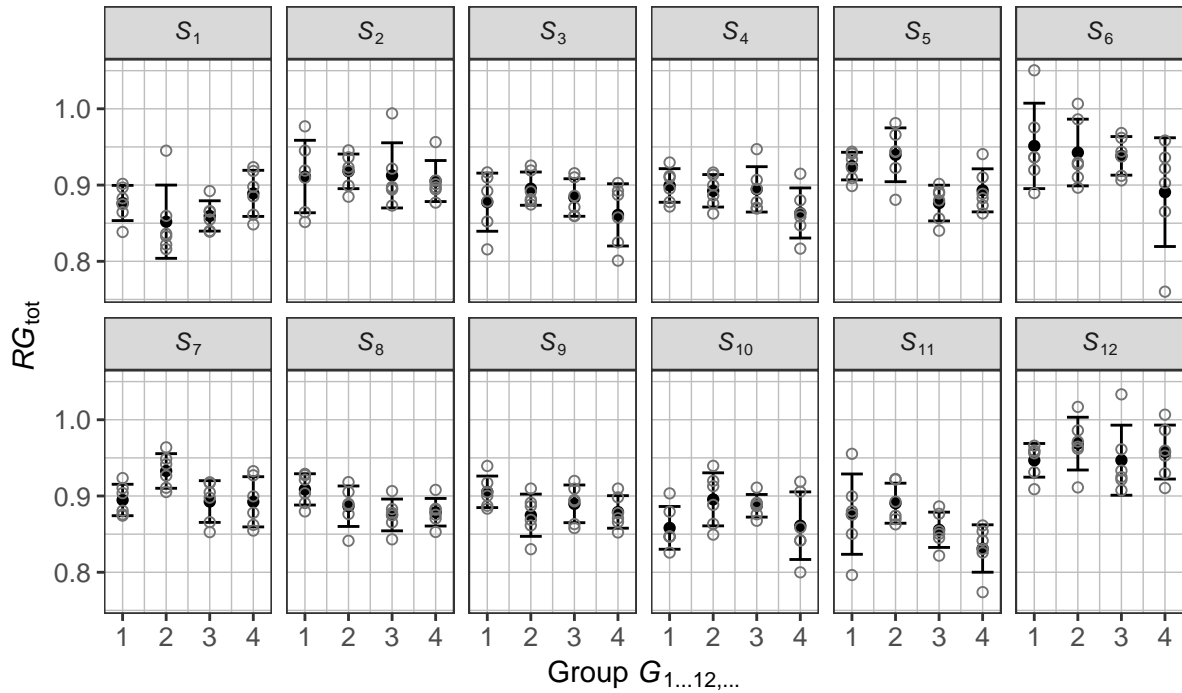
Figure 10: Total relative growth by group
Total relative growth RG_{tot} assessed on the level of assay groups $G_{1...12,...}$ (gray: single values, black: grouped mean $\pm SD$)
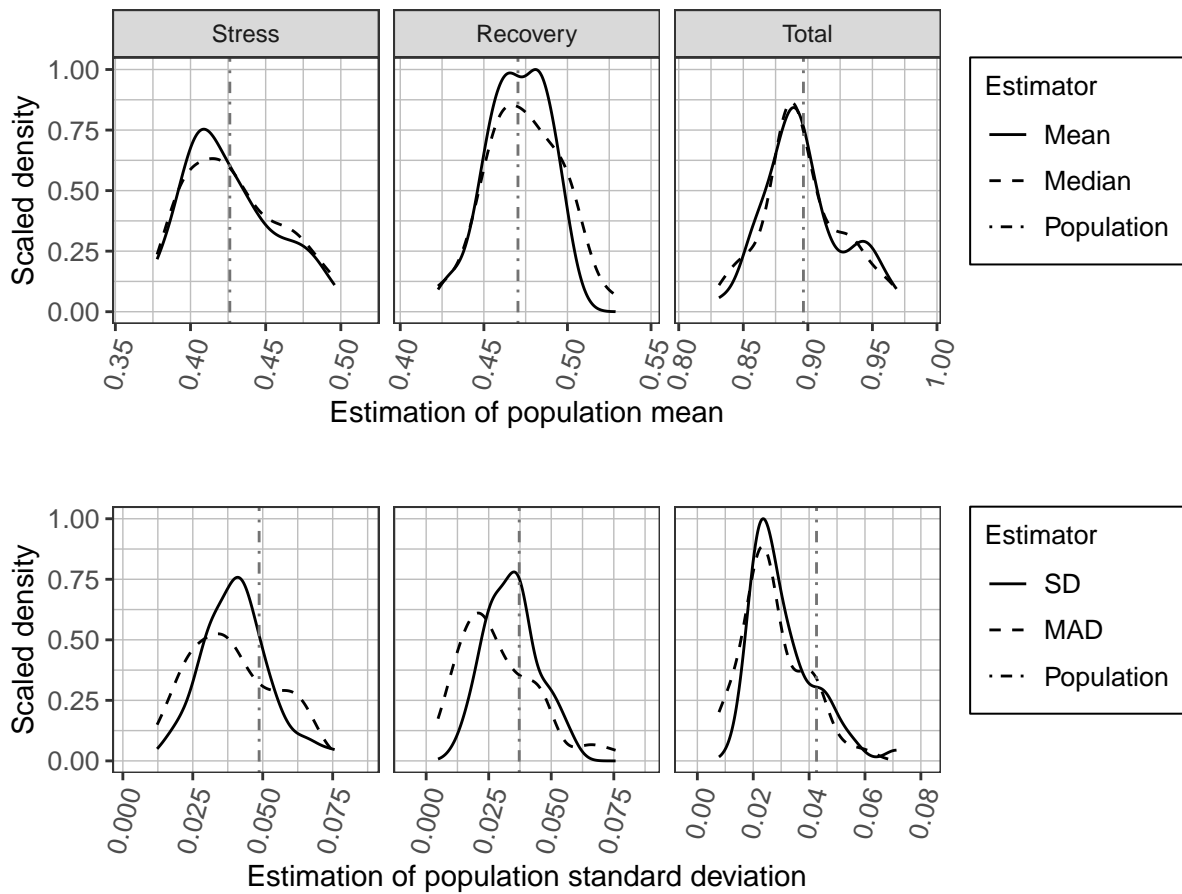
Figure 11: Comparison of growth parameter estimators
Distribution of $G_{1...12,...}$ group parameters as estimators for population mean (upper plot) and standard deviation (lower plot)

▷ For the stress phase both mean and median seem to underestimate the target value slightly, while the maxima for the recovery phase and the total relative growth are in agreement with the target value.

▷ For both stress and recovery phase, the distribution of medians shows a higher dispersion, indicated by the less intense maxima.

▷ Therefore, the group mean can be deemed the least biased central value estimate for a group G belonging to the population P_0.

The lower plot presents the data obtained on the variability measures of all groups: the standard deviation and the median absolute deviation (MAD) are plotted against the standard deviation attributed to the population, the target value (see tbl. 5). Summarizing, the plot contains the following information:

▷ The MAD shows a higher dispersion than the SD for all three growth parameters, indicated by the less intense maxima.

▷ The distribution of SD in the recovery phase is in agreement with the target value, while both SD and MAD greatly underestimate the target value for all other growth parameters – for RG_{tot} the target value is underestimated by approx. 50 %.

▷ Therefore, neither the group standard deviation SD, nor the median absolute deviation MAD are reliable estimators of the population standard deviation.

Establishment of a robust effect size measure

The results discussed above highlight a basic problem in plant-based experiments: the already high biological variability of plant populations – as indicated e. g. by the total relative growth RG_{tot} ranging from 0.760 to 1.051 – can hardly be captured within samples of a size as small as $n = 6$ (or even smaller). Variability due to biased sampling and experimental conditions taken into account, the problem intensifies.

The differences between groups shown in fig. 10 can hardly be explained by a specific (chemical) treatment since all plants were grown under control conditions (untreated). The range of between-group differences simply sums up the variability of all framework conditions: biological fitness, bias in sampling and fluctuations in the experimental conditions. In order to not mistake such fluctuations as true effects, a critical effect size needs to be

defined by answering the following question: Which size of an observed effect E_0 between two groups is most likely attributable to the experimental setup? Ideally, with an answer at hand, all effects $E < E_0$ could be judged random, while all effects $E > E_0$ could be assigned to a certain compound treatment. In reality, most compounds will only have a slight (positive or negative) effect onto the relative growth, causing measured effects to be close to E_0. In these cases – if applied as hard limit – the defined effect size E_0 will influence the probability of type I and type II errors:

  ▷ With decreasing E_0 the rate of effects incorrectly judged to be caused by treatment will increase (false positives, type I error).
  ▷ With increasing E_0 the rate of real effects caused by treatment that are incorrectly deemed random will increase (false negatives, type II error).

In the first case – E_0 set too low – an experiment will probably yield many "active" compounds, a vast share of which will prove ineffective in follow-up experiments – a rather costly strategy, taken personnel and experimental expenses into account. In the second case, the experiment will only yield a few "top players" (if any), failing to recognize promising candidates that may have a lower absolute activity, but could exhibit a promising alternative mode of action. If one has to decide in one direction or the other, false positives are usually considered less problematic as these can be reevaluated in validation experiments. False negatives, on the other side, are usually lost, since reevaluation of discarded compounds is rarely in scope of such projects. However, the risk of commiting both type I and type II errors can be minimized by defining a rationale for finding an optimal value for E_0. Moreover, different levels of effects can be defined, as proposed by COHEN who distinguished between small, medium and large effects [69].

Before a critical effect size can be defined, a proper measure has to be found. All three introduced effect sizes (see section 2.2.1) standardize a difference of means in some way. As discussed in relation to fig. 11, the group mean is the most unbiased estimator of the true population mean, therefore the group means of treated groups and control group will be used in effect size estimation. Regarding the standardization, of the three introduced effect sizes, HEDGES' g is to be ruled out as measure because of its bias with small sample sizes [76]. Moreover, a correction for a difference in sample sizes – for which HEDGES' g was originally proposed – is unnecessary with the experimental design at hand, since group sizes will not differ nor change. Both COHEN's d and GLASS's Δ use the standard deviation of the

compared groups to standardize the mean difference. Keeping in mind the results discussed in relation to the distribution of variability estimators in fig. 11, this could prove problematic since the observed group standard deviation shows a broad distribution and underestimates the population's standard deviation considerably. A, by chance, small standard deviation in the control (or treated) group could cause an excessive growth of the effect size, likely leading to an overestimation of the true effect. By employing COHEN's d as measure under replacement of the observed standard deviations of both control and treatment group with the "true" population's standard deviation SD_{P} assessed on 288 plants, the estimated effect sizes tend to become smaller, thus reducing the risk of type I errors. Derived from COHEN's d (eqn. 2.5), the effect size measures for the three different growth parameters are therefore defined as follows:

$$d_{\mathrm{st}} = \frac{\overline{RG}_{\mathrm{st,T}} - \overline{RG}_{\mathrm{st,C}}}{\sqrt{\frac{SD_{\mathrm{st,P}}^2 + SD_{\mathrm{st,P}}^2}{2}}} = \frac{\overline{RG}_{\mathrm{st,T}} - \overline{RG}_{\mathrm{st,C}}}{SD_{\mathrm{st,P}}} \tag{2.8a}$$

$$d_{\mathrm{rec}} = \frac{\overline{RG}_{\mathrm{rec,T}} - \overline{RG}_{\mathrm{rec,C}}}{\sqrt{\frac{SD_{\mathrm{rec,P}}^2 + SD_{\mathrm{rec,P}}^2}{2}}} = \frac{\overline{RG}_{\mathrm{rec,T}} - \overline{RG}_{\mathrm{rec,C}}}{SD_{\mathrm{rec,P}}} \tag{2.8b}$$

$$d_{\mathrm{tot}} = \frac{\overline{RG}_{\mathrm{tot,T}} - \overline{RG}_{\mathrm{tot,C}}}{\sqrt{\frac{SD_{\mathrm{tot,P}}^2 + SD_{\mathrm{tot,P}}^2}{2}}} = \frac{\overline{RG}_{\mathrm{tot,T}} - \overline{RG}_{\mathrm{tot,C}}}{SD_{\mathrm{tot,P}}} \tag{2.8c}$$

To define optimal levels of effect sizes, we first need to estimate the size of the system's inherent variability – the observed between-group effect under similar treatment. Detailed analysis of the data shown in fig. 10 reveals that the largest difference in $\overline{RG}_{\mathrm{tot}}$ among the four groups of a plate is to be found between $G_{5,2}$ and $G_{5,3}$ with

$$0.940 - 0.876 = \underline{0.0633}$$

Applying the effect size measure as shown above results in a value of

$$d_{\mathrm{tot}} = \frac{\overline{RG}_{\mathrm{tot}}(G_{5,2}) - \overline{RG}_{\mathrm{tot}}(G_{5,3})}{SD_{\mathrm{tot,P}}} = \frac{0.940 - 0.876}{0.043} = 1.484 \approx \underline{1.5}$$

In conclusion, the biggest difference in $\overline{RG}_{\text{tot}}$ between groups under identical experimental conditions due to inherent variability of the experimental setup corresponds to an effect size of $d_{\text{tot}} = 1.5$, which shall be defined as critical effect size $E_{0,\text{tot}}$. Observed effect sizes higher than $E_{0,\text{tot}}$ will be considered small effects. For the purpose of this work medium and large effects shall be defined in steps of $0.5 \cdot SD_{\text{tot,P}}$, meaning that an effect is deemed large only if the difference in $\overline{RG}_{\text{tot}}$ between control and treated group is $\geq 2.5 \cdot SD_{\text{tot,P}}$. The different magnitudes in terms of effect sizes are therefore:

   ▷ no effect: $d_{\text{tot}} < 1.5$
   ▷ small: $1.5 \leq d_{\text{tot}} < 2.0$
   ▷ medium: $2.0 \leq d_{\text{tot}} < 2.5$
   ▷ large: $2.5 \leq d_{\text{tot}}$

By applying similar rules, different magnitudes of effects can be found for RG_{st} and RG_{rec} as well (see tbl. 6, p. 33). As mentioned earlier, different confidence intervals for different types of effect size measures have been proposed, many of them available as part of statistics software. Exact 95 % confidence intervals for the parameters d were constructed using the R package MBESS [72].

Merging of replicate measurements – a meta-analytical approach

The term "meta-analysis" refers to a "set of techniques for integrating the results from a number of studies on the same or similar issues" [77]. If reported in an appropriate format, namely group and effect sizes and confidence intervals rather than single P-values, published studies can contribute to the development of generalized knowledge on a certain topic, independent from differences between single experimental setups and methods. However, the outcome of a meta-analysis does not only depend on the studies involved, but also on the meta-analytical technique used: integrating the underlying studies within a fixed-effects model (FE) can give results differing considerably from ones obtained by applying a random-effects model (RE) – an important distinction that was studied in detail by SCHMIDT *et al.* [78]. Both methodologies can be valid in a certain case, depending on the goal that is to be achieved: If inference is seeked exclusively within the limitations of the underlying studies without generalizing for non-considered past or future studies, an FE model is a legitimate choice (so-called conditional inference [79]). If, on the other hand, generalized knowledge –

unconditional inference – is sought, RE models will give less biased, more reliable statements, where FE models tend to underestimate variability [78, 79, 80]. The difference between FE and RE models lies within the assumption about the true value underlying each single study: FE models assume a constant true value (homogeneity) across all studies, meaning the standard deviation of the true value δ of COHEN's d (eqn. 2.5) equals zero ($SD_\delta = 0$). Thus, between-study variability is considered to be exclusively due to simple sampling error. In contrast, RE models can also accurately describe cases in which the true value differs between single studies (heterogeneity), meaning that the overall sampling error consists of basic sampling error and an additional term for changes in the true value SD_δ. In conclusion, FE models can be considered special cases of RE models for $SD_\delta = 0$.

As discussed previously, the observed variability between groups of plants subjected to similar treatment is non-negligible due to inherent biological variability combined with small sample sizes. Utilizing a meta-analytic approach within this work provides a powerful method to increase certainty about a compounds' influence towards plant growth by merging repeated measurements, rather than increasing sample size in a single experiment.

The true value, the effect size that is approximated by the observed effect size d (eqns. 2.8a – 2.8c), is not assumed to change between repeated experiments using the same compound at the same concentration level in an identical setup – if this was the case, the experimental setup would be flawed. Therefore, using an FE model to combine repeated measurements appears appropriate. The estimation of a mean effect size $\overline{d}$ for the described measures d in this work is done by weighting the individual effect sizes using the inverse-variance-weighted average method (see [79, 78]):

$$\overline{d} = \frac{\sum \omega_i d_i}{\sum \omega_i} \quad . \tag{2.9}$$

The 95 % confidence interval is constructed as

$$CI_{\overline{d}, 0.95} = \overline{d} \pm 1.96 \cdot SE_{\overline{d}} \quad . \tag{2.10}$$

Careful examination of the underlying formulae shows that higher effect sizes d have less weight ω in calculating $\overline{d}$. This way, the influence of single (extremely) high effects, which are more likely to be due to sampling error, is reduced. For details and derivation of the equations shown above see section 7.3.2, p. 109. For the calculation of the described parameters within this work, the R package metafor was used [81].

Table 6: Summary of critical values for the classification of effect sizes

	RG_{st}	RG_{rec}	RG_{tot}
SD_{P}	0.049	0.037	0.043
Small effect	$1.3 \le d_{\mathrm{st}} < 1.8$	$1.8 \le d_{\mathrm{rec}} < 2.3$	$1.5 \le d_{\mathrm{tot}} < 2.0$
Medium effect	$1.8 \le d_{\mathrm{st}} < 2.3$	$2.3 \le d_{\mathrm{rec}} < 2.8$	$2.0 \le d_{\mathrm{tot}} < 2.5$
Large effect	$2.3 \le d_{\mathrm{st}}$	$2.8 \le d_{\mathrm{rec}}$	$2.5 \le d_{\mathrm{tot}}$

Summary of the statistical evaluation of screening results

The evaluation of plant growth in terms of effect sizes throughout the screening of compounds includes the following steps:

1. Measurement of frond areas A_0, A_{48} and A_{72}
2. Calculation of parameters RG_{st}, RG_{rec} and RG_{tot} using the ln-transformed frond areas
3. Calculation of group means $\overline{RG}_{\mathrm{st}}$, $\overline{RG}_{\mathrm{rec}}$ and $\overline{RG}_{\mathrm{tot}}$ for control and test groups
4. Calculation of the effect sizes d_{st}, d_{rec} and d_{tot} by standardizing the difference in group means between control and test group using the populations' standard deviation. Tbl. 6 informs about the relevant SD_{P} and the different magnitudes of effects.
5. In case of replication of measurements: calculation of $\overline{d}$, its standard error $SE_{\overline{d}}$ and its 95 %-confidence interval $CI_{\overline{d},0.95}$ using all individually obtained d_i.

2.2.3 *In vivo* database screening and comparison with *in silico* docking studies

As mentioned earlier, the compound library used for the *in vivo* screening in this work originated from the work of HEYM, who performed an *in silico* screening of compound databases [24]. Using docking studies and visual inspection for structural features, 121 commercially available compounds were selected from KeyOrganics, of which 119 were screened within this work. These 119 compounds can be divided into distinct groups and subgroups, based on key structural features related to the PARP pharmacophore (fig. 6): 71 compounds comprised the structure of a bicyclic lactam, as it is known from many inhibitors of *Hs*PARP-1. Most prominent among them are the classes of 4-substituted phthalazin-1(2*H*)-ones **8** (Pht, $n = 26$), 2-substituted quinazolin-4(3*H*)-ones **9** (Qui, $n = 27$) and 2-substituted
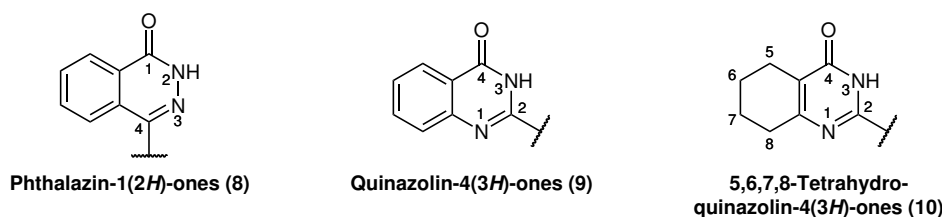
Figure 12: Classes of bicyclic lactams included in the screened compound library

5,6,7,8-tetrahydroquinazolin-4(3*H*)-ones **10** (ThQui, $n = 11$) (see fig. 12). The second group (48 compounds) consisted of acyclic amides, ureas and hydrazides ($n = 35$) as well as several compounds lacking the amide group, incorporating a carboxylic acid function instead ($n = 13$). All tested compounds were applied as solutions in pure DMSO at a final concentration of 10 µM. Their chemical structures, consecutive numbers and screening results are listed in the appendix.

Fig. 13, p. 35, gives an overview of the results for the total relative growth effect size d_{tot} obtained in the screening of the compound library, grouped by basic chemical structure (lactam or miscellaneous). It can be seen that both groups exhibit a distribution in influence onto plant growth from slight adverse to distinctly positive effects – single non-cyclic amides have to be taken into consideration for growth-enhancing activity, though the topmost lactams clearly show superior activity. As expected, only a small fraction of compounds showed an acceleration of growth equal to or greater than the critical effect size of $E_{0,tot} = 1.5$. In total, 19 out of 119 compounds (16 %) could be assigned a small, medium or large effect. Tbl. 7 informs about number and share of actives in both groups in greater detail. Several points have to be considered in judging this hit ratio:

▷ The selection of compounds was based on their estimated ability of being coordinated inside the active site of an *At*PARP-1 homology model – first *in vitro* enzyme inhibition studies showed rather poor correlation with the predicted docking strength [26].

Table 7: Number and share of effective compounds in library screening by level and group; percentages relate to the within-group ratio

	Criterium	Lactams	Other
Small effect	$1.5 \leq d_{tot} < 2.0$	7 (10 %)	2 (4 %)
Medium effect	$2.0 \leq d_{tot} < 2.5$	3 (4 %)	4 (8 %)
Large effect	$2.5 \leq d_{tot}$	3 (4 %)	0
Total		13 (18 %)	6 (12 %)
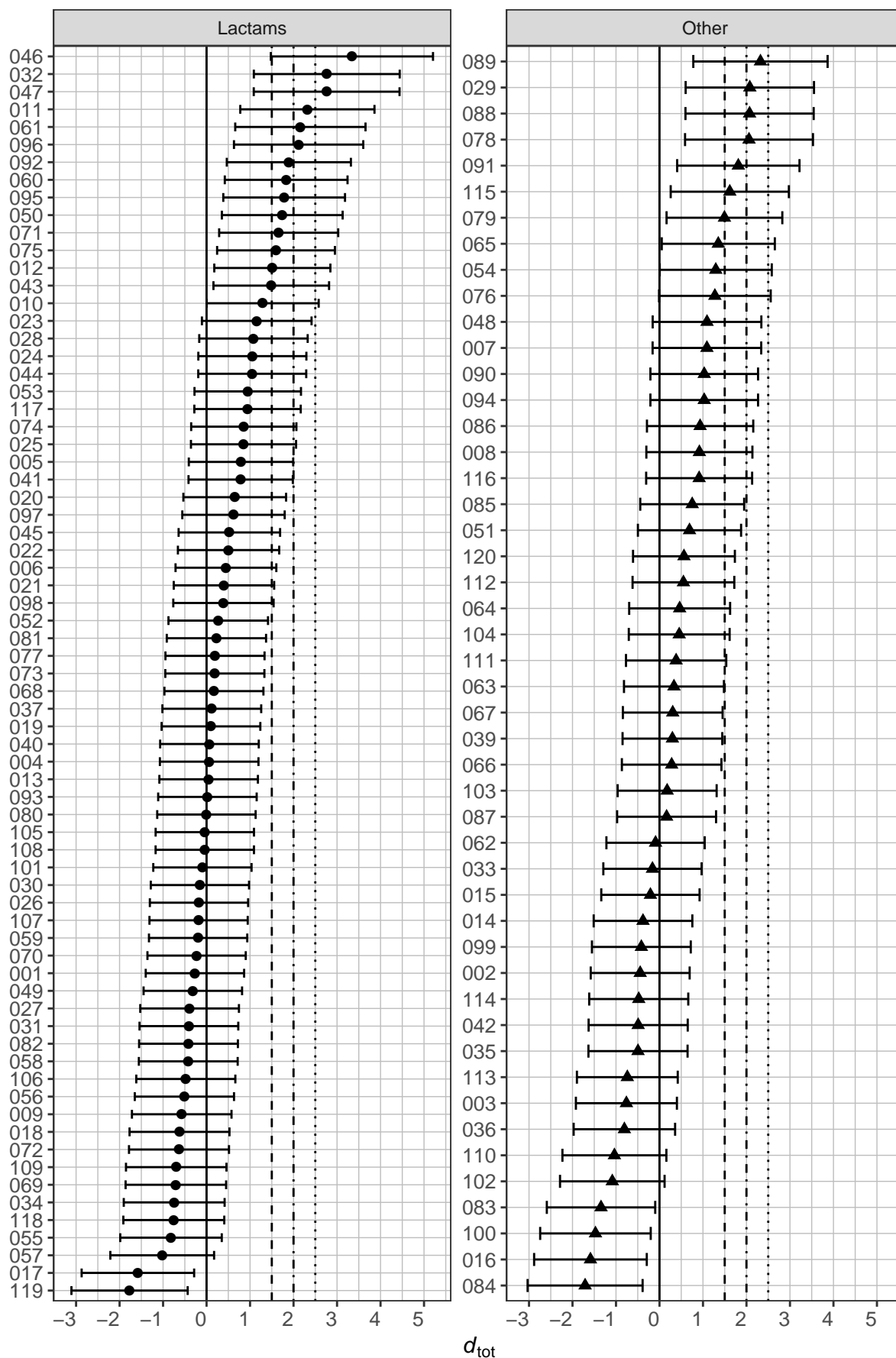
Figure 13: Overview screening results of compound library
Total relative growth effect size $d_{tot} \pm CI_{0.95}$ for all 119 compounds tested, grouped according to basic chemical structure; highlighted vertical lines indicate effect size levels (see tbl. 6, dashed – small, dotdash – medium, dotted – large)
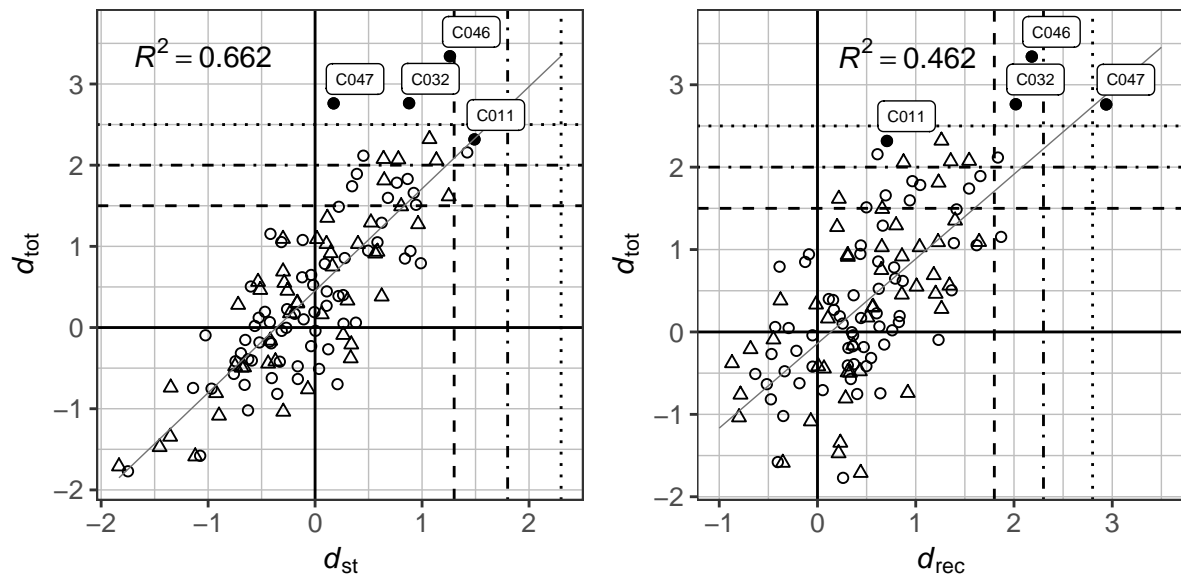
Figure 14: **Correlation between growth parameters** d_{tot} and d_{st} (left) and d_{rec} (right); circle: lactams, triangle: other; highlighted horizontal and vertical lines indicate effect size levels (see tbl. 6, dashed – small, dotdash – medium, dotted – large)

Hence, confirmation of PARP enzymes being the targets of the tested compounds is still pending.

▷ On the contrary, PARP-1 is known to be highly conserved among eukaryotes which made it possible to build a homology model for the *A. thaliana* enzyme based on the crystal structure of *Hs*PARP-1 as template in the first place. Thus, a high structural similarity between *At*PARP-1 and *Lm*PARP-1 seems likely, too.

▷ All compounds were tested on whole *Lemna* plants rather than on an isolated enzyme. Therefore, the activity of each compound does not only rely on the ability of inhibiting (or activating) its target, but also on its physicochemical properties which control e. g. resorption via root and/or leaf, transport and possible metabolism within the plant.

▷ The defined levels of effect sizes are type I error-optimized, meaning the activity of compounds tends to be underestimated. The share of compounds deemed active could be raised by lowering the critical effect size E_0 – at the expense of risking a higher share of false positives.

In the discussion of a compounds' activity not only the total relative growth, but also the performance within stress and recovery phase is of relevance. By plotting d_{tot} against d_{st} and d_{rec} (fig. 14, p. 36) it can be estimated, whether an acceleration of growth dominates in one of the two phases of the assay. As indicated by the coefficients of determination $R^2 = 0.662$ and 0.462, respectively, a moderate correlation between the total relative growth and both the relative growth in stress and recovery phase seems to exist. On average, a compounds'

activity cannot be fixed to a single phase, but is rather present throughout the complete time of the assay. The four compounds labeled in the plot illustrate the different effects observed: compounds **C046** and **C032** could be found among the highest ranking actives in both the stress and the recovery phase, thus taking ranks 1 and 2 in total relative growth. **C047** performed poorly in the stress phase without measurable effect but superseded all other compounds in the recovery phase, thus ranking third in terms of total relative growth. In contrast, compound **C011** ranked highest in the stress phase, but appeared to have no effect in the recovery phase, therefore ranking lower in total activity.

Of particular interest is the question how well the *in vivo* activity correlates with the activity predicted through the *in silico* studies. The docking scores obtained by Heym basically represent the calculated strength of interaction between the molecule and the model of *At*PARP-1 [24]. Thereby, similar to an enthalpic term, a lower (more negative) value represents a more favorable state – meaning the lower the score value obtained for a certain compound, the higher the probability for the molecule to bind inside the active site of the enzyme, possibly leading to an inhibition of the catalytic activity. The relation between d_{tot} of the three major classes of lactams employed in the screening and their assigned docking scores failed to show any distinct correlation (fig. 15, p. 38). The group of Pht – with one exception – clusters well in terms of docking scores, including the topmost predicted activities (most negative scores). However, the spread within the *in vivo* activity is large, including adverse effects and inactives, and shows no sign of correlation with the docking scores. For the groups of Qui and ThQui a different, but similarly unexpected distribution is observed: Most interestingly, the lowest-ranked derivative in terms of docking scores in both groups proved to be the most effective in the *in vivo* system, completely contradicting the hypothesized correlation.

These results indicate that the *in silico* screening docking scores cannot be used to predict growth accelerating effects in *L. minor* – the virtual model does not serve as key in understanding the mode of action of the screened compounds. Based on these observations two scenarios are imaginable:

1. A high structural similarity between *At*PARP-1 and *Lm*PARP-1 exists and the basic mode of action of small molecules can be explained with the proposed model. Yet, the influence of physicochemical properties of compounds, their resorption and bioavailability within the plant dictate whether a compound is able to deploy its activity after all. In
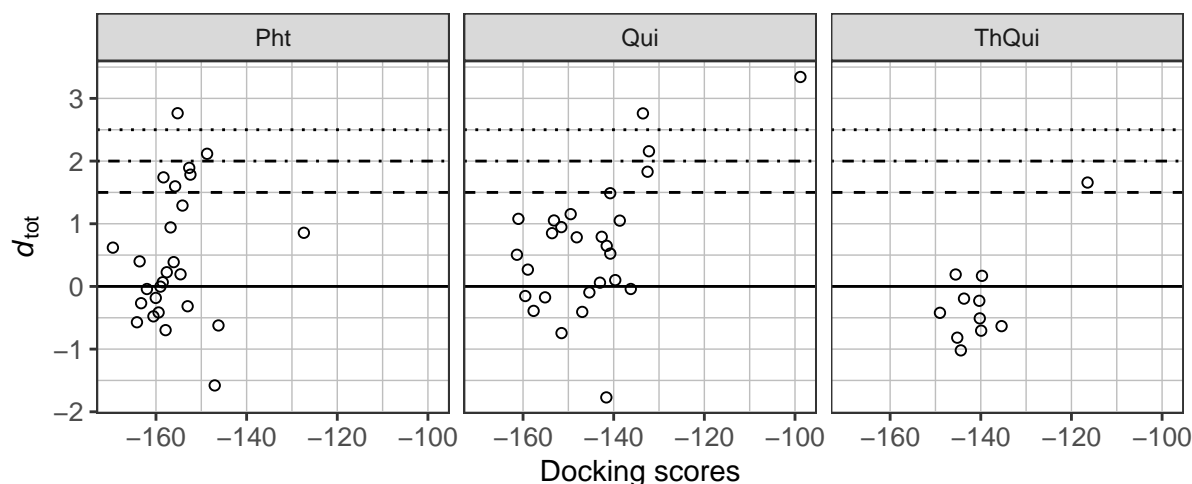
Figure 15: Comparison of docking scores and total relative growth effect size d_{tot} for the three major classes of lactams employed in the *in vivo* screening; for docking scores and their calculation see [24]; highlighted horizontal and vertical lines indicate effect size levels (see tbl. 6, dashed – small, dotdash – medium, dotted – large)

this case, many derivatives deemed inactive could actually be actives "handicapped" by unfavorable structural features, that hinder access to the target enzyme.

2. The measured *in vivo* effects are not attributable to inhibition of PARP enzymes but are rather connected to an entirely different target, which coincidentally is susceptible to compounds bearing the basic structural features of PARP inhibitors. In this case, the presented *in vivo* activities can only be the starting point of much more comprehensive investigations towards the true target.

2.2.4 Structure-activity relationships

The first step in clarifying the connection between the chemical structure of the screened compounds and their experimentally observed growth-enhancing effects consists in analyzing the distribution of activity between and within the groups of compounds sharing similar basic scaffolds, as classified earlier (see previous section). This distribution is detailed in fig. 16, p. 39, as violin plot – a synergy of box and density plots [82] – in which each point indicates the effect size of a single compound and the embracing body refers to the density of results at a certain activity level. At first glance, the plot reveals that both Qui and Pht show effects distributed over the whole range obtained in the library screening, whereas ThQui are highly concentrated around and below $d_{\text{tot}} = 0$ with only a single exception. Obviously, in both Qui and Pht, the substituents rather than the bicyclic core determine the nature and strength of the compounds' activity.
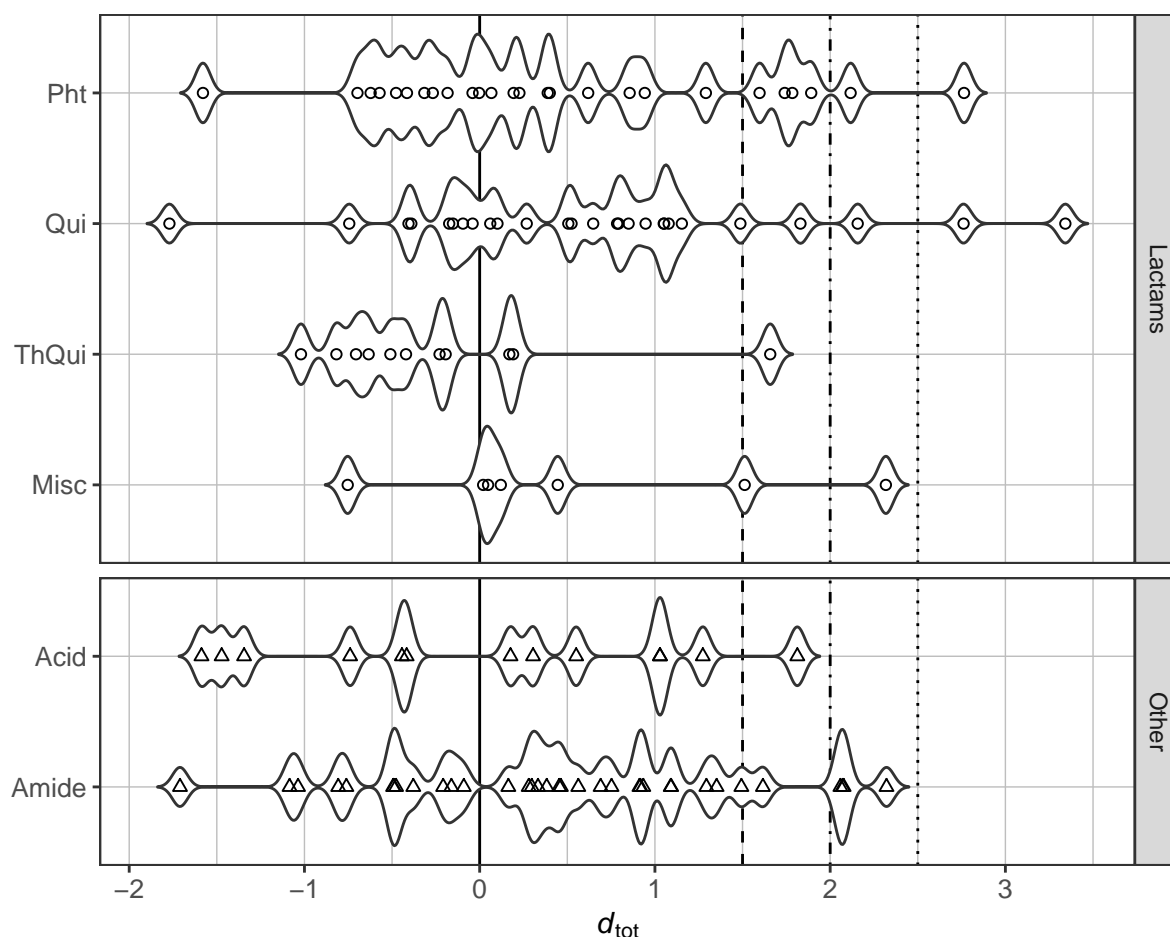
Figure 16: Violin plot of total relative growth effect size distribution by scaffold
Scaled to common width across groups; highlighted horizontal and vertical lines indicate effect size levels (see tbl. 6, dashed – small, dotdash – medium, dotted – large)

Considering the results for ThQui derivatives, one could be tempted to judge the saturated lactam core as disqualifying for an improvement in plant stress tolerance. In fact, also the substituents in this class show much less variation than in the classes of Qui and Pht. The single ThQui compound with a small effect is **C071**, its structure is shown in fig. 17. Besides the lactam core, all eleven derivatives share the acylated nitrogen substitution in 2-position – structural differences occur only regarding the substitution of the phenyl ring with the *o*-Cl-substitution in **C071** possibly being favorable for the compounds' activity. However, the corresponding *m*-Cl-, *p*-Cl- and *o,p*-di-Cl-derivatives (**C073**, **C056**, **C069**), as well as the *o,o*-di-F- and *o*-Me-substituted ones (**C072**, **C070**) are found to be inactive. Among the
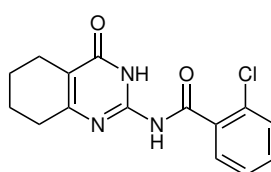
Figure 17: Compound C071

remaining five compounds, carrying different Me- and OMe-substituents, not a single one with a positive effect could be found either. This naturally raises the question if the effect found for **C071** truly is an effect – which leaves two possible explanations:

1. The effect is real and is determined by the compounds' highly specialized structure. In this case – as already suggested by the ineffectivity of the other class members – small structural changes would result in complete loss of activity and there is little to no design space for an improvement of the structure.
2. The effect is not real but rather an artifact, though a remarkably big one. This case can only be excluded by replication of the experiment and confirmation of the found effect.

To decide if the effect is real, replication measurements were carried out. The results of this experiment are detailed in section 2.2.5, p. 42, where the discussion will be continued.

Quinazolinones include both the highest (**C046**) and lowest (**C119**) ranking compounds with the majority concentrating around $d_{tot} = 0$, as well as in the range of $0.3 \leq d_{tot} \leq 1.2$. Single compounds enter the range of small, medium and large effects. Seemingly, the influence of substituents is especially high in this compound class, which makes it necessary to analyze their constitution in greater detail. In the top panel of fig. 18, p. 41, the Qui activity distribution is shown again as starting point for the step-wise refinement of substituent structures. Three different elements occur as adjacent atoms in the 2-position of the Qui core: sp^3-carbon (methylene and methine groups), nitrogen (secondary and tertiary amine groups) and sulfur (alkyl sulfides). Grouping the activity according to these atom types generates the plot in the middle panel, showing that both carbon- (lilac) and sulfur-based substituents (orange) fail to reach remarkable effect sizes, while nitrogen-based substituents (green) show a distribution of step-wise increasing activity in the range of $0.4 \leq d_{tot} \leq 3.4$. If these seven observations are further labeled according to the type of substitution at the nitrogen (lower panel), a clear separation between N-alkyl (lilac) and N-aryl (pink) groups is found. Of the three structures incorporating an aliphatic amine in 2-position (shown in fig. 19, p. 41), only **C043** comes near to a promising effect size, while all four aniline-substituted Qui derivatives (shown in fig. 20) have at least small, two of them even large positive effects onto the growth of *L. minor*. This clear superiority of compounds carrying aromatic amines gives a first hint at distinct structural features, that lead to an increased drought stress tolerance *in vivo*. To gain more certainty in this effect, these four compounds were also included in the replication experiments described in the following section.
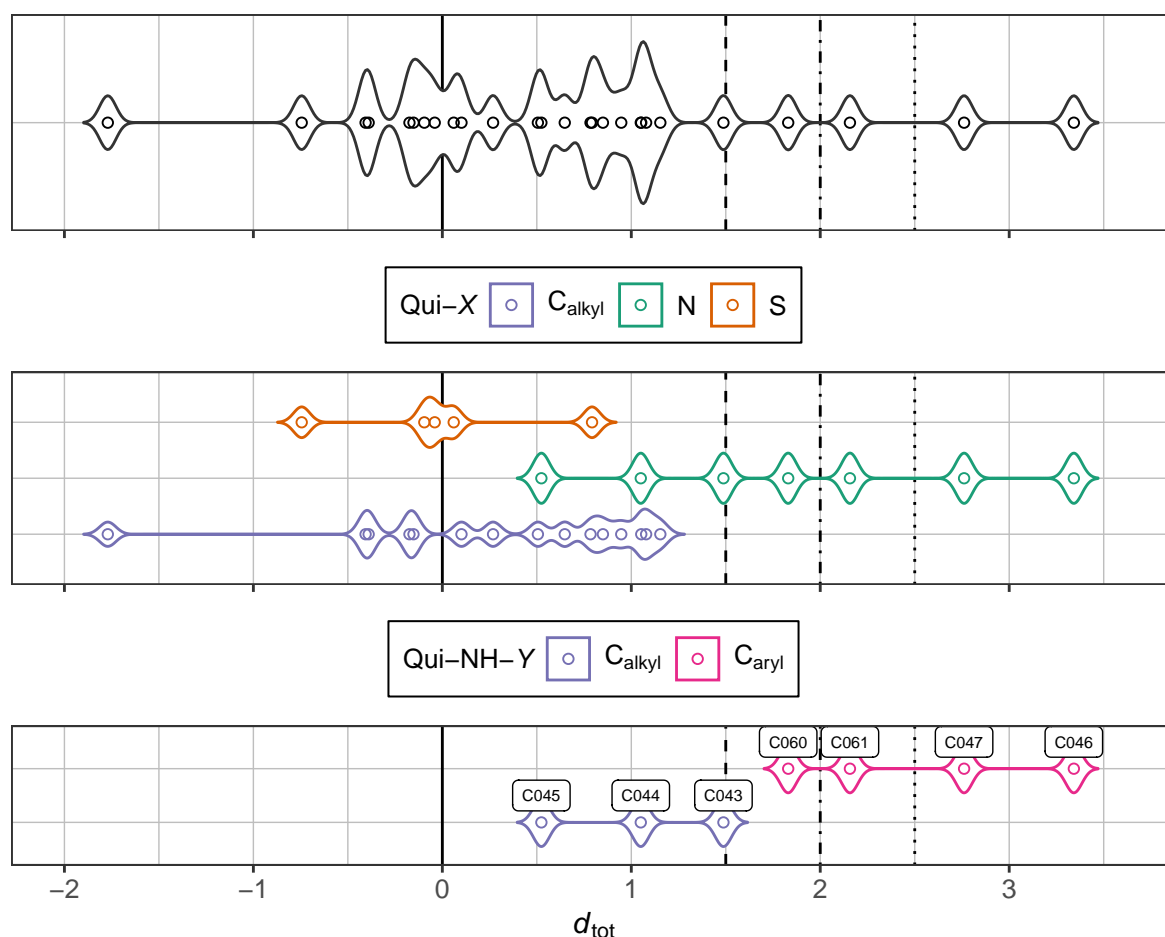
Figure 18: Violin plot of Qui activity profile (total relative growth effect size)
Complete set (upper plot), grouped by substituent in 2-position (middle plot) and grouped by type of following atom in the substituent chain (lower plot); highlighted horizontal and vertical lines indicate effect size levels (see tbl. 6, dashed – small, dotdash – medium, dotted – large)

In the class of Pht, the structural diversity of substituents is comparable to the class of Qui. However, many combinations of elements with aliphatic or aromatic groups are only realized in one to three compounds, which makes a stepwise refinement of substituent constitution less descriptive. However, a first glance at the six top-ranked compounds with at least small effects already yields a clear picture of the activity-defining structural features for this class (see fig. 21): Four out of these six compounds show a high structural similarity – not only among themselves, but also to the members of the Qui group with highest activities. This similarity can hardly be neglected and is especially high in the group **C046 – C061 – C032 – C050**. Considering the additional methylene group and the freely rotatable bonds between
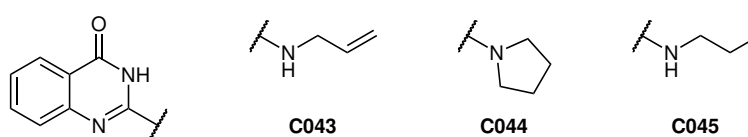
Figure 19: 2-(Alkylamino)-quinazolin-4(3*H***)-ones** included in the compound library
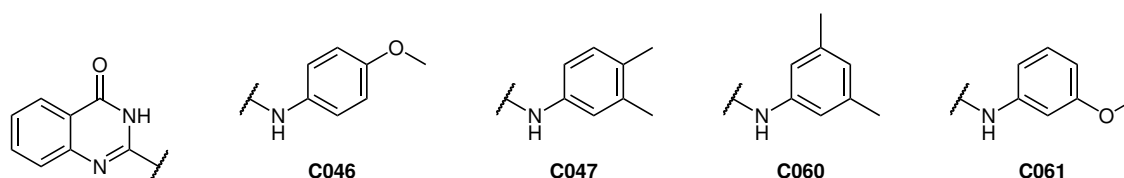
Figure 20: 2-(Arylamino)-quinazolin-4(3*H*)-ones included in the compound library

core and substituent, it is easily imaginable that the Pht structures can pose their substituents in analogous manner to the Qui structures, possibly enabling comparable coordination in the active site of a common target enzyme. The small effect exhibited by **C095** (4-(phenylmethyl)-Pht) could be seen as additional confirmation for the necessity of a flexible aromatic system being part of the substituent. However, not all derivatives incorporating these flexible aniline-derived substituents are active – single compounds even seem to have slightly adverse effects onto the growth of *L. minor*, especially those with electron-withdrawing substituents like p-NO$_2$ (**C049**), p-OCF$_3$ (**C109**) or heteroaromatic systems (**C077**).

Apart from the lactam classes, 8 more compounds exhibited small or medium effects. Their small number and structural diversity prevents making statements about any relation between structure and activity. To clarify if the observed effects are real, five of these compounds were part of the replication experiments and are discussed there.

2.2.5 Confirmation of screening results

Definition of effect size levels

The combination of replicate measurements for single compounds in a meta-analytical model as described in section 2.2.2 aims at increasing certainty about obtained effect sizes. The weight for a single experiment in calculating the mean effect size $\overline{d}$ decreases with increasing effect size to correct for extreme high results, likely to be caused by sampling error. Thus, initially observed large effects tend to be reduced to a lower level. At the same time, the
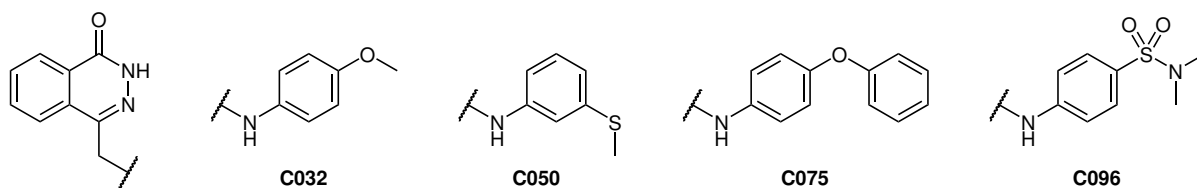
Figure 21: Top-ranked 4-((arylamino)methyl)-phthalazin-1(2*H*)-ones in terms of *in vivo* plant growth acceleration
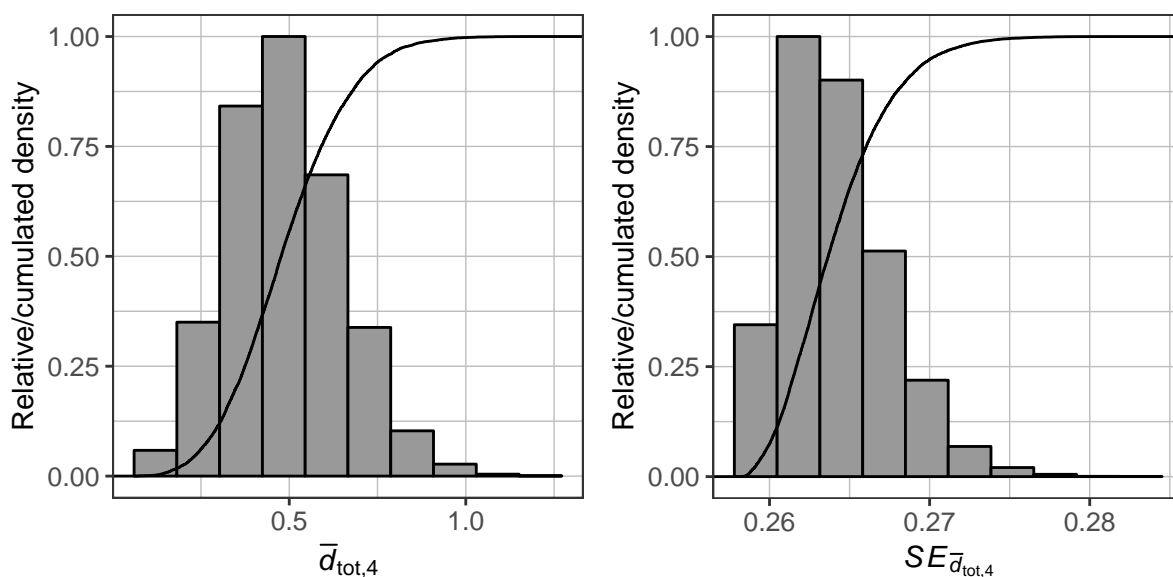
Figure 22: Distribution of bootstrap sampled mean effect size and its standard error
Histogram and cumulative distribution function (CDF); each observation calculated from four randomly sampled by-chance effect sizes of the control experiment (see fig. 10) according to eqns. 2.9 – 2.10; left: mean effect size $\overline{d}_{tot,4}$, right: standard error $SE_{\overline{d}_{tot,4}}$

increased certainty is reflected in a smaller standard error ($SE_{\overline{d}}$) and narrowing confidence intervals.

For the single determinations in the initial screening, resonable limits for the ranking of small, medium and large effects could be assigned by quantifying the inherent variability of the assay system and finding the "worst-case" effect size, that is likely not due to an effective treatment. This type I error-optimized effect size was taken as lower limit for a small effect – medium and large effects were assigned in steps of $0.5 \cdot SD_{P}$. In the light of increased certainty and the tendency for reduction of the effect size level through applying the fixed-effect model, these limits will no longer allow to assign reasonable levels of effects for repeated measurements. Therefore, new limits for four-fold replications were determined by the following procedure: For the twelve plates (with samples $S_{1...12}$) used in the initial control experiment, shown in fig. 10, all pair-wise effect sizes d_{tot} between groups on the same plate were calculated ($G_{6,1}$ against $G_{6,2}$, $G_{6,1}$ against $G_{6,3}$ and so on). With four groups on each plate this results in six effect sizes per plate or 72 effect sizes in total for all twelve plates. These build a pool of effect sizes that could be observed just by chance, without any chemical treatment. Particularly interesting is the question how large a calculated mean effect size $\overline{d}_{tot}$ is likely to be, if determined out of these by-chance effects.

For each compound considered in the replication experiment, three measurements were carried out in addition to the first screening, resulting in a total of four experiments. To obtain

comparable results, the number of replicate measurements in compound screening and limit determination should be equal. Hence, critical effect size limits were determined on the basis of four by-chance effects out of the pool of 72 from the control experiment. Since a single calculation does not give a reliable statement about what is to be expected, a simulation with $n = 10000$ repetitions was carried out. In each repetition, four out of the 72 by-chance effect sizes were randomly sampled with replacement (so-called bootstrap sampling [83]). Out of these, the mean effect size $\overline{d}_{\text{tot},4}$ and its standard error $SE_{\overline{d}_{\text{tot},4}}$ were calculated, which, summed up over all repetitions, characterize the space of by-chance effects that need to be considered when judging meta screening results. Fig. 22 details the distribution of both parameters over the 10000 repetitions. Here again, the choice of suitable limits for effect levels decides about the share of type I and II errors in evaluating compound data as discussed in section 2.2.2. The effect size levels for the one-fold screening have been chosen to be type I error-optimized, meaning that the hurdle for a compound to enter in-depth analysis and replication experiments have been set comparably high. This approach was deemed most promising within the scope of this work, where the main goal was a proof of concept and the identification of one or two lead compound classes. Upon other terms – especially when time, workforce and costs are not considered limiting factors – these levels may be defined differently, in order to increase the number of promising candidates. However, at this point, with using the 95 % quantile of the $\overline{d}_{\text{tot},4}$ distribution ($\overline{d}_{\text{tot},4} = 0.8$) as critical limit, a slightly more moderate treshold is applied for the evaluation of compound meta results. As increment between small, medium and large effects the width of the confidence interval of the mean, using the 95 % quantile of the standard error ($SE_{\overline{d}_{\text{tot},4}} = 0.3$), is chosen. Consequently, the following levels of effect sizes for $n = 4$ are defined:

▷ no effect: $\overline{d}_{\text{tot},4} < 0.8$

▷ small: $0.8 \leq \overline{d}_{\text{tot},4} < 1.4$

▷ medium: $1.4 \leq \overline{d}_{\text{tot},4} < 2.0$

▷ large: $2.0 \leq \overline{d}_{\text{tot},4}$

Meta screening results of the compound library

Of the 19 active compounds exhibiting small, medium and large effects in the initial screening, 14 were chosen for the replication experiment. In addition, 6 compounds deemed inactive
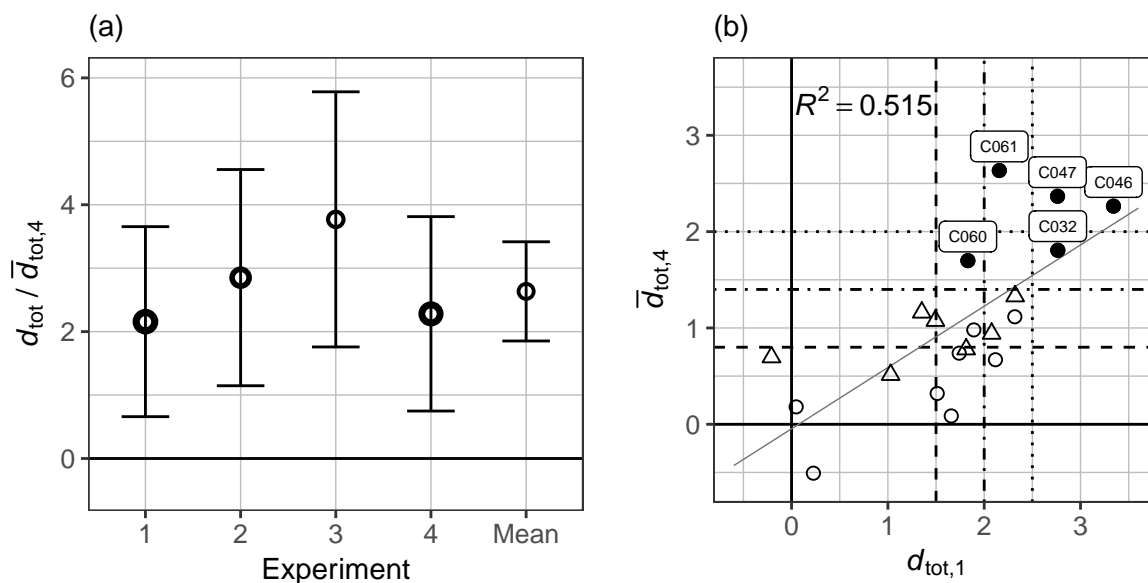
Figure 23: Meta-analysis of screening results
(a) Combination of four individual effect sizes into a mean effect size exemplified for compound **C061**, stroke indicates weight of the individual $d_{tot,i}$ in calculating $\bar{d}_{tot,4}$; (b) Correlation between initial screening and overall effect size based on four replicates, highlighted horizontal and vertical lines indicate effect size levels (dashed – small, dotdash – medium, dotted – large)

were retested as negative control, since the experimental setup should also be able to confirm negative results. For each compound, the mean relative growth effect size $\bar{d}_{tot,4}$ was calculated from four replicate measurements as described in section 2.2.2. Fig. 23a gives an example of merging individual experiments into a mean effect size – the stroke indicates the weight with which each individual result contributed to $\bar{d}_{tot,4}$. It is easily recognizable, how much less weight is assigned to higher effect sizes through the inverse-variance-methodology, accounting for possible high sampling error in individual experiments. The gain in certainty is represented by the confidence interval width of the mean effect size, which is reduced by about 50 % compared to the individual effects.

Before the activity of the individual compounds is discussed, the central question is whether the model system is able to deliver reproducible results. To address this question, the correlation between the results of the initial screening $d_{tot,1}$ and the mean effect size $\bar{d}_{tot,4}$ was investigated. In an optimal setup, a perfect correlation between both quantities could be expected, since each replicate should confirm the initially observed effect and the mean of all replicates would therefore take a value identical to the individual $d_{tot,1}$. However, keeping the uncertainty of the observed effect sizes in mind – expressed in terms of their comparably wide confidence intervals (see section 2.2.3) – variability among replicate measurements is to be expected. Fig. 23b shows the individual effect sizes of the initial screening plotted against the corresponding mean effect sizes for the 20 compounds chosen. The coefficient of
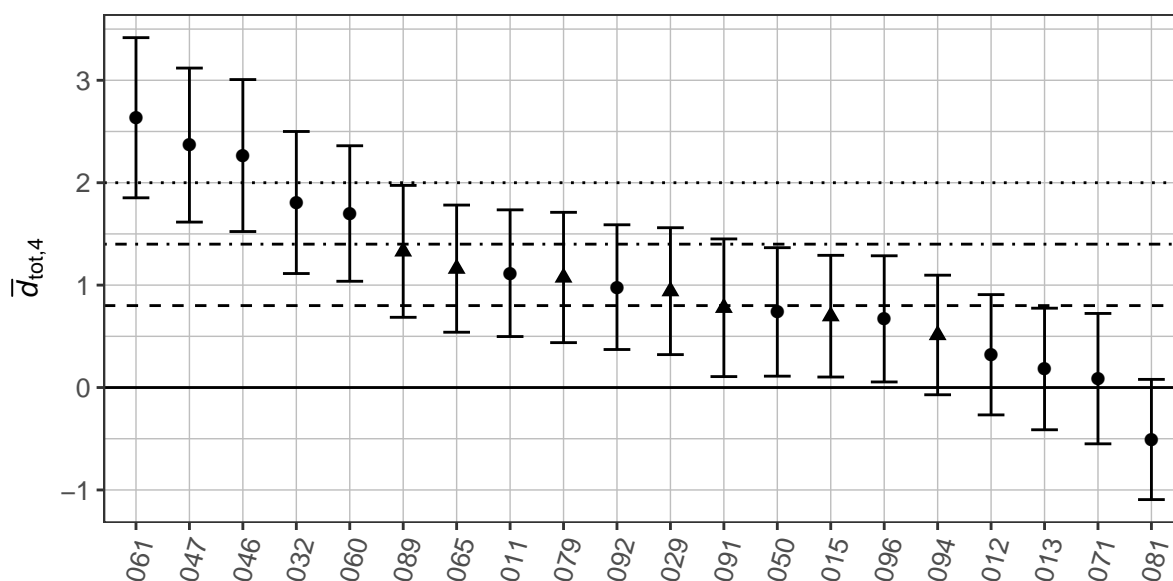
Figure 24: Results of meta-analysis of four-fold measurement
Mean total relative growth effect size $\bar{d}_{\text{tot},4} \pm CI_{\bar{d}_{\text{tot},4},0.95}$ for 20 compounds; highlighted vertical lines indicate effect size levels (dashed – small, dotdash – medium, dotted – large)

determination ($R^2 = 0.515$) indicates a moderate correlation between the two parameters as expected. Compounds above the regression line ranked higher in overall activity than could be expected from the first experiment, while compounds below the line seemed to be overestimated in the initial screening. Summarizing, both actives as well as inactives shifted to higher or lower overall activities, while the basic trend in activity distribution was confirmed. Fig. 24 details the mean effect sizes for all 20 compounds tested. Once more, a distribution over all levels of activity from slightly adverse to distinctly positive effects onto the growth of *L. minor* is observed. Interestingly, the five highest ranking compounds in mean effect size (labeled in fig. 23b) are exclusively Qui and Pht, bearing aniline-based substituents – this fact can be seen as first confirmation of the structural motif, which was identified as mandatory for growth acceleration based on the library screening (see section 2.2.4). In terms of mean effect sizes, two of the five compounds were confirmed to have a large effect (**C046** and **C047**), two of them showed even bigger effects than in the first screening (**C061** and **C060**). Pht **C032** (see fig. 21) descended from a large to a medium effect – still ranking high among the structurally related Qui compounds – while the highly related **C050** and **C096** failed to exhibit even small mean effects, despite the first promising measurements. The single ThQui compound **C071** that was found to be among the first actives was shown to have no effect at all ($\bar{d}_{\text{tot},4} = 0.087$) – it can therefore be concluded that the first result has to be regarded an artifact, which the experimental setup was able to identify eventually. By this, the class of ThQui as a whole is rendered inactive in the *in vivo* system.

The following conclusions can be drawn from the data shown:

▷ A moderate correlation exists between single experiments and mean effect sizes merged from replicate measurements.

▷ The experimental system can lead to false positives (or negatives), if conclusions are drawn solely from single measurements.

▷ Merging replicate measurements in a meta-analytical fashion increases certainty about observed effects, helps sorting out artifacts and separates true actives from inactive compounds.

2.3 Conclusions and perspective

Starting from the original *in vivo* assay system described by Geissler, a more robust experimental setup was developed, which allows for the investigation of drought stress tolerance-inducing effects in stress and recovery phase. It was shown that the model plant *L. minor* experiences water stress, despite its natural habitat being water. If equipped with a suitable effect size measure, the assay is able to identify compounds that exhibit both positive and negative effects, while still keeping balance between the number of actives and inactives, thus reducing the share of both false positives and false negatives. In general, this type of assay system can easily be modified and even upscaled to allow application in different eco-toxicological or plant physiological studies, e. g. heavy metal toxicity or nutrient deficiency. By adjusting the composition of the nutrient media, different types of abiological stressors can be imposed onto the plants, while still keeping the benefit of a quick, easy and highly automated evaluation of plant growth.

In a first broad screening comprising 119 virtually preselected compounds from different classes of cyclic and acyclic amides, as well as carboxylic acids, 19 active structures emerged with small to large effects onto the plants' growth under water stress, giving first hints at beneficial structural motifs. Especially the class of 2-(arylamino)-quinazolin-4(3*H*)-ones stood out among the actives. 20 compounds were selected for further investigation – measurements were replicated and combined in a meta-analytical fashion to provide a more reliable mean effect size. Actives as well as inactives could be confirmed in their individual activity, single compounds were shown to be intially overestimated. In summary, replicate

experiments helped separating truly active from inactive compounds. Since the bioassay is cost-effective and results are obtained within days, the number of screenable compounds is virtually unlimited. In combination with the possibility of employing different stressors, a vast range of applications is imaginable.

The achieved identification of a lead structural motif can be seen as promising starting point for further investigations: structural refinement aiming at more striking effects, transfer of the observed effects to other, more specialized assay systems using agriculturally important model plants (e. g. barley or wheat), and affinity-based protein profiling aiming at the identification of one or more target enzymes. As soon as promising target candidates evolve, the found effects can further be confirmed in more biomolecular assay systems employing the isolated targets. The comparison of the identified pharmacophore to the traditional PARP motif (described in section 2.1.2) reveals an agreement in certain features:

▷ The essential binding-motif of a fixed s-*cis*-amide is the main structural feature mandatory for activity in both pharmacophores. Among the 20 structures investigated in depth, 11 showed small, medium or large effects – only two of them comprised open-chained secondary amide structures, that do not guarantee the availability of a hydrogen atom in *cis*-position to the carbonyl group – but could still pose accordingly.

▷ A bicyclic aromatic core is beneficial for the activity in both pharmacophores. The screened class of ThQui – incorporating a saturated A-ring – showed low chemical diversity, yet all derivatives proved to be inactive.

▷ Substituents to the core lactam system are able to control potency and physicochemical properties in PARP inhibitors. Similar effects could be attributed to substituents in the most active compounds found in the *in vivo* system – however, their chemical space seems to be much more confined. Only aniline-based substituents are found to be beneficial, while aliphatic amines, sulfur- and carbon-based substituents are diminishing the observed effect strongly.

Within this work the focus lies on structural modifications that (a) maximize *in vivo* activity, (b) provide deeper insight into possible modes of action and (c) allow attachment of active structures to reporter molecules or solid phases. Such conjugated derivatives could prove helpful in sub-celullar localization studies and enrichment of possible targets like proteins. The results concerning these goals are detailed in the following chapter.

3 Synthesis of Novel Quinazolinones as Drought Stress Tolerance Inducers

This chapter   is based on experimental work carried out by R. BERGER.

Abstract   Based on insights gained from the screening of a comprehensive compound library, a lead pharmacophore connected to growth enhancement in *L. minor* was formulated. Targeting this pharmacophore, the synthesis of new, previously undescribed 2-arylaminoquinazolin-4(3*H*)-ones was probed using two different approaches. One of the approaches led to the development of a synthetic sequence that is flexible enough to offer a wide range of obtainable diversity in the target compounds. At the same time, it comprises only three synthetic steps starting from anthranilic acid esters, operates on affordable bulk chemicals and was shown to be upscalable on laboratory level, which promises suitability for an industrial-scale application. In total, the synthesis yielded 23 compounds exhibiting 3-point structural diversity: 15 compounds comprise varying aniline-based substituents in 2-position of the quinazolin-4(3*H*)-one core, ranging from electron-rich to electron-deficient structures with differing sterical demand. Four additional compounds bearing different *N*-methylation motifs were derived from the basic 2-(phenylamino)-quinazolin-4(3*H*)-one as model compounds to study the influence of NH-donor ability onto the biological activity. Ultimately, four compounds with nitro- and amino-substituents attached to the quinazolinone core were obtained, which may serve as promising starting points for affinity-based protein profiling investigations.

3.1 Introduction

An extensive screening for drought stress tolerance-inducing effects in a library of small molecules using an *in vivo L. minor*-based bioassay yielded a romising lead pharmacophore. Highest activity could be found amongst compounds of two chemical classes: Quinazolin-4(3*H*)-ones (Qui) and phthalazin-1(2*H*)-ones (Pht), bearing a monosubstitution in 2- or 4-position, respectively. The five compounds with the most promising effects in the *in vivo* system are shown in fig. 25, p. 51. The high structural similarity instantly becomes evident as all four Qui (top row) are substituted with electron-donating aniline derivatives composing two pairs of constitutional isomers (**C046** – **C061** and **C047** – **C060**). The single Pht **C032** comprises *p*-anisidine (4-methoxyaniline) as substituent – alike compound **C046** – attached to the core lactam via an additional methylene bridge. In terms of their individual three-dimensional structure – which is the determining factor for e. g. effective binding to an enzyme – it is easily imaginable that compound **C032** is able to pose its substituent similar to **C046** due to higher flexibility allowed for by the spacer. In conclusion, *in vivo* activity is found within a very confined chemical space of similar physico-chemical properties and structural features crucial for interaction with their still unknown target.

Alas, availability of related derivatives of these two compound classes was utterly limited at the time of the investigation. To gain deeper insight into the mode of action, to further improve *in vivo* activity and to clarify if the observed effects can be explained by interaction with PARP enzymes (see chapter 2), new derivatives had to be synthesized aiming to address the importance of the following structural features:

▷ **Nature of the primary substituent:** The four different aniline derivatives most promising to induce significant drought stress tolerance are highly structurally related: They are of comparable size and π-electron density – attributes which mainly govern the compounds' ability, e. g. to take up space inside an enzymatic cavity and effectively bind via $\pi-\pi$-interactions. New compounds were laid out to incorporate other aniline derivatives varying in number, type, position and size of substitutions on the phenyl ring.

▷ **H-bond-donor ability:** As discussed in relation to the PARP pharmacophore, the fixed s-*cis*-amide realized by the lactam core in known inhibitors is crucial for an effective binding to the enzyme via an H-bond to a neighbouring glycine residue (see fig. 3, p. 9).
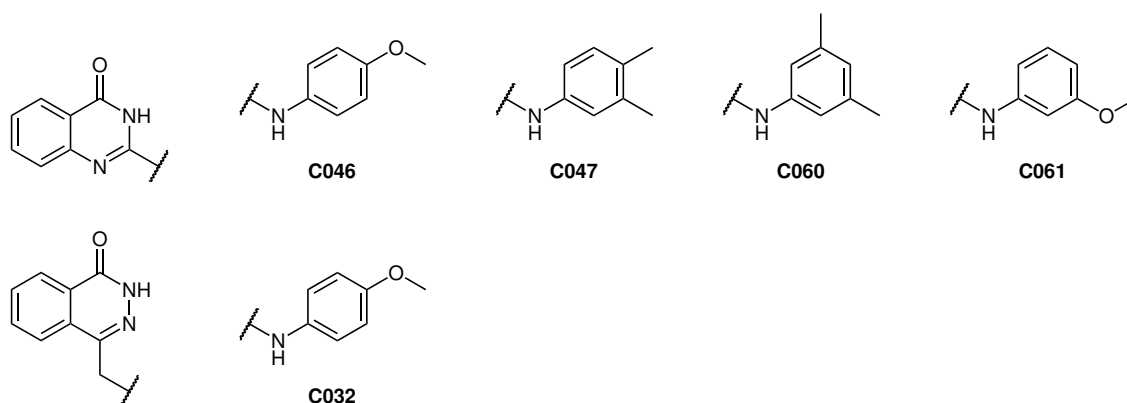
Figure 25: Highest ranking active compounds found in *in vivo* library screening

If PARP interaction is the basis for the compounds' effect on water stress tolerance, additional *N*-substitution (e. g. through methylation) should yield inactive derivatives. In addition to the lactam group, the importance of the exocyclic NH-group is to be investigated which, in theory, could play a role in target binding as well.

▷ **Constitution of the bicyclic core:** The possibility and benefit of substitutions at the core system need to be investigated in order to (a) control activity and (b) open options for structural modification, which may enable e. g. solid-phase binding of actives for the enrichment of possible targets (affinity-based protein profiling).

In the light of the superior activity of Qui over the single Pht – and under the assumption of a common mode of action – it was decided to focus on the synthesis of new quinazolinone derivatives, for which various synthetic procedures have been published. A selection thereof is presented in the following section.

3.1.1 Synthesis and applications of quinazolinones

Quinazolin-4(3*H*)-ones constitute a diverse class of naturally occuring and synthetically accessible compounds, which share the general hetero-bicyclic structure shown in fig. 26. Different synthetic routes have been developed to maximize control over the three main
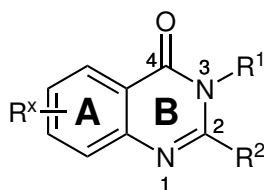
Figure 26: General structure of quinazolin-4(3*H*)-ones with 3-point diversity
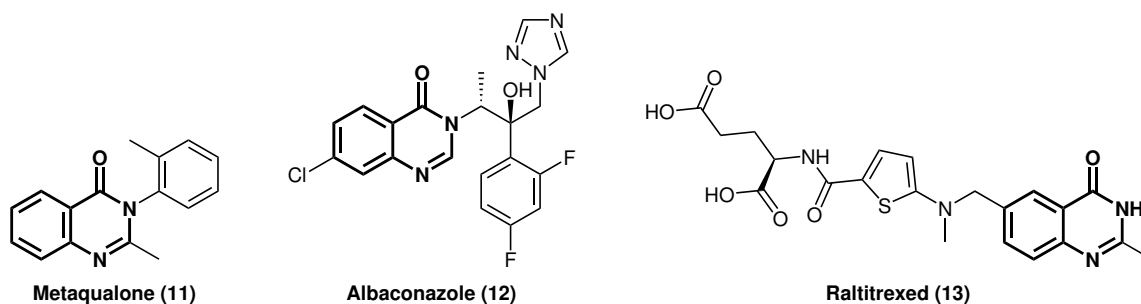
Figure 27: Examples of quinazolinones exhibiting biological activity

points of diversity indicated by R^1, R^2 and R^x. Both pharmaceutically used and naturally occuring quinazolinones make use of this range of diversity, resulting in a vast amount of possible structures (see fig. 27) that can be found to exhibit sedative (e.g. metaqualone **11**), antimicrobial, antiinflammatory, antifungal (e.g. albaconazole **12**) and anticancer (raltitrexed **13**) activity – for an extensive review of pharmaceutically active derivatives see HAMEED [84].

The synthesis of the most simple derivative, quinazolin-4(3*H*)-one ($R^1 = R^2 = R^x = H$), by condensation of anthranilic acid (2-aminobenzoic acid) with formamide (pathway A in fig. 28) was published in 1895 and is known as NIEMENTOWSKI reaction [85]. The reaction most likely proceeds via two condensation steps forming an *o*-amidine intermediate in the first step, followed by a nucleophilic attack of the amide nitrogen on the carboxyl group [86]. Substitution in 2- and 3-position, and at the A-ring can easily be controlled by the choice of educts. Major drawbacks of the reaction, such as reaction temperatures often exceeding 130 °C, considerably long reaction times and moderate yields can be mitigated by employing microwave irradiation, which nowadays is a well established heating technique [86, 87]. Thereby, the NIEMENTOWSKI reaction renders a wide variety of multiply substituted quinazolin-4(3*H*)-ones accessible – however, substitution in 2-position is limited to alkyl and aryl groups.

The incorporation of amines as substituents in 2-position is more challenging: In analogy to the NIEMENTOWSKI reaction, one could assume the reaction between anthranilic acid
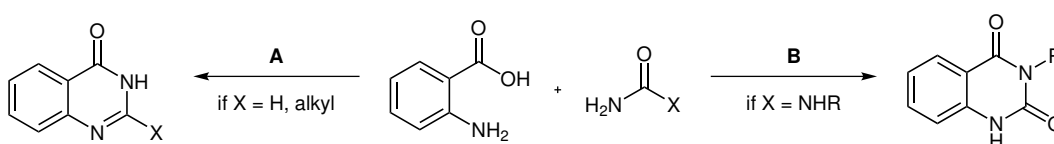
Figure 28: **Expected synthesis products** based on the choice of educts
A: NIEMENTOWSKI reaction with formamide or alkyl amides; B: Reaction with substituted ureas

and a substituted urea might yield the desired product. In fact, this reaction rather leads to quinazolin-2,4-diones carrying the substitution in 3-position (pathway B, fig. 28) [87]. Upon examination of the general structure of 2-aminoquinazolin-4(3*H*)-ones, it becomes apparent that the crucial step of the synthesis lies in the formation of a guanidine-like structure, formed between the two endocyclic and the exocyclic nitrogen atoms. For this reason, many synthetic approaches make use of building blocks and reaction principles known from the synthesis of guanidine compounds. In general, all synthetic pathways presented herein depend on the preparation of two C−N-bonds in the first steps, activation and formation of a third C−N-bond in the final step. In a retrosynthetic sense, the product formation can be imagined starting from anthranilic acid and aniline via

▹ introduction of a $^+$C≡N-synthon forming a cyanamide

▹ nucleophilic addition of a second amino group to the cyanamide and

▹ cyclization through nucleophilic attack of the newly formed guanidine onto the carboxyl group.

In theory, the introduction of the $^+$C≡N-synthon can be achieved on either side of the educts, which adds a certain flexibility to synthetic sequences and helps avoiding incompatibilities of reaction conditions and instable or multifunctional reactants (see fig. 29).

Precursors from aromatic amines

Since cyanamides are sufficiently stable, it is the obvious approach to study the reaction between anthranilic acid (and its derivatives) and aryl cyanamides as done by SHIKHALIEV *et al.* (see fig. 30, p. 54) [88]: The authors aimed at a direct addition of methyl anthranilate **14** to *N*-(methoxyphenyl)-cyanamides **15**, but found that the nucleophilicity of the amino group (respectively the electrophilicity of the cyanamide group) did not suffice to observe product formation. Only in presence of equimolar amounts of hydrochloric acid did the reaction proceed as contemplated – this was attributed to an activation of the cyanamide by *in situ* formation of a chloroformamidine intermediate. The newly formed guanidine is then
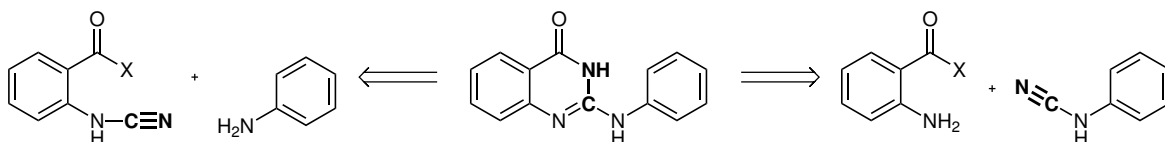
Figure 29: Retrosynthesis of 2-(Arylamino)-quinazolin-4(3*H*)-one via introduction of a CN-synthon
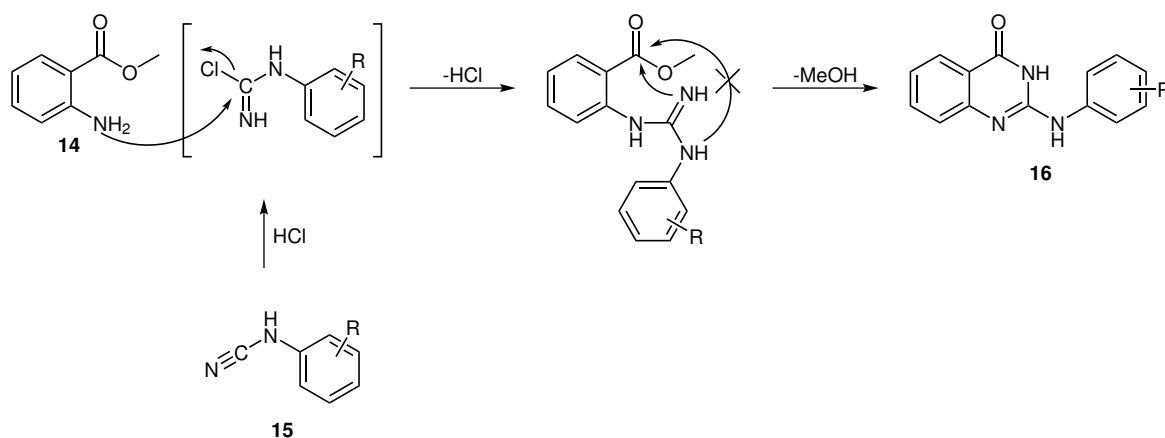
Figure 30: Mechanism of cyclization between anthranilates and aryl cyanamides leading to 2-(arylamino)-quinazolin-4(3*H*)-ones according to Shikhaliev *et al.* [88]

believed to attack the carboxyl moiety with its unsubstituted nitrogen, leading to cyclization and formation of the 2-substituted quinazolinone **16**. Although the authors explicitly state that a cyclization under participation of the substituted amino group, leading to 2-amino-3-substituted quinazolin-4(3*H*)-ones, is imaginable, they exclusively isolated the 2-substituted isomers in 25 % (R = 4-OMe), respectively 21 % (R = 2-OMe) yield. However, when Shishoo *et al.* studied the formation of structurally similar thienopyrimidin-4(3*H*)-ones, they were able to isolate both the desired 2-substituted as well as the 2-amino-3-substituted derivatives in varying ratios of 3:1 to 1:1 [89].

A different approach, studied by Liu *et al.* and Zhang *et al.* involves the preformation of guanidines and their fusion to 2-halobenzoic acids under copper or iron catalysis. Alas, the 2-amino-substituted quinazolinones included in these studies could be prepared in moderate to fair yields only (45 – 59 %) and originated exclusively from un- or *N,N*-disubstituted guanidines and none of them derived from aromatic amines [90, 91].
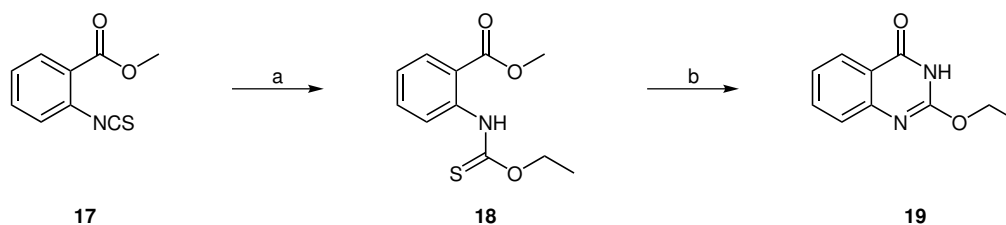
Figure 31: Synthesis of a precursor to 2-aminoquinazolin-4(3*H*)-ones according to Dean *et al.* [92]
a: EtOH, reflux (79 %); b: NH$_3$, EtOH (94 %)
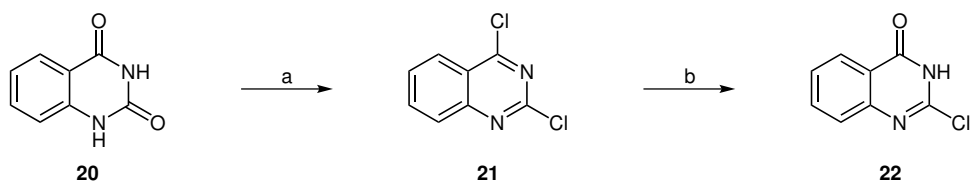
Figure 32: Synthesis of a precursor to 2-aminoquinazolin-4(3*H***)-ones** according to DERUITER *et al.* [93]
a: POCl$_3$, PhNMe$_2$ (87 %); b: NaOH, MeOH, H$_2$O (96 %)

Precursors from anthranilic acids

The syntheses presented above rely on the conversion of the aromatic amine into a suitable reactand. Since the anthranilic acid derivative is required only in the final step, these syntheses offer high flexibility in varying the functionalization pattern of the quinazolinone A-ring. However, if the focus of diversification lies on the substitution in 2-position, such synthetic sequences may prove beneficial, which are based upon the preparation of the bicyclic core bearing a potential leaving group. This leaving group could then be replaced by the respective amine in the final step. Investigating derivatives of methyl 2-isothiocyanatobenzoate **17**, DEAN *et al.* isolated the stable thiocarbamate product **18**, formed upon treatment with ethanol, which could be converted into 2-ethoxyl-quinazolin-4(3*H*)-one **19** using ethanolic ammonia (see fig. 31, p. 54). The authors were able to isolate the product in good yield (74 % over two steps) although a long reaction time was required (4 d in the second step). Substitution of the ethoxyl group by aliphatic amines provided 2-(alkylamino)-quinazolinones in good yields – however, reactivity towards aromatic amines was not investigated. Besides the long reaction time, the poor availability of 2-isothiocyanatobenzoate is a major drawback in utilizing the reaction on a greater scale.

DERUITER *et al.* chose commercially available 2,4-quinazolin-(1*H*, 3*H*)-dione **20** as starting material and used phosphorus oxychloride to convert it into 2,4-dichloroquinazoline **21**, which was selectively hydrolyzed to give 2-chloroquinazolin-4(3*H*)-one **22** (see fig. 32) [93]. In terms of human and environmental safety, phosphorus oxychloride is not the reagent of choice. On the other hand, this synthetic sequence yields a precursor, which can be considered

Figure 33: Synthesis of a precursor to 2-aminoquinazolin-4(3*H***)-ones** according to ERB *et al.* [94]
a: (H$_2$N)$_2$CS, 180 °C (57 %); b: MeI, NaOH (73 %)

superior amongst the ones discussed herein in terms of reactivity towards nucleophiles. The authors present five examples of 2-(arylamino)-quinazolin-4(3*H*)-ones incorporating different types of functionalized anilines, which were obtained in fair to very good yields (57 – 89 %).

The third precursor of interest is 2-(methylthio)-quinazolin-4(3*H*)-one, which was employed in the synthesis of 2-substituted quinazolinones by several groups [94, 95, 96, 97]. ERB *et al.* used harsh reaction conditions to fuse thiourea to isatoic anhydride **23**, yielding 2-thioxo-2,3-dihydroquinazolin-4(1*H*)-one **24**, which could be alkylated regioselectively to give 2-methylthioquinazolin-4(3*H*)-one **25** (see fig. 33, p. 55) [94]. This approach uses readily available and cheap starting materials – nonetheless, milder protocols are known that allow access to the corresponding 2-thioxoquinazolinones **24** even from more sensitive or highly functionalized anthranilic acids [95, 96]. Precursor **25** is supposed to be more stable under storage conditions than its 2-chloro analogue **22**, which may be compared to a carboxylic acid chloride – still, it is expected to exhibit good reactivity towards nucleophiles, since the displacement reaction produces methanethiol as gaseous by-product, which easily evades the reaction and helps shifting the equilibrium to the side of the reaction products.

3.1.2 Requirements for an industrial-scale synthesis

The presented syntheses offer a versatile set of techniques to access new quinazolinone derivatives. Depending on the desired application, one or another approach may promise better results. Since the aim of this work lies in the discovery of new actives, which may eventually enter commercial development for agricultural application, several constraints have to be addressed – especially in contrast to research on pharmaceuticals for human use:

> ▷ **Development and production costs** are the key limiting parameter. Promising substances have to be accessible from precursors that are easily synthesized from basic materials or which are readily available and cost-effective. While development costs for pharmaceuticals can easily enter eight- to nine-digit figures over several years [98], possibly resulting in a single substance being marketed for more than $ 500,000/patient and year [99], agrochemical agents are usually produced in much larger scale for a fraction of that price and achievable profit margin.

▷ **Complexity** and **scalability** of the reaction sequence go hand in hand with production costs. Generally, the number of synthesis steps and the number of reactands in each step directly influence final product yield and therefore costs. The need for a catalyst, its chemical nature (e. g. simple acids, rare metal-based complexes or even enzymes), application form (homogeneous/heterogeneous catalysis) as well as the ecological criticality of the reaction medium (in terms of waste management) can have severe impact, both on the scalability of the synthesis as well as production costs.

▷ **Selectivity** is one of the most important attributes for pharmaceuticals – the perfect drug substance targets e. g. a single enzyme in humans or a pathogenic microorganism without causing any side effects. This aim is increasingly accomplished by developing highly sophisticated and complex structures like peptides or proteins, which demand much higher production costs at the benefit of low effective doses. In agrochemical applications, agents may be preferred that could target homologous enzymes in a number of weeds (herbicides) or pests (insecticides, acaricides, molluscicides) – these are usually less structurally complex, less selective and need therefore be administered in higher doses to compensate for their low selectivity. Likewise, a broad spectrum of treatable crops is desired in the development of stress tolerance-inducing compounds.

In summary, the developed synthetic route is planned to put emphasis on the following characteristics:

▷ Starting materials are cost-effective and readily available,

▷ the number of synthetic steps and educts in each step is as low as possible (two component-reactions are preferred),

▷ no high cost catalyst is needed and

▷ the reaction should give access to the desired products on a multi-gram scale in the laboratory.

3.2 Results and discussion

The focus of this work lies on the development of compounds with maximized activity in the *in vivo* model, which requires the incorporation of different aniline-based sustituents, first and foremost. To achieve this goal, a synthetic route via an activated quinazolinone

seems most promising to obtain numerous derivatives. However, modifications at the A-ring of the core lactam may open additional possibilities for solid-phase attachment of active compounds. Therefore, a synthetic procedure that allows a facile exchange of the anthranilic acid building block would be preferred. For this reason, two separate synthetic routes have been investigated, one based on the work of SHIKHALIEV *et al.* employing aryl cyanamides **15** [88] and another one based on 2-(methylthio)-quinazolin-4(3*H*)-one **25** as described by different authors [94, 95, 96, 97]. The results are presented in this section, detailed synthetic procedures are described in experimental section 7.4, p. 110.

3.2.1 The cyanamide route

SHIKHALIEV's synthesis requires methyl anthranilate to be fused with aryl cyanamides, which are sufficiently stable to be isolated but are not commercially available. Numerous protocols exist for the conversion of primary and secondary amines into cyanamides – yet, most of them either make use of highly toxic reagents (cyanogen bromide, trichloracetonitrile [100]) or rely on sophisticated catalysis (for extensive review see [101, 102]). One possible route makes use of substituted thioureas, which can be desulfurized to give the corresponding cyanamides or carbodiimides (in case of *N,N'*-disubstituted thioureas) using e. g. silicon-based reagents [103] or metal catalysis [104]. Noteworthy in several ways is the procedure used by NATH *et al.* and ALI *et al.* which achieve clean desulfurization of thioureas using molecular iodine and triethylamine [105, 106]. Carried out in organic solvents, the reaction yields only elemental sulfur and triethylammonium iodide as by-products which readily precipitate, thus simplifying purification of the desired product significantly. The required thioureas are accessible from anilines by direct reaction with alkali metal isothiocyanates and strong acids, e. g. trifluoroacetic acid, although yields are low and reaction conditions are harsh [107]. For this reason, the more effective 2-step synthesis of thioureas developed by RASMUSSEN *et al.* was the preferred choice [108]: A thiocyanate anion is activated in form of benzoylthiocyanate by reaction with benzoyl chloride, followed by addition of an (aromatic) amine to yield a benzoyl-protected thiourea. The benzoyl group is subsequently cleaved off under strong basic conditions yielding the *N*-monosubstituted thiourea.

In their publication SHIKHALIEV *et al.* describe the synthesis of 2-((4-methoxyphenyl)amino)-quinazolin-4(3*H*)-one yielding 25 % of the desired product [88], which is identical to com-

pound **C046** of the screened library (see fig. 25). Because of its considerable activity in the *in vivo* system and readily available spectroscopic data for comparison, it was decided to use it as model compound for establishing a synthetic procedure. The theoretical route to access the compound shown in fig. 34 assembles the most promising synthetic steps of the literature discussed.

Starting from *p*-Anisidine **26**, the benzoyl-protected thiourea was synthesized as described by HAY *et al.* [107] with minor modifications. The product started to precipiate immediately when the reaction mixture was poured on ice and was easily separated by filtration. Since the removal of the benzoyl moiety was to be conducted in aqueous solution, purification and drying of the product were deemed unnecessary. Instead, deprotection was directly carried out by adding the crude product to warm sodium hydroxide solution. Cooling of the solution and pH adjustment in turn forced compound **27** to precipitate, which – after filtration, washing with water and drying – was obtained in sufficient purity and excellent yield (96 % over two steps).

For the conversion of **27** into the corresponding cyanamide, the thiourea was dissolved in ethyl acetate containing triethylamine. The mixture was cooled in an ice bath, giving a clear, almost colorless solution. By dropwise addition of molecular iodine in ethyl acetate, the course of the reaction was easily observable as known from a titration: the first drop of dark violet iodine solution discolored immediately due to quick and complete consumption. To the same extent the time required for discoloration of additional iodine grew, more fine off-white powder of elemental sulfur precipitated from the solution. Upon complete turnover of the thiourea, any additional drop of iodine solution lead to a persistent dark purple color,
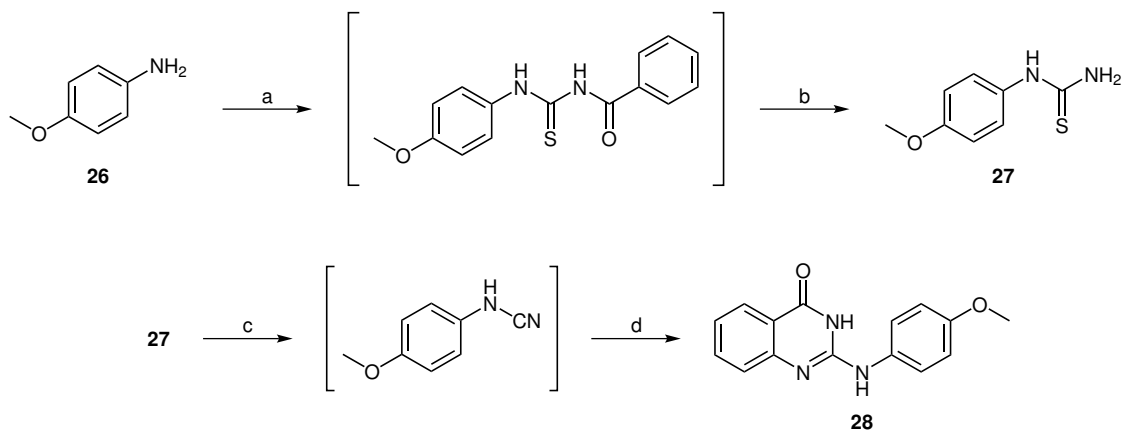
Figure 34: Synthesis of 2-((4-methoxyphenyl)amino)-quinazolin-4(3*H***)-one** via *N*-(4-methoxyphenyl)-cyanamide
a: KSCN, PhCOCl, acetone (not purified); b: 10 % NaOH in H_2O (96 % over 2 steps); c: I_2, NEt_3, EtOAc (not purified); d: HCl, 2-aminobenzonitrile, DMF or dioxane, then H_2O (desired product not obtained)

29
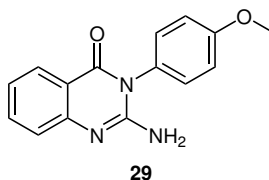
Figure 35: Synthesis product obtained using the procedure of Shikhaliev *et al.* [88]

indicating the end of the reaction. Although aryl cyanamides are described stable enough for isolation, the protocol of Nath *et al.* promised to yield the product in solution with only minor amounts of by-products. For this reason, it was decided to proceed with minimal purification efforts. The solid by-products were filtered off, the crude product was dried *in vacuo* and then added to DMF together with 2-aminobenzonitrile (an analogue to anthranilic acid). Aqueous hydrochloric acid was added to activate the cyanamide (as proposed in [88], also see fig. 30). After heating (85 °C, 90 min), a single major product could be observed by TLC, which was purified into an almost colorless, crystalline solid. Contrary to the expectation, mass and NMR spectra proved the product to be *N*-(4-methoxyphenyl)-urea (yield: 48 %), a logical hydrolysis product of the chloroformamidine intermediate – the reactive form of the cyanamide. Obviously, the amino group of 2-aminobenzonitrile did not show sufficient nucleophilicity to compete with hydrolysis by water present in the reaction mixture.

Therefore, in a second attempt, the crude cyanamide was dissolved in dry dioxane and HCl in dioxane was added to catalyze the reaction. After 6 h of heating, the mixture was diluted with water and stirred for additional 2 h to facilitate hydrolysis of the supposedly present imido moiety (formed from the nitrile group through cyclization) to the required lactam group. After extraction and purification, the major reaction product was obtained as colorless crystalline solid in 62 % yield. HR-MS proved that the product was of the expected elemental composition. However, the NMR spectrum showed a single N–H-signal with an intensity corresponding to two hydrogen atoms, while the infrared spectrum comprised two absorption bands, one from symmetrical and one from asymmetrical stretching of an NH_2-group – thus, the compound could be identified as 2-amino-3-(4-methoxyphenyl)-quinazolin-4(3*H*)-one **29**, the incorrectly cyclized constitutional isomer of the desired product **28**. Since Shikhaliev *et al.* could isolate only 25 % of the correctly cyclized product, the two results may be regarded in accordance.

A shifted product ratio in favor of the 2-substituted quinazolinones may be imaginable with more electron-deficient anilines due to reduced nucleophilicity of the substituted nitrogen in

the cyanamide/guanidine intermediate – however, based on the clear excess of unwanted by-product, this synthesis route was regarded unfit for general and broad access to 2-(arylamino)-quinazolin-4(3*H*)-ones.

3.2.2 Synthesis via an activated quinazolinone core

As discussed earlier, 2-(methylthio)-quinazolin-4(3*H*)-one **25** is a promising precursor for the desired 2-substituted products and practical protocols exist that allow its synthesis from commercially available substances in reasonable yields (see section 3.1.1). Yet, based on the experiences made with the simple and effective preparation of thioureas via benzoylisothiocyanate presented in section 3.2.1, a possible application for the preparation of precursor **25** was desirable. Considering the fusion reaction between isatoic anhydride **23** and thiourea carried out by ERB *et al.*, the question arose if the formation of the thiourea moiety could be accomplished directly, involving the amino group of anthranilic acid rather than forcing it into the molecule from an external source.

In theory, the reaction between an anthranilic acid derivative and benzoylisothiocyanate should yield the corresponding benzoyl-protected thiourea shown in fig. 36. Upon cleavage of the benzoyl group, rapid cyclization under substitution of the leaving group X is supposed to take place. To test this possibility, ethyl anthranilate **30** was brought to reaction with benzoylisothiocyanate as described in section 3.2.1. As expected, a bright yellow-orange solid could easily be precipitated from cooled aqueous solution. ESI-mass and NMR spectra proved the identity of the benzoyl-protected thiourea of methyl anthranilate. When added to pre-heated sodium hydroxide solution, the solid instantly dissolved, indicating conversion. After short reaction time, a fine white precipitate was obtained from the cooled, acidified solution – filtration and recrystallization yielded the expected 2-Thioxo-2,3-dihydroquinazolin-4(1*H*)-one **24** as white needles in excellent yield (94 %).
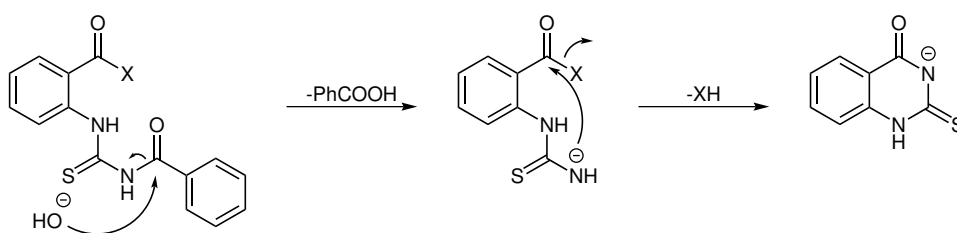
Figure 36: Hypothesized cyclization mechanism leading to the formation of 2-thioxo-2,3-dihydroquinazolin-4(1*H*)-one **24**
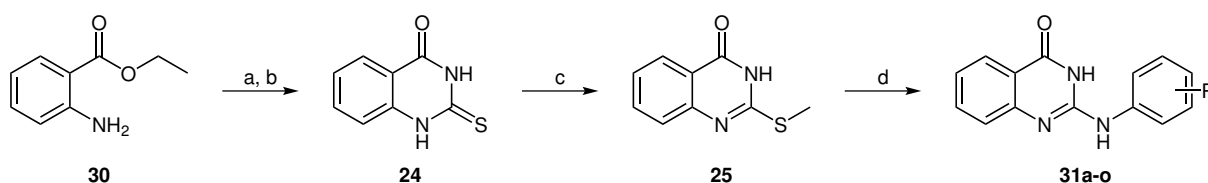
Figure 37: Complete synthesis route to 2-(arylamino)-quinazolin-4(3*H*)-ones
a: KSCN, PhCOCl, acetone; b: 10% NaOH (94%, recrystallized); c: MeI, NaH, DMF (90%, recrystallized); d: aryl amine, AcOH (43 – 94%, recrystallized)

For the methylation of **24**, the protocol used by ERB *et al.* was modified. Instead of using sodium hydroxide as base in aqueous solution, the reaction was carried out in dry DMF with sodium hydride (suspended in mineral oil). Moreover, all three reagents were used in equimolar amounts with dropwise addition of methyl iodide. These modifications served two purposes: Firstly, sodium hydride effectively deprotonated **24** without hydrolyzing methyl iodide due to its non-nucleophilic character. Secondly, gradual addition of equimolar alkylating agent guaranteed regioselective mono-*S*-alkylation without obtaining *N(3)*-alkylated or *N(3),S*-dialkylated products. This way, the precursor **25** could be obtained in excellent yield (90%) and purity after recrystallization.

All authors describing the use of **25** as precursor to 2-aminoquinazolin-4(3*H*)-ones state that the reactions were carried out under neat conditions with excess amine being reagent and solvent at the same time. While this may be practical for liquid amines, the approach did not promise acceptable results with the mainly solid aromatic amines in scope of this work. In order to develop a general method, different high-boiling solvents were considered as reaction medium. In a first attempt to synthesize compound **31b**, precursor **25** was refluxed with a minor excess (1.2 eq.) of *p*-anisidine in a small volume of bis-(2-methoxyethyl)-ether (diglyme) for 6 h, which yielded the desired compound after recrystallization as blue-greyish powder in 69% yield. Considering the reaction mechanism being a nucleophilic substitution, it was thought beneficial to use an even more polar solvent, possibly a protic one to support leaving of the $^-$SCH$_3$-group as methanethiol. On that account, the reaction was carried out in glacial acetic acid: as reflux temperature was reached, a strong rotten odour immediately indicated a reaction. The target compound could be isolated as blueish-white solid in 79% yield. As logical by-product of the reaction, *N*-acetyl-4-methoxyaniline could be observed by ESI-MS, formed through reaction of the amine with acetic acid. To keep this side reaction from lowering the product yield, the amine concentration was raised to 2 eq. (relative to **25**), resulting in an improved yield of 94% after recrystallization.

The general synthetic protocol used to obtain 15 different 2-(arylamino)-quinazolin-4(3*H*)-ones starting from commercially available substances, is summarized in fig. 37. Precursor **25** (5 mmol), together with 1.5 eq. of aryl amine, was refluxed in glacial acetic acid (7.5 ml) while monitoring educt consumption. Where inactivated aryl amines were employed or competing formation of *N*-acetylated aryl amine was observed, another 0.5 eq. aryl amine were added as indicated in tbl. 8. Towards maximal conversion of the starting materials, most products tended to precipitate from the solution – additional acetic acid was added dropwise where necessary to keep the mixtures stirrable. Finally, crude products could effectively be precipitated by dilution of the reaction mixture with water. After recrystallization, the products were obtained in moderate to excellent yields.

Table 8: Synthesized quinazolinones; Reaction conditions: 5 mmol 2-methylthio-4(3*H*)-quinazolinone, amine, glacial acetic acid, reflux, recrystallization

Entry	C*xxx*	Product	Amine [eq.]/ Time [h]	Recryst.	Yield [%]
31a	126		1.5/6	DMF/water	79
31b	121		2.0/5	DMF/water	94
31c	122		2.0/5	DMF/water	88
31d	123		2.0/5	DMF/water	79
31e	128		1.5/5	DMF/water	65
31f	173		2.0/5	DMF/*n*-PrOH	43
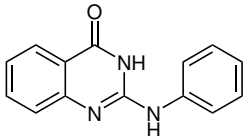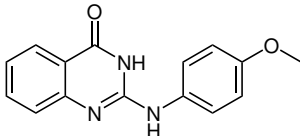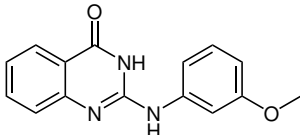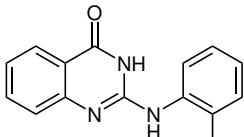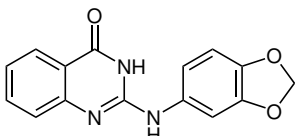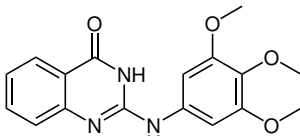
[1] synthesized on 15 mmol scale

[2] synthesized on 30 mmol scale

Table 8: continued

Entry	Cxxx	Product	Amine [eq.]/ Time [h]	Recryst.	Yield [%]
31g	127		1.5/5	DMF/water	81
31h	178		1.5/10 2.0/16	DMF/n-PrOH DMF/water	59[1] 72[2]
31i	179		1.5/10	DMF/n-PrOH	62[1]
31j	125		1.5/3	DMF/water	74
31k	124		1.5/3	DMF/water	71
31l	130		2.0/7	DMF/water	73
31m	129		2.0/18	DMF/water	46
31n	174		2.0/72	DMF/n-PrOH	56
31o	172		1.5/4	DMF/n-PrOH	71
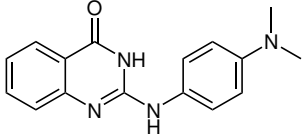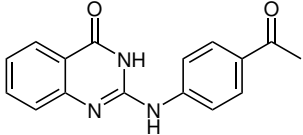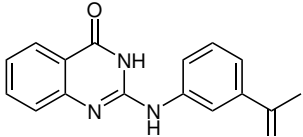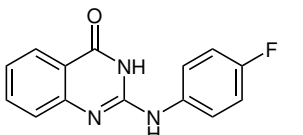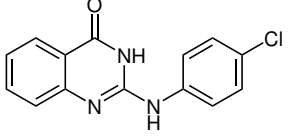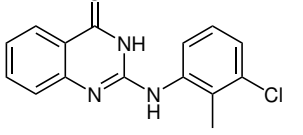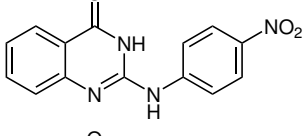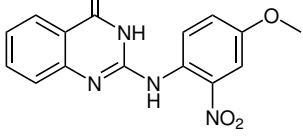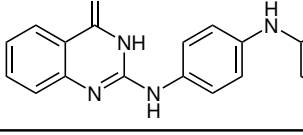
[1] synthesized on 15 mmol scale

[2] synthesized on 30 mmol scale

The yields presented vary considerably among homologous and structurally similar derivatives. While **31b** was isolated in 94 % yield, both shifting of the methoxy group (**31b**, **31d**) as well as additional substitution by similar groups (**31e**, **31f**) seemed unfavourable for the

amount of isolated product. This cannot be explained by the reactivity of the respective anilines, but is rather due to the solubility of the products. Solubility both in polar (water, lower alcohols, acetic acid, acetonitrile) and unpolar (ethers, higher alcohols, dichloromethane) solvents was generally poor for all listed derivatives. Considerable dissolution under ambient conditions could only be achieved in DMSO, while boiling DMF was the only solvent giving satisfying results in recrystallization. Due to this, changes in the crystallization procedure were virtually impossible – however, in almost all cases the products crystallized in excellent purity which was the main interest. Moderate upscaling of the last synthetic step was shown to be unproblematic – 15 mmol- or even 30 mmol-scale preparations proceeded as expected, yielding e. g. more than 6 g of compound **31h** (see tbl. 8).

In summary – keeping the required characteristics discussed in section 3.1.2 in mind – the employed synthetic procedure promises good applicability for an upscaled industrial process:

▷ The required starting materials (anthranilic acid esters, benzoyl chloride, potassium thiocyanate, aryl amines) are cheap and available as bulk chemicals. Additionally, a wide variety of aryl amines is synthetically accessible through industrial scale processes, e. g. from phenols and aryl halides (e. g. Buchwald-Hartwig amination) or from aniline (electrophilic aromatic substitution by halogens, nitration, diazotation etc.).

▷ By-products throughout the synthetic pathway are either environmentally uncritical (e. g. alcohols and benzoic acid) or recyclable by distillation (DMF, acetic acid).

▷ No additional catalyst is required, apart from acetic acid as solvent in the last synthetic step.

▷ Crystallization affords highly pure products without the need for chromatographic purification, which usually is complex, expensive and complicated to upscale.

3.2.3 *N*-methylated derivatives for mechanistic investigations

Besides improvement of the biological activity, a deeper understanding of the mode of action in enhancing stress tolerance of the obtained compounds was seeked. In connection to the PARP pharmacophore presented in section 2.1.2, the relevance of the NH-donor activity of the quinazolinone core was to be investigated. Since the exocyclic NH-group could also be part of the binding motif, evaluation of the H-donor ability in this position promised to
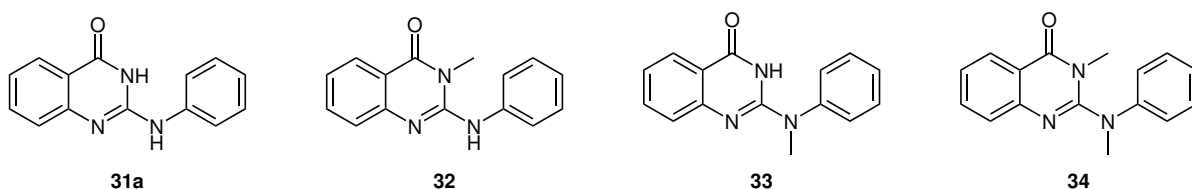
Figure 38: Compounds synthesized for investigating the importance of the H-**bond-donor capacity** bearing 0, 1 or 2 N-methylations

provide additional mechanistic insights. Therefore, in addition to the basic 2-(phenylamino)-quinazolin-4(3*H*)-one **31a**, three more compounds were targeted for synthesis as shown in fig. 38, p. 66, bearing either a single *endo-* (**32**) or *exo-N*-methylation (**33**), or both (**34**).

Compound **33** could be obtained by employing the same procedure used to synthesize the variety of quinazolinones listed in tbl. 8. Reaction between precursor **25** and *N*-methylaniline (2 eq.) yielded compound **33** as expected in very good yield (88 %) and high purity after recrystallization. In order to gain access to compounds **32** and **34**, methylation of **31a** seemed a viable approach. However, regiospecific methylation could hardly be expected due to the structure of the anion of **31a**, which allows the formulation of multiple possible resonance and tautomeric structures – two of them with the negative charge located at either *endo-* or *exo*-nitrogen and one with an oxygen-located charge (see fig. 39). Upon reaction with 1 eq. of alkylating reagent, the formation of five different products is possible – three mono- and two dialkylated – their ratios depending on the relative nucleophilicity of the three positions. Indeed, when **31a** was brought to reaction with equimolar sodium hydride and methyl iodide, a mixture of compounds was obtained (see fig. 40, p. 67). Following chromatographic separation, the two major products could be identified by means of ESI-MS and (2D-)NMR as the desired product 3-methyl-2-(phenylamino)-quinazolin-4(3*H*)-one **32** (47 %) and its *O*-methylated isomer **35** (16 %). A third fraction (16 %) was shown to contain a mixture of the two possible dimethylated products (*exo-N/endo-N, exo-N/O*). In a similar fashion, the reaction between compound **33** and methyl iodide led to a mixture of the two possible dimethylated products **34** and **36** in 55 % and 27 % yield, respectively (see fig. 41, p. 67).
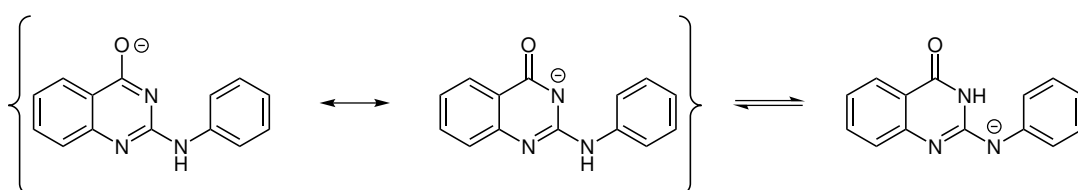
Figure 39: Resonance and tautomeric structures of the anion of compound 31a
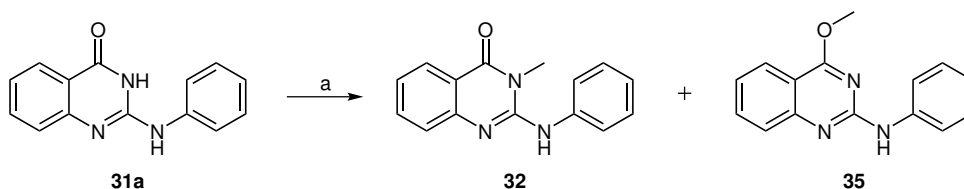
Figure 40: Alkylation reaction of compound 31a leading to mono- and di-methylated products
a: equimolar MeI, NaH (**32**: 46 %, **35**: 16 %)

3.2.4 Core-modified derivatives for solid-phase coupling

The newly synthesized 2-(arylamino)-quinazolin-4(3*H*)-ones presented so far were designed with focus on varying anilines as substituents in 2-position of the quinazolinone core. Assuming that both the *endo*- and *exo*-NH-moieties are indispensable for the biological activity of the given compound class, only few of the newly synthesized derivatives leave viable options for further regiospecific modification, e. g. through reductive amination of the ketones in **31h** and **31i** or reduction of the nitro group in **31m**. However, the presence of modifiable groups in biologically active derivatives can offer manifold options for (a) simple tuning of the physico-chemical properties by attaching hydrophilic or lipophilic substituents in order to increase activity, (b) attachment of different reporter groups like fluorescent dyes that support e. g. subcellular localization or (c) solid-phase attachment of active motifs usable in target enrichment studies. Since even the slightest modification in a single position of the molecule may decrease or increase the biological activity considerably, a set of different, usually isomeric structures need to be investigated to find the most suitable attachment position for a given application. In order to widen the space for chemical modifications beyond the 2-substituent, a set of core-modified compounds was targeted within this work, incorporating functional groups thta offer a broad spectrum of possible chemical transformations, namely amino groups (acylation, alkylation, conversion to isocyanides, etc.) and carboxylic esters (transesterification, amidation, reduction, etc.).

Investigation of the model compound **31a** reveals four different positions on the A-ring of the
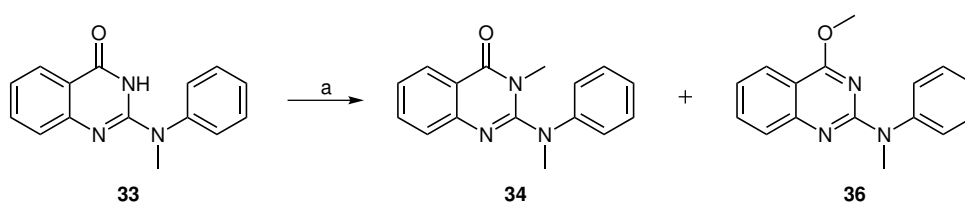
Figure 41: Alkylation reaction of compound 33 leading to di-methylated products
a: MeI, NaH (**34**: 55 %, **36**: 27 %)
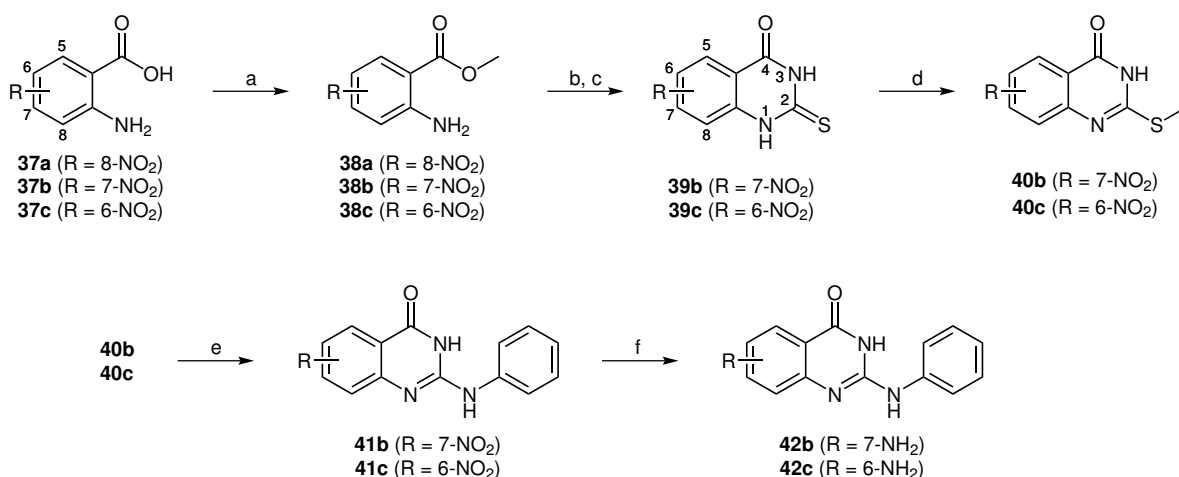
Figure 42: Synthetic route to quinazolinones with core-amino-substitution (for consistency, position numbering of nitroanthranilic acids **37** follows IUPAC rules for the final product here; correct numbering is applied in the experimental section)
a: MeOH, H$_2$SO$_4$, reflux (quantitative); b: KSCN, PhCOCl, acetone; c: 3 % NaOMe in MeOH (**39b**: 98 %; **39c**: 62 % recryst.);
d: MeI, NaH, DMF (**40b**: 38 % recryst.; **40c**: 94 % recryst.); e: PhNH$_2$, AcOH (**41b**: 69 % recryst.; **41c**: 79 % recryst.); f: Fe,
AcOH, EtOH (**42b**: 16 % chrom.; **42c**: 30 % chrom.)

quinazolinone core available for attachment of additional functionalities like nitro groups.
For three of the four possible structures, the corresponding nitroanthranilic acids **37** were
commercially available in amounts suitable for multistep syntheses (see fig. 42, p. 68). Since
aromatic nitro groups are stable to a broad range of chemical transformations, the construc-
tion of nitro-substituted 2-(phenylamino)-quinazolin-4(3*H*)-ones **41** from the respective
nitroanthranilic acids seemed promising. Reduction of the nitro group to an amino function
could then be accomplished in the final step of the synthesis – under conditions most likely
harmless to the quinazolinone motif – yielding the further modifiable amino-substituted
compounds **42**. Due to the unsatisfactory results obtained using the synthetic procedure
via *N*-arylcyanamides (see section 3.2.1), it was decided to prepare the corresponding acti-
vated 2-(methylthio)-quinazolin-4(3*H*)-ones **40** from the respective acids, following a similar
synthetic route as employed in the synthesis of compound **31**.

The three commercially available nitroanthranilic acids **37** were smoothly converted to their
respective methyl esters **38** using a standard protocol for acid-catalyzed esterification in
methanol. All three esters were obtained in quantitative yield though full conversion took 72 –
96 h. In the next step the esters needed to be transformed into the cyclized thioxo-compounds
39 – in analogy to the reactions described in section 3.2.2, the intermediate product may
be formed by nucleophilic addition of the anthranilic ester amino group to benzoylisothio-
cyanate. While the nucleophilicity of the amino group in unsubstituted anthranilic acid is
already low due to the neighbouring carboxyl function, an even lower reactivity towards
the isothiocyanate was expected for the esters **38**, especially **38a** and **38c**, which carry the

desactivating nitro group in *ortho-*, respectively *para*-position to the amine group. Compound **39b** could be obtained after a moderate reaction time of 3 h in excellent yield (98 %) and a purity sufficiently high to make recrystallization obsolete. However, conversion of **38c** yielded only 62 % of product **39c** (after recrystallization) in the same reaction time. For **38a** it was not possible to isolate considerable amounts of product even after 7 h – obviously both desactivation and steric hindrance of the neighbouring nitro and carboxyl groups lowered the reactivity of the amino group to a level unsuitable for this conversion.

S-methylation of **39b** and **39c** was carried out according to the synthetic procedure for **25** with minor modifications. Although full conversion was accomplished for both derivatives, only **40c** was obtained in excellent yield (94 % after recrystallization). Compound **40b** crystallized only partially from DMF/water and gave an unsatisfying yield of 38 %. However, incorporation of aniline as substituent in 2-position could be carried out without problems: after a mildly prolonged reaction time of 18 h both **41b** and **41c** were isolated in fair to good yields comparable to those of the products **31** (69 %and 79 %, respectively, after recrystallization).

For the final step in the synthetic sequence – the reduction of an aromatic nitro into an amino group – a standard protocol utilizing elemental iron to generate hydrogen radicals *in situ* was employed (Beauchamp reaction). Here, instead of hydrochloric acid, a mixture of acetic acid and ethanol was used as reaction medium to improve solubility of the quinazolinones. However, the desired products **42** did not crystallize purely and could only be isolated in poor yields of 16 % and 30 %, respectively, after chromatographic purification.

In summary, 2-(arylamino)-quinazolin-4(3*H*)-ones with regioisomeric amino substitutions at the quinazolinone core are accessible via the five-step synthesis shown. While the procedure is easy to handle, the overall yields of 4 % (**42b**) and 14 % (**42c**) for the two obtained products are not satisfying if required in larger amounts. The yields are definitely improvable by altering the established synthetic route regarding reaction times, reagent loads and purification procedures, which could be done only in a limited fashion within the scope of this work.

3.3 Conclusions and perspective

The scientific literature offers numerous synthetic approaches to the synthesis of quinazolin-4(3*H*)-ones. Depending on the desired application, one or another may promise more flexibility in varying substituents in different positions of the molecule. However, only few of them are suited for the incorporation of amine substituents in 2-position and even fewer make use of inexpensive bulk chemicals which is a central requirement for a robust, upscalable process. Two different routes were experimentally evaluated in regard to their applicability in the synthesis of 2-(arylamino)-quinazolin-4(3*H*)-ones: Firstly, the fusion of anthranilic acid to aryl cyanamides was tested in order to make derivatives with varying substitution patterns at the quinazolinone core easily available. Contrary to the expectation, the major product of this reaction was found to be the incorrectly cyclized 3-aryl isomer of the target compound. In a second approach, an activated quinazolinone core was prepared that could be converted to the targeted 2-(arylamino)-quinazolin-4(3*H*)-ones in a single step, offering higher flexibility in exchanging the 2-substitution. Thereby, an operationally simple conversion of anthranilic acid esters was developed that gives rise to the precursor 2-thioxo-2,3-dihydroquinazolin-4(1*H*)-one in excellent yield and purity which – to current knowledge – has not been described in the literature. In total, the synthesis starting from anthranilic acid esters and aryl amines comprises three steps and made 15 compounds in overall yields of 36 – 80 % available. While all final compounds crystallized in excellent purity, in some cases yields were considerably diminished by this procedure due to incomplete precipitation. Optimization of the purification may improve individual yields in the final step remarkably.

Using a simple and effective alkylation procedure, 2-(phenylamino)-quinazolin-4(3*H*)-one could be converted into three additional derivatives bearing *endo-* and/or *exo-N*-methylations. Through blockage of the central lactam binding motif, the *endo-N*-methylated compound promises further insights into the relevance of PARP enzyme inhibition regarding the observed *in vivo* activity. Follow-up investigations will also focus on a possible involvement of the *endo*-NH-group in target coordination for the first time.

Although the developed synthetic sequence primarily allows flexible exchange of the 2-substitution, core-modified quinazolinones have also been shown to be accessible starting from different anthranilic acid derivatives. As proof of concept, the synthesis of two re-

gioisomeric core-amino-functionalized quinazolinones was demonstrated in five steps from nitroanthranilic acids. Here again, overall yields were poor but are most likely improvable through optimization of reaction and purification conditions. If found active in the *in vivo* assay, these amino-functionalized agents can be subjected to manifold modifications aiming at target localization and enrichment. However, the main focus of this work lies in the evaluation of the *in vivo* activity of the newly synthesized compounds in regard to drought stress tolerance-induction. The respective results are presented in the next chapter.

4 Assessment of the Biological Activity of Novel Quinazolinones

This chapter is based on experimental work carried out by R. BERGER, with support from A. KIM and G. WESTPHAL.

Abstract The growth-enhancing activity towards *Lemna minor* hypothesized to be inherent in 2-(arylamino)-quinazolin-4(3*H*)-ones was confirmed by means of the developed *in vivo* assay. Ten newly synthesized and diversely substituted derivatives were found to impose small to large stress tolerance-inducing effects onto the plants. Following this confirmation, the complete set of 22 synthesis products, alongside two reference compounds, was subjected to concentration-dependent activity profiling, which yielded valuable information towards the refinement of the quinazolinone pharmacophore. A general trend was derived, correlating a gain in activity to an increasing electron density in the 2-substituting anilines. While electron-donating groups attached to the quinazolinone core do not affect the observed activity negatively, different N-methylation patterns lead to entirely inactive compounds. The gathered data allow for a partial confirmation of a connection between the mandatory structural motifs of known PARP inhibitors and the observed *in vivo* stress tolerance-enhancing activity. At the same time, an extension to the PARP pharmacophore was proposed, which is necessary in order to explain the observed activity of quinazolinones. However, based purely on the insights gained from the phenotypic assay, a mode of action involving inhibition of PARP enzymes by quinazolinone derivatives could neither be excluded nor confirmed. After all, with the delivered proof of a general, not necessarily stress-related plant growth-regulating activity, a wider range of regulatory networks needs to be considered as targets for this class of compounds.

4.1 Introduction

Based on the broad screening of small molecules aiming at the identification of water stress tolerance-inducing effects in the model plant *L. minor* a set of 23, for the most part previously undescribed compounds was synthesized. All of these compounds incoporate 2-(phenylamino)-quinazolin-4(3*H*)-one as basic scaffold and furthermore exhibit different substitution patterns in regard to (a) the aniline-based substituent in 2-position, (b) the endo- and exocyclic secondary amino functions and (c) the A-ring (see fig. 26) of the quinazolinone core. By assessing their *in vivo* activity using the previously developed *L. minor* bioassay, a confirmation of the actives found in the library screening and a distinction between structural motifs more and less beneficial to the biological activity is sought.

Additionally, the question is to be answered whether an observed growth-enhancing activity is either present exclusively under water stress conditions and subsequent recovery or can also be confirmed under normal physiological conditions. As discussed in section 1.2, general plant growth regulation and plant abiotic stress response involve similar signaling pathways. Therefore, if growth enhancement could also be observed in unstressed plants, it would suggest that one or more targets of quinazoline-based effectors may be found within the plants' regulatory networks.

4.2 Results and discussion

4.2.1 Mean screening results of novel 2-(arylamino)-quinazolin-4(3*H*)-ones

As discussed in section 2.2.5, only a moderate correlation was found between the initial activity screening of compounds and the mean results of repeated measurements in the *L. minor* phenotypic assay. Therefore, conclusions regarding the activity of a specific compound and its magnitude shall not be drawn based on single measurements, but rather on a series of repeated experiments to decrease the rate of both false positive and false negative results. For this reason, ten of the synthesized 2-(arylamino)-quinazolin-4(3*H*)-ones shown in section 3.2.2 were subjected to threefold testing at a concentration of $10\,\mu M$ in an identical experimental setup as described in section 2.2.1. The corresponding effect size classification

for mean effect sizes of $n = 3$ experiments, lower and higher numbers, was calculated as pointed out in section 2.2.5 with the critical values for $n = [2...5]$ replicates given in tbl. 9.

The results obtained from repeated testing are shown fig. 43, ranked according to mean effect sizes. The respective chemical structures and numeric values are given in tbl. 10 alongside meta results from the initial library screening (see section 2.2.5) for identical structures, where available. Firstly, it becomes evident that all ten compounds exhibit an effect upon the growth of *L. minor* – three of them achieving a large, three a medium and four compounds a small effect. This fact can be deemed an important proof of concept since the biological activity that was proposed to be inherent for this chemical class could be confirmed in all derivatives tested. Two out of these ten compounds have been investigated earlier as part of the screening library: compound **C046** (identical to **C121**) ranked third in the initial screening with an effect size of $\bar{d}_{tot,4} = 2.265 \pm 0.742$, classified a large effect. This effect size was confirmed almost exactly following synthesis of the compound with $\bar{d}_{tot,3} = 2.224 \pm 0.832$, corresponding to a medium effect. It is to be noted that the difference in confidence interval width as well as in effect classification both account for the unequal number of replicate tests. Commercially available compound **C061** originally ranked highest in activity ($\bar{d}_{tot,4} = 2.635 \pm 0.782$) while the identical, in-house synthesized **C122** shows a diminished effect ($\bar{d}_{tot,3} = 2.035 \pm 0.807$) which classifies only as medium. This discrepance may appear remarkable since mean effect sizes calculated from a number of individual experiments tend to overestimate the true effect with smaller numbers of replicates, as discussed earlier (see section 2.2.5). However, since both mean effect sizes lie well within the 95 % confidence interval of the respective other, it needs to be concluded that there is no ground for proving statistical difference between the results.

Apart from the two previously known structures, the set comprised four compounds ranking higher in activity (**C123**, **C127**, **C128** and **C126**) as well as four compounds ranking lower (**C130**, **C124**, **C129** and **C125**). Among them, the basic scaffold of the compound class **C126**

Table 9: Summary of critical values for the mean effect size assessment depending on number of replicates

	$n = 2$	$n = 3$	$n = 4$	$n = 5$
Small effect	1.0 – 1.8	0.9 – 1.7	0.8 – 1.4	0.8 – 1.4
Medium effect	1.8 – 2.6	1.7 – 2.5	1.4 – 2.0	1.4 – 2.0
Large effect	> 2.6	> 2.5	> 2.0	> 2.0
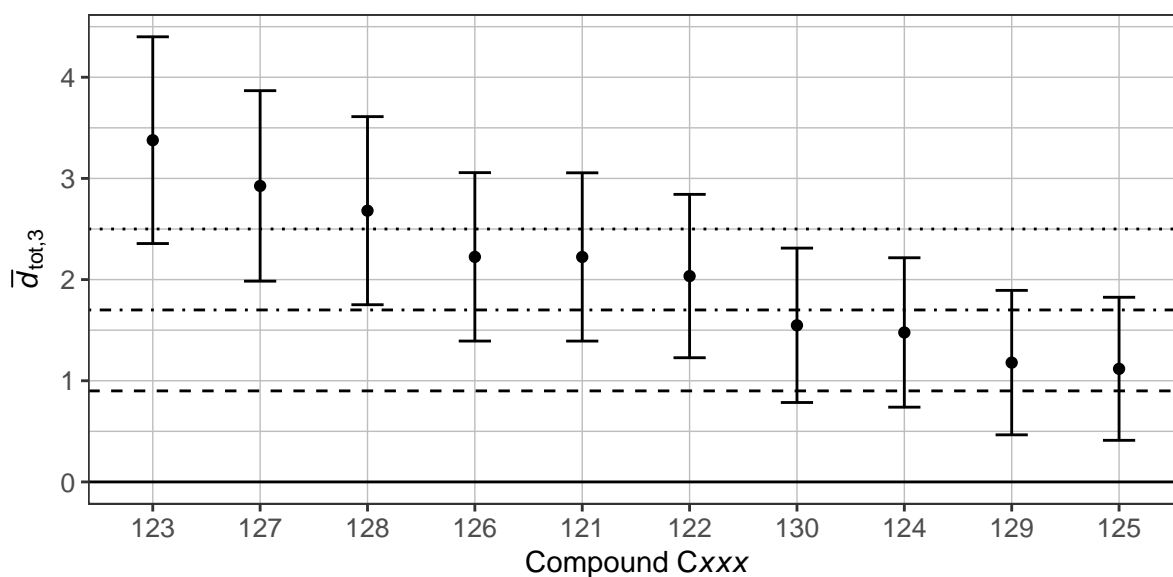
Figure 43: Results of mean effect sizes of three-fold measurement
Mean total relative growth effect size $\bar{d}_{\text{tot},3} \pm CI_{\bar{d}_{\text{tot},3},0.95}$ for 10 compounds tested at $10\,\mu$M concentration ranked according to effect size; highlighted vertical lines indicate effect size levels for $n = 3$ replicates

is found to have a positive influence onto the growth of *L. minor*, similar in size to its *p*- and *m*-methoxy derivatives **C121** and **C122**. Upon assessment of their chemical constitution, it appears that electron-rich aniline substituents tend to positively influence effect sizes, while electron-deficient substituents seem to diminish activity compared to the unsubstituted **C126**. This observation gives a first hint towards a functional relationship between structural motifs and activity within the class of 2-(arylamino)-quinazolin-4(3*H*)-ones.

4.2.2 Concentration-dependent activity profiles

So far, all compounds were tested exclusively on $10\,\mu$M level to guarantee maximal comparability of results. However, gaining knowledge of the concentration dependency is crucial in assessing the compounds' potency and applicability. Ideally, a compounds' activity, when plotted against the applied concentration on a logarithmic scale, yields a sigmoidal curve starting from low concentration levels without any observable effect to higher concentration levels with a maximal effect (saturation) onto the (biological) system. The shape of the curve, its slope and the location of the half maximal effective concentration (EC_{50}) define the therapeutic bandwith and optimal dose. To probe their concentration dependency, the synthesis products were tested over concentration ranges spanning at least four orders of magnitude (factor of 1000) using the previously described *L. minor* assay setup. The number of concentration levels and the maximal concentration applied differ among the tested

Table 10: **Screening results of newly synthesized quinazolinones**; Combined results of $n = 3$ replicate tests; Equivalent compounds of screening library shown where available with combined results of $n = 4$ replicate tests

Cxxx	Structure	$\bar{d}_{tot,3} \pm CI_{\bar{d}_{tot,3},0.95}$	Equiv. to Cxxx	$\bar{d}_{tot,4} \pm CI_{\bar{d}_{tot,4},0.95}$
123		3.378 ± 1.022		
127		2.926 ± 0.941		
128		2.681 ± 0.930		
126		2.225 ± 0.832		
121		2.224 ± 0.832	046	2.265 ± 0.742
122		2.035 ± 0.807	061	2.635 ± 0.782
130		1.548 ± 0.763		
124		1.477 ± 0.738		
129		1.179 ± 0.714		
125		1.118 ± 0.707		
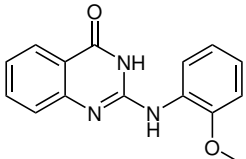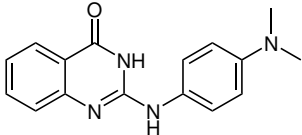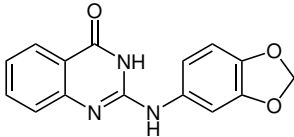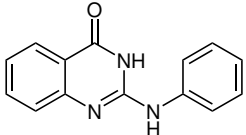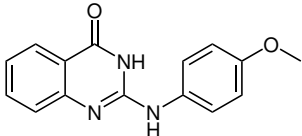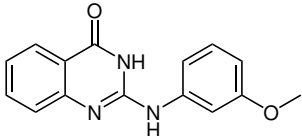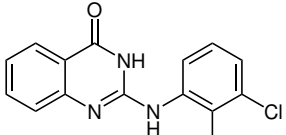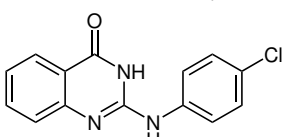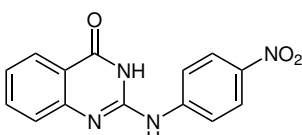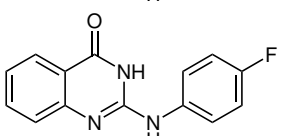
compounds due to distinct differences in solubility. Moreover, the number of replicate tests is not equal for all concentration levels of a specific compound – several tests were carried out at $\leq 10\,\mu M$ while higher concentrations were only applied in later stages of the investigation when the obtained data had not yet shown an indication for reaching a maximum effect.

As discussed earlier, comparability of mean effect sizes based on inconsistent numbers of replicate tests is limited. Still, all results obtained are shown and discussed since the main focus lies on the identification of general trends of concentration dependency rather than exact measurements of activity for specific concentration levels.

Comparison of model scaffolds

Compound **C126** represents the structurally least complex 2-(arylamino)-quinazolin-4(3*H*)-one, all other synthesized compounds can be regarded derivatives of this structure. Therefore, the observed activity of this compound serves as benchmark for the evaluation of all other derivatives in terms of growth enhancement.

C126 was applied over a concentration range of 1 nm to 100 μM as depicted in fig. 44. As indicated by point size, the number of replicates varied from 1 to 5 for specific concentration levels – the reliability of the estimated effects naturally increases with growing number of replicates, which is expressed through the width of the corresponding confidence intervals on the mean effect sizes. The overall trend of the relation corresponds to the characteristic shape of a sigmoidal curve left of its EC_{50} value. If extrapolated, the curve would reach its inflection point – which marks the compounds' EC_{50} value – and steadily rise towards its maximal value $\bar{d}_{tot,max}$. Concludingly, the estimated EC_{50} value for this compound would lie beyond a concentration of 100 μM. Such high concentrations may be judged uneconomical in the light of EC_{50} values commonly found in *in vitro* assays. Here again, it must be noted that the observed growth-enhancing effects apply to a whole plant rather than an isolated enzyme. On the way to their still unknown targets, the quinazolinone compounds have to overcome several physiological barriers either by active or (most likely) passive transport. Until an active transporter for this chemical class is found in plants it has to be assumed that the compounds enter the plant purely by passive transport, namely diffusion and osmosis. Both require a large gradient in concentration between compartments, thus explaining the necessity for applying rather high concentrations.

A detailed analysis of the dose-response curve confirms the agreement between the expected and observed concentration dependency of **C126**:

  ▷ Below a concentration of 1 μM no growth-enhancing effect is observable, the obtained effect sizes are statistically equivalent to zero at 95 % confidence level.
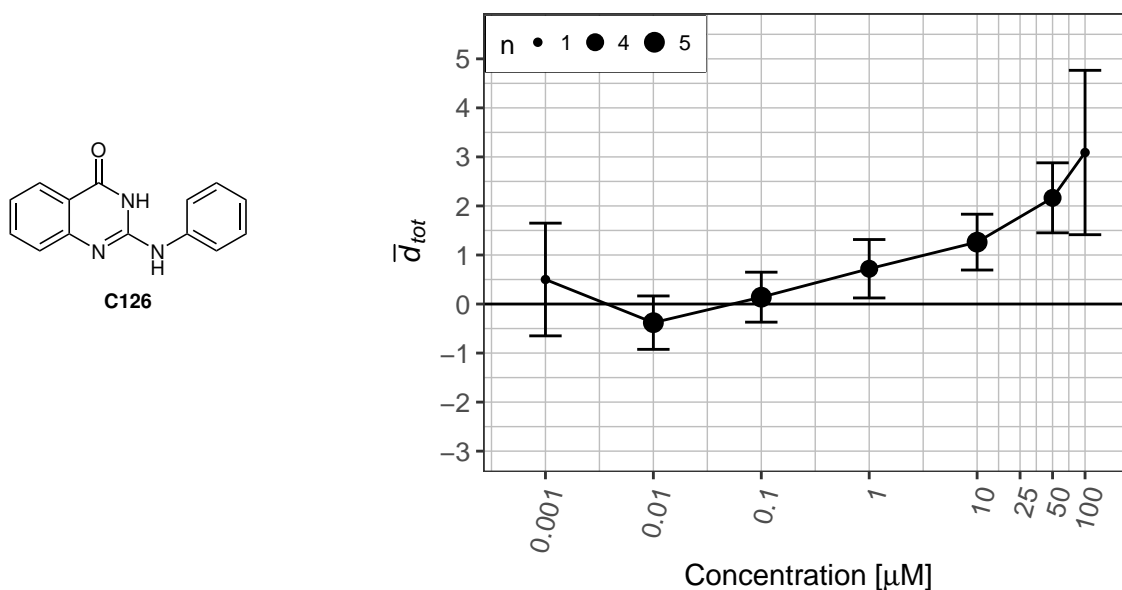
Figure 44: **Structure and concentration-activity profile** of compound **C126**

▷ At $1\,\mu M$ a first measurable effect of 0.720 ± 0.596 is found which still fails to reach a noteworthy magnitude (below the critical limit for small effects).

▷ At a concentration of $10\,\mu M$ compound **C126** exhibits a small, almost medium effect of 1.263 ± 0.569.

▷ A large effect (2.166 ± 0.714) is observed when the compound is applied at $50\,\mu M$ level.

▷ Application of higher concentrations ($100\,\mu M$) seems to further enhance plant growth or at least confirm the effect size obtained for $50\,\mu M$.

In an attempt to establish comparability between earlier investigations and the present work, the lead compound identified by GEISSLER (4-ANI, **C153**) was subjected to the concentration-dependent activity profiling. The respective data are shown in fig. 45. While the compound was claimed to enhance growth of *L. minor* by 16.3 % ($10\,\mu M$), respectively 12.6 % ($1\,\mu M$) [25], no growth enhancement could be proven in the present setup. On the contrary, a diminishment in growth compared to the controls was found when applied in doses higher than $10\,\mu M$. The data at hand suggests that for the concentration levels found by GEISSLER to positively affect plant growth, the true effect equals zero, meaning the compound was falsely labeled active. As discussed in section 2.2.1 this discrepancy may well be tied to the shortcomings of a first exploratory experimental setup and the statistical evaluation in the original setup of the assay.
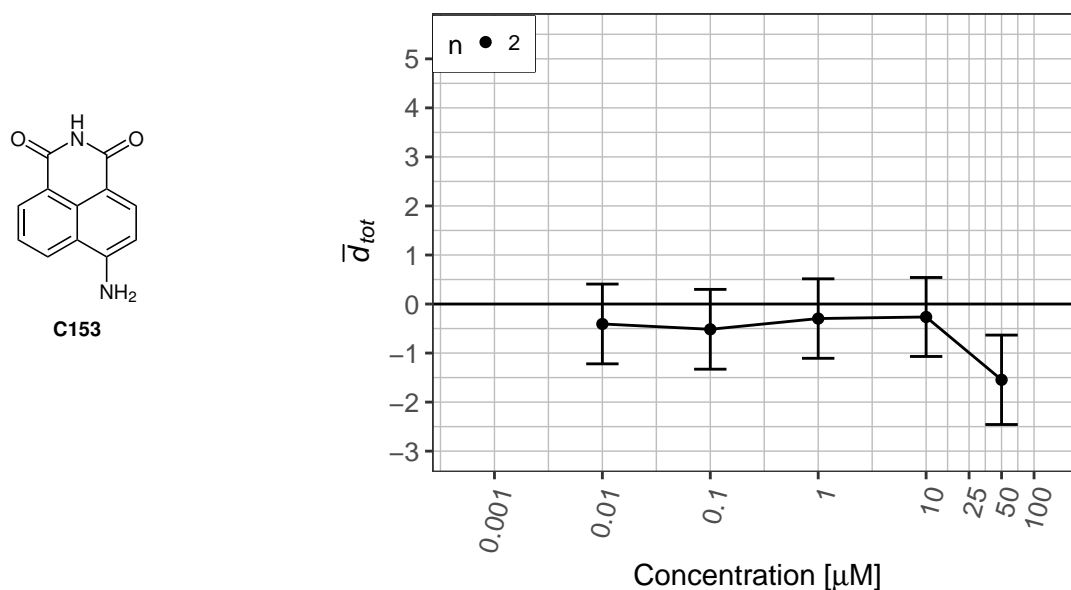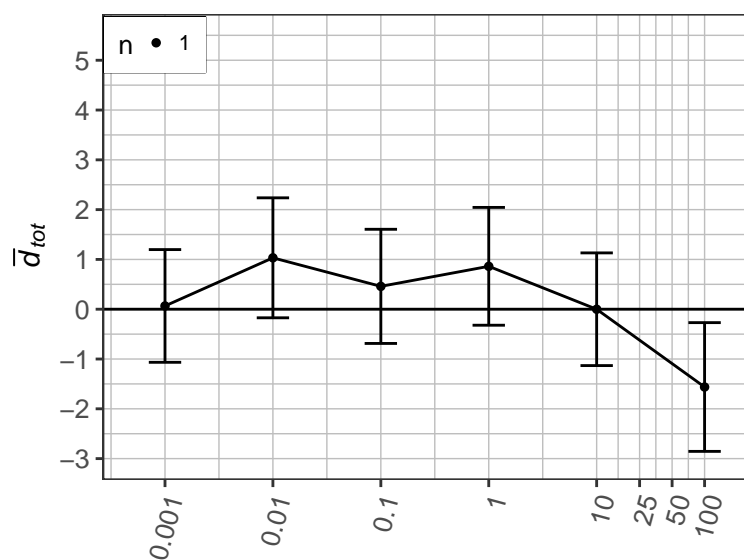
Figure 45: Structure and concentration-activity profile of compound **C153** identified as active and employed as reference compound by GEISSLER [25, 26]

To further explore the design space of active structures, a compound closely related to the 2-(arylamino)-quinazolin-4(3H)-ones was tested, bearing a 2-substituent based on an aminopyrimidine rather than aniline. The compound was synthesized in the IPB by G. WESTPHAL and kindly provided for testing. The chemical structure of **C184** (see fig. 46) can be understood as derivative of compound **C060** obtained by twofold exchange CH →N in the aromatic system of the substituent. The synthesis of the compound comprised a condensation reaction of 2-guanidinoquinazolin-4(3H)-one and pentane-2,4-dione as crucial step to the formation of the substituent (not shown here). While the related compound **C060** reached a medium effect (see section 2.2.5) at 10 μM level, **C184** was found to be completely inactive over the concentration range of 10 nm – 50 μM. This finding enables a deeper understanding of the structural motifs connected to activity in the *in vivo* assay: while the exchange CH →N has little influence on the sterical demand of the compound, the electronic structure within the substituent and mesomerization between substituent and quinazolinone core are changed fundamentally. These differences can easily alter the compounds' pose within or prevent its interaction with, e. g. a target enzyme. However, until the molecular target of the compound class and the mode of action have been identified, it can only be empirically assessed that this structural change within the substituent leads to complete diminishment of the observed growth-enhancement.
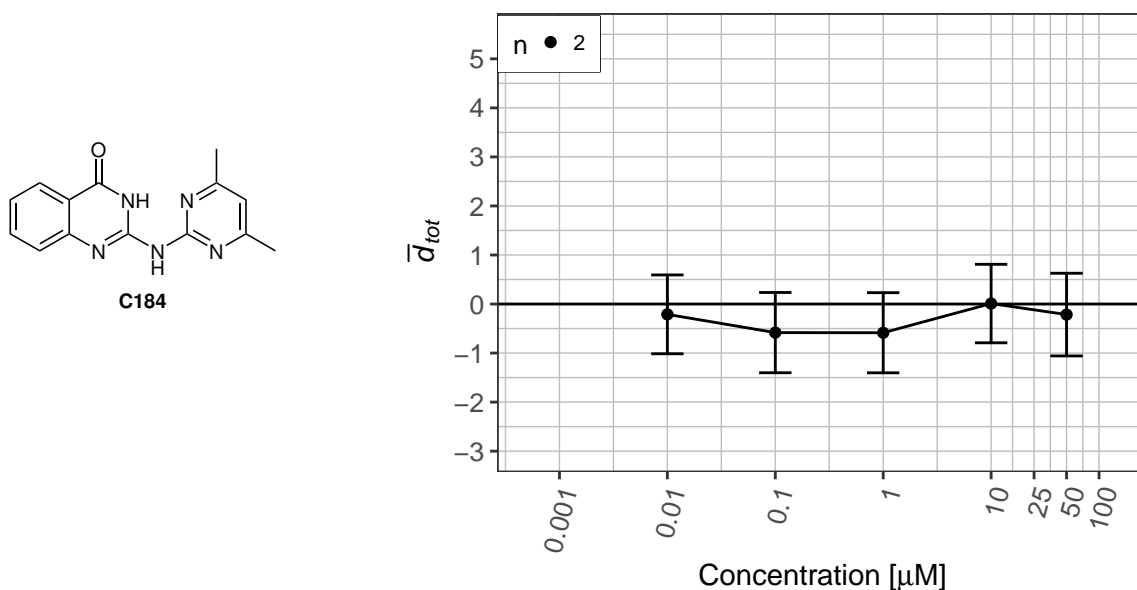
Figure 46: Structure and concentration-activity profile of compound **C184**

Electron-rich substituents

Among the first synthesis products, the quinazolinones bearing electron-rich (methoxyl-, dimethylamino-, methylendioxyl-) substituents showed a tendency to outperform rather electron-deficient halogen- and nitro-substituted derivatives (see fig. 43). Figs. 47 and 48, pp. 81 – 82, inform about the activity profiles of the respective compounds.

At a first glance all six compounds exhibit dose-response relationships that match the expectations gained from the model compound **C126** for the most part. No growth enhancement is found on concentration levels lower than $1\,\mu$M. Except for **C173**, doses of $1\,\mu$M to $10\,\mu$M begin to enhance the growth of *L. minor* with small to medium, or even large effects until a peak in activity is reached at a concentration of $25\,\mu$M. Interestingly, for all compounds (except **C173**) the observable activity drops dramatically for a concentration of $50\,\mu$M. However, activity seems to be recovered at $100\,\mu$M to an extent at least comparable to $25\,\mu$M. Point size and width of confidence intervals indicate that only 1 – 2 tests were performed for these concentration levels. Here again, the theoretical overestimation of the true effect by poorly powered meta results (calculated from a small number of replicates) is contradicted: the effect sizes for concentrations of $50\,\mu$M seem to underestimate the expected progress of the dose-response curve greatly. Such an agreement in counter-intuitive data among a set of compounds suggests a systematic flaw in the experimental setup. Indeed, the data for the $50\,\mu$M level was generated in only two consecutive experiments (BER352, BER353)
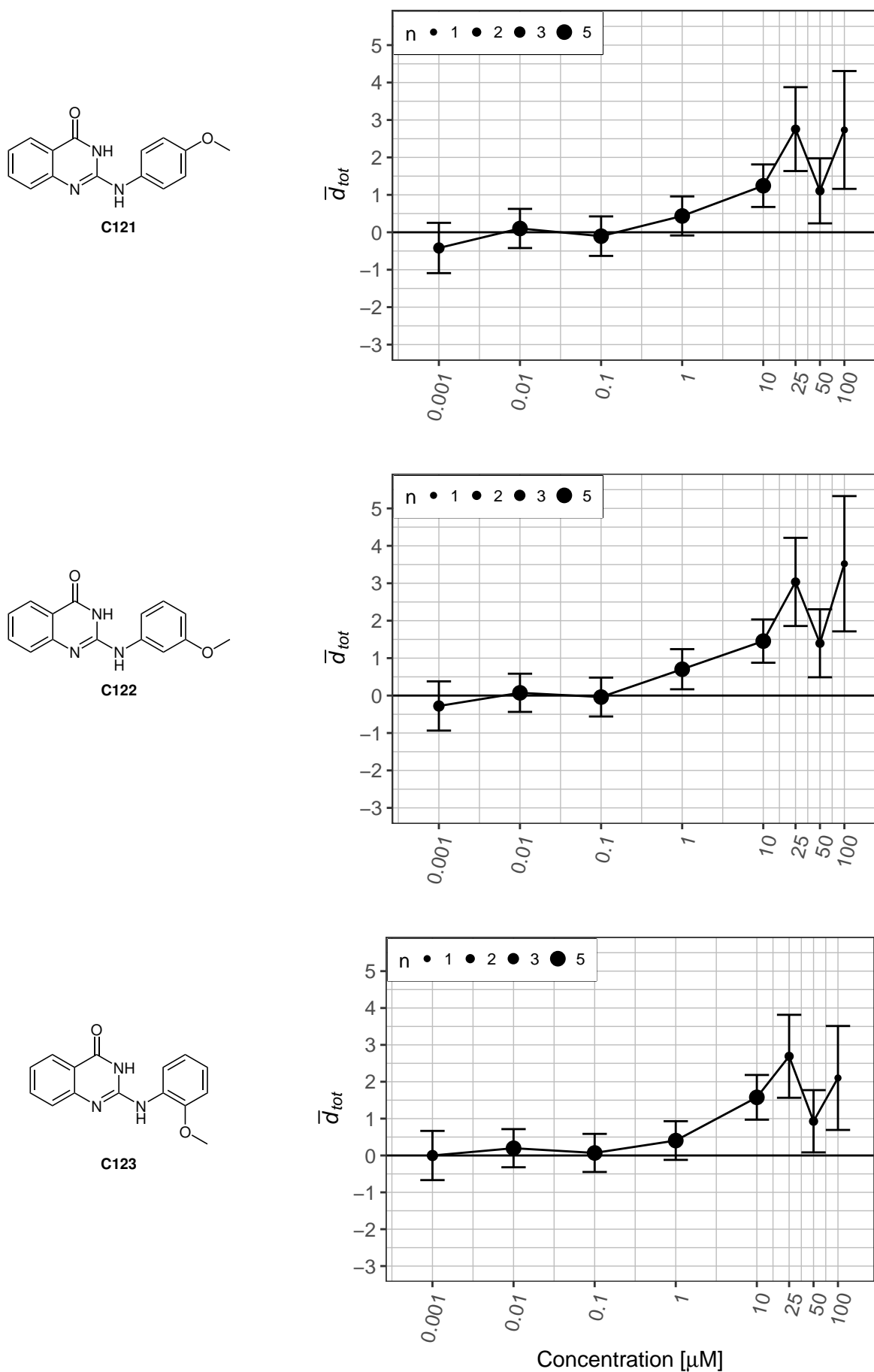
C121

C122

C123

Figure 47: Structure and concentration-activity profile of compounds **C121**, **C122** and **C123**
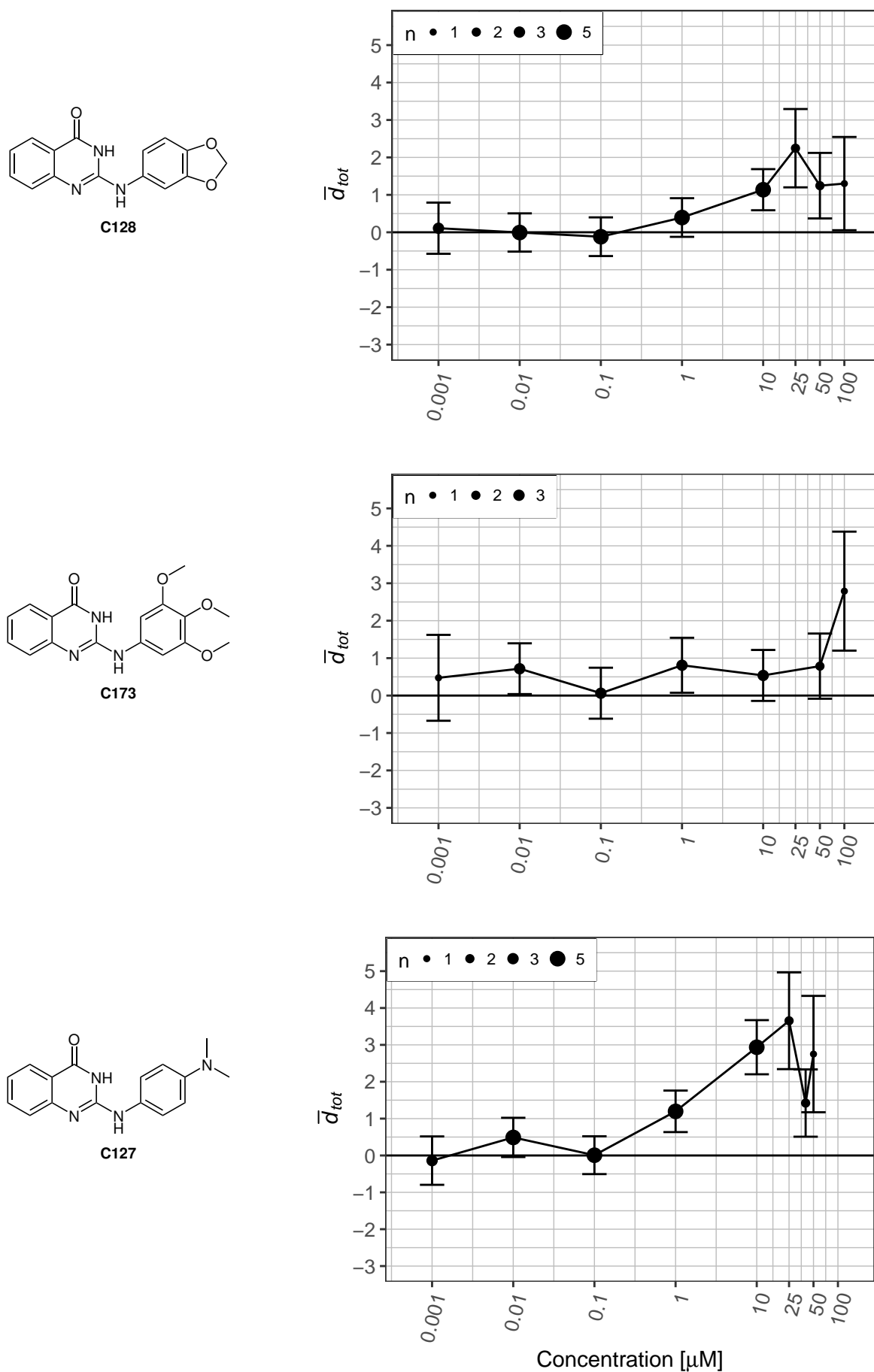
Figure 48: Structure and concentration-activity profile of compounds **C128**, **C173** and **C127**

while the data e. g. for 25 µM was obtained in an independent experiment. This leaves the possibility of altered conditions between the experiments, even though the protocol was not changed. An alternative scenario might explain the decrease in activity with adverse side-effects of the applied compounds that outweigh their growth-enhancing effects in high concentrations. However, since activity seems to increase again on a level of 100 µM, this explanation does not sustain. Therefore, it must be assumed that an unrecognized change in experimental conditions paired with an insufficient statistical power led to the observation of such implausible effects for the concentration level of 50 µM. For that reason, further discussion and comparison will focus mainly on effect sizes obtained for concentration levels of 10 µM and 25 µM.

Compounds **C121**, **C122** and **C123** appear as constitutional isomers and show comparable activity profiles, both qualitatively and quantitatively. All three of them exhibit statistically evident growth enhancement in *L. minor* corresponding to small and medium effects at 10 µM level (**C121**: 1.244 ± 0.568; **C122**: 1.455 ± 0.578; **C123**: 1.577 ± 0.606) and large effects at 25 µM (**C121**: 2.756 ± 1.120; **C122**: 3.036 ± 1.178; **C123**: 2.690 ± 1.125) that surpass the model compound **C126**. As concluded from the comparison between **C126** and **C184**, the sterical demand of the 2-substituent seems to influence a compounds' activity much less than its electronic structure (see previous section). This finding is confirmed by these three derivatives: the +*M*-effect of the methoxyl group causes a considerable increase in growth enhancement compared to the model compound **C126**, while its position on the phenyl ring merely finetunes the effect size. Even the bulkier methylendioxyl group in **C128** fails to quench growth enhancement – though activity is clearly decreased in comparison to the methoxyl derivatives, it still matches **C126** in effect size. A limit seems to be reached only with the triple methoxyl substitution in **C173**: while no or only neglectable effects could be observed in the concentration range of 1 nm to 50 µM, a single determination at 100 µM could be judged a large effect. Even if this effect was confirmed in follow-up investigations **C173** would fail to compete with the lower effective doses of its related, less substituted compounds.

Compound **127** is the only synthesized derivative incorporating an electron-donating amino group in the aromatic substituent. At the same time, it shows the highest growth-enhancing activity towards *L. minor* of the whole set (10 µM: 2.937 ± 0.734; 25 µM: 3.654 ± 1.312). Since dialkylamino groups are considered to induce a stronger +*M*-effect than alkoxyl groups,

the superiority of **C127** over **C121**, **C122** and **C123** serves as additional evidence for the key importance of the substituents' electronic structure in general and its electron density in particular.

Based on the activity found for concentration levels of $10\,\mu$M and $25\,\mu$M, the ranking shown in fig. 49 can be derived, which attributes a gain in activity to quinazolinones bearing electron-rich, not too sterically demanding aniline derivatives as substituent in 2-position. Compared to the order obtained in the repetitive testing of the first synthesis products (see tbl. 10) at $10\,\mu$M level, the overall trend is confirmed. In fact, the three methoxyl derivatives were previously judged to be of different potency with **C123** outperforming the other two. However, a difference could not be statistically justified due to the substantial overlap of confidence intervals. Depending on the concentration level considered, one or another derivative shows higher effect sizes in the activity profiling. Therefore, they are considered to be of comparable potency – with a higher number of replicate measurements a clearer distinction could be achieved, but this is not the aim of the presented investigations.

Electron-deficient and mixed substituents

The set of synthesized quinazolinones bearing rather electron-deficient 2-substituents comprise *p*-chloro-, -fluoro- and -nitro-substituted anilines (**C124**, **C125** and **C129**), as well as *m*- and *p*-aminoacetophenone (**C178** and **C179**). Their structures and activity profiles are presented in fig. 50, respectively fig. 51. Additionally, three more diversely substituted anilines were chosen for incorporation into the quinazolinone molecule, which are displayed in fig. 52 (**C130**, **C174** and **C172**).
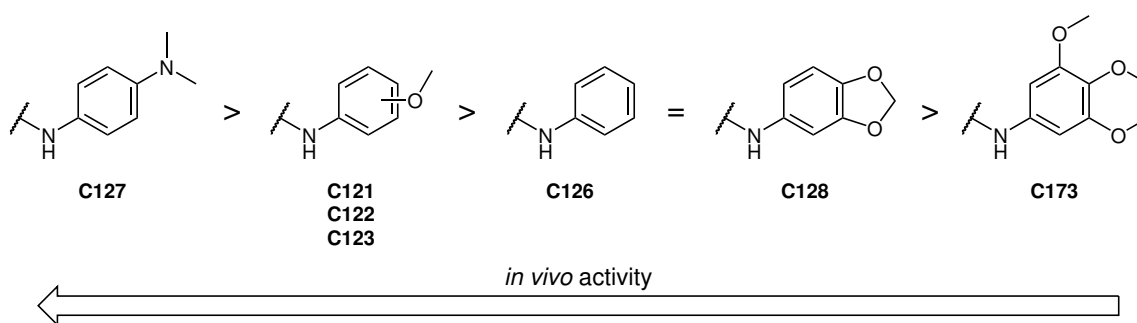
Figure 49: Ranking of synthesized electron-rich quinazolinone derivatives according to effects exhibited in the *in vivo* assay at $10\,\mu$M and $25\,\mu$M concentration

All of these compounds failed to show any remarkable effect onto the growth of *L. minor* up to a concentration of $10\,\mu M$. Still, single small effects were observed, e. g. for **C124** at $1\,\mu M$, which cannot be regarded promising activity but rather need to be judged artifacts, considering the overall trend of the profile. Above concentrations of $10\,\mu M$ the compounds **C124** and **C125** exhibit small to medium effects with the *p*-fluoro-derivative performing slightly better ($50\,\mu M$: 2.174 ± 1.010; $100\,\mu M$: 2.493 ± 1.594). The corresponding *p*-nitro-derivative on the other hand renders completely inactive. While these structures are comparable to **C127** and **C121** in terms of sterical demand, the electron density of the aromatic system is strongly reduced due to the substantial $-I$-effect of the halogens, respectively the $-I$- and $-M$-effect of the nitro group. This reduction in electron density seems to be accompanied by a reduction in *in vivo* activity up to its complete loss, which serves as additional confirmation of the hypothesized crucial role of the substituents' electronic structure. In the compounds **C178** and **C179** the carbonyl group negatively affects the electron density within the phenyl ring both through a $-I$- as well as a $-M$-effect. Consequently, both substances affect the growth of *L. minor* only to a minor extent (**C178**: 1.044 ± 0.613; **C179**: 0.983 ± 0.715; both small effects at $50\,\mu M$), which ranks far from the top actives.

The compounds **C130** and **C174** provide a less clear picture. Based on the hypothesized influence of the substituents' electron density, it could be expected that **C130** exhibits an activity at least comparable to **C124** due to the mixed influences of the attached methyl group and chloro-atom. However, no effect was found up to concentrations of $50\,\mu M$ and even the single determination at $100\,\mu M$ does not reach the treshold for qualifiying as small effect. For **C174** a small effect is found at $10\,\mu M$, which could not be confirmed by application of higher doses. Eventually, the absence of growth enhancement in the very bulky derivative **C172** fails to surprise considering the findings regarding the sterical demand of the substituent in e. g. **C128** and **C173**. Indeed, this compound appears to have a minor activity only in low doses with an effect size of 1.337 ± 0.726 ($10\,nM$) which contradicts the expected relation between concentration and activity.

N-methylated derivatives

So far, all investigated derivatives aimed at understanding the influence of the aniline-based substituent in 2-position. The quinazolinone core of the molecule was therefore left
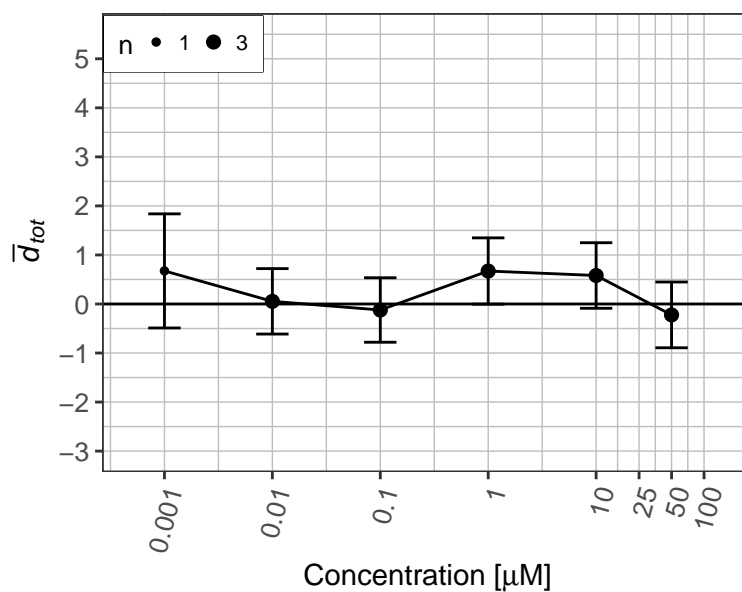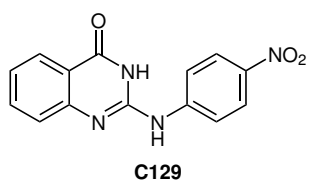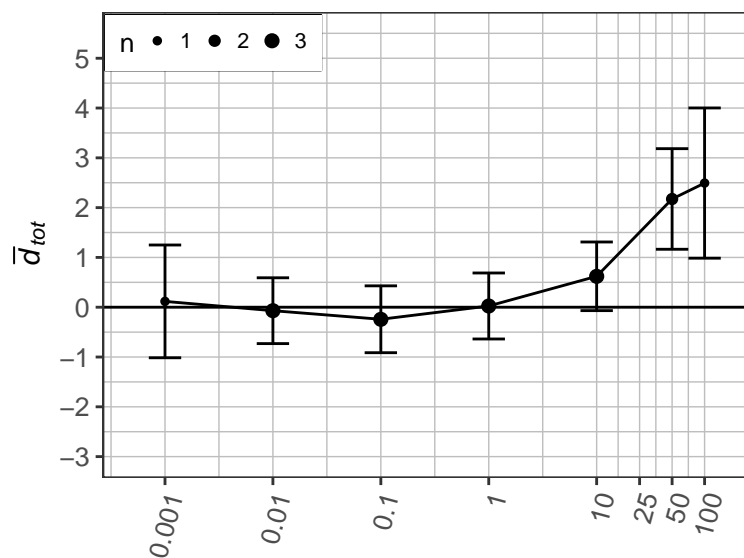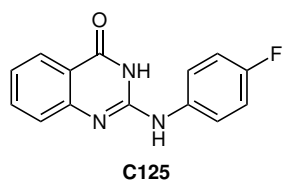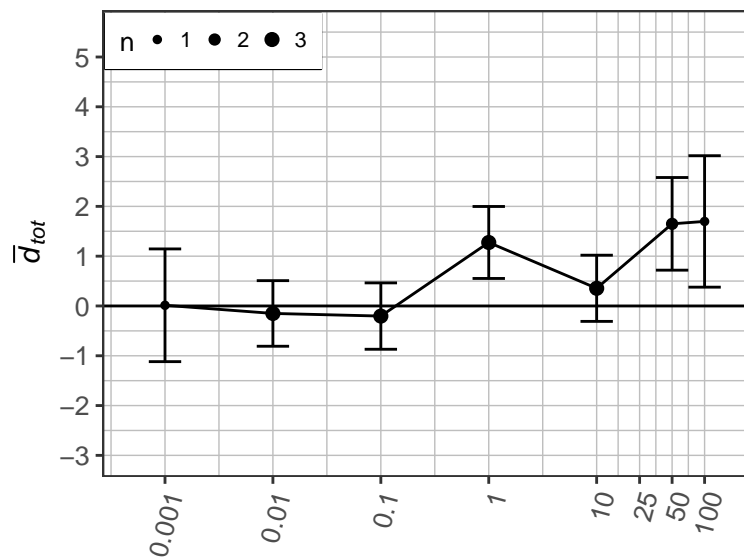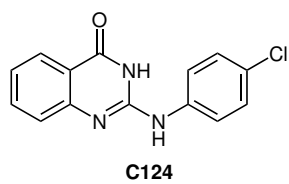
Figure 50: Structure and concentration-activity profile of compounds C124, C125, C129
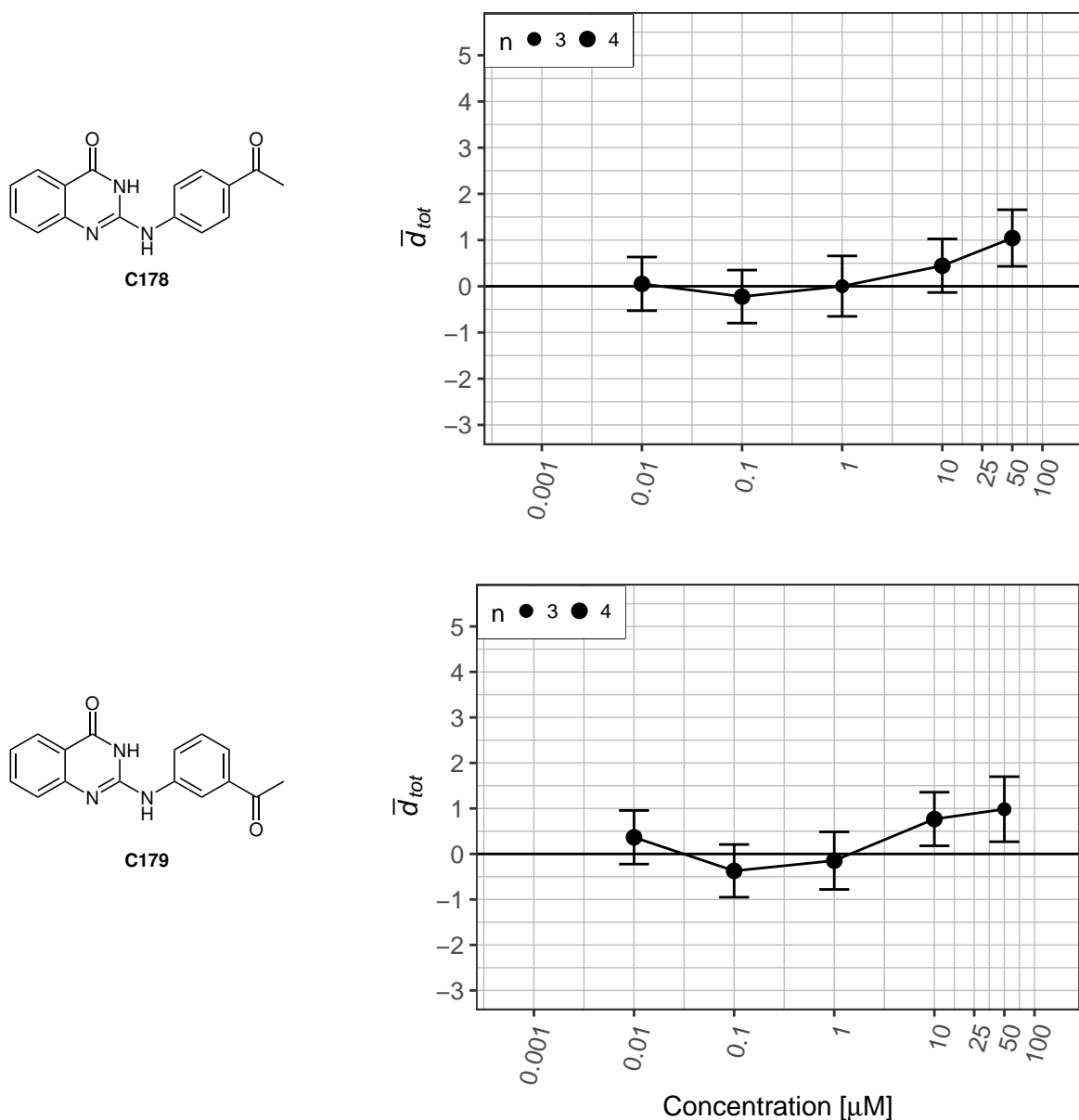
Figure 51: **Structure and concentration-activity profile** of compounds **C178** and **C179**

unaltered, including the capability of donating and accepting H-bonds via the lactam group in the B-ring, which was proven to be a mandatory motif in small molecules to interact (and possibly inhibit) enzymes of the PARP-family (see section 2.1.2). The structural modifications realized in **C175**, **C176** and **C177** represent the least sterically demanding way of blocking the H-bond-donating function of either the endocyclic or the exocyclic NH-group, or both. Thus, comparison of the activity profiles against the model compound **C126** should yield a picture of the influence of different methylation patterns onto the growth enhancement of the studied quinazolinones. The chemical structures of the mono- and dimethylated compounds are depicted in fig. 53, alongside their respective concentration-activity profiles. Although tested only once per concentration level the collective data for all three compounds
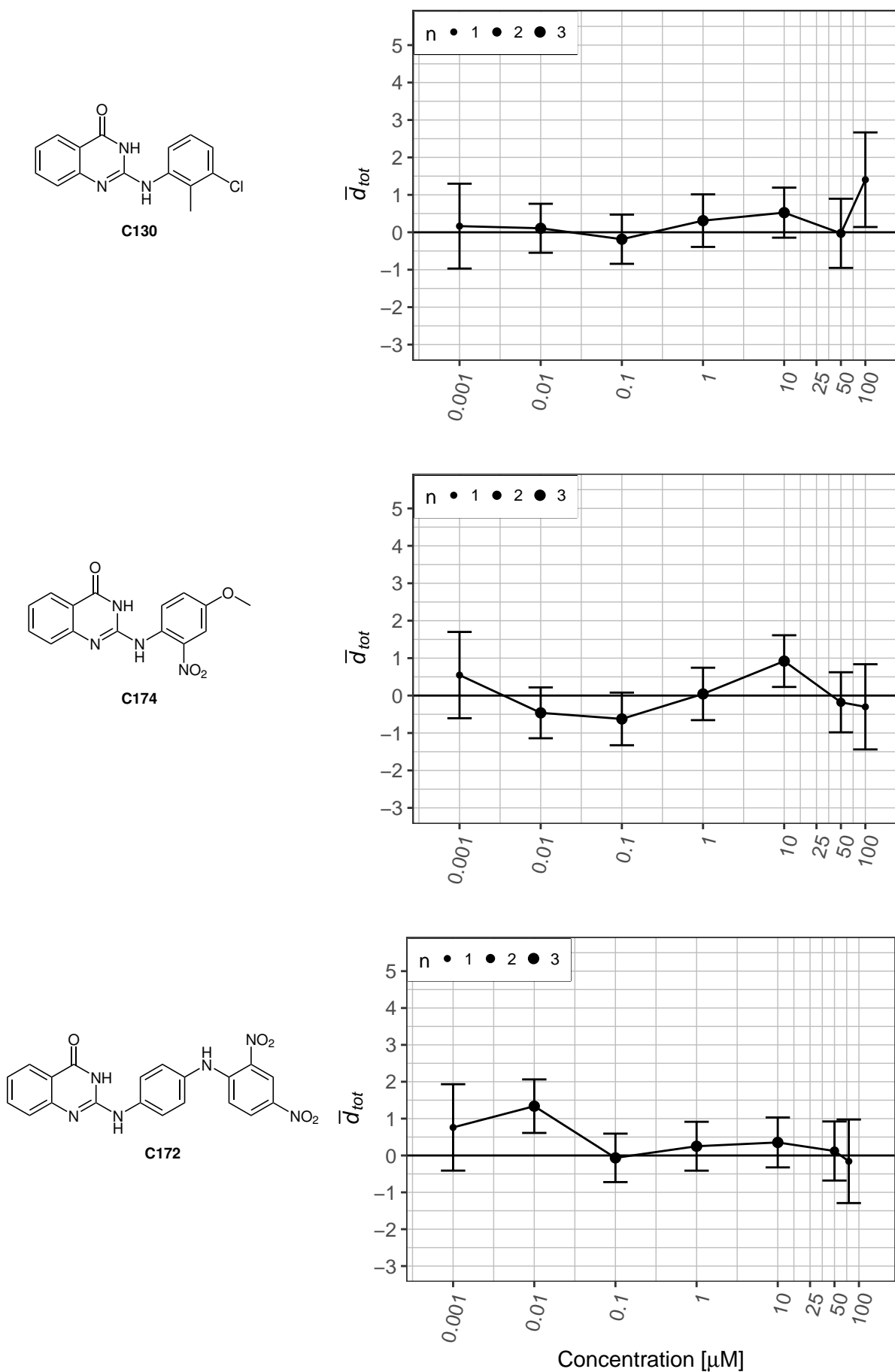
Figure 52: Structure and concentration-activity profile of compounds **C130**, **C174** and **C172**

indicate the absence of growth-enhancing activity with a tendency for adverse effects in higher doses. Compared to the single determination of **C126** at $100\,\mu$M (3.090 ± 1.781) the huge discrepancy in activity becomes evident (**C175**: -0.401 ± 1.135; **C176**: -1.562 ± 1.290; **C177**: -1.303 ± 1.238).

In the light of the hypothesis attributing *in vivo* activity to inhibition of the PARP enzyme family, the absence of said activity in compound **C176** and consequently **C177** could have been expected due to the crucial role of the lactam group in coordination within the PARP enzyme (see section 2.1.2). Aprt from that, the inactivity of **175** provides valuable information regarding the refinement of the proposed pharmacophore. Based on the limited data available so far, not only the *endo-* but also the *exo*-NH-group has to be considered mandatory for a growth-enhancing activity *in vivo*. If confirmed, three possible root causes for this observation may be considered:

1. Under the assumption of equal effectiveness of **C126** and **C175** towards a common target, methylation of the exocyclic nitrogen-atom alters the physico-chemical properties in comparison to **C126** to a degree that prevents **C175** from being taken up by the plant via – presumably – passive transport. Considering the structural diversity of all previously presented compounds found to be active in *L. minor*, an allegedly small modification such as a methylation does not appear significant enough to result in complete abolishment of uptake.

2. Although still undescribed, it is possible that the quinazolinone structures in scope enter the plant via an active transport mechanism. Such a mechanism is unlikely to have evolved for the purpose of transporting these very compounds – a more probable scenario is their "accidental" uptake through a less specialized active transporter originally designed for carrying structurally related, naturally-occuring compounds like secondary plant metabolites. In this case, the additional methylation in **C175** would keep the compound from being recognized by the transporter. However, since no published data provides insights into possible carriers for quinazolinones, there is no justification for pursuing such theory at this point.

3. Under the assumption of a mutual transport mechanism and comparable concentrations of both compounds within the plant, the structural difference represented by the N-methylation could render **C175** inactive towards the target enzyme if a highly specialized binding mechanism between the enzyme and the model compound **C126**
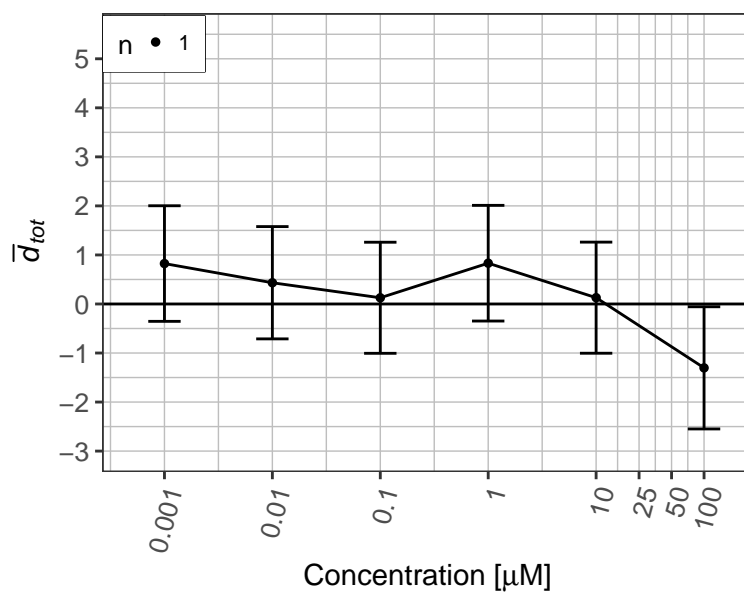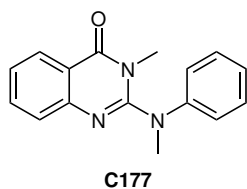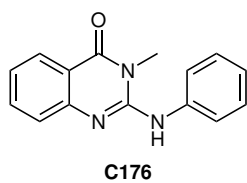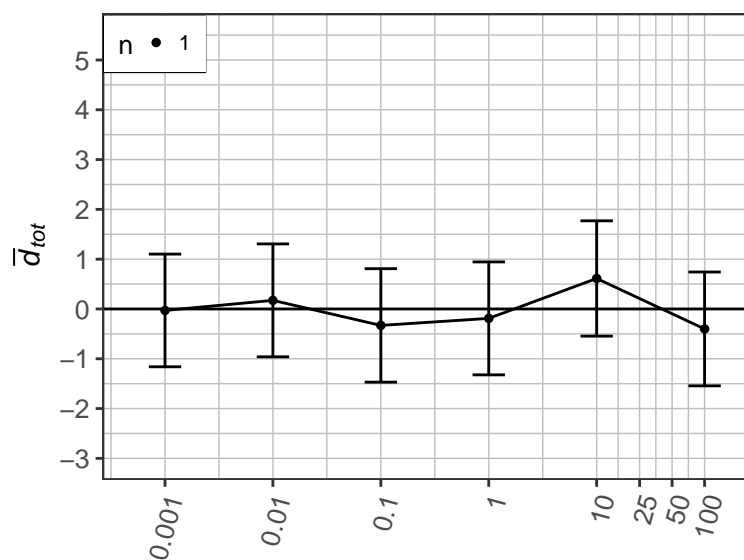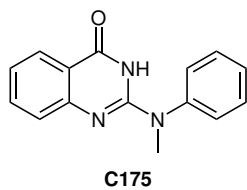
Figure 53: Structure and concentration-activity profile of compounds **C175**, **C176** and **177**

(and other active derivatives) truly exists. Since the presented investigations originated in the assumption of an inhibitory activity of small molecules towards PARP enzymes, this scenario appears most likely at this point. Consequently, the question arises whether the *exo*-NH-group is either a mandatory part of an extended PARP binding motif – possibly relevant only in *L. minor* – or if the binding motif relates to another target which might not even be of enzymatic origin.

To conclusively address the question of the influence of different methylation patterns regarding the pharmacophore, a confirmed target has to be identified first which exceeds the scope of this work.

Core-modified derivatives

After obtaining valuable information on advantageous structural features of the aniline-based substituent and the two NH-groups, possible modifications involving the A-ring of the quinazolinone core were deemed worthy of being investigated in order to obtain a comprehensive picture of the design space for growth-enhancing quinazolinones. For this purpose, two compounds comprising nitro-groups in 6-, respectively 7-position of the quinazolinone core, namely **C180** and **C181**, were synthesized and tested regarding their *in vivo* activity. Being mere intermediates within synthetic sequences targeting core-modifiable derivatives, both compounds were designed to give rise to their 6- and 7-amino analogues. This conversion was realized through reductive amination, resulting in the compounds **C182** and **C183**. The chemical structures of both pairs of compounds alongside their dose-response curves are depicted in figs. 54 and 55.

Both nitro-substituted compounds were subjected to fourfold activity determination covering the concentration range of 10 nm to 50 μM. As observed in the model compound **C126**, doses below 1 μM did not show any effect onto the growth of *L. minor*. Alas, even higher doses failed to affect the plant growth positively. Across the whole concentration range investigated, effect sizes were statistically equal to zero for both **C180** and **C181**. Most interestingly, the biological activity inherent to the model compound **C126** seems to be recovered following conversion of the nitro- into amino-groups, at least partially. At 50 μM concentration small (**C183**: 1.718 ± 0.938) and medium (**C182**: 2.516 ± 1.073) effects were observed.
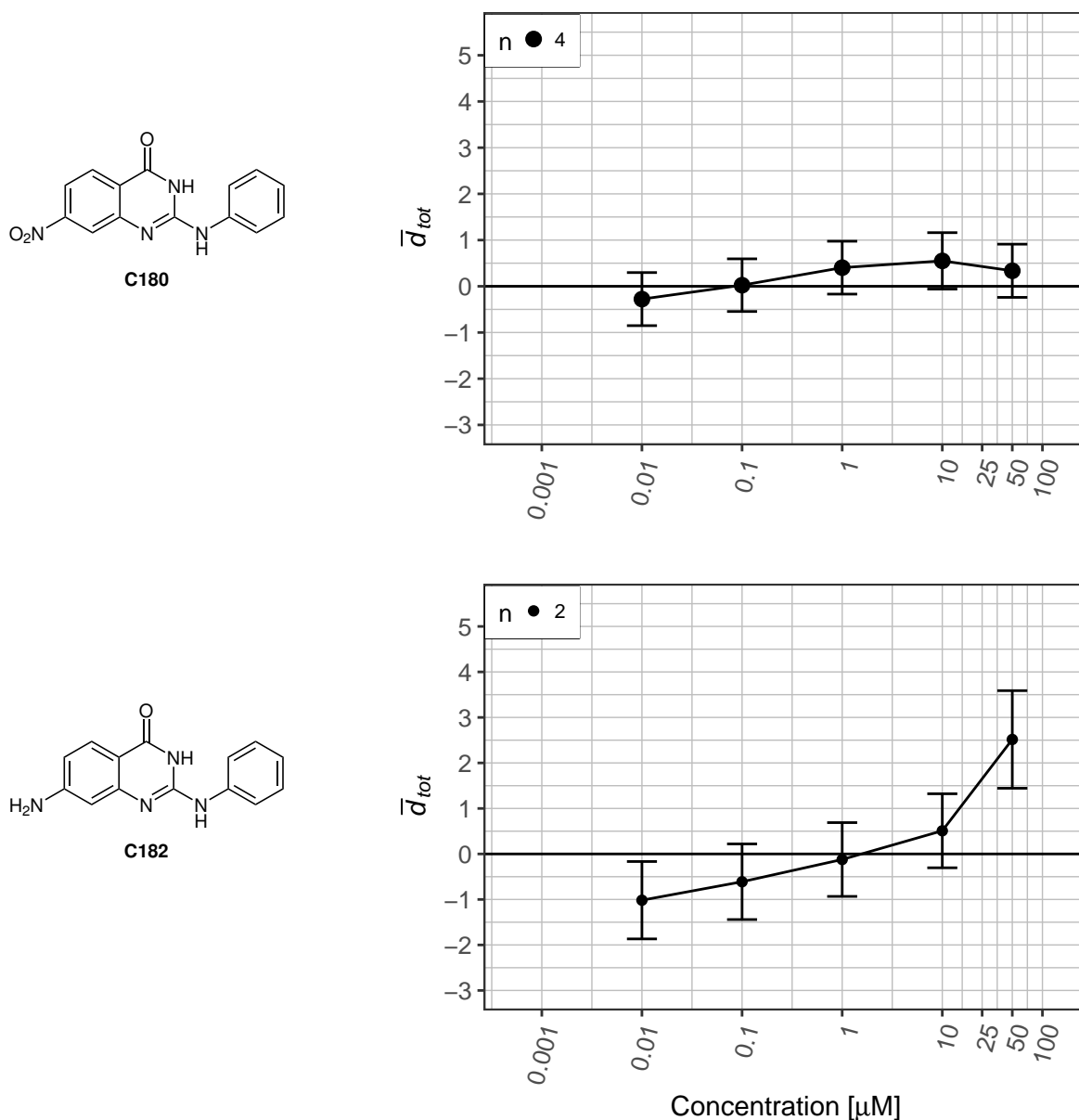
Figure 54: **Structure and concentration-activity profile** of compounds **C180** and **C182**

Apparently, manipulation of the electron-density influences the *in vivo* activity not only when the affecting substituents are located in the side chain, but also when attached to the quinazolinone core: the two pairs of nitro-amino-analogues **C180** – **C182** and **C181** – **C183** follow the same trend as the compounds **129** – **C127**, with the nitro-compound being more or less inactive and the amino-compound showing distinct growth enhancement in *L. minor*. Following this rationale, **C182** and **C183** ought to show even larger effects when modified by *N*-mono- or *N,N*-dialkylation, which ought to further increase the +*M*-effect of the amino group.
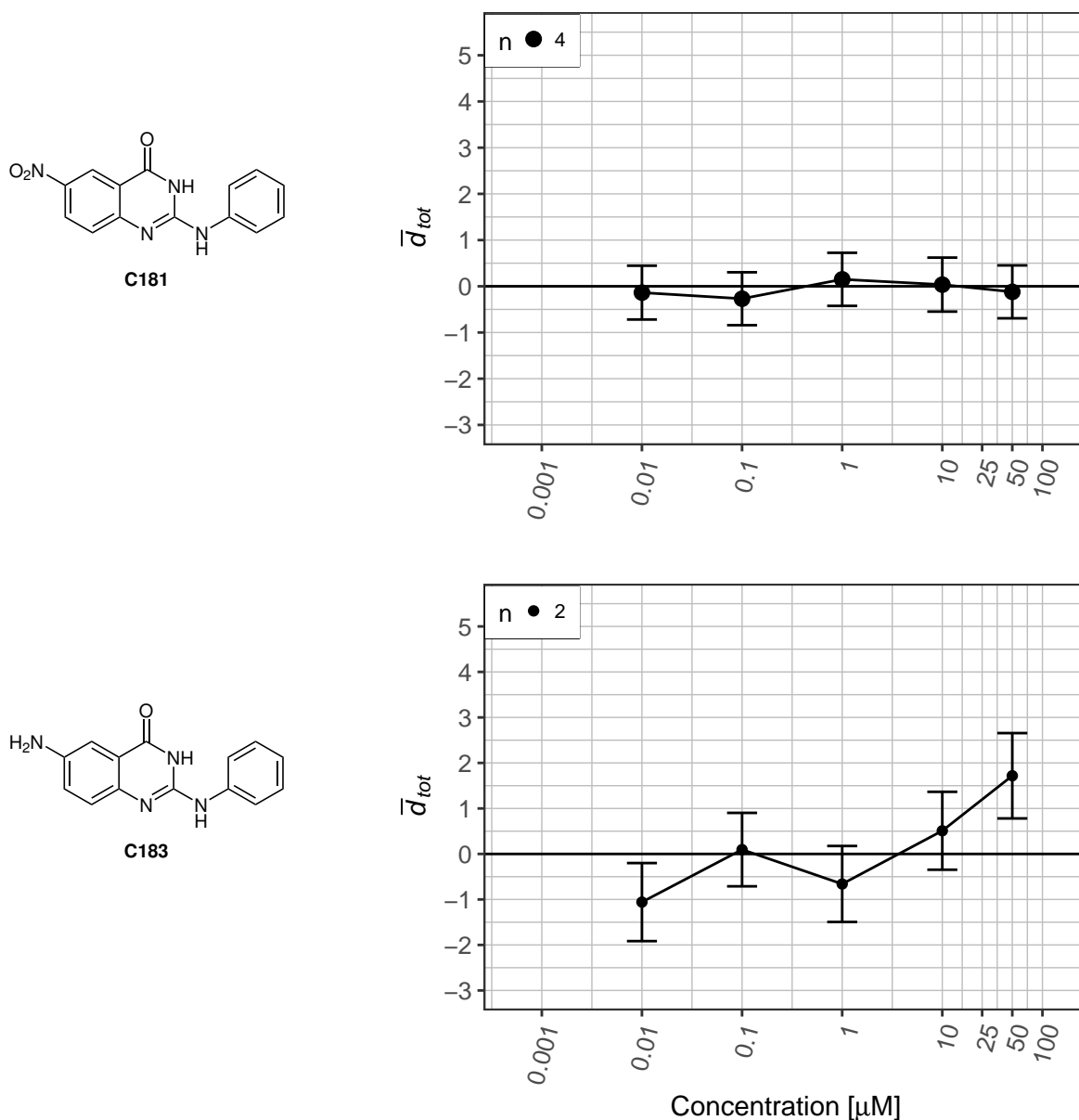
Figure 55: Structure and concentration-activity profile of compounds **C181** and **C183**

4.2.3 Assessment of growth enhancement under stress and non-stress conditions

As detailed in the introduction (see section 1.3), stress tolerance-inducing agents likely exhibit plant growth-regulating activity in general, even under normal physiological conditions. With a stress tolerance induction already demonstrated for different 2-(arylamino)-quinazolin-4(3H)-ones, the question arises whether a promotion of plant growth could be observed in absence of water stress as well. For the experimental investigation, **C126** was chosen as the model compound for the class of synthesized quinazolinones. The compound was applied to groups of *L. minor* plants at t_0 that were subjected to (a) water stress conditions
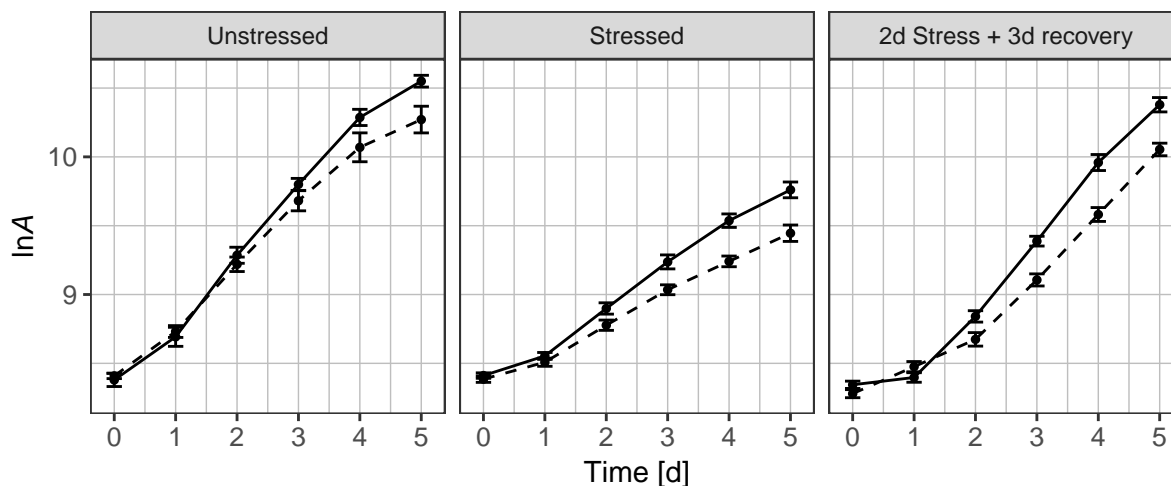
Figure 56: Assessment of growth enhancement under stress and non-stress conditions demonstrated by single application of $100\,\mu M$ **C126** at t_0; shown is the logarithmic frond area $\ln A \pm CI_{0.95}$ for groups of $n = 6$ plants, dashed line: negative control (DMSO), solid line: test group
left: Non-stress conditions (without PEG); middle: Stress conditions (full strength PEG); right: Stress application for $2\,d$ followed by recovery for $3\,d$

(b) non-stress conditions and (c) a combination of a two-day stress and three-day recovery phase. The main experimental parameters as described in section 2.2.1 were applied with a single modification: 12-well microtiter plates were used instead of 24-well plates, in order to enable plant growth for periods longer than three days without physical limitation by the vessels. This way, a test group could be hosted alongside a DMSO-treated control group in a single plate (both groups with $n = 6$ plants) and monitored for periods of five days. The growth profiles for control and test groups based on logarithmic frond areas are shown in fig. 56, reflecting the different conditions. Tbl. 11 further informs about the growth rates μ of control and test groups subjected to the different conditions, which were obtained by linear regression of the mean logarithmic leaf area in the period of days 2 – 4 where maximal growth could be observed. In addition, the calculated frond area doubling time t_{dbl} is given for all groups as more intuitive measure of plant growth.

The growth profiles for the control groups under stress and non-stress conditions agree with the expected trend. Starting with a decelerated growth within the first $24\,h$, likely due to physiological adjustment to the "new" environment, both groups pass into an almost linear growth on logarithmic scale which corresponds to an exponential growth in terms of frond area, respectively biomass (see section 2.2.1 for the mathematical description). The growth rate, which is reflected by the slope of the linear phase, is considerably lower under water stress ($\mu = 0.232\,\frac{1}{d}$) compared to non-stress conditions ($\mu = 0.425\,\frac{1}{d}$). This is also reflected in the respective doubling times of $2.989\,d$ and $1.631\,d$. In this experimental setup,

Table 11: Growth rates and doubling times of *L. minor* under different stress conditions and treatments

Treatment		Unstressed	Stressed	2 d Stress + 3 d recovery
C126	$\mu\left[\frac{1}{d}\right]$	0.501	0.319	0.559
	$t_{dbl}[d]$	1.384	2.173	1.240
DMSO	$\mu\left[\frac{1}{d}\right]$	0.425	0.232	0.454
	$t_{dbl}[d]$	1.631	2.989	1.528

a doubling time of the unstressed DMSO-treated plants with 1.631 d can be considered the benchmark for optimal growth of *L. minor* which is in agreement with previously reported values [55]. Accordingly, the control group in the stress/recovery experiment shows a delayed growth comparable to the stressed control within the first 48 h and a subsequent acceleration in the recovery phase reflected by an unprecedented shortening in doubling time to 1.528 d. With this acceleration in the recovery period, the stressed control group recovers to a state comparable to the unstressed control. The obtained growth parameters clearly demonstrate that even plants like *L. minor* experience water stress and show distinct physiological adaptations to a change in water potential, despite their natural habitat being water.

The comparison between controls and test groups yields a clear picture at first glance: The test groups treated with 100 μM 2-(phenylamino)-quinazolin-4(3*H*)-one outperform their respective controls in all cases. Under permanent stress conditions the treatment accelerates growth by approximately 38 %, assessed on basis of the growth rates $\mu = 0.319 \frac{1}{d}$ (treated) and $\mu = 0.232 \frac{1}{d}$ (control). Although applied only once, the beneficial effect of **C126** is present throughout the whole monitored period, which promises a sustainable long-term effect in a possible field application as well. Interestingly, a positive effect of **C126** is also observed under normal physiological conditions which is reflected by a growth rate increase of 18 % compared to the control. This result suggests that 2-(arylamino)-4(3*H*)-ones indeed exhibit general plant growth-regulating activity, most possibly through interaction with the central regulatory pathways discussed (see section 1.3). In agreement, the treatment with **C126** leads to an enhancement in growth by 23 % in the recovery phase, when applied at the beginning of a two-day stress period. It needs to be highlighted that the effect of the chemical treatment is still observable in the recovery phase, although no further applicaton was performed at the shift from stress to recovery conditions, which was achieved by complete exchange of the medium including the chemical agent.

In conclusion, the highest overall growth rate, respectively the lowest doubling time of 1.240 d, could be observed in the recovering plants under treatment with **C126**. The pairwise comparison of treated and non-treated groups under identical conditions reveals the great potential of this class of compounds regarding growth promotion, both under water stress and normal physiological conditions. Regarding the objective of this work, especially the improved production of biomass during stress situations, as well as the accompanying accelerated recovery seem promising towards a future mitigation of shortfalls in crop production.

4.2.4 Refinement of the lead pharmacophore

Starting from the initial hypothesis of PARP inhibitors being promising drought stress tolerance-inducing agents, many insights into more and less beneficial structural motifs could be gained by directed synthesis and *in vivo* experimental evaluation. In reference to the well established pharmacophore of *Hs*PARP-1 inhibitors shown in fig. 6, p. 6, several modifications are necessary to correctly describe the quinazolinone pharmacophore based on the obtained experimental evidence of the library screening (see section 2.2.4) and activity profiling of the synthesized derivatives presented in this chapter. The pharmacophore shown in fig. 57 summarizes all information obtained on the constitution of active structures:

▷ The essential amide binding motif (red) needs to be extended: All quinazolinones found to be active comprise the H-bond donor function through the lactam group as known from PARP inhibitors. The available experimental results indicate that blocking of this function through *N*-alkylation leads to an extinction of *in vivo* activity. Moreover, the exocyclic secondary amino function seems to be mandatory for activity since *N*-methylation in this position renders the derivatives inactive as well.
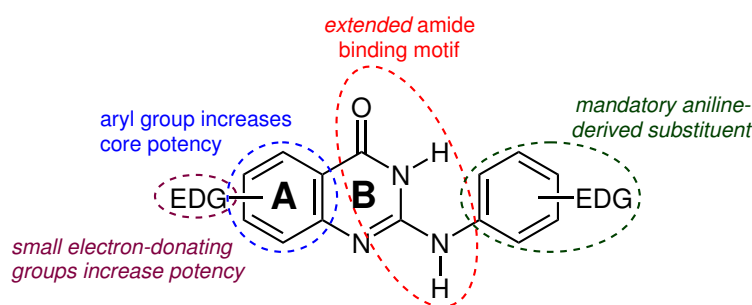
Figure 57: Revised pharmacophore of active quinazolinone structures based on experimental results

▷ The increase in potency through an aromatic A-ring in the quinazolinone core (blue) can be confirmed. Though all screened ThQui compounds eventually rendered inactive, this effect cannot be attributed exclusively to the saturated A-ring since all derivatives also comprised a 2-substituent which is likely to negatively influence *in vivo* activity. However, based on the structural agreement amongst the active quinazolinones, an aromatic A-ring is regarded mandatory at this point.

▷ An extension of the PARP motif is necessary for the substituent in 2-position (darkgreen): of all screened compounds, only those could be judged active which carried an aniline-based side chain. Sulfur-, oxygen- and carbon-based substituents as well as *N*-alkyl groups failed to enhance growth in *L. minor*. In addition, the structurally highly related compound **C184**, incorporating an aminopyrimidine substituent, rendered completely inactive as well. Therefore, within the limitations of the available data, an aniline-based substituent in 2-position is regarded mandatory.

▷ Further refinement of the substituents' structure was achieved by comparison of derivatives incorporating different anilines covering a wide range of electron-donating (EDG) to electron-withdrawing groups (EWG), as well as variability in terms of size, position and number of substituents. In summary, *in vivo* activity was shown to be enhanced in comparison to the basic scaffold 2-(phenylamino)-quinazolin-4(3*H*)-one by small numbers of sterically undemanding electron-donating (methoxyl- and dimethylamino-) groups. Meanwhile, the position of the substituent on the phenyl ring seems to be less influential.

▷ Regarding the substitution pattern of the A-ring (violet), the PARP pharmacophore describes a tolerance towards small substituents. In the quinazolinones, it was found that the type of substitution (more than its position) has considerable influence onto the activity, as was demonstrated through two pairs of nitro-amino-analogues. Here again, sterically undemanding, electron-donating groups appear to be beneficial towards growth enhancement in *L. minor*, while groups with strong $-M$- and $-I$-effects lead to a reduction or even extinction of activity.

By application of these rules, a single chemical structure can be postulated which combines all structural features found to be beneficial. This compound ought to show the highest growth enhancement in *L. minor* which can be hypothesized based, on the assembled data. The respective structure as shown in fig. 58 is expected to be accessible with only minor modifications of the synthetic route shown in fig. 42, p. 68. While the introduction of
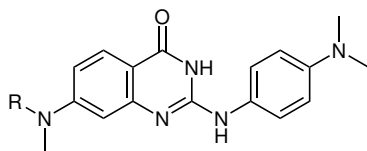
Figure 58: Hypothesized optimal structure of quinazolinones based on the rules formulated for the pharmacophore

p-(dimethylamino)-aniline in 2-position ought to proceed without problems, challenges may arise from the alkylation of the amino-group in 7-position, during which all other secondary and tertiary amino groups need to be protected from alkylation. However, if achieved, the resulting derivatives could not only outperform all compounds presented herein, but also be promising probes (with R being e. g. a solid-phase-attached spacer) for affinity-based profiling studies aiming at the identification of targets.

4.3 Conclusions and perspective

Following the identification of 2-(arylamino)-quinazolin-4(3*H*)-ones as promising stress tolerance-inducing agents from the library screening and the exploration of a wider range of chemical diversity through synthesis, the final aim of this work lay in the description of the concentration dependency of quinazolinone *in vivo* activity and the deduction of a comprehensive pharmacophore for this class of compounds.

By the example of 2-(phenylamino)-quinazolin-4(3*H*)-one, which can considered the common scaffold of all newly synthesized derivatives, it could be shown that the stress tolerance-inducing effect in the *in vivo* assay follows a concentration dependency as expected. Alas, a characterization across the whole therapeutic bandwith has not been accomplished due to the fact that even at a concentration of $100\,\mu M$ the half maximal effective concentration (EC_{50}) was not reached. Nevertheless, small to large effects in growth enhancement were statistically proven for concentrations $\geq 1\,\mu M$, confirming the hypothesized potency of the compound class. At the same time, previously assumed beneficial effects of 4-ANI onto *L. minor* were not confirmed, the compound is rather be considered inactive under the current assay conditions.

With additional, more diversely substituted quinazolinone derivatives, a tuning of *in vivo* activity was accomplished: An overall trend towards improved growth enhancement by substitution with electron-rich anilines in 2-position could be identified, while electron-deficient

anilines and pyrimidine-based substituents led to a diminishment in activity. Furthermore, different *N*-alkylations resulted in entirely inactive compounds, which provides a striking similarity to the insights obtained by PURNELL *et al.* on PARP inhibitors (see section 2.1.2) [42]. Electron-donating groups attached to the quinazolinone core seemed to preserve activity. Based on the gathered data, the earlier formulated structure-activity relationship (see section 2.2.4) could be refined into a more detailed pharmacophore connecting the observed activity to distinct structural features.

The presented investigations are based on the hypothesis of PARP enzymes being viable targets of small molecule effectors for the enhancement of water stress tolerance induction. By comparison of the "traditional" PARP pharmacophore (see section 2.1.2) and the defined quinazolinone motif neither proof nor disproof of this hypothesis are possible yet. While essential structural features of PARP inhibitors like the lactam group or the aromatic A-ring are still present in and mandatory for the activity of quinazolinones, the compounds found active also include important features exceeding the PARP pharmacophore. On the one hand, it is possible that enzymes of the PARP family are targeted by quinazolinones within *L. minor* and that their distinct binding motif requires these additional functional groups to enhance binding strength and facilitate an effective inhibition. On the other hand, entirely different targets and modes of action cannot be excluded yet: considering the fact that **C126** exhibits growth-enhancing activity under stress as well as non-stress conditions points to a general plant growth-promoting activity as described for several agrochemicals already in use (see section 1.3). These agents usually interfer with the plants' regulatory networks. Moreover, in the light of the central function of PARP/ART proteins within the plant cell, it is questionable to which extent their inhibition may prove beneficial towards plant growth under optimal, non-stress conditions.

In summary, the presented investigations have to be considered a starting point to in-depth investigations on a molecular level. While the phenotypical proof of action is now well established for a single plant species, profound conclusions about the mode of action can only be drawn through identification of the target(s) affected. If accomplished, these new insights ought to provide valuable approaches both towards the tuning of *in vivo* activity as well as a broad applicability of quinazolinone compounds in economically important crops.

5 Summary

The presented thesis follows a research project conducted in the group of Bioorganic Chemistry, Leibniz Institute of Plant Biochemistry in Halle, aiming at the identification of drought stress tolerance-inducing effects in small molecules by means of phenotypical screening. Aiming to confirm and extend previously gained knowledge, the main objective of the thesis lay in the investigation of a possible connection between plant PARP enzyme inhibition and an increase in drought stress tolerance induction.

Starting from the original setup of the *Lemna minor* bioassay, several improvements were implemented, targeting at a reduction in required time and manual labour, as well as a higher robustness in statistical evaluation and reliability of obtained results. To these ends, the assay duration was reduced while simultaneously dividing the term into a stress and a subsequent recovery phase. Through introduction of script-based batch processing of images with optical recognition of plants, a high level of automatization and accuracy could be achieved, while reducing manual efforts required in data evaluation to a minimum. Downstream data processing utilized effect size determinations to distinguish between small, medium and large drought stress tolerance-enhancing effects (or growth-accelerating effects in general) in a compound library comprising 119 compounds previously described to be promising candidates for inhibition of PARP enzymes, thus assumed to positively affect plant energy homeostasis under abiotic stress conditions. Both actives and inactives were subjected to replicate measurements that were combined in a meta-analytical fashion to yield a robust assessment of the compounds' *in vivo* activity. Detailed analysis of these screening results in relation to the structural features of the compounds allowed for the attribution of stress tolerance induction to two classes of heterocyclic structures, namely 2-substituted quinazolin-4(3*H*)-ones and 4-substituted phthalazin-1(2*H*)-ones, both with substituents derived from aniline.

Targeting the quinazolinone pharmacophore, previously undescribed 2-arylaminoquinazolin-4(3*H*)-ones were synthesized in a three-step sequence starting from anthranilic acid esters in order to further explore the potency of this compound class. In total, 23 compounds were synthesized exhibiting 3-point structural diversity with (a) varying aniline derivatives in 2-position, (b) different *N*-methylation patterns or (c) differing substitution patterns at the A-ring of the quinazolinone core. These products were analyzed regarding their stress tolerance-enhancing activity in the *in vivo* assay system, yielding small to large positive effects onto the plants. Further concentration-dependent activity profiling allowed for the refinement of the first proposed quinazolinone pharmacophore, attributing differences in the chemical nature of substitutions, their positions and patterns to either an enhancement or diminishment in biological activity.

The gathered data may be regarded a partial confirmation of a connection between the mandatory structural motifs of known PARP inhibitors and the observed *in vivo* stress tolerance-enhancing activity. However, based purely on the insights gained from the phenotypic assay, a mode of action involving inhibition of PARP enzymes by quinazolinone derivatives could neither be excluded nor confirmed. Follow-up studies are necessary to achieve identification of the molecular target(s) of the described quinazolinones and to yield a quantitative structure-activity-relationship beneficial for structural optimization.

6 Zusammenfassung

Die vorliegende Arbeit stellt die Fortführung eines Forschungsprojektes dar, welches in der Gruppe Natur- und Wirkstoffchemie des Leibniz-Instituts für Pflanzenbiochemie in Halle durchgeführt wurde. Zur Bestätigung und Erweiterung der daraus hervorgegangenen Erkenntnisse, lag der Fokus der Arbeit in der Untersuchung eines möglichen Zusammenhangs zwischen der Inhibition pflanzlicher PARP-Enzyme und einer verbesserten Trockenstresstoleranz.

Ausgehend vom usprünglich verwendeten Design des *Lemna minor*-Bioassays wurden einige Verbesserungen implementiert, welche sowohl die Dauer und den operativen Aufwand reduzieren, als auch zu einer robusteren statistischen Evaluation und einer höheren Verlässlichkeit der erhaltenen Resultate führen sollten. Um dies zu erreichen, wurde die Assaydauer reduziert und in eine Stress- und eine Erholungsphase geteilt. Durch die Einführung skriptbasierter Stapelverarbeitung von Bildern mit optischer Erkennung der Pflanzen konnte ein hohes Maß an Automatisierung und Genauigkeit erreicht werden, während die Notwendigkeit manueller Eingriffe im Rahmen der Datenverarbeitung auf ein Minimum reduziert wurde. Die nachfolgende Datenanalyse basiert auf der Bestimmung von Effektgrößen zur Unterscheidung geringer, mittlerer und starker Verbesserung der Trockenstresstoleranz (bzw. wachstumsfördernder Effekte im Allgemeinen) durch 119 Substanzen einer Screening-Bibliothek, welche im Vorfeld als vielversprechende Kandidaten für die Inhibition von PARP-Enzymen, und damit als mutmaßlich förderlich für den pflanzlichen Energiehaushalt unter abiotischem Stress, identifiziert wurden. Aktive sowie inaktive Substanzen wurden in wiederholten Messungen untersucht, welche in Art einer Meta-Analyse kombiniert wurden um eine möglichst verlässliche Aussage über die *in vivo*-Aktivität der Substanzen zu erhalten. Detaillierte Analyse dieser Ergebnisse in Bezug auf die strukturellen Eigenschaften der Verbindungen deutete auf Stresstoleranz-fördernde Aktivität in zwei Klassen heterocyclischer

Verbindungen hin, im Speziellen 2-substituierte Chinazolin-4(3*H*)-one und 4-substituierte Phthalazin-1(2*H*)-one, jeweils substituiert durch Abkömmlinge des Anilins.

Abzielend auf das Chinazolinon-Pharmakophor wurden vormals nicht beschriebene 2-Aryl-aminochinazolin-4(3*H*)-one in einer dreistufigen Sequenz ausgehend von Anthranilsäure-estern synthetisiert um die Potenz dieser Substanzklasse weitergehend zu untersuchen. Insgesamt wurden 23 Verbindungen synthetisiert, welche sich in drei strukturellen Merk-malen unterscheiden: (a) variierende Anilinderivate als -substituenten in 2-Position, (b) ver-schiedene Muster von *N*-Methylierungen und (c) unterschiedliche Substitutionsmuster am A-Ring des Chinazolinon-Grundkörpers. Die erhaltenen Produkte wurden im *in vivo*-Bioassay hinsichtlich ihrer Stresstoleranz-fördernden Aktivität untersucht, wobei geringe bis starke Effekte auf die Pflanzen festgestellt werden konnten. Weiterführende Untersuchungen zum konzentrationsabhängigen Aktivitätsprofil erlaubten die Verfeinerung des ersten vorgeschla-genen Chinazolinon-Pharmakophors, welches Unterschiede in der chemischen Natur von Substituenten, deren Position und Muster mit einer Steigerung bzw. Senkung der biologi-schen Aktivität in Verbindung bringt.

Die erhobenen Daten können als teilweise Bestätigung der Verbindung zwischen verbindlichen strukturellen Motiven bekannter PARP-Inhibitoren und der beobachteten *in vivo* Stresstoleranz-fördernden Aktivität betrachtet werden. Jedoch kann ausschließlich auf Grundlage der Ergebnisse des phänotypischen Screenings ein funktioneller Zusammenhang zwischen der beobachteten Aktivität und der Inhibition pflanzlicher PARP-Enzyme durch Chinazolinone weder ausgeschlossen noch bestätigt werden. Nachfolgende Studien sind nötig um die molekularen Targets der Chinazolinone identifizieren und quantitative Struktur-Aktivitäts-Beziehungen zur strukturellen Optimierung ableiten zu können.

7 Experimental Section

7.1 General remarks

If not stated otherwise, all working steps in relation to bioassays were carried out under sterile conditions inside a laminar flow cabinet. Plant growth media were sterilized by autoclaving (121 °C, 20 min). Materials and tools were either purchased as sterile or sterilized under identical conditions.

7.1.1 Chemicals and materials

All components for plant growth media were purchased from commercial suppliers in grades suitable for biological application. DMSO 99.9 % and MS medium were obtained from Duchefa Biochemie, Haarlem (Netherlands), PEG6000 (Ph. Eur.) and PEG8000 (Ph. Eur.) from Carl Roth GmbH & Co. KG, Karlsruhe (Germany). Screening compounds were obtained from Key Organics Ltd. (Highfield Road Industrial Estate Camelford, Cornwall PL32 9RA, UK). Bottle top sterile filters (PES, 0.2 μm) and 24-well and 12-well microtiter plates (Thermo Fisher Nunc© Multidish: PS, sterile, flat bottom, 128 x 86 mm) were obtained from VWR International GmbH, Darmstadt (Germany).

All reagents used in the synthetic procedures were obtained from commercial suppliers with a purity of at least 95 % and directly used without further purification. THF and dichloromethane were dried by distillation over suitable drying agents, following standard procedures, and stored over molecular sieves 3 Å. Anhydrous DMF was purchased from Sigma-Aldrich and stored over molecular sieves 3 Å. All other solvents were distilled in-house and dried, if necessary, over molecular sieves.

7.1.2 Instrumentation

Recording of *L. minor* assay images was carried out on a LemnaTec Scanalyser system using the built-in software. Images of size 1280 x 980 px were exported to the computer's hard drive. Batch analysis of image series was carried out using the software ImageJ (version 1.49v) using an appropriate algorithm (see 7.2.4, p. 107) [56].

Analytical thin-layer chromatography was conducted with silica coated aluminium plates (silica 60 F_{254}) obtained from Merck, Germany. Compound detection was achieved either by UV irradiation (254 nm) or staining and subsequent heating ($> 100\,°C$) using cerium(IV)-molybdatophosphoric acid.

One- and two-dimensional NMR spectra were recorded on Varian Mercury 300, 400 and 600 spectrometers. Chemical shifts are reported relative to tetramethylsilane (TMS) ($\delta = 0.00$) for ^{1}H spectra and DMSO ($\delta = 39.52$) or chloroform ($\delta = 77.16$) for ^{13}C spectra. Signal multiplicities are reported using the following abbreviations: s (singlet), d (duplet), t (triplet), q (quartet), m (multiplet).

Standard mass spectra were recorded on an API-150 device (Applied Biosystems) in positive and negative electrospray mode. High resolution mass spectra in both positive and negative mode were recorded either on a Bruker Apex III Fourier transform ion cyclotron resonance (FT-ICR) mass spectrometer (Bruker Daltonics, Billerica, USA) equipped with an external APOLLO electrospray ion source (Agilent Technologies, Santa Clara, USA), or an Orbitrap Elite mass spectrometer (Thermofisher Scientific, Bremen, Germany) equipped with an HESI electrospray ion source in positive or negative electrospray mode.

HPLC traces were recorded on a VWR Hitachi LaChrom Elite instrument (L-2 series) using a YMC C-18 column (150 x 4.6 mm, particle size: 5 μm, pore size: 120 Å). The eluents used were MeCN + 0.1 % TFA (A) and water + 0.1 % TFA (B) at a flow rate of 0.8 ml/min with the following gradient: 5 % A (4 min) / 5 % A → 100 % A (15 min) / 100 % A (5 min). Detection of the analytes was performed in the UV range at 254 nm. Signals present in the solvent blank were excluded upon determation of analyte purity.

7.2 Microtiter plate assay with *Lemna minor*

7.2.1 Culture medium and maintenance

Axenic cultures of *Lemna minor* were originally provided by the Canadian Phycological Culture Centre (strain number CPCC 490). Cultures were maintained under sterile conditions in 500 ml Erlenmeyer flasks, equipped with cellulose plugs in a Sanyo MLR-351H Environmental Test Chamber at constant illumination ($\sim 120\,\mu\text{mol} \cdot \text{m}^{-2} \cdot \text{s}^{-1}$, 27 °C). Every seven days, 10 – 15 plants were transferred to a new flask containing 200 ml of sterile STEINBERG medium with the composition given in table 12, p. 107. For the preparation of one litre of STEINBERG medium, 20 ml each of stock solutions 1 – 3 were mixed with 1 ml each of stock solutions 4 and 5. The mixture was diluted to 950 ml with distilled water, the pH was adjusted to 5.5 with 1 M hydrochloric acid, the solution was filled up to 1000 ml with distilled water and sterilized.

7.2.2 Stress medium

For the preparation of one litre of STEINBERG stress medium, the stock solutions were mixed as described above and diluted to 500 ml. Under stirring, 150 g PEG6000 were dissolved and the solution was further diluted to 950 ml with distilled water. After adjusting the pH to 5.5, the solution was filled up to 1000 ml and sterilized by suction filtration through a bottle top filter (PES, 0.2 μm pore size).

7.2.3 Preparation and maintenance of assay plates

A 24-well microtiter plate was divided horizontally and vertically into four groups of six wells each. Each well was equipped with 2 ml of stress medium and 2 μl of test substance (DMSO for control or compound stock in DMSO), resulting in a final DMSO concentration of 0.1 %. After all wells were filled, 20 ml of stress medium was spread within the cavity between the wells to reduce water evaporation from the medium within the wells. For each plate, three-fronded plants of comparable size were taken from a single culture flask using an inoculation loop and were distributed randomly across the wells. The plate was closed

Table 12: Composition of Steinberg medium (modified according to Altenburger)

Solution	Compound	M [g/mol]	Final medium		Stock
			β [mg/l]	c [mmol/l]	β [g/l]
1	KNO_3	101.12	350.00	3.461	17.50
	KH_2PO_4	136.09	90.00	0.661	4.50
	K_2HPO_4	174.18	12.60	0.072	0.63
2	$MgSO_4 \cdot 7\,H_2O$	246.37	100.00	0.406	5.00
3	$Ca(NO_3)_2 \cdot 4\,H_2O$	236.15	295.00	1.249	14.75
			β [μg/l]	c [μmol/l]	β [mg/l]
4	H_3BO_3	61.83	120.00	1.941	120.00
	$ZnSO_4 \cdot 7\,H_2O$	287.43	180.00	0.626	180.00
	$Na_2MoO_4 \cdot 2\,H_2O$	241.92	44.00	0.182	44.00
	$MnCl_2 \cdot 4\,H_2O$	197.84	180.00	0.910	180.00
5	$FeCl_3 \cdot 6\,H_2O$	270.21	760.00	2.813	760.00
	$Na_2EDTA \cdot 2\,H_2O$	372.24	1500.00	4.030	1500.00

and the lid was fixed with tape. Subsequently, the first image was taken. After incubation for 48 h the plate was opened, the wells were carefully drained using a pipette (Eppendorf, Germany) and refilled with 2 ml of PEG-free Steinberg medium after which the second image was taken. After further incubation for 24 h the third image was taken.

In a variation of the assay, 12-well plates were used, containing 4 μl of test substance (or DMSO) in 4 ml medium. Application of this setup is indicated in the text.

7.2.4 Imaging of assay plates, processing and statistical analysis

The following processing steps were applied to all assay images using the software ImageJ:

  ▷ enhance contrast

  ▷ split channels, select blue channel

  ▷ set treshold (method: "Intermodes")

  ▷ analyze particles (size: 900 – ∞, circularity: 0.10 – 1.00)

The results containing x and y coordinates as well as frond areas for each plant were saved into a text file.

Data processing, statistical analysis and graphical presentation of data was entirely performed using the open-source statistical software R version 3.5.2 (2018-12-20) [109], equipped with the following packages: bindrcpp (version 0.2.2), data.tree (version 0.7.8), dplyr (version 0.7.8), fitdistrplus (version 1.0-11), ggplot2 (version 3.1.0), ggstance (version 0.3.1), gridExtra (version 2.3), knitr (version 1.21), lsei (version 1.2-0), magrittr (version 1.5), MASS (version 7.3-51.1), Matrix (version 1.2-15), MBESS (version 4.4.3), metafor (version 2.0-0), moments (version 0.14), npsurv (version 0.4-0), plyr (version 1.8.4), reshape2 (version 1.4.3), stringr (version 1.3.1), survival (version 2.43-3), tibble (version 2.0.1), tidyr (version 0.8.2), xlsx (version 0.6.1).

7.3 Statistical inference and mathematical formalism

7.3.1 Basic statistical formulae

The following formulae apply to univariate samples assumed to be normally distributed.

Arithmetic mean:

$$\bar{x} = \frac{1}{n} \sum_{i=1}^{n} x_i$$

Median:

$$\tilde{x} = \begin{cases} x_{\frac{n+1}{2}} & \text{for odd } n \\ \frac{1}{2}\left(x_{\frac{n}{2}} + x_{\frac{n}{2}+1}\right) & \text{for even } n \end{cases}$$

Standard deviation:

$$s = \sqrt{\frac{\sum_{i=1}^{n}(x_i - \bar{x})^2}{n-1}}$$

Median absolute deviation:

$$MAD = \text{median}(|x_i - \tilde{x}|)$$

Confidence interval of the arithmetic mean:

$$CI = \bar{x} \pm \frac{s}{\sqrt{n}} \cdot t_{1-\frac{\alpha}{2}, n-1}$$

7.3.2 Derivation of a mean effect size across experiments

The following formalism is derived from [79, 80, 78]. For the calculation of the mean effect size $\overline{d}$ across i experiments with effect sizes d_i, the simple sampling error of each measurement is needed which is defined as

$$V_i = \frac{N_T + N_C}{N_T N_C} + \frac{d_i^2}{2(N_T + N_C)}.$$

Group sizes $N_T = N_C = 6$ are held constant throughout the screening, therefore

$$V_i = \frac{6+6}{6 \cdot 6} + \frac{d_i^2}{2(6+6)} = \frac{8 + d_i^2}{24}$$

The weighting factor ω is the reciprocal of the simple sampling error:

$$\omega_i = \frac{1}{V_i} = \frac{24}{8 + d_i^2}$$

The standard error of the mean effect size defined as

$$SE_{\overline{d}} = \sqrt{\sum \frac{1}{\omega_i}} = \sqrt{\sum \frac{8 + d_i^2}{24}}$$

can be used to construct the 95 % confidence interval for the mean effect size:

$$\overline{d} - 1.96 \cdot SE_{\overline{d}} \leq \overline{d} \leq \overline{d} + 1.96 \cdot SE_{\overline{d}}$$

7.4 Synthetic procedures

7.4.1 The cyanamide route

N-(4-Methoxyphenyl)-thiourea (27, BER193)
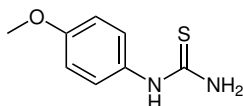
To a solution of potassium thiocyanate (2.48 g, 25 mmol) in dry acetone (30 ml), benzoyl chloride (2.56 ml, 22 mmol) was added dropwise upon which a white precipitate formed immediately. The suspension was heated to reflux (oil bath) for 10 min, then the oil bath was removed and *p*-anisidine (2.49 g, 20 mmol) was added pinchwise. The mixture was refluxed for further 30 min, then cooled to room temperature, poured on ice and stirred for 30 min. The product was filtered off, washed with water and directly added to preheated (80 °C) sodium hydroxide solution (50 ml, 10 % w/v). The solution was stirred for 1.5 h, then cooled to room temperature and poured on ice. After acidification with hydrochloric acid (5 M, pH ~ 3), the pH was adjusted to ~ 10 with ammonia solution (25 %). After stirring for 30 min, the product was filtered off, washed with water and dried *in vacuo*. Further purification was not necessary.

N-(4-Methoxyphenyl)thiourea (27, BER193)
Yield 96 % (off-white solid);
^{1}H-NMR (400 MHz, DMSO-d_6) δ 9.46 (s, 1 H), 7.23 (d, $J = 8.7$ Hz, 2 H), 6.90 (d, $J = 8.9$ Hz, 2 H), 3.74 (s, 3 H); **^{13}C-NMR** (100 MHz, DMSO-d_6) δ 181.12, 156.56, 131.71, 125.52, 113.96, 55.23; **HR-MS** *m/z* 183.0590 (found), 183.0587 (calc.) [M+H]$^+$;

2-Amino-3-(4-methoxyphenyl)-quinazolin-4(3*H*)-one (29, BER220)
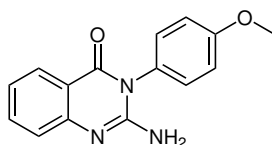
Compound **27** (547 mg, 3.00 mmol) and triethylamine (846 μl, 6.05 mmol) were dissolved in 15 ml ethyl acetate and cooled to 0 °C (ice bath). A solution of iodine (763 mg, 3.00 mmol) in

10 ml ethyl acetate was added dropwise over a period of 20 min. The ice bath was removed and the reaction mixture was stirred for 30 min at room temperature. Then, the mixture was filtered into a separation funnel, the filter was washed with additional ethyl acetate (70 ml) and diethyl ether (50 ml). The organic phase was washed with water and brine (100 ml each), dried over sodium sulfate and eventually *in vacuo*.

2-Aminobenzonitrile (362 mg, 3.00 mmol) was then added to the dried product, the flask was sealed and flushed with nitrogen. Under nitrogen atmosphere, the reagents were dissolved in 20 ml of dry dioxane and hydrogen chloride solution in dioxane (4 M, 1.00 ml) was added through a syringe. The reaction mixture was heated to 80 °C for 6 h, then diluted with 80 ml of water and stirred at room temperature for further 2 h. The pH was adjusted to ~ 7 and the product was extracted with ethyl acetate (3 x 80 ml). The combined organic phases were dried over sodium sulfate, then *in vacuo*. Column chromatography with hexane/acetone (1:1) as eluent yielded the pure title compound.

2-Amino-3-(4-methoxyphenyl)-quinazolin-4(3*H*)-one (29, BER220)
Yield 62 % (off-white solid);
^{1}H-NMR (600 MHz, DMSO-d_6) δ 7.88 (dd, $J = 7.9, 1.3$ Hz, 1 H), 7.60 (ddd, $J = 8.5, 7.1, 1.6$ Hz, 1 H), 7.29 – 7.24 (m, 2 H), 7.23 (d, $J = 7.9$ Hz, 1 H), 7.13 – 7.07 (m, 3 H), 6.26 (s, 2 H), 3.83 (s, 3 H); **^{13}C-NMR** (150 MHz, DMSO-d_6) δ 162.01, 159.47, 152.04, 150.11, 134.30, 129.90, 127.85, 126.50, 123.86, 121.36, 116.77, 115.15, 55.38; **HR-MS** m/z 268.1078 (found), 268.1081 (calc.) [M+H]$^+$;

7.4.2 Precursors to 2-(arylamino)-quinazolin-4(3*H*)-ones

2-Thioxo-2,3-dihydroquinazolin-4(1*H*)-one (24, BER242)
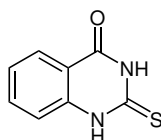
To a well stirred solution of potassium thiocyanate (6.20 g, 62.5 mmol) in 75 ml dry acetone was added benzoyl chloride (6.41 ml, 55.0 mmol) dropwise and the mixture was heated to reflux (oil bath). After 15 min the oil bath was removed and ethyl anthranilate (7.47 ml, 50.0 mmol) was added dropwise. The mixture was refluxed for further 60 min, poured on

ice water (350 ml) and stirred for 30 min. The precipitate was filtered off, washed with water and added portionwise to preheated (80 °C) sodium hydroxide solution (125 ml, 10 % w/v) with stirring. After complete dissolution, the mixture was stirred for further 30 min, cooled to room temperature, then poured on ice. The pH was adjusted to 2 – 3 with conc. hydrochloric acid and the mixture was stirred for 30 min. Finally, the product was filtered off, washed with water and recrystallized from DMF/water.

2-Thioxo-2,3-dihydroquinazolin-4(1H)-one (24, BER242)

Yield 94 % (white needles);

^{1}H-NMR (400 MHz, DMSO-d_6) δ 12.82 – 12.31 (m, 2H), 7.93 (dd, $J = 7.9$, 1.2 Hz, 1H), 7.73 (ddd, $J = 8.5$, 7.4, 1.5 Hz, 1H), 7.39 – 7.29 (m, 2H); **^{13}C-NMR** (100 MHz, DMSO-d_6) δ 174.28, 159.61, 140.42, 135.37, 126.72, 124.35, 116.18, 115.84; **HR-MS** m/z 177.0123 (found), 177.0128 (calc.) [M-H]$^-$;

2-(Methylthio)-quinazolin-4(3H)-one (25, BER239)
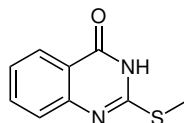
To a stirred suspension of sodium hydride (60 % suspension in mineral oil, 1.60 g, 40 mmol) in dry DMF (60 ml) at room temperature (water bath), compound **24** (7.13 g, 40 mmol) was added pinchwise. Upon complete dissolution, methyl iodide (2.49 ml, 40 mmol) was added dropwise and the mixture was heated to 40 °C for 3 h. After that, the mixture was cooled to room temperature, poured on ice and stirred for 30 min. The precipitated product was filtered off and washed with water and diethyl ether. Following recrystallization from DMF/water, the pure title compound was obtained.

2-(Methylthio)-quinazolin-4(3H)-one (25, BER239)

Yield 90 % (white needles);

^{1}H-NMR (400 MHz, DMSO-d_6) δ 12.58 (s, 1H), 8.04 (dd, $J = 7.9$, 1.2 Hz, 1H), 7.80 – 7.72 (m, 1H), 7.54 (d, $J = 8.1$ Hz, 1H), 7.45 – 7.38 (m, 1H), 2.58 (s, 3H); **^{13}C-NMR** (100 MHz, DMSO-d_6) δ 161.14, 156.33, 148.39, 134.55, 126.02, 125.93, 125.53, 119.89, 12.72; **HR-MS** m/z 191.0282 (found), 191.0285 (calc.) [M-H]$^-$;

General procedure A: Esterification of substituted nitroanthranilic acids (38a – 38b)

To a solution of nitro-substituted anthranilic acid (9.11 g, 50 mmol) in methanol (135 ml), conc. sulfuric acid (2.67 ml, 50 mmol) was added dropwise at room temperature. The mixture was refluxed for 72 – 96 h until complete conversion of the starting material was observed (judged by TLC). The reaction mixture was cooled to room temperature, then put into an ice bath. The pH of the mixture was adjusted to ~ 10 using sodium hydroxide solution (1 M) prior to extraction with ethyl acetate (4 x 200 ml). The combined organic phases were dried over sodium sulfate, the solvent was evaporated *in vacuo.*
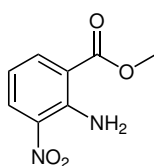
3-Nitro-2-aminobenzoic acid (38a, BER399)

Yield quantitative (red-orange solid);

^{1}H-NMR (400 MHz, Chloroform-*d*) δ 8.45 (s, 2 H), 8.38 (dd, $J = 8.4$, 1.7 Hz, 1 H), 8.24 (dd, $J = 7.7$, 1.7 Hz, 1 H), 6.65 (t, $J = 8.1$ Hz, 1 H), 3.92 (s, 3 H); **^{13}C-NMR** (100 MHz, Chloroform-*d*) δ 167.57, 147.44, 139.48, 133.39, 132.40, 114.56, 114.10, 52.41;
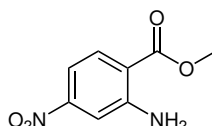
4-Nitro-2-aminobenzoic acid (38b, BER383)

Yield quantitative (orange solid);

^{1}H-NMR (400 MHz, Chloroform-*d*) δ 8.00 (d, $J = 8.8$ Hz, 1 H), 7.50 (d, $J = 2.3$ Hz, 1 H), 7.40 (dd, $J = 8.8$, 2.2 Hz, 1 H), 6.05 (s, 2 H), 3.92 (s, 3 H); **^{13}C-NMR** (100 MHz, Chloroform-*d*) δ 167.26, 151.34, 150.67, 132.81, 114.92, 111.11, 110.06, 52.19;
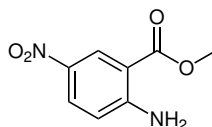
5-Nitro-2-aminobenzoic acid (38c, BER392)

Yield quantitative (yellow solid);

^{1}H-NMR (400 MHz, Chloroform-*d*) δ 8.83 (d, $J = 2.7$ Hz, 1 H), 8.13 (dd, $J = 9.2$, 2.7 Hz, 1 H),

6.67 (d, $J = 9.1\,\text{Hz}$, 1 H), 6.54 (s, 2 H), 3.93 (s, 3 H); ^{13}**C-NMR** (100 MHz, Chloroform-d) δ 167.21, 154.69, 137.29, 129.20, 128.88, 116.19, 116.12, 109.24, 52.15;

7-Nitro-2-thioxo-2,3-dihydroquinazolin-4(1H)-one (39b, BER386)
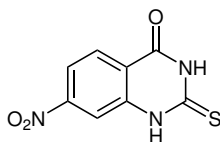
To a well stirred solution of potassium thiocyanate (6.08 g, 62.5 mmol) in 125 ml dry acetone was added benzoyl chloride (6.38 ml, 55.0 mmol) dropwise and the mixture was heated to reflux (oil bath). After 15 min, the oil bath was removed and compound **38b** (9.81 g, 50.0 mmol) was added pinchwise. The mixture was refluxed for further 3 h, poured on ice water (350 ml) and stirred for 30 min. The precipitate was filtered off and suspended in methanol (150 ml), to which sodium methoxide (25 % w/v in methanol, 20 ml) was added. The mixture was heated to 50 °C and stirred for 20 min, then cooled to room temperature and poured on ice. The pH was adjusted to ~ 4 with conc. hydrochloric acid and the mixture was stirred for 30 min. Finally, the precipitated product was filtered off, washed with diethyl ether (2 x 200 ml) and dried *in vacuo*.

7-Nitro-2-thioxo-2,3-dihydroquinazolin-4(1H)-one (39b, BER386)
Yield yellow solid (98 %);
^{1}**H-NMR** (400 MHz, DMSO-d_6) δ 12.88 (m, 2 H), 8.16 – 7.99 (m, 3 H); ^{13}**C-NMR** (100 MHz, DMSO-d_6) δ 175.15, 158.55, 151.16, 140.88, 128.93, 120.57, 117.93, 111.08; **HR-MS** m/z 221.9977 (found), 221.9979 (calc.) [M-H]$^-$;

6-Nitro-2-thioxo-2,3-dihydroquinazolin-4(1H)-one (39c, BER396)
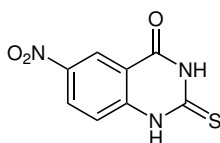
To a well stirred solution of potassium thiocyanate (5.38 g, 55.4 mmol) in 125 ml dry acetone was added benzoyl chloride (5.65 ml, 48.7 mmol) dropwise and the mixture was heated to reflux (oil bath). After 15 min the oil bath was removed and compound **38c** (8.69 g,

44.3 mmol) was added pinchwise. The mixture was refluxed for further 3 h, poured on ice water (350 ml) and stirred for 30 min. The precipitate was filtered off and suspended in methanol (150 ml) to which then sodium methoxide (25 % w/v in methanol, 20 ml) was added. The mixture was heated to 50 °C and stirred for 20 min, then cooled to room temperature and poured on ice. The pH was adjusted to ~ 2 with conc. hydrochloric acid and the mixture was stirred for 30 min. Finally, the crude product was filtered off, dried *in vacuo* and recrystallized from DMF/water. The product was isolated as 1:1-complex with DMF (judged by NMR analysis).

6-Nitro-2-thioxo-2,3-dihydroquinazolin-4(1*H*)-one (39c, BER396)

Yield yellow solid (62 %);

^{1}H-NMR (400 MHz, DMSO-d_6) δ 13.10 (s, 1 H), 12.88 (s, 1 H), 8.58 (d, $J = 2.6$ Hz, 1 H), 8.51 (dd, $J = 9.0, 2.7$ Hz, 1 H), 7.95 (s, 1 H), 7.48 (d, $J = 9.0$ Hz, 1 H), 3.32 (s, 2 H), 2.73 (s, 3 H); **^{13}C-NMR** (100 MHz, DMSO-d_6) δ 175.50, 162.25, 158.57, 144.45, 142.83, 129.88, 122.75, 117.27, 116.46, 35.74, 30.73; **HR-MS** m/z 221.9980 (found), 221.9979 (calc.) [M-H]$^-$;

**7-Nitro-2-(methylthio)-quinazolin-4(3*H*)-one (40b, BER408)**
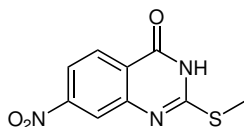
To a stirred suspension of sodium hydride (60 % suspension in mineral oil, 1.77 g, 44.3 mmol) in dry DMF (50 ml) at room temperature (water bath) was slowly added compound **39b** (9.89 g, 44.3 mmol). Upon complete dissolution, methyl iodide (2.76 ml, 44.3 mmol) was added dropwise and the mixture was stirred for 3 h at 45 °C. After that, the mixture was cooled to room temperature, poured on ice, acidified with few drops of conc. hydrochloric acid and stirred for 30 min. The product was filtered off and washed with water. Following recrystallization from DMF/water the pure title compound was obtained.

7-Nitro-2-(methylthio)-quinazolin-4(3*H*)-one (40b, BER408)

Yield yellow solid (38 %);

^{1}H-NMR (400 MHz, DMSO-d_6) δ 12.98 (s, 1 H), 8.27 – 8.07 (m, 3 H), 2.60 (s, 3 H); **^{13}C-NMR**

(100 MHz, DMSO-d_6) δ 160.03, 159.47, 151.16, 148.64, 128.25, 124.26, 120.73, 118.97, 12.85; **HR-MS** m/z 236.0140 (found), 236.0135 (calc.) [M-H]$^-$;

6-Nitro-2-(methylthio)-quinazolin-4(3*H*)-one (40c, BER407)
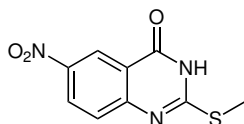
To a stirred suspension of sodium hydride (1.00 g, 25 mmol, 60 % suspension in mineral oil) in dry DMF (40 ml) at room temperature (water bath) was slowly added compound **39c** (7.41 g, 25 mmol). Upon complete dissolution, methyl iodide (1.56 ml, 25 mmol) was added dropwise and the mixture was stirred for 7 h at 55 °C. After that the mixture was cooled to room temperature, poured on ice, acidified with few drops of conc. HCl and stirred for 30 min. The product was filtered off and washed with water. Following recrystallization from DMF/water the pure title compound was obtained.

6-Nitro-2-(methylthio)-quinazolin-4(3*H*)-one (40c, BER407)

Yield yellow solid (94 %);

^{1}H-NMR (400 MHz, DMSO-d_6) δ 13.06 (s, 1 H), 8.69 (d, $J = 2.7$ Hz, 1 H), 8.46 (dd, $J = 9.0, 2.8$ Hz, 1 H), 7.66 (d, $J = 9.0$ Hz, 1 H), 2.61 (s, 3 H); **^{13}C-NMR** (100 MHz, DMSO-d_6) δ 161.44, 160.16, 152.29, 143.77, 128.57, 127.50, 122.21, 119.82, 12.95; **HR-MS** m/z 236.0133 (found), 236.0135 (calc.) [M-H]$^-$;

7.4.3 2-(Arylamino)-quinazolin-4(3*H*)-ones

General Procedure B: synthesis of 2-(arylamino)-quinazolin-4(3*H*)-ones (31a – 31o)

A solution of compound **25** (961 mg, 5.0 mmol) and aryl amine (7.5 mmol) in glacial acetic acid (7.5 ml) was heated to reflux under stirring for the time given in tbl. 8 (p. 63), while checking conversion of starting materials by TLC. Where indicated, additional 2.5 mmol of aryl amine were added within the first 2 h of the reaction. If product started to precipitate during the course of the reaction, acetic acid was added dropwise to keep the reaction mixture from solidifying. After the indicated time, the heating was removed and water was added dropwise under stirring until a fine precipitate formed. The slurry was cooled to room temperature and additional water was added until a volume of 80 – 90 ml was reached. The mixture was cooled in the fridge for at least 3 h, the crude product was filtered off.

If the filtrate was free of product (judged by ESI-MS), the crude product was dried *in vacuo* and directly recrystallized from the solvent mixtures indicated in tbl. 8 (p. 63). If product could still be found in the filtrate, it was extracted once with dichloromethane and ethyl acetate (125 ml each). The crude product and the organic phases were combined, the solvent was removed *in vacuo* and pure products were obtained by recrystallization.
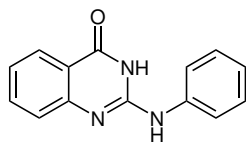
2-(Phenylamino)-quinazolin-4(3*H*)-one (31a, BER291)

Yield 79 % (white solid);

¹H-NMR (400 MHz, DMSO-d_6) δ 10.80 (s, 1H), 8.64 (s, 1H), 7.97 (dd, $J = 7.9$, 1.0 Hz, 1H), 7.75 (d, $J = 7.9$ Hz, 2H), 7.69 – 7.62 (m, 1H), 7.41 (d, $J = 8.1$ Hz, 1H), 7.36 (t, $J = 7.9$ Hz, 2H), 7.27 – 7.20 (m, 1H), 7.05 (t, $J = 7.3$ Hz, 1H); **¹³C-NMR** (100 MHz, DMSO-d_6) δ 161.55, 149.98, 147.35, 138.94, 134.43, 128.81, 125.85, 125.32, 123.03, 122.45, 119.26, 118.36; **HR-MS** m/z 236.0829 (found), 236.0829 (calc.) [M-H]⁻; **Purity** (HPLC, 254 nm) 99.3 %;
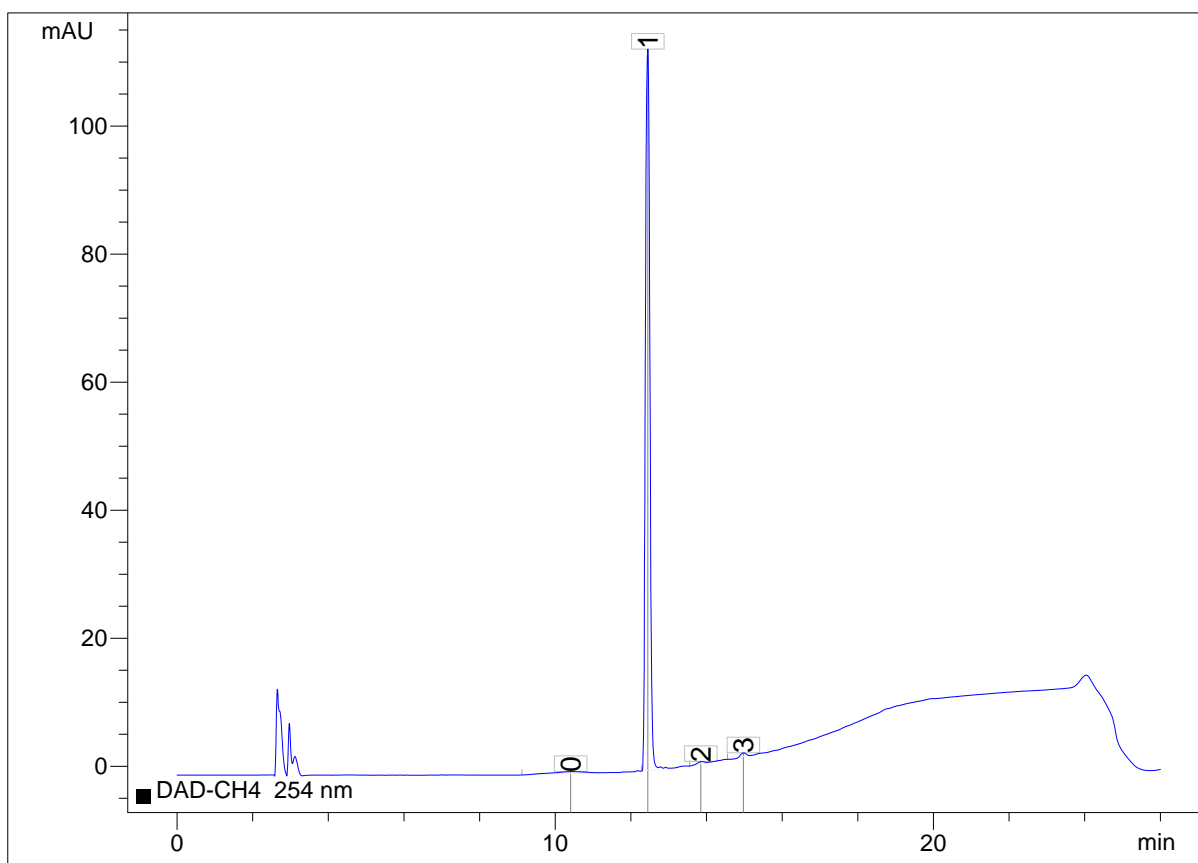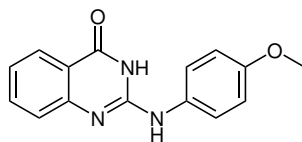
2-((4-Methoxyphenyl)amino)-quinazolin-4(3*H*)-one (31b, BER292)

Yield 94 % (off-white solid);

¹H-NMR (400 MHz, DMSO-d_6) δ 10.76 (s, 1 H), 8.46 (s, 1 H), 7.95 (dd, J = 8.0, 1.2 Hz, 1 H), 7.69 – 7.54 (m, 3 H), 7.34 (d, J = 8.1 Hz, 1 H), 7.20 (t, J = 7.4 Hz, 1 H), 6.98 – 6.89 (m, 2 H), 3.75 (s, 3 H); **¹³C-NMR** (100 MHz, DMSO-d_6) δ 161.69, 155.04, 150.26, 147.75, 134.34, 131.81, 125.88, 125.11, 122.66, 121.41, 118.14, 114.01, 55.21; **HR-MS** m/z 266.0926 (found), 266.0935 (calc.) [M-H]$^-$; **Purity** (HPLC, 254 nm) 98.9 %;
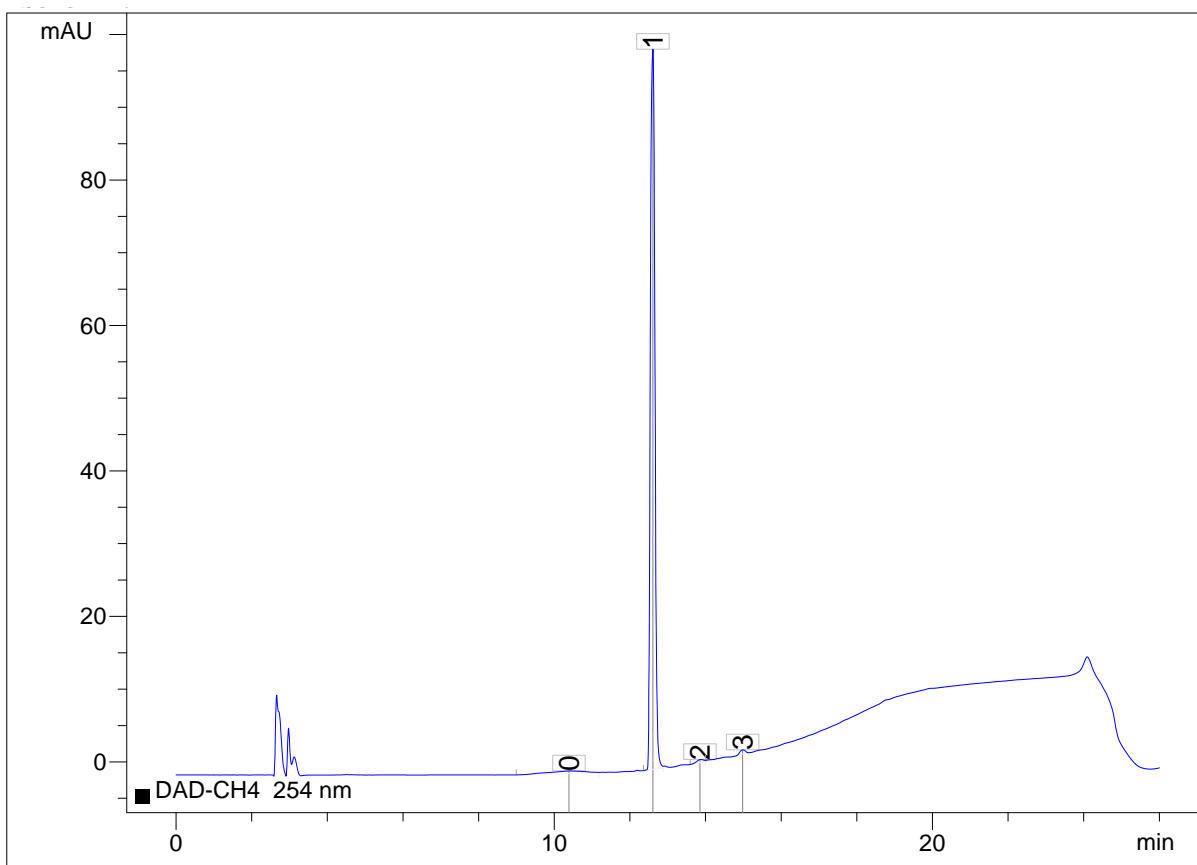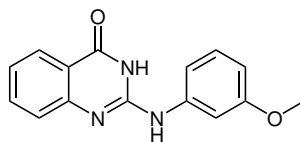
2-((3-Methoxyphenyl)amino)-quinazolin-4(3*H*)-one (31c, BER293)

Yield 88 % (off-white solid);

¹H-NMR (400 MHz, DMSO-d_6) δ 10.77 (s, 1 H), 8.66 (s, 1 H), 7.97 (dd, $J = 7.8, 1.0$ Hz, 1 H), 7.71 – 7.63 (m, 1 H), 7.60 (s, 1 H), 7.42 (d, $J = 8.1$ Hz, 1 H), 7.29 – 7.21 (m, 2 H), 7.15 (d, $J = 8.1$ Hz, 1 H), 6.63 (dd, $J = 8.1, 2.0$ Hz, 1 H), 3.79 (s, 3 H); **¹³C-NMR** (100 MHz, DMSO-d_6) δ 161.50, 159.64, 149.87, 147.25, 140.12, 134.46, 129.54, 125.84, 125.38, 123.12, 118.37, 111.45, 107.83, 105.07, 54.97; **HR-MS** m/z 266.0938 (found), 266.0935 (calc.) [M-H]⁻; **Purity** (HPLC, 254 nm) 99.2 %;
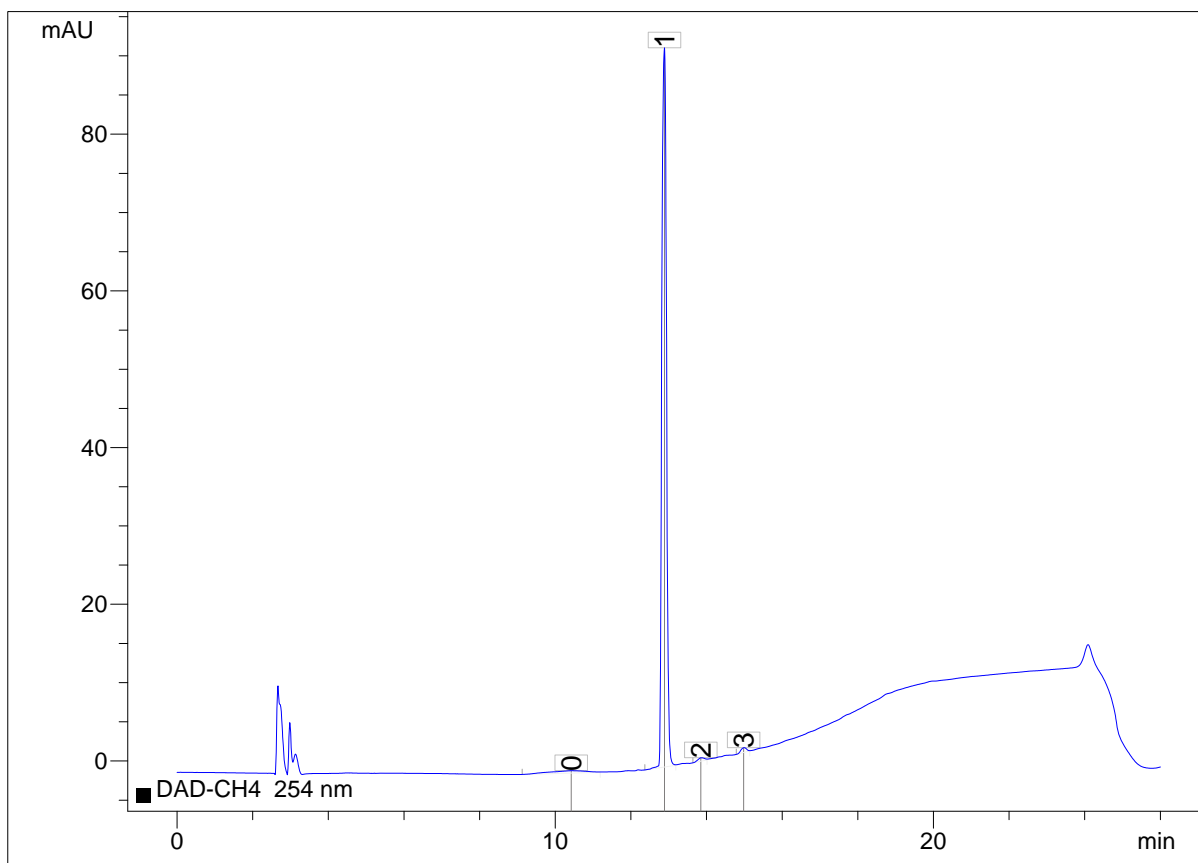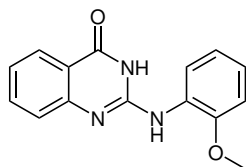
2-((2-Methoxyphenyl)amino)-quinazolin-4(3*H*)-one (31d, BER287)

Yield 79 % (white solid);

¹H-NMR (400 MHz, DMSO-d_6) δ 11.46 (s, 1 H), 8.69 (d, $J = 8.6$ Hz, 1 H), 8.35 (s, 1 H), 7.97 (dd, $J = 7.8, 0.9$ Hz, 1 H), 7.70 – 7.62 (m, 1 H), 7.43 (d, $J = 8.2$ Hz, 1 H), 7.29 – 7.19 (m, 1 H), 7.10 – 6.95 (m, 3 H), 3.91 (s, 3 H); **¹³C-NMR** (100 MHz, DMSO-d_6) δ 161.59, 149.97, 148.08, 147.42, 134.38, 127.99, 125.82, 125.38, 123.04, 122.46, 120.51, 119.39, 118.40, 110.74, 55.92; **HR-MS** m/z 266.0936 (found), 266.0935 (calc.) [M-H]⁻; **Purity** (HPLC, 254 nm) 98.9 %;
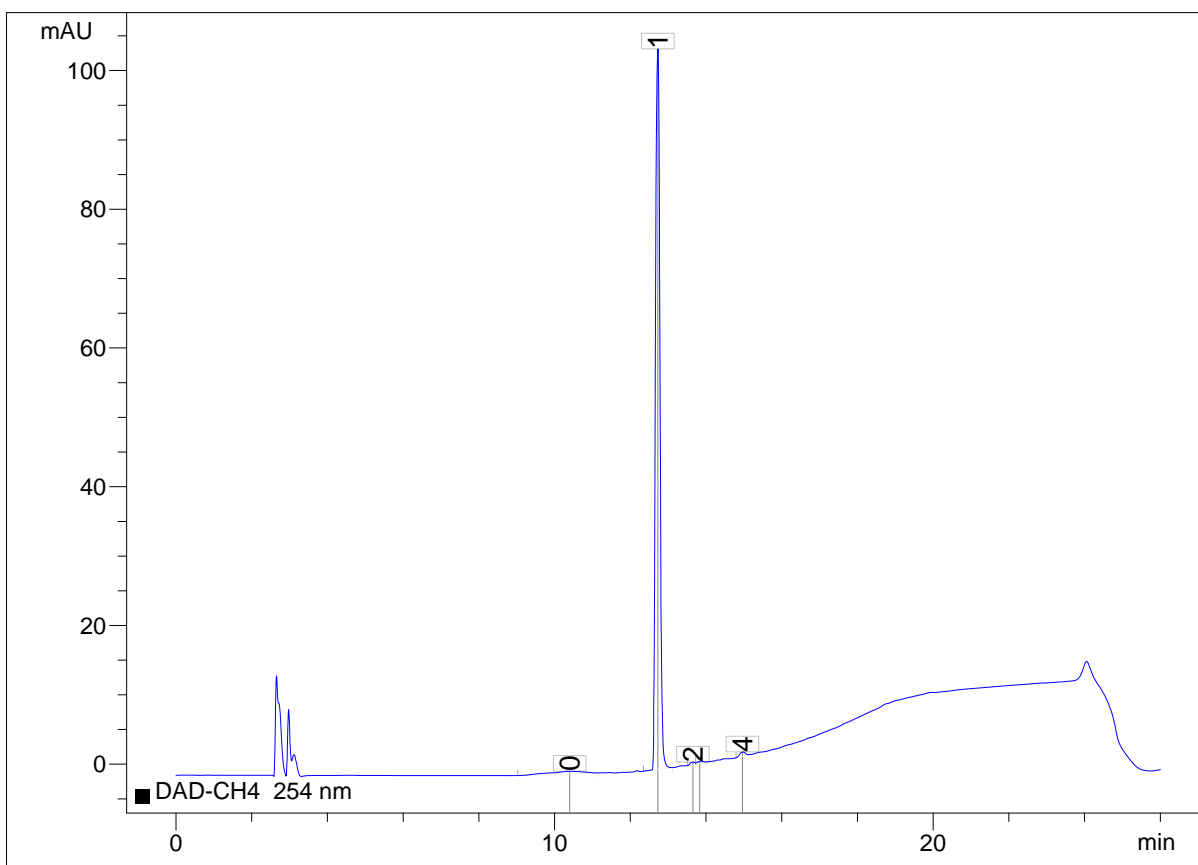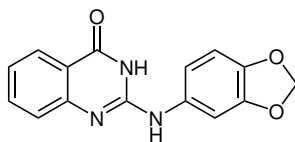
2-((3,4-Methylenedioxyphenyl)amino)-quinazolin-4(3*H*)-one (31e, BER299)

Yield 65 % (off-white solid);

¹H-NMR (400 MHz, DMSO-d_6) δ 10.75 (s, 1 H), 8.52 (s, 1 H), 7.95 (dd, J = 7.9, 1.0 Hz, 1 H), 7.68 – 7.59 (m, 1 H), 7.54 (d, J = 1.9 Hz, 1 H), 7.37 (d, J = 8.0 Hz, 1 H), 7.25 – 7.17 (m, 1 H), 6.98 (dd, J = 8.4, 2.0 Hz, 1 H), 6.89 (d, J = 8.3 Hz, 1 H), 6.02 (s, 2 H); **¹³C-NMR** (100 MHz, DMSO-d_6) δ 161.58, 150.07, 147.60, 147.18, 142.65, 134.41, 133.17, 125.84, 125.18, 122.81, 118.22, 112.49, 108.09, 102.22, 101.00; **HR-MS** m/z 280.0730 (found), 280.0728 (calc.) [M-H]⁻; **Purity** (HPLC, 254 nm) 98.9 %;
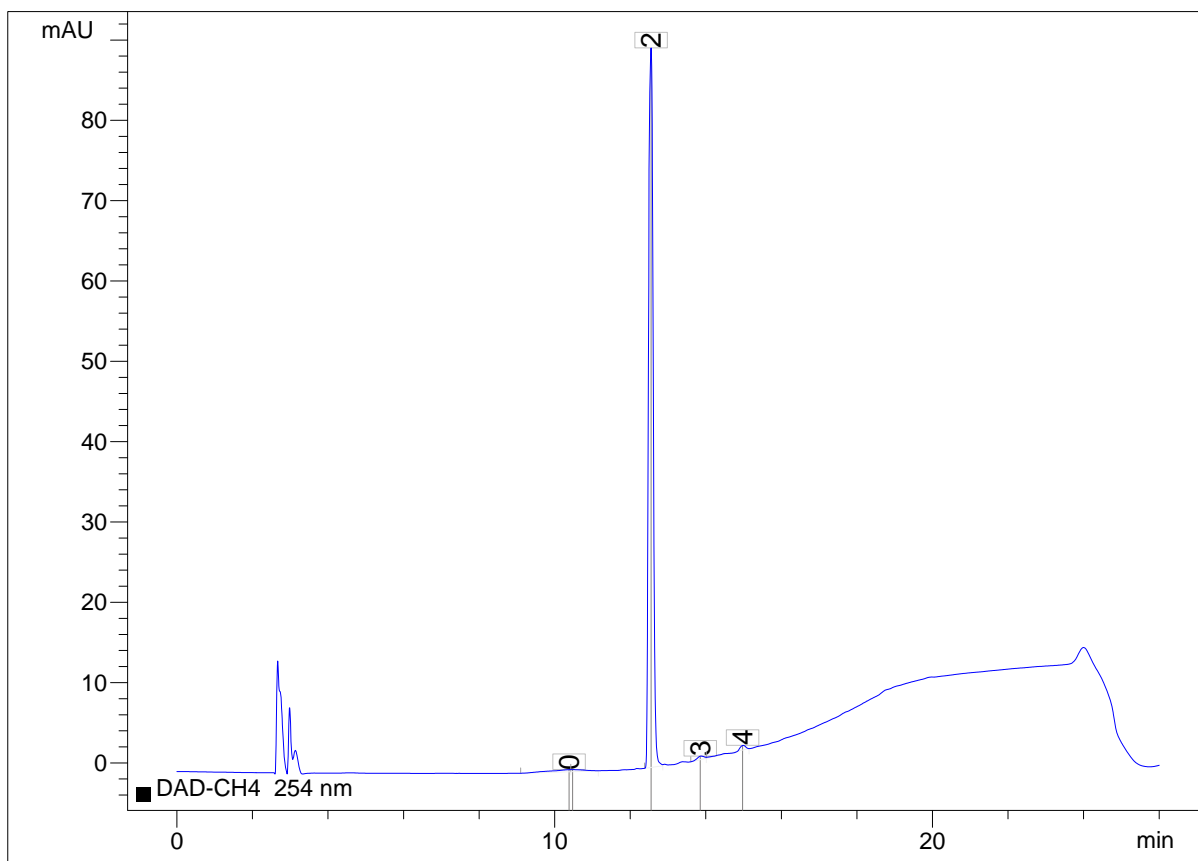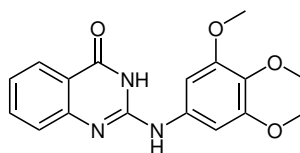
2-((3,4,5-Trimethoxyphenyl)amino)-quinazolin-4(3*H*)-one (31f, BER300)

Yield 43 % (white solid);

¹H-NMR (400 MHz, DMSO-d_6) δ 10.77 (s, 1H), 8.61 (s, 1H), 7.97 (dd, $J = 7.9, 0.9$ Hz, 1H), 7.69 – 7.62 (m, 1H), 7.41 (d, $J = 8.0$ Hz, 1H), 7.26 – 7.20 (m, 1H), 7.14 (s, 2H), 3.81 (s, 6H), 3.64 (s, 3H); **¹³C-NMR** (100 MHz, DMSO-d_6) δ 161.58, 152.77, 149.88, 147.36, 134.95, 134.44, 132.87, 125.83, 125.43, 123.01, 118.29, 97.23, 60.12, 55.73; **HR-MS** m/z 326.1143 (found), 326.1146 (calc.) $[M\text{-}H]^-$; **Purity** (HPLC, 254 nm) 99.1 %;
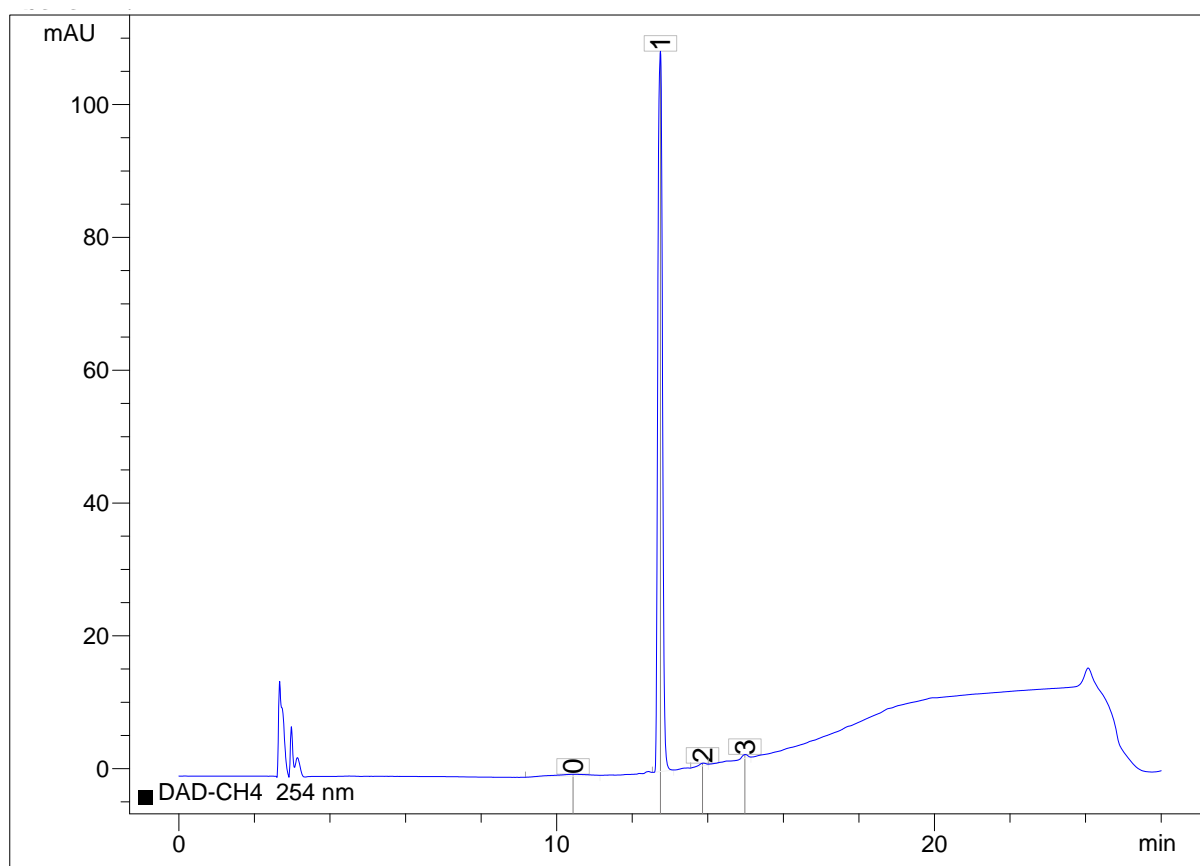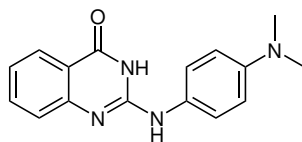
2-((4-(Dimethylamino)phenyl)amino)-quinazolin-4(3*H*)-one (31g, BER294)

Yield 81 % (blue-grey solid);

¹H-NMR (400 MHz, DMSO-d_6) δ 10.69 (s, 1 H), 8.28 (s, 1 H), 7.93 (d, $J = 7.2$ Hz, 1 H), 7.66 – 7.55 (m, 1 H), 7.49 (d, $J = 8.9$ Hz, 2 H), 7.30 (d, $J = 8.1$ Hz, 1 H), 7.17 (t, $J = 7.4$ Hz, 1 H), 6.75 (d, $J = 9.0$ Hz, 2 H), 2.87 (s, 6 H); **¹³C-NMR** (100 MHz, DMSO-d_6) δ 161.67, 150.52, 147.94, 146.96, 134.31, 128.32, 125.84, 125.00, 122.33, 121.60, 118.01, 112.88, 40.55; **HR-MS** m/z 279.1253 (found), 279.1251 (calc.) $[\text{M-H}]^-$; **Purity** (HPLC, 254 nm) 98.2 %;
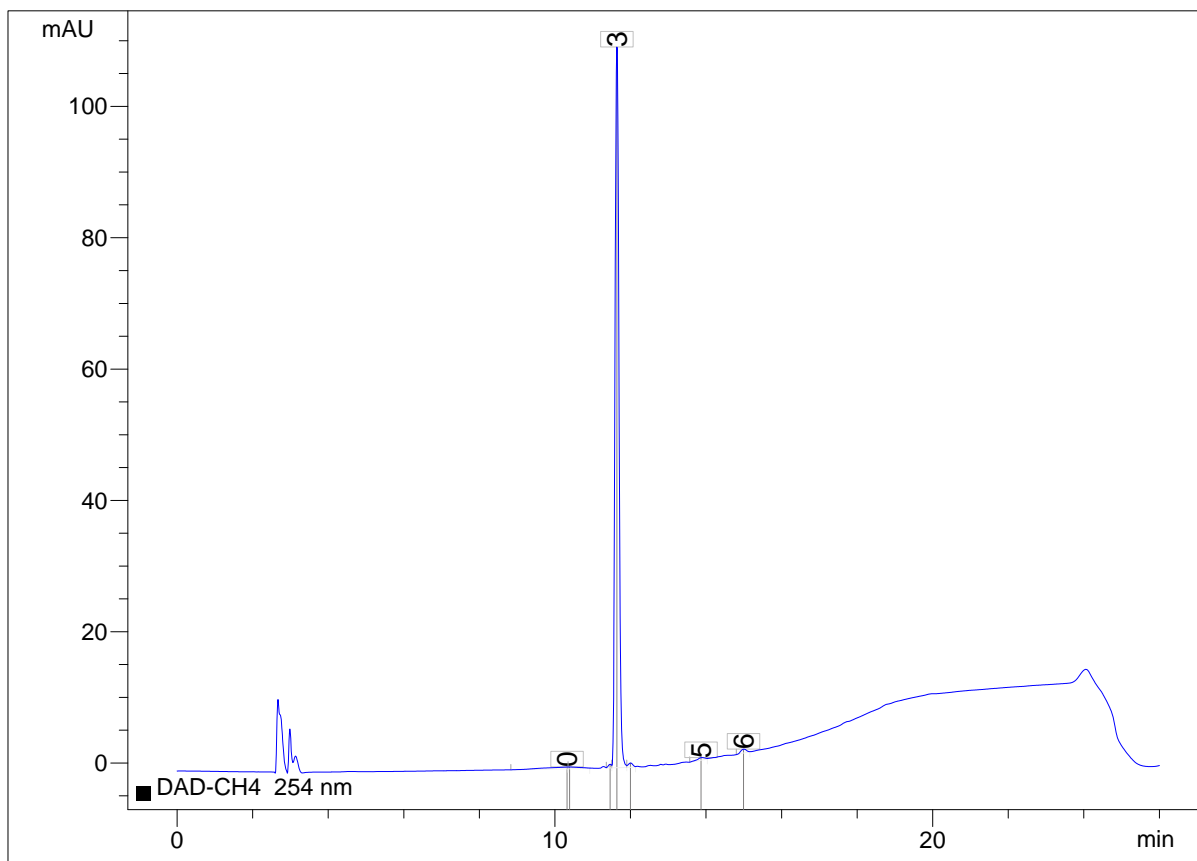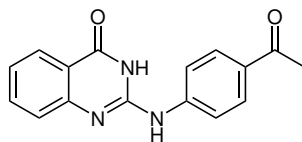
2-((4-Acetylphenyl)amino)-quinazolin-4(3*H*)-one (31h, BER328)

Yield 59 %, prepared in 15 mmol scale (yellowish solid);

^{1}H-NMR (400 MHz, DMSO-d_6) δ 10.93 (s, 1 H), 9.09 (s, 1 H), 8.03 – 7.85 (m, 5 H), 7.74 – 7.66 (m, 1 H), 7.48 (d, $J = 8.1$ Hz, 1 H), 7.33 – 7.26 (m, 1 H), 2.55 (s, 3 H); **^{13}C-NMR** (100 MHz, DMSO-d_6) δ 196.28, 161.49, 149.49, 146.86, 143.50, 134.55, 130.78, 129.56, 125.90, 125.55, 123.64, 118.68, 118.17, 26.39; **HR-MS** *m/z* 278.0933 (found), 278.0935 (calc.) $[\text{M-H}]^-$; **Purity** (HPLC, 254 nm) 99.0 %;
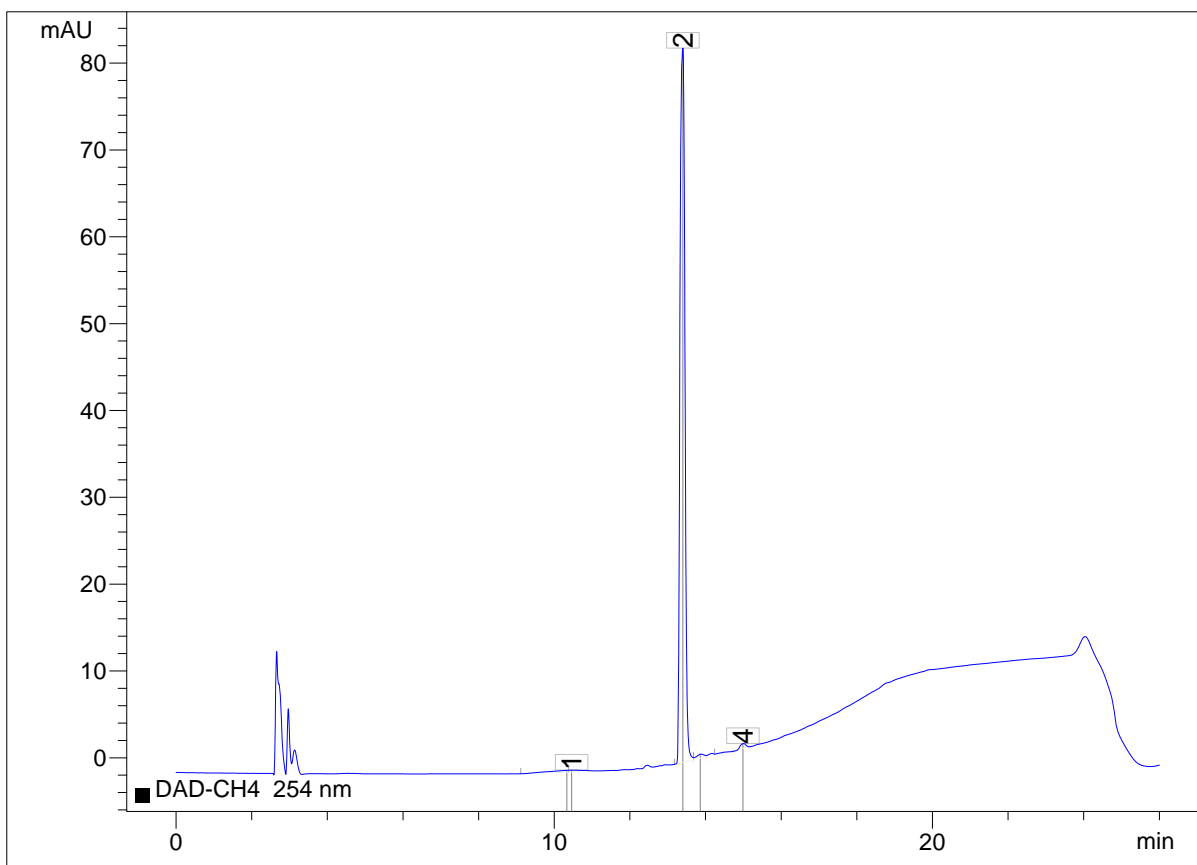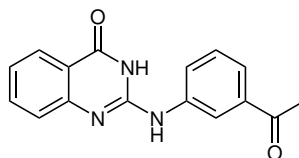
2-((3-Acetylphenyl)amino)-quinazolin-4(3*H*)-one (31i, BER329)

Yield 62 %, prepared in 15 mmol scale (brown solid);

¹H-NMR (400 MHz, DMSO-d_6) δ 10.90 (s, 1 H), 8.89 (s, 1 H), 8.38 (s, 1 H), 7.99 (d, J = 7.8 Hz, 2 H), 7.72 – 7.61 (m, 3 H), 7.51 (t, J = 7.9 Hz, 1 H), 7.42 (d, J = 8.1 Hz, 1 H), 7.29 – 7.23 (m, 1 H); **¹³C-NMR** (100 MHz, DMSO-d_6) δ 197.66, 161.59, 149.72, 147.32, 139.41, 137.36, 134.51, 129.18, 125.89, 125.38, 123.77, 123.28, 122.27, 118.69, 118.49, 26.77; **HR-MS** m/z 280.1076 (found), 280.1081 (calc.) $[M+H]^+$; **Purity** (HPLC, 254 nm) 98.2 %;
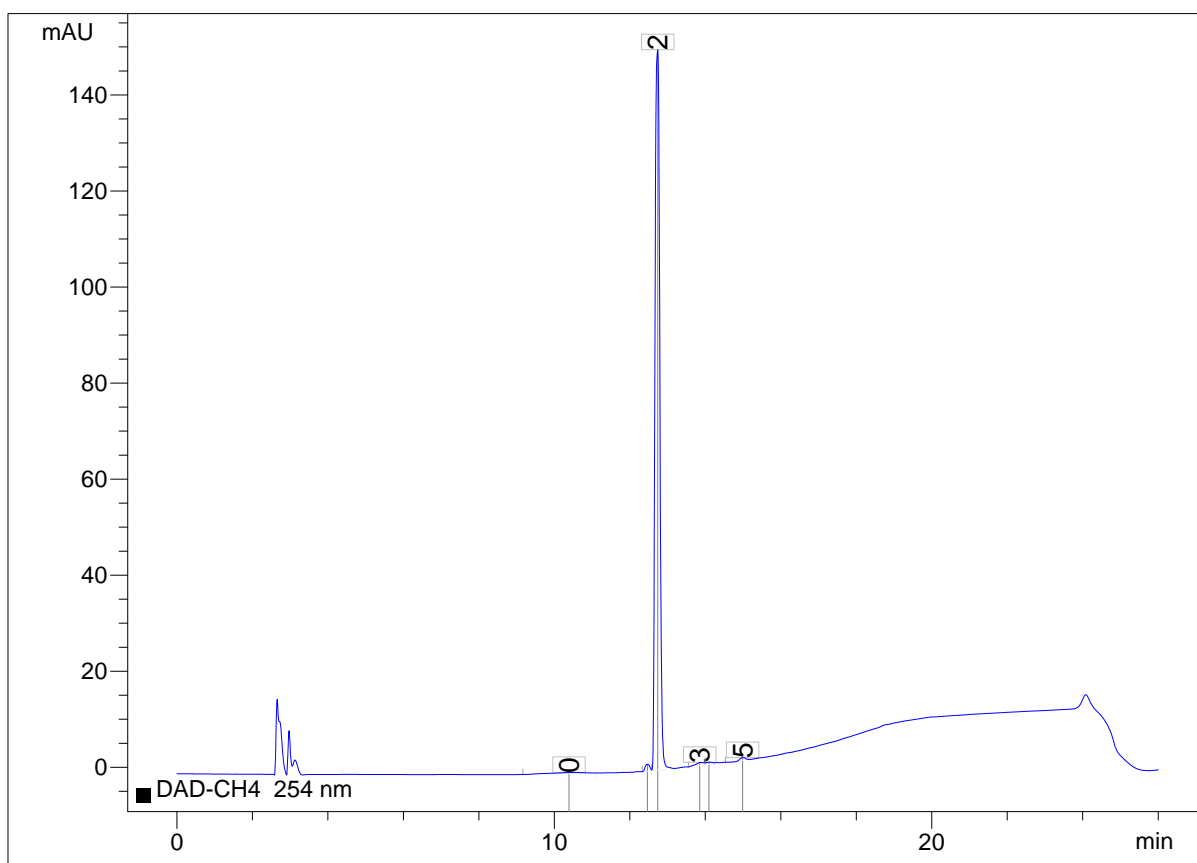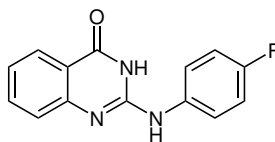
2-((4-Fluorophenyl)amino)-quinazolin-4(3*H*)-one (31j, BER305)

Yield 74 % (white solid);

¹H-NMR (400 MHz, DMSO-d_6) δ 10.84 (s, 1 H), 8.67 (s, 1 H), 7.97 (d, J = 7.7 Hz, 1 H), 7.75 (dd, J = 8.8, 4.9 Hz, 2 H), 7.68 – 7.61 (m, 1 H), 7.38 (d, J = 8.1 Hz, 1 H), 7.27 – 7.15 (m, 3 H); **¹³C-NMR** (100 MHz, DMSO-d_6) δ 161.61, 157.69 (d, J = 239.1 Hz), 149.93, 147.50, 135.28, 134.43, 125.86, 125.23, 123.01, 121.25 (d, J = 7.8 Hz), 118.35, 115.33 (d, J = 22.3 Hz); **HR-MS** m/z 256.0885 (found), 256.0881 (calc.) $[M+H]^+$; **Purity** (HPLC, 254 nm) 98.9 %;
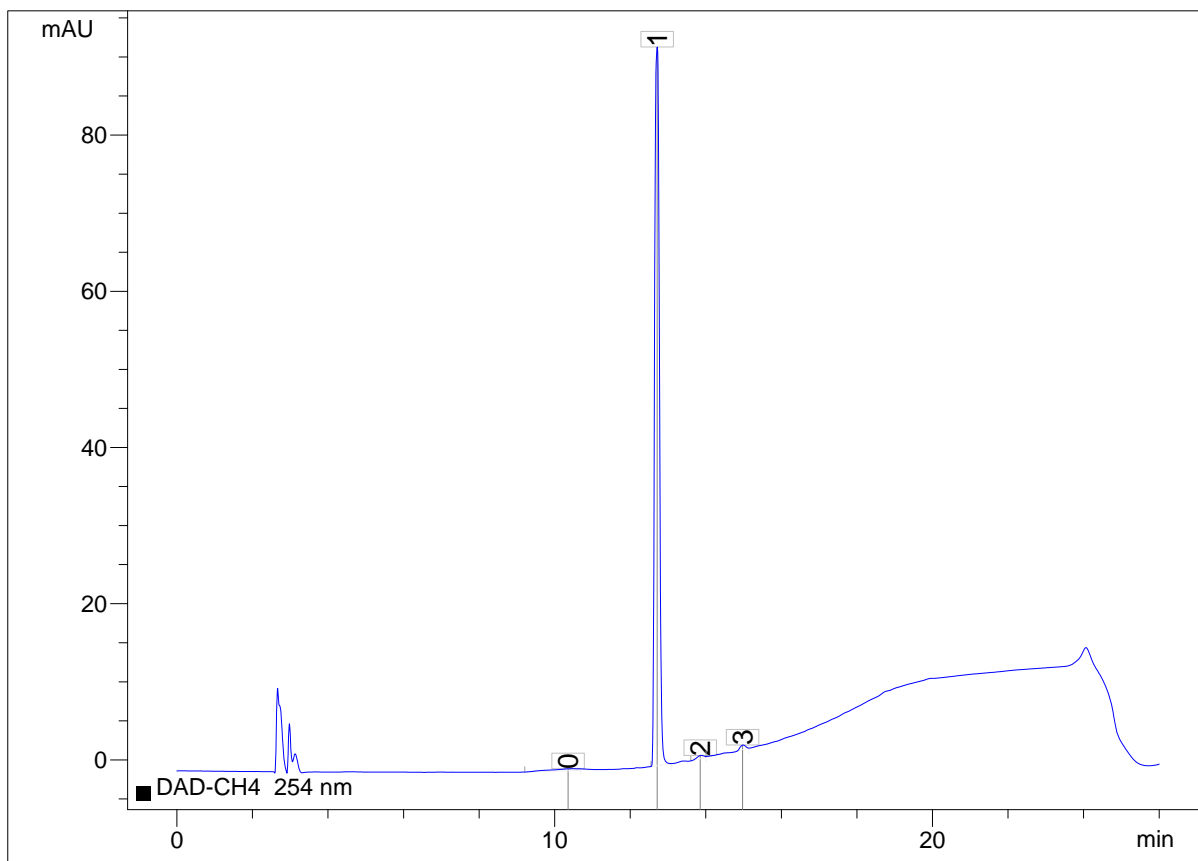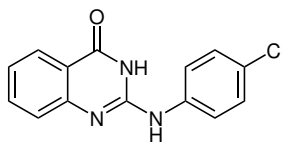
2-((4-Chlorophenyl)amino)-quinazolin-4(3*H*)-one (31k, BER304)

Yield 71 % (white solid);

¹H-NMR (400 MHz, DMSO-d_6) δ 10.86 (s, 1 H), 8.79 (s, 1 H), 7.98 (d, $J = 7.6$ Hz, 1 H), 7.78 (d, $J = 8.6$ Hz, 2 H), 7.70 – 7.63 (m, 1 H), 7.45 – 7.36 (m, 3 H), 7.25 (t, $J = 7.3$ Hz, 1 H); **¹³C-NMR** (100 MHz, DMSO-d_6) δ 161.54, 149.74, 147.21, 137.97, 134.47, 128.62, 125.97, 125.87, 125.33, 123.24, 120.84, 118.45; **HR-MS** m/z 270.0442 (found), 270.0440 (calc.) [M-H]⁻; **Purity** (HPLC, 254 nm) 99.2 %;
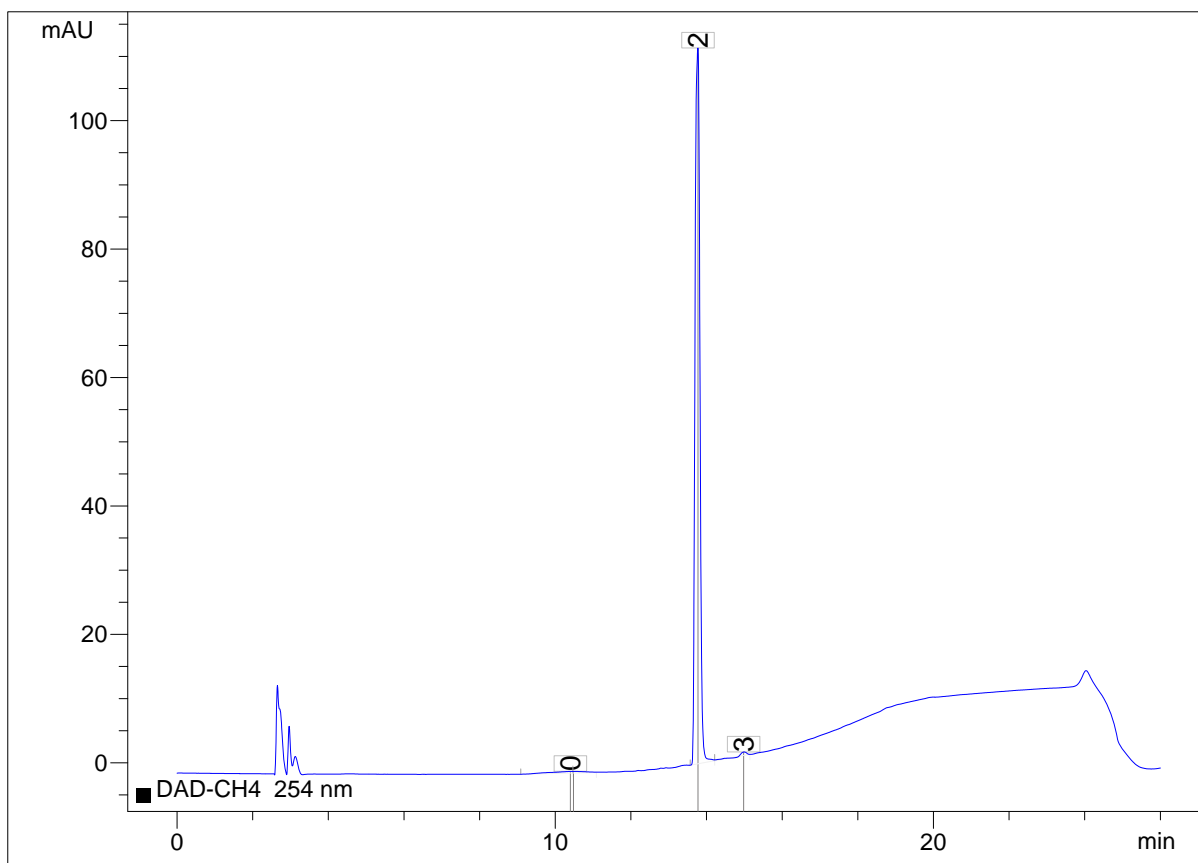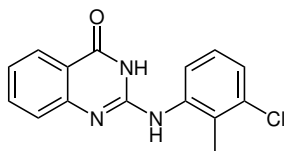
2-((3-Chloro-2-methylphenyl)amino)-quinazolin-4(3*H*)-one (31l, BER306)

Yield 73 % (off-white solid);

¹H-NMR (400 MHz, DMSO-d_6) δ 11.25 (s, 1H), 8.15 (s, 1H), 7.96 (d, J = 7.3 Hz, 2H), 7.65 – 7.57 (m, 1H), 7.30 (d, J = 8.1 Hz, 1H), 7.27 – 7.18 (m, 3H), 2.31 (s, 3H); **¹³C-NMR** (100 MHz, DMSO-d_6) δ 161.75, 149.98, 148.17, 138.41, 134.34, 133.62, 128.31, 127.00, 125.89, 125.11, 124.75, 122.92, 122.49, 118.28, 14.85; **HR-MS** m/z 284.0600 (found), 284.0596 (calc.) [M-H]⁻; **Purity** (HPLC, 254 nm) 99.1 %;
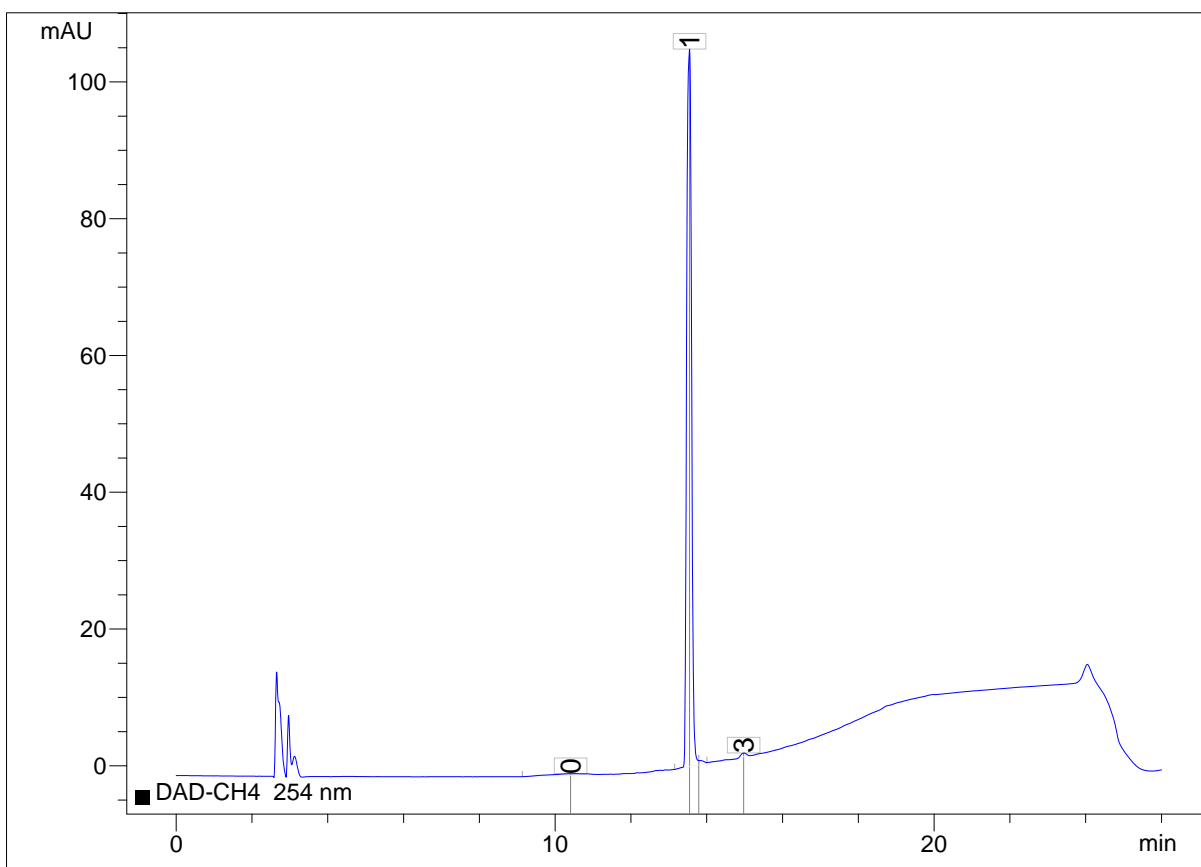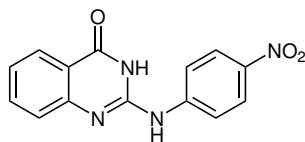
2-((4-Nitrophenyl)amino)-quinazolin-4(3*H*)-one (31m, BER288)

Yield 46 % (yellow solid);

¹H-NMR (400 MHz, DMSO-d_6) δ 11.05 (s, 1 H), 9.42 (s, 1 H), 8.28 – 8.21 (m, 2 H), 8.06 – 7.97 (m, 3 H), 7.76 – 7.69 (m, 1 H), 7.51 (d, J = 8.1 Hz, 1 H), 7.32 (t, J = 7.3 Hz, 1 H); **¹³C-NMR** (100 MHz, DMSO-d_6) δ 161.46, 149.14, 146.58, 145.52, 141.24, 134.62, 125.93, 125.68, 125.04, 124.07, 118.89, 118.47; **HR-MS** m/z 281.0680 (found), 281.0680 (calc.) [M-H]⁻; **Purity** (HPLC, 254 nm) 100.0 %;
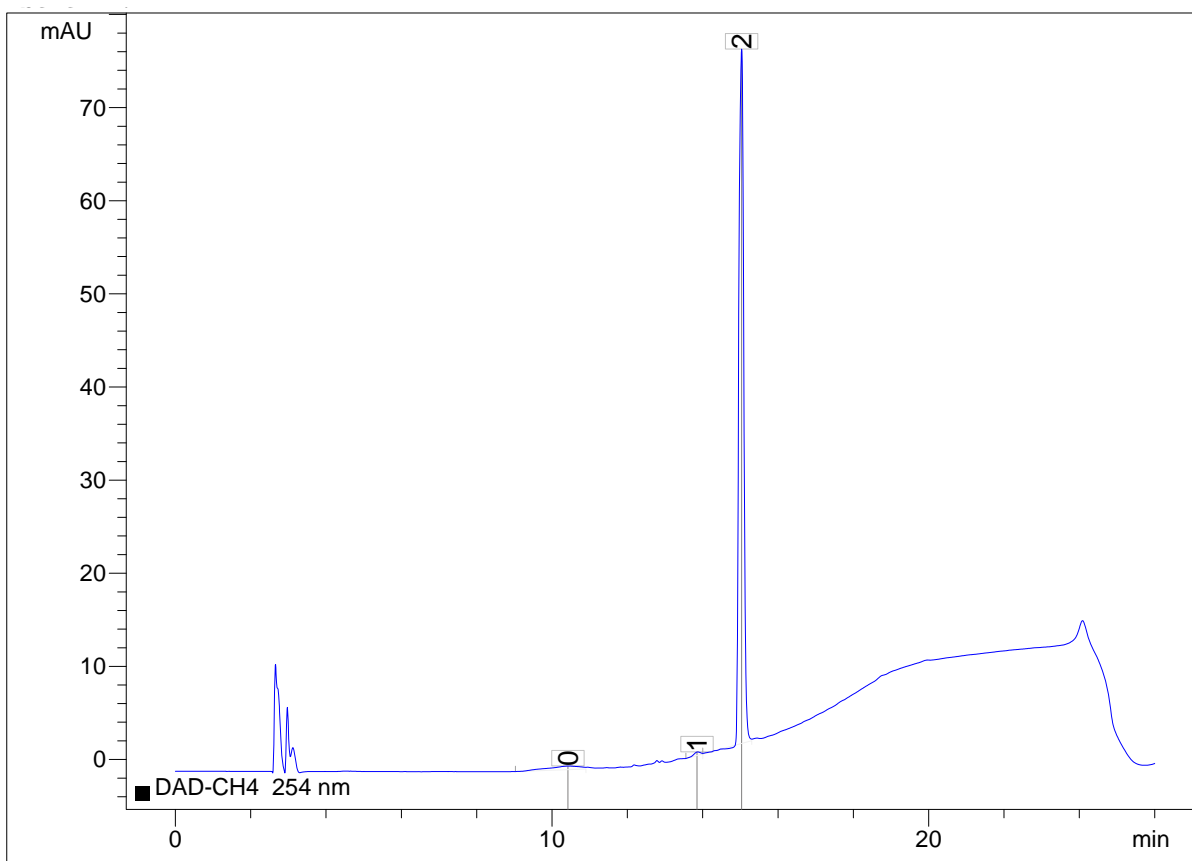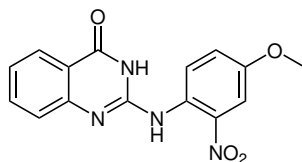
2-((4-Methoxy-2-nitrophenyl)amino)-quinazolin-4(3*H*)-one (31n, BER315)

Yield 56 % (orange needles);

¹H-NMR (400 MHz, DMSO-d_6) δ 11.87 (s, 1 H), 9.21 (s, 1 H), 8.29 (s, 1 H), 7.97 (d, $J =$ 7.7 Hz, 1 H), 7.67 – 7.61 (m, 1 H), 7.59 (d, $J = 2.9$ Hz, 1 H), 7.40 (dd, $J = 9.1$, 2.5 Hz, 1 H), 7.30 – 7.22 (m, 2 H), 3.86 (s, 3 H); **¹³C-NMR** (150 MHz, DMSO-d_6) δ 161.90, 154.77, 149.25, 147.49, 140.39, 134.43, 126.67, 125.93, 125.21, 123.48, 121.62, 118.66, 108.62, 55.96; **HR-MS** m/z 311.0792 (found), 311.0786 (calc.) $[\text{M-H}]^-$; **Purity** (HPLC, 254 nm) 99.0 %;
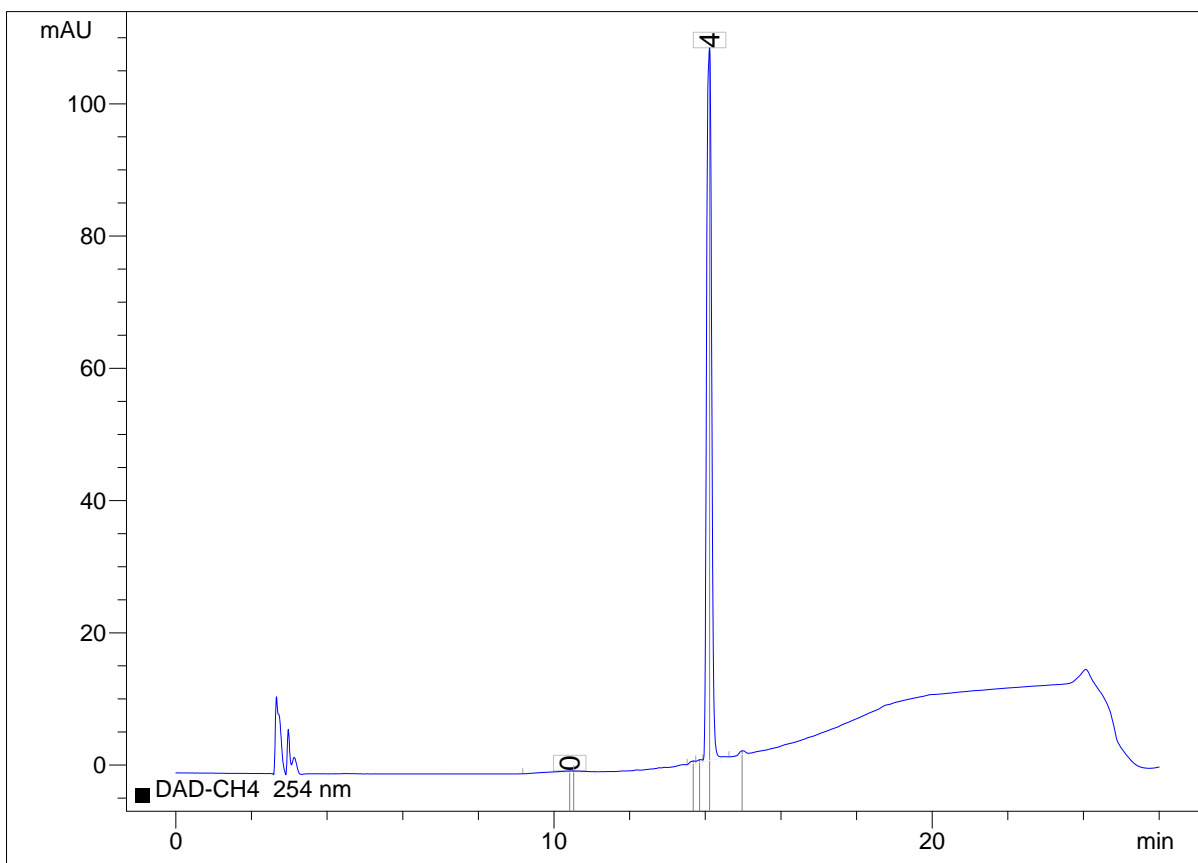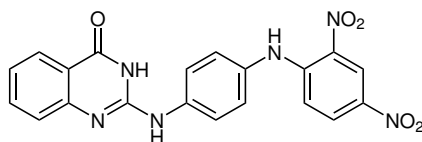
2-((4-((2,4-Dinitrophenyl)amino)phenyl)amino)-quinazolin-4(3H)-one (31o, BER295)

Yield 71 % (red solid);

^{1}H-NMR (400 MHz, DMSO-d_6) δ 10.87 (s, 1 H), 10.15 (s, 1 H), 8.90 (d, $J = 2.7$ Hz, 1 H), 8.89 (s, 1 H), 8.86 (s, 1 H), 8.22 (dd, $J = 9.6, 2.7$ Hz, 1 H), 7.98 (d, $J = 7.8$ Hz, 1 H), 7.89 (d, $J = 8.6$ Hz, 2 H), 7.70 – 7.63 (m, 1 H), 7.44 (d, $J = 8.1$ Hz, 1 H), 7.37 (d, $J = 8.8$ Hz, 2 H), 7.29 – 7.22 (m, 1 H), 7.09 (d, $J = 9.6$ Hz, 1 H); **^{13}C-NMR** (100 MHz, DMSO-d_6) δ 161.55, 149.82, 147.23, 147.12, 137.91, 136.05, 134.48, 131.73, 130.81, 129.75, 126.64, 125.88, 125.35, 123.46, 123.21, 120.16, 118.45, 116.85; **HR-MS** m/z 417.0948 (found), 417.0953 (calc.) [M-H]$^-$; **Purity** (HPLC, 254 nm) 96.5 %;
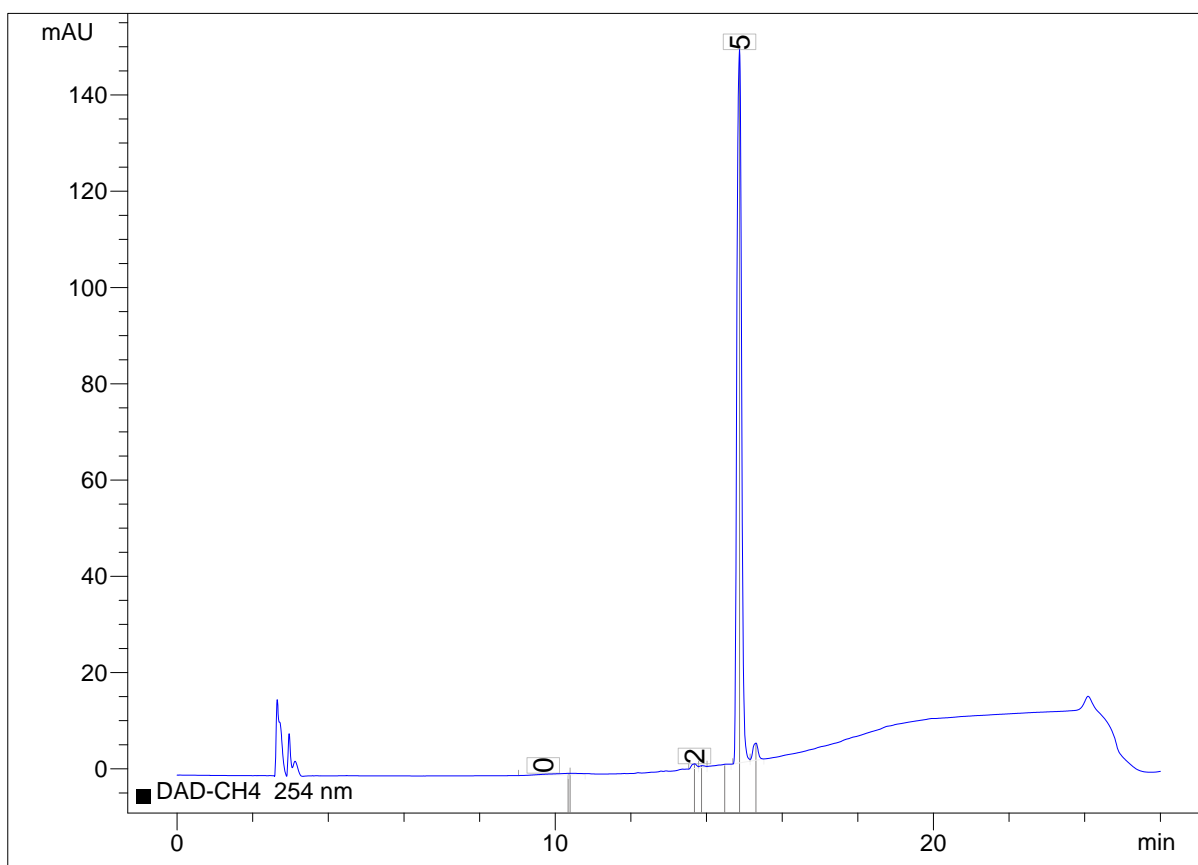
7.4.4 *N*-Methylated 2-(phenylamino)-quinazolin-4(3*H*)-ones

2-(*N*-Methyl-*N*-phenylamino)-quinazolin-4(3*H*)-one (33, BER324)
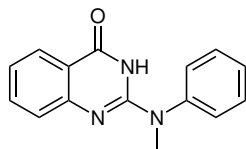
A solution of compound **25** (1.92 g, 10 mmol) and *N*-methylaniline (2.17 ml, 20 mmol) in glacial acetic acid (15 ml) was heated to reflux for 10 h. Upon cooling, water was added dropwise to the solution and a white precipitate started to form. The solution was further diluted with water to a volume of 200 ml and stored in the fridge for 3 h. After filtration, the filtrate was extracted with dichloromethane and ethyl acetate (250 ml each). The organic phases were combined with the filtered precipitate and dried *in vacuo*. Recrystallization from DMF/*n*-propanol yielded the pure title compound.

2-(*N*-Methyl-*N*-phenylamino)-quinazolin-4(3*H*)-one (33, BER324)
Yield 88 % (off-white crystals);
^{1}H-NMR (400 MHz, DMSO-d_6) δ 10.89 (s, 1 H), 7.92 (dd, J = 7.9, 1.2 Hz, 1 H), 7.60 (t, J = 7.4 Hz, 1 H), 7.45 (t, J = 7.7 Hz, 2 H), 7.39 – 7.26 (m, 4 H), 7.22 – 7.16 (m, 1 H), 3.41 (s, 3 H); **^{13}C-NMR** (150 MHz, DMSO-d_6) δ 162.43, 150.44, 150.20, 144.03, 134.30, 129.62, 126.35, 125.91, 125.10, 122.60, 117.71, 39.29; **HR-MS** *m/z* 250.0992 (found), 250.0990 (calc.) $[M\text{-H}]^-$; **Purity** (HPLC, 254 nm) 98.3 %;
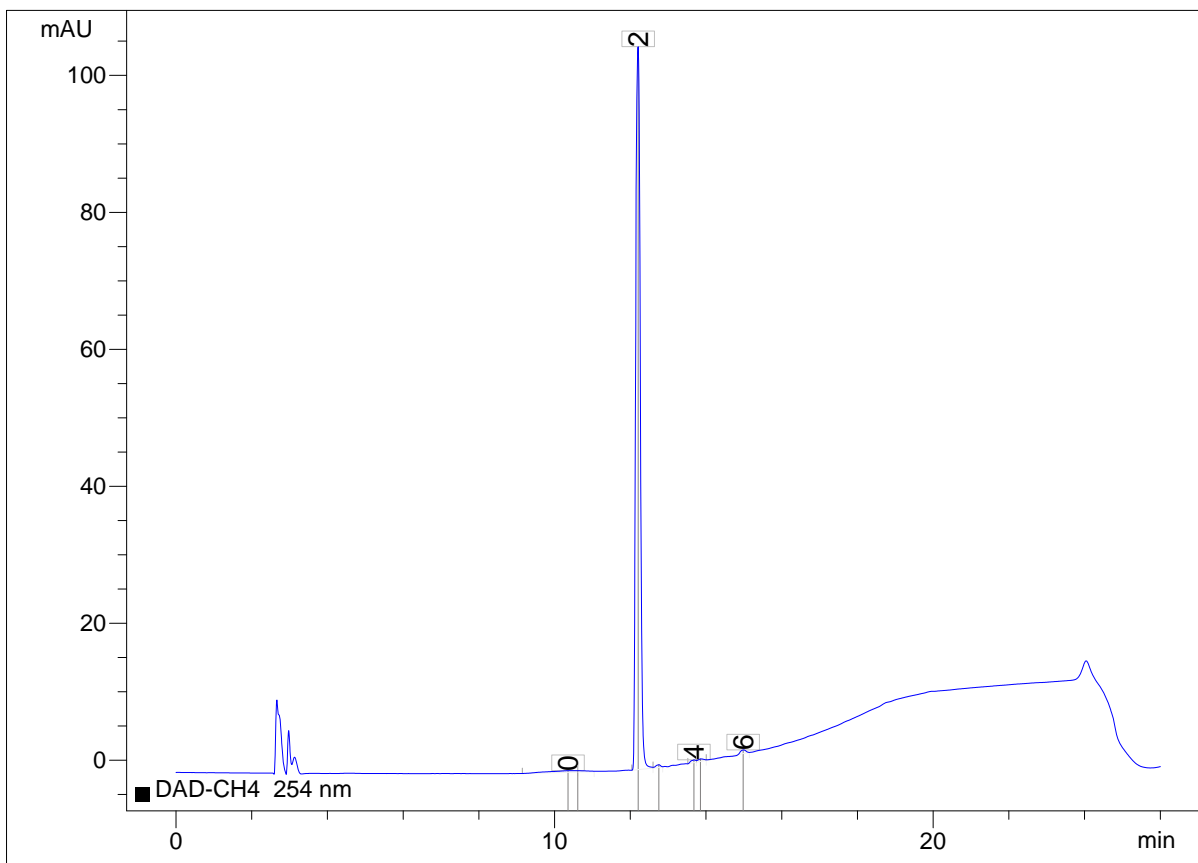
3-Methyl-2-(phenylamino)-quinazolin-4(3*H*)-one (32, BER341a)
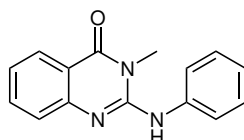
To a stirred suspension of sodium hydride (60 % suspension in mineral oil, 80 mg, 2 mmol) in dry DMF (5 ml) at room temperature (water bath) was added compound **31a** (475 mg, 2 mmol). Then, methyl iodide (125 μl, 2 mmol) was added dropwise and the mixture was stirred for 3 h at 50 °C. The mixture was poured on ice, stirred for 30 min and extracted with ethyl acetate (3 x 150 ml). After evaporation of the solvent *in vacuo,* the crude product was redissolved in ethyl acetate and adsorbed on silica gel (9 g). The pure product was isolated by column chromatography on an Isolera system (100 g silica column) eluting with a hexane/ethyl acetate gradient.

3-Methyl-2-(phenylamino)-quinazolin-4(3*H*)-one (32, BER341a)

Yield 46 % (colorless solid);

¹H-NMR (400 MHz, DMSO-d_6) δ 8.65 (s, 1H), 7.98 (d, J = 7.3 Hz, 1H), 7.74 – 7.65 (m, 2H), 7.65 – 7.57 (m, 1H), 7.40 – 7.32 (m, 2H), 7.27 (d, J = 8.1 Hz, 1H), 7.21 (t, J = 7.4 Hz, 1H), 7.10 (t, J = 7.4 Hz, 1H), 3.61 (s, 3H); **¹³C-NMR** (100 MHz, DMSO-d_6) δ 161.75, 148.61, 148.08, 139.30, 134.11, 128.33, 126.38, 124.87, 123.32, 122.73, 122.61, 117.10, 28.79; **HR-MS** *m/z* 252.1124 (found), 252.1131 (calc.) [M+H]⁺; **Purity** (HPLC, 254 nm) 97.6 %;
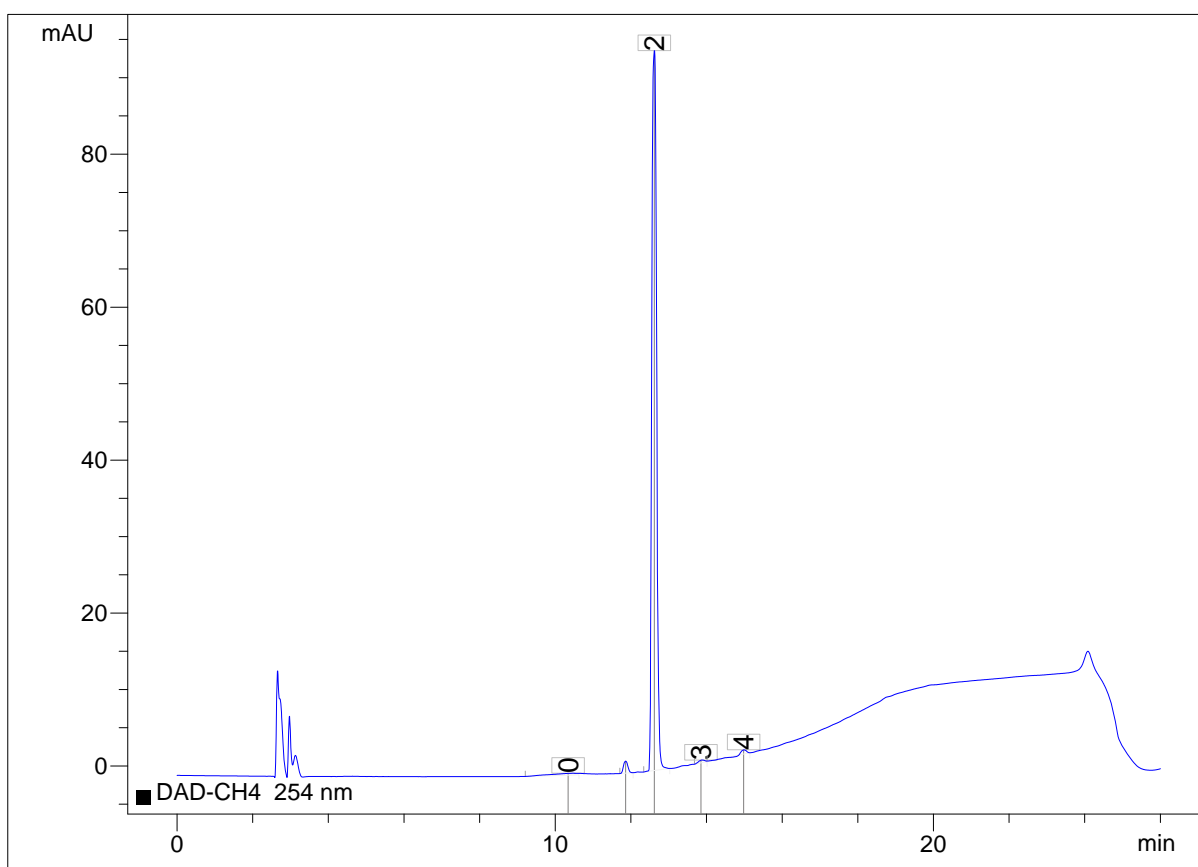
3-Methyl-2-(*N*-methyl-*N*-phenylamino)-quinazolin-4(3*H*)-one (34, BER330a)
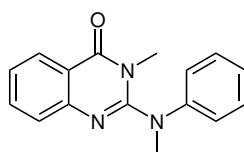
To a stirred suspension of sodium hydride (60 % suspension in mineral oil, 352 mg, 8.8 mmol) in dry DMF (15 ml) at room temperature (water bath) was added compound **33** (2.21 g, 8.8 mmol). Then, methyl iodide (560 µl, 9 mmol) was added dropwise and the mixture was

stirred for 3 h at 50 °C. The mixture was poured on ice, stirred for 30 min and extracted with ethyl acetate (3 x 150 ml). After evaporation of the solvent *in vacuo,* the crude product was redissolved in ethyl acetate and adsorbed on silica gel (7.5 g). The pure product was isolated by column chromatography on an Isolera system (100 g silica column) eluting with a hexane/ethyl acetate gradient.

3-Methyl-2-(*N*-methyl-*N*-phenylamino)-quinazolin-4(3*H*)-one (34, BER330a)

Yield 55 % (colorless crystals);

^{1}H-NMR (400 MHz, DMSO-d_6) δ 8.10 (dd, J = 7.9, 1.2 Hz, 1 H), 7.79 – 7.73 (m, 1 H), 7.57 (d, J = 8.0 Hz, 1 H), 7.44 – 7.34 (m, 3 H), 7.16 (t, J = 7.4 Hz, 1 H), 7.09 (d, J = 7.6 Hz, 2 H), 3.41 (s, 3 H), 3.04 (s, 3 H); **^{13}C-NMR** (100 MHz, DMSO-d_6) δ 162.86, 152.64, 147.17, 146.87, 134.15, 129.75, 126.23, 125.86, 124.72, 124.10, 121.83, 118.82, 41.59, 31.99; **HR-MS** m/z 266.1290 (found), 266.1288 (calc.) $[M+H]^+$; **Purity** (HPLC, 254 nm) 97.9 %;
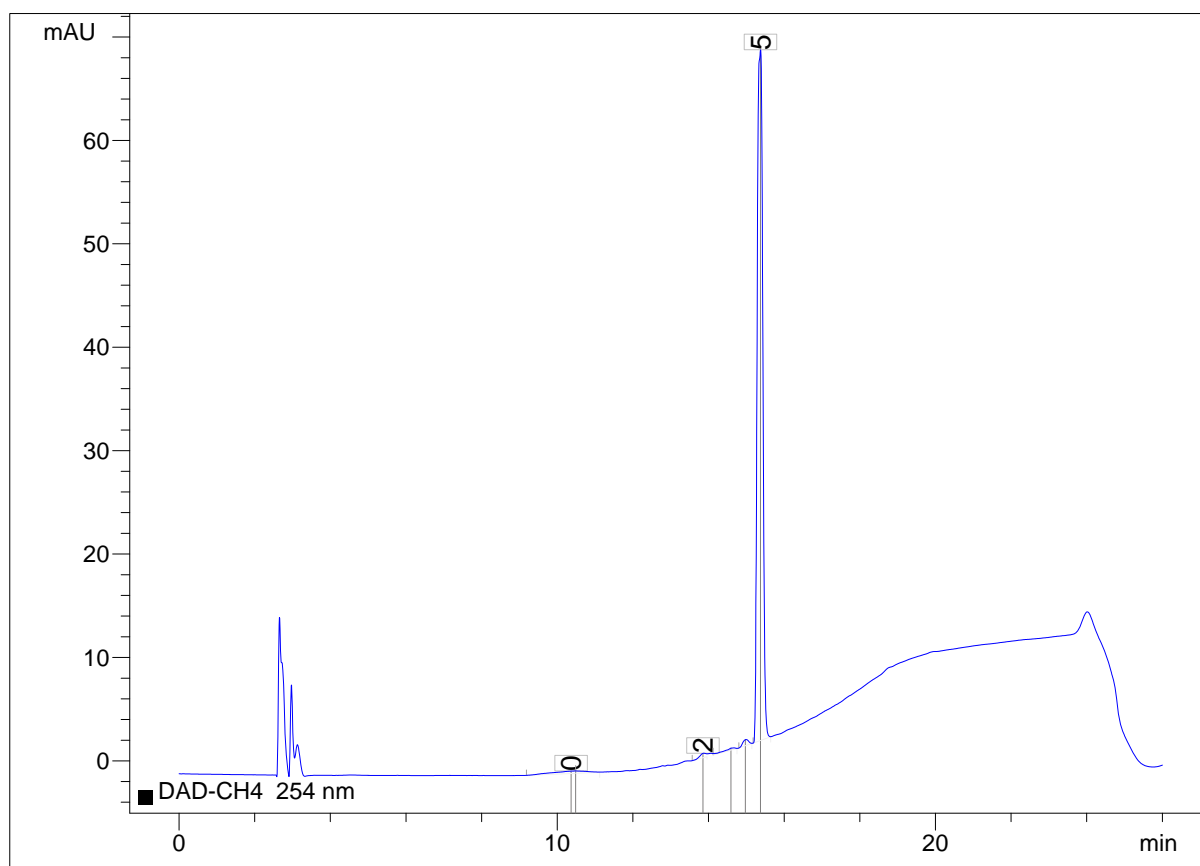
7.4.5 Core-modified 2-(phenylamino)-quinazolin-4(3*H*)-ones

7-Nitro-2-(phenylamino)-quinazolin-4(3*H*)-one (41b, BER413)
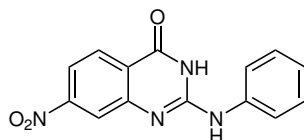
Compound **40b** (3.56 g, 15 mmol) and aniline (2.74 ml, 30 mmol) were dissolved in glacial acetic acid and the mixture was refluxed for 18 h. Upon cooling, the reaction was quenched with water resulting in a final volume of 200 ml. After storing the mixture for 3 h in the fridge, the raw product was filtered off, the filtrate was extracted with dichloromethane (2 x 150 ml) and ethyl actetate (150 ml). The crude product and the organic phases were combined and dried *in vacuo*. Recrystallization from DMF/water yielded the pure title compound.

7-Nitro-2-(phenylamino)-quinazolin-4(3*H*)-one (41b, BER413)

Yield orange solid (69 %);

^{1}H-NMR (400 MHz, DMSO-d_6) δ 11.13 (s, 1 H), 8.85 (s, 1 H), 8.16 (d, $J = 8.7$ Hz, 1 H), 8.10 (d, $J = 2.2$ Hz, 1 H), 7.93 (dd, $J = 8.7, 2.3$ Hz, 1 H), 7.75 (d, $J = 8.0$ Hz, 2 H), 7.38 (t, $J = 7.8$ Hz, 2 H), 7.10 (t, $J = 7.3$ Hz, 1 H); **^{13}C-NMR** (100 MHz, DMSO-d_6) δ 160.57, 151.42, 150.70, 148.82, 138.33, 128.88, 127.98, 123.08, 122.69, 119.99, 119.81, 116.33; **HR-MS** *m/z* 281.0679 (found), 281.0680 (calc.) [M-H]$^-$; **Purity** (HPLC, 254 nm) 99.7 %;
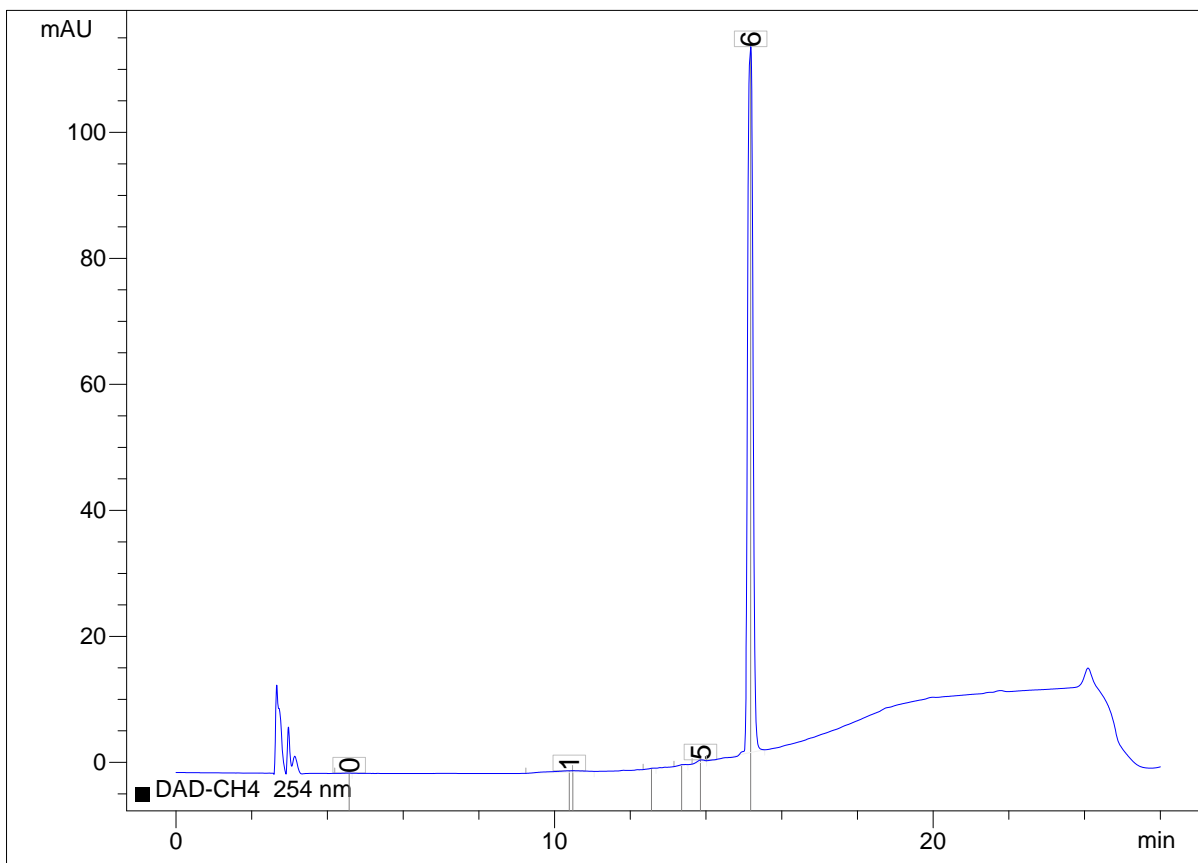
6-Nitro-2-(phenylamino)-quinazolin-4(3*H*)-one (41c, BER416)
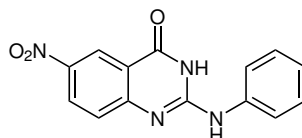
Compound **40c** (4.75 g, 20 mmol) and aniline (3.65 ml, 40 mmol) were dissolved in glacial acetic acid and the mixture was refluxed for 18 h. Upon cooling, the reaction was quenched with water resulting in a final volume of 200 ml. After storing the mixture for 3 h in the fridge, the raw product was filtered off, dried *in vacuo* and recrystallized from DMF/water.

6-Nitro-2-(phenylamino)-quinazolin-4(3*H*)-one (41c, BER416)

Yield yellow solid (79 %);

^{1}H-NMR (400 MHz, DMSO-d_6) δ 11.22 (s, 1 H), 9.06 (s, 1 H), 8.68 (d, $J = 2.7$ Hz, 1 H), 8.38 (dd, $J = 9.1, 2.8$ Hz, 1 H), 7.73 (d, $J = 8.0$ Hz, 2 H), 7.51 (d, $J = 9.1$ Hz, 1UnH), 7.44 – 7.35 (m, 2 H), 7.17 – 7.08 (m, 1 H); **^{13}C-NMR** (100 MHz, DMSO-d_6) δ 160.77, 155.18, 149.95, 141.85, 137.96, 128.90, 128.53, 126.43, 123.58, 122.31, 120.40, 117.81; **HR-MS** *m/z* 281.0679 (found), 281.0680 (calc.) $[\text{M-H}]^-$; **Purity** (HPLC, 254 nm) 99.5 %;
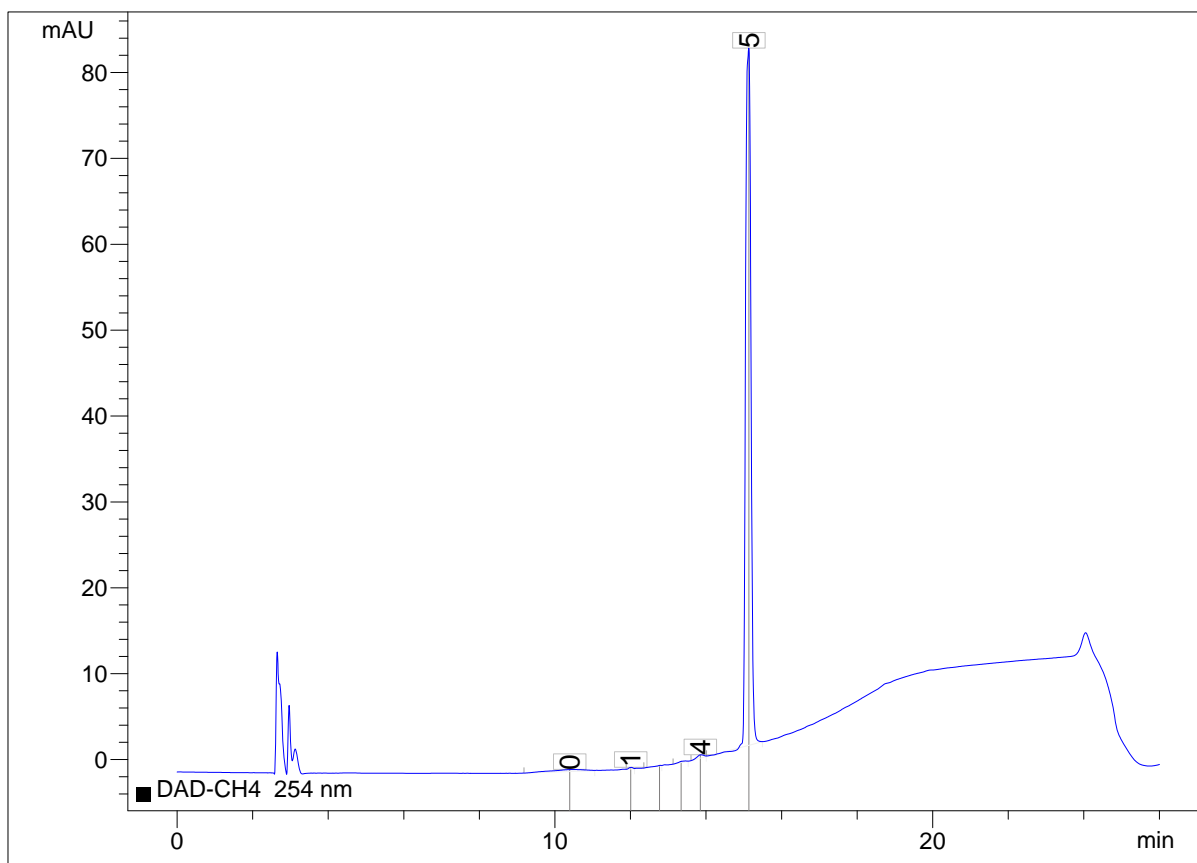
7-Amino-2-(phenylamino)-quinazolin-4(3*H*)-one (42b, BER419)
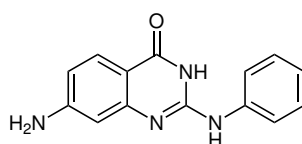
To a suspension of compound **41b** (2.12 g, 7.5 mmol) in ethanol (35 ml), acetic acid (35 ml) and iron filings (1.68 g, 30.0 mmol) were added. The mixture was refluxed for 90 min, then cooled to room temperature. After evaporation of the solvent *in vacuo*, the residue was resuspended in sodium hydroxide solution (5 M, 50 ml) and methanol (50 ml). Leftover iron filings were separated by vacuum filtration, the filtrate was cooled externally with ice, the pH was adjusted to 5 – 6 with conc. hydrochloric acid. After 30 min of stirring, the crude product was filtered off and recrystallized from DMF/water. Since this did not afford pure product, the crystallized solid was subjected to purification by column chromatography on an Isolera system (100 g silica column) eluting with an ethyl acetate/methanol gradient.

7-Amino-2-(phenylamino)-quinazolin-4(3*H*)-one (42b, BER419)

Yield pale yellow solid (16 %);

^{1}H-NMR (400 MHz, DMSO-d_6) δ 10.22 (s, 1 H), 8.53 (s, 1 H), 7.72 (d, J = 7.9 Hz, 2 H), 7.63 (d, J = 8.4 Hz, 1 H), 7.40 – 7.29 (m, 2 H), 7.01 (t, J = 7.4 Hz, 1 H), 6.51 – 6.42 (m, 2 H), 5.89 (s, 2 H); **^{13}C-NMR** (100 MHz, DMSO-d_6) δ 161.01, 154.52, 151.71, 147.25, 139.34, 128.72, 127.16, 121.99, 118.90, 111.63, 107.40, 105.79; **HR-MS** m/z 253.1082 (found), 253.1084 (calc.) $[M+H]^+$; **Purity** (HPLC, 254 nm) 98.4 %;
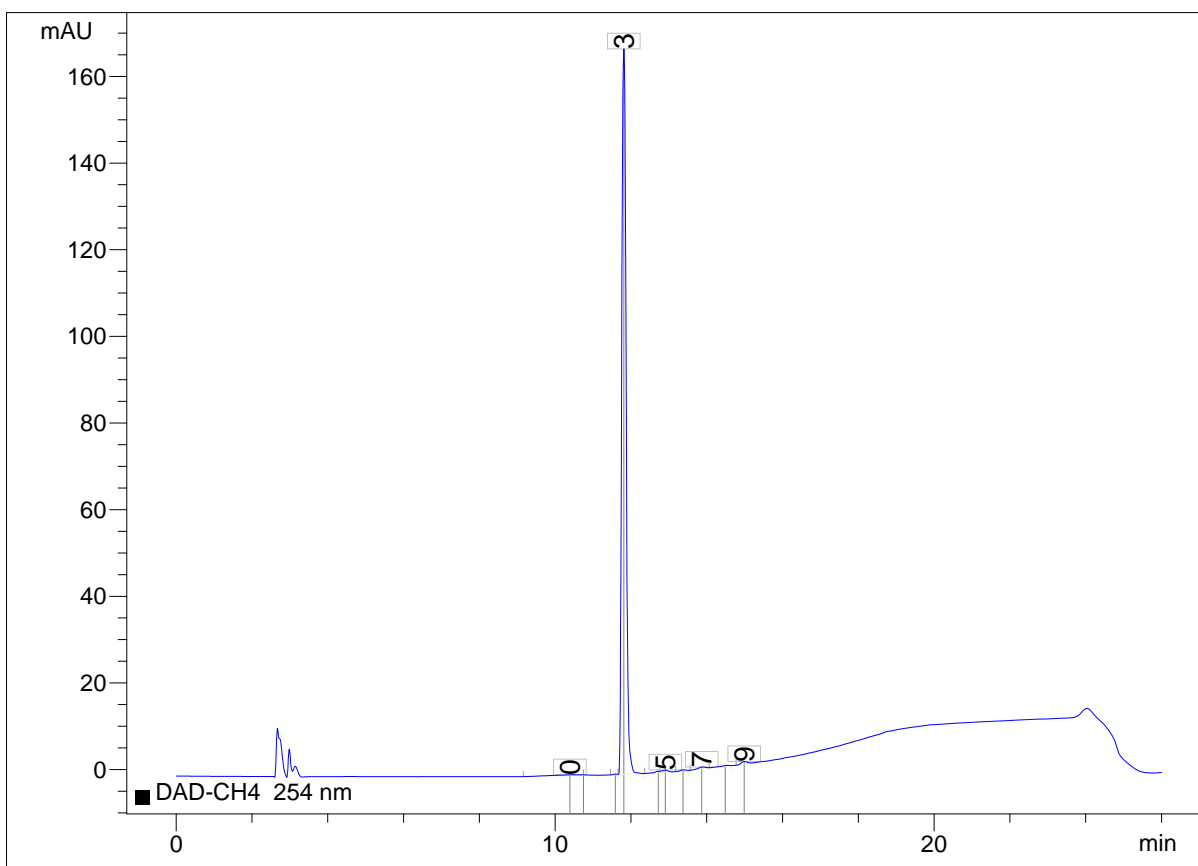
6-Amino-2-(phenylamino)-quinazolin-4(3*H*)-one (42c, BER420)

To a suspension of compound **41c** (3.95 g, 14 mmol) in ethanol (65 ml), acetic acid (65 ml) and iron filings (3.13 g, 56 mmol) were added. The mixture was refluxed for 8 h, then cooled to room temperature. After evaporation of the solvent *in vacuo*, the residue was resuspended in sodium hydroxide solution (5 M, 150 ml). Leftover iron filings were separated by vacuum

filtration, the filtrate was cooled externally with ice, the pH was adjusted to 5 – 6 with conc. hydrochloric acid. After 30 min of stirring, the crude product was filtered off and recrystallized from DMF/water. Since this did not afford pure product, the crystallized solid was subjected to purification by column chromatography on an Isolera system (340 g silica column) eluting with an ethyl acetate/methanol gradient.

6-Amino-2-(phenylamino)-quinazolin-4(3*H*)-one (42c, BER420)

Yield pale yellow solid (30 %);

^{1}H-NMR (400 MHz, DMSO-d_6) δ 10.55 (s, 1 H), 8.38 (s, 1 H), 7.71 (d, J = 8.0 Hz, 2 H), 7.41 – 7.27 (m, 2 H), 7.22 – 7.10 (m, 2 H), 7.03 – 6.94 (m, 2 H), 5.23 (s, 2 H); **^{13}C-NMR** (100 MHz, DMSO-d_6) δ 161.54, 145.03, 144.17, 140.60, 139.62, 128.74, 126.06, 122.82, 121.59, 119.06, 118.39, 107.16; **HR-MS** m/z 251.0938 (found), 251.0938 (calc.) [M-H]$^-$; **Purity** (HPLC, 254 nm) 95.2 %;
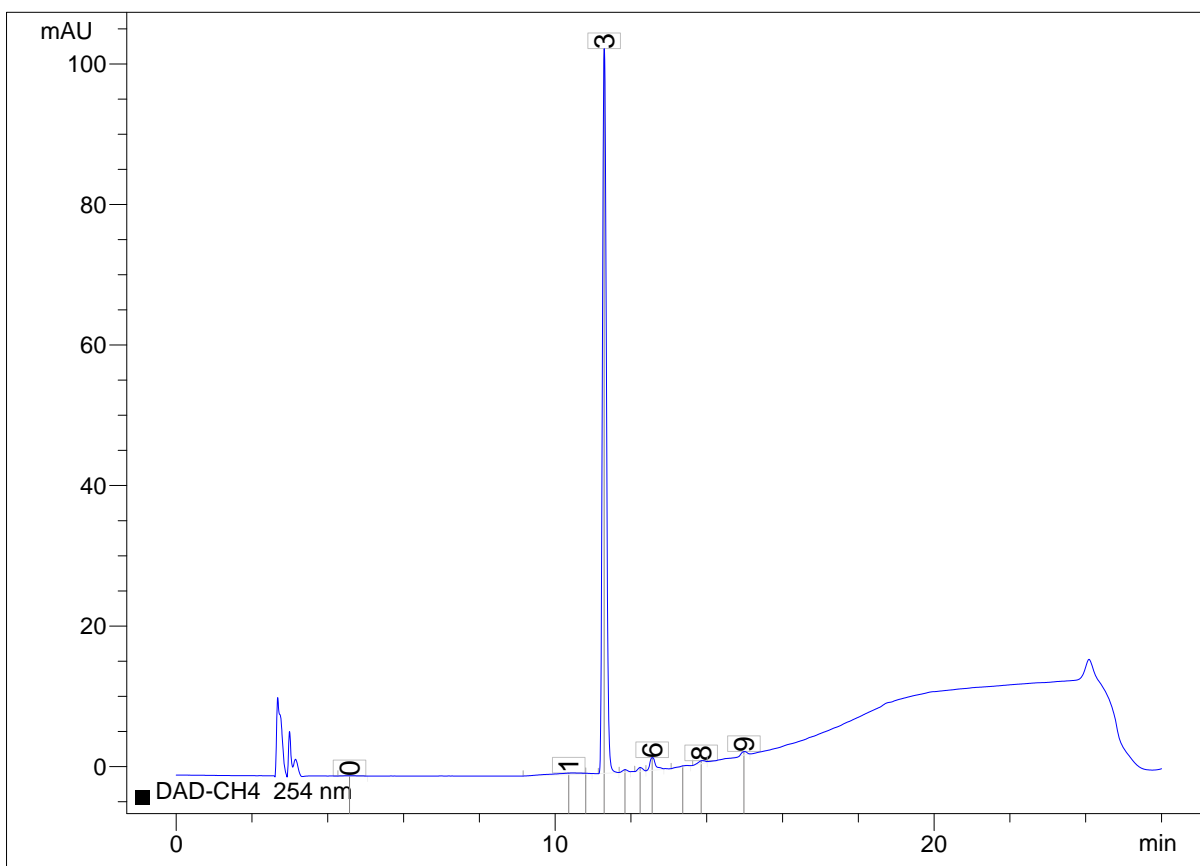
References

[1] David Rhodes and Anna Nadolska-Orczyk. "Plant Stress Physiology". In: *Encyclopedia of Life Sciences* (2001). DOI: 10.1038/npg.els.0001297 (cit. on pp. 1, 2).

[2] *Agri-Environmental Statistics*. 2019. URL: http://www.fao.org/economic/ess/environment/en/ (visited on 11/18/2020) (cit. on p. 1).

[3] Food and Agriculture Organization of the United Nations. *The State of Food Security and Nutrition in the World*. 2018 (cit. on p. 1).

[4] *Disasters causing billions in agricultural losses, with drought leading the way*. 2017. URL: http://www.fao.org/news/story/en/item/1106977/icode/ (visited on 11/18/2020) (cit. on p. 1).

[5] Seyed Y.S. Lisar, Rouhollah Motafakkerazad, Mosharraf M. Hossain, and Ismail M.M. Rahman, eds. *Water Stress in Plants: Causes, Effects and Responses*. DOI: 10.5772/39363 (cit. on p. 2).

[6] Yuriko Osakabe, Keishi Osakabe, Kazuo Shinozaki, and Lam-Son P. Tran. "Response of plants to water stress". In: *Frontiers in Plant Science* 5 (2014), p. 86. DOI: 10.3389/fpls.2014.00086 (cit. on pp. 2, 4).

[7] Theodore C. Hsiao. "Plant Responses to Water Stress". In: *Annual Review of Plant Physiology* 24.1 (1973), pp. 519–570. DOI: 10.1146/annurev.pp.24.060173.002511 (cit. on p. 2).

[8] Park S. Nobel. *Physicochemical and Environmental Plant Physiology*. Elsevier, 2009 (cit. on p. 3).

[9] Tibor Kalapos. "Leaf water potential-leaf water deficit relationship for ten species of a semiarid grassland community". In: *Plant and Soil* 160.1 (1994), pp. 105–112. DOI: 10.1007/BF00150351 (cit. on p. 3).

[10] Louis G. Nickell, ed. *Controlling Biological Behavior of Plants with Synthetic Plant Growth Regulating Chemicals*. Vol. 111. 1979. DOI: 10.1021/bk-1979-0111.ch010 (cit. on p. 5).

[11] M. Halmann. "Synthetic Plant Growth Regulators". In: *Advances in Agronomy* 43 (1990), pp. 47–105. DOI: 10.1016/S0065-2113(08)60476-9 (cit. on p. 5).

[12] Naohiko Ohama, Hikaru Sato, Kazuo Shinozaki, and Kazuko Yamaguchi-Shinozaki. "Transcriptional Regulatory Network of Plant Heat Stress Response". In: *Trends in Plant Science* 22.1 (2017), pp. 53–65. DOI: 10.1016/j.tplants.2016.08.015 (cit. on p. 5).

[13] Hoang-Chinh Nguyen, Kuan-Hung Lin, Shin-Lon Ho, Chih-Ming Chiang, and Chi-Ming Yang. "Enhancing the abiotic stress tolerance of plants: from chemical treatment to biotechnological approaches". In: *Physiologia Plantarum* 164.4 (2018), pp. 452–466. DOI: 10.1111/ppl.12812 (cit. on p. 5).

[14] Andreas Savvides, Shawkat Ali, Mark Tester, and Vasileios Fotopoulos. "Chemical Priming of Plants Against Multiple Abiotic Stresses: Mission Possible". In: *Trends in Plant Science* 21.4 (2016), pp. 329–340. DOI: 10.1016/j.tplants.2015.11.003 (cit. on p. 5).

[15] Solmaz Irani and Christopher D. Todd. "Exogenous allantoin increases *Arabidopsis* seedlings tolerance to NaCl stress and regulates expression of oxidative stress response genes". In: *Journal of Plant Physiology* 221 (2018), pp. 43–50. DOI: 10.1016/ j.jplph.2017.11.011 (cit. on p. 5).

[16] Tijen Demiral and Ismail Türkan. "Exogenous glycinebetaine affects growth and proline accumulation and retards senescence in two rice cultivars under NaCl stress". In: *Environmental and Experimental Botany* 56.1 (2006), pp. 72–79. DOI: 10.1016/j. envexpbot.2005.01.005 (cit. on p. 5).

[17] R. A. Fletcher and V. Nath. "Triadimefon reduces transpiration and increases yield in water stressed plants". In: *Physiologia Plantarum* 62.3 (1984), pp. 422–426. DOI: 10.1111/j.1399-3054.1984.tb04596.x (cit. on p. 6).

[18] R. A. Fletcher and G. Hofstra. "Triadimefon a Plant Multi-Protectant". In: *Plant and Cell Physiology* 26.4 (1985), pp. 775–780. DOI: 10.1093/oxfordjournals.pcp.a076970 (cit. on p. 6).

[19]   C. Abdul Jaleel, G.M.A. Lakshmanan, M. Gomathinayagam, and R. Panneerselvam. "Triadimefon induced salt stress tolerance in *Withania somnifera* and its relationship to antioxidant defense system". In: *South African Journal of Botany* 74.1 (2008), pp. 126–132. DOI: 10.1016/j.sajb.2007.10.003 (cit. on p. 6).

[20]   C. Abdul Jaleel, P. Manivannan, B. Sankar, A. Kishorekumar, R. Gopi, R. Somasundaram, and R. Panneerselvam. "Induction of drought stress tolerance by ketoconazole in *Catharanthus roseus* is mediated by enhanced antioxidant potentials and secondary metabolite accumulation". In: *Colloids and Surfaces. B, Biointerfaces* 60.2 (2007), pp. 201–206. DOI: 10.1016/j.colsurfb.2007.06.010 (cit. on p. 6).

[21]   Ali Ahsan Bajwa, Muhammad Farooq, and Ahmad Nawaz. "Seed priming with sorghum extracts and benzyl aminopurine improves the tolerance against salt stress in wheat (*Triticum aestivum* L.)" In: *Physiology and Molecular Biology of Plants : an International Journal of Functional Plant Biology* 24.2 (2018), pp. 239–249. DOI: 10.1007/s12298-018-0512-9 (cit. on p. 6).

[22]   Wolfgang Thielert. "A unique product: The story of the imidacloprid stress shield". In: *Pflanzenschutz-Nachrichten Bayer* 59 (2006), pp. 73–86 (cit. on p. 6).

[23]   *Imidacloprid: Weit mehr als nur das meistverkaufte Insektizid weltweit*. 2006. URL: https://www.proplanta.de/agrar-nachrichten/unternehmen/imidacloprid-weit-mehr-als-nur-das-meistverkaufte-insektizid-weltweit_article1162910583.html (visited on 11/18/2020) (cit. on p. 6).

[24]   Peter Paul Heym. "*In silico* characterisation of AtPARP1 and virtual screening for AtPARP inhibitors to increase resistance to abiotic stress". PhD thesis. Halle (Saale): Martin-Luther-Universität Halle-Wittenberg, 2016 (cit. on pp. 7, 10, 33, 37, 38).

[25]   Torsten Geißler and Ludger A. Wessjohann. "A Whole-Plant Microtiter Plate Assay for Drought Stress Tolerance-Inducing Effects". In: *Journal of Plant Growth Regulation* 30.4 (2011), pp. 504–511 (cit. on pp. 7, 13–15, 17, 78, 79).

[26]   Torsten Geißler. "Entwicklung von Assays zur Untersuchung chemisch induzierter Trockenstresstoleranz". PhD thesis. Halle (Saale): Martin-Luther-Universität Halle-Wittenberg, 2012 (cit. on pp. 7, 13, 34, 79).

[27]   A. Ruf, Josiane Ménissier de Murcia, Gilbert Ménissier de Murcia, and Georg E. Schulz. "Structure of the catalytic fragment of poly(ADP-ribose) polymerase from

chicken". In: *Proceedings of the National Academy of Sciences of the United States of America* 93 (1996), pp. 7481–7485 (cit. on pp. 9, 12).

[28] Prakash Jagtap and Csaba Szabó. "Poly(ADP-ribose) polymerase and the therapeutic effects of its inhibitors". In: *Nature Reviews Drug Discovery* 4.5 (2005), pp. 421–440. DOI: 10.1038/nrd1718 (cit. on pp. 9, 10).

[29] P. Chambon, J. D. Weill, and P. Mandel. "Nicotinamide mononucleotide activation of a new DNA-dependent polyadenylic acid synthesizing nuclear enzyme". In: *Biochemical and Biophysical Research Communications* 11.1 (1963), pp. 39–43. DOI: 10.1016/ 0006-291X(63)90024-X (cit. on p. 9).

[30] Jean-Christophe Amé, Catherine Spenlehauer, and Gilbert de Murcia. "The PARP superfamily". In: *BioEssays* 26.8 (2004), pp. 882–893. DOI: 10.1002/bies.20085 (cit. on p. 9).

[31] Zdenko Herceg and Zhao-Qi Wang. "Functions of poly(ADP-ribose) polymerase (PARP) in DNA repair, genomic integrity and cell death". In: *Mutation Research/Fundamental and Molecular Mechanisms of Mutagenesis* 477.1-2 (2001), pp. 97–110. DOI: 10.1016/ S0027-5107(01)00111-7 (cit. on p. 9).

[32] Chad V. Kuny and Christopher S. Sullivan. "Virus-Host Interactions and the ARTD/PARP Family of Enzymes". In: *PLoS Pathogens* 12.3 (2016), e1005453. DOI: 10.1371/ journal.ppat.1005453 (cit. on p. 9).

[33] Michael O. Hottiger, Paul O. Hassa, Bernhard Lüscher, Herwig Schüler, and Friedrich Koch-Nolte. "Toward a unified nomenclature for mammalian ADP-ribosyltransferases". In: *Trends in Biochemical Sciences* 35.4 (2010), pp. 208–219. DOI: 10.1016/j.tibs. 2009.12.003 (cit. on p. 9).

[34] Bryan A. Gibson and W. Lee Kraus. "New insights into the molecular and cellular functions of poly(ADP-ribose) and PARPs". In: *Nature Reviews. Molecular Cell Biology* 13.7 (2012), pp. 411–424. DOI: 10.1038/nrm3376 (cit. on p. 9).

[35] C. C. Kiehlbauch, N. Aboulela, E. L. Jacobson, D. P. Ringer, and M. K. Jacobson. "High Resolution Fractionation and Characterization of ADP-Ribose Polymers". In: *Analytical Biochemistry* 208.1 (1993), pp. 26–34. DOI: 10.1006/abio.1993.1004 (cit. on p. 9).

[36]   Dana V. Ferraris. "Evolution of Poly(ADP-ribose) Polymerase-1 (PARP-1) Inhibitors. From Concept to Clinic". In: *Journal of Medicinal Chemistry* 53.12 (2010), pp. 4561–4584. DOI: 10.1021/jm100012m (cit. on pp. 10–13).

[37]   László Virág and Csaba Szabó. "The therapeutic potential of poly(ADP-ribose) polymerase inhibitors". In: *Pharmacological Reviews* 54.3 (2002), pp. 375–429 (cit. on p. 10).

[38]   Marc de Block, Christoph Verduyn, Dirk de Brouwer, and Marc Cornelissen. "Poly(ADP-ribose) polymerase in plants affects energy homeostasis, cell death and stress tolerance". In: *The Plant Journal for Cell and Molecular Biology* 41.1 (2005), pp. 95–106. DOI: 10.1111/j.1365-313X.2004.02277.x (cit. on p. 10).

[39]   Philipp Schulz, Jenny Neukermans, Katrien van der Kelen, Per Mühlenbock, Frank van Breusegem, Graham Noctor, Markus Teige, Michael Metzlaff, and Matthew A. Hannah. "Chemical PARP inhibition enhances growth of *Arabidopsis* and reduces anthocyanin accumulation and the activation of stress protective mechanisms". In: *PloS One* 7.5 (2012), e37287. DOI: 10.1371/journal.pone.0037287 (cit. on p. 10).

[40]   Philipp Schulz, Karel Jansseune, Thomas Degenkolbe, Michaël Méret, Hannes Claeys, Aleksandra Skirycz, Markus Teige, Lothar Willmitzer, and Matthew A. Hannah. "Poly(ADP-ribose)polymerase activity controls plant growth by promoting leaf cell number". In: *PloS One* 9.2 (2014), e90322. DOI: 10.1371/journal.pone.0090322 (cit. on p. 10).

[41]   Sandy Vanderauwera, Marc de Block, Nancy van de Steene, Brigitte van de Cotte, Michael Metzlaff, and Frank van Breusegem. "Silencing of poly(ADP-ribose) polymerase in plants alters abiotic stress signal transduction". In: *Proceedings of the National Academy of Sciences of the United States of America* 104.38 (2007), pp. 15150–15155. DOI: 10.1073/pnas.0706668104 (cit. on p. 10).

[42]   M. R. Purnell and W. J. Whish. "Novel inhibitors of poly(ADP-ribose) synthetase". In: *The Biochemical Journal* 185.3 (1980), pp. 775–777 (cit. on pp. 11, 99).

[43]   Ming Tao, Chung Ho Park, Ron Bihovsky, Gregory J. Wells, Jean Husten, Mark A. Ator, and Robert L. Hudkins. "Synthesis and structure-activity relationships of novel poly(ADP-ribose) polymerase-1 inhibitors". In: *Bioorganic & Medicinal Chemistry Letters* 16.4 (2006), pp. 938–942. DOI: 10.1016/j.bmcl.2005.10.099 (cit. on p. 12).

[44] M. Banasik, H. Komura, M. Shimoyama, and K. Ueda. "Specific inhibitors of poly(ADP-ribose) synthetase and mono(ADP-ribosyl)transferase". In: *The Journal of Biological Chemistry* 267.3 (1992), pp. 1569–1575 (cit. on p. 12).

[45] R. J. Griffin, L. C. Pemberton, D. Rhodes, C. Bleasdale, K. Bowman, A. H. Calvert, N. J. Curtin, B. W. Durkacz, D. R. Newell, and J. K. Porteous. "Novel potent inhibitors of the DNA repair enzyme poly(ADP-ribose)polymerase (PARP)". In: *Anti-Cancer Drug Design* 10.6 (1995), pp. 507–514. DOI: 10.1177/0956797611435133 (cit. on p. 12).

[46] Stacie S. Canan Koch, Lars H. Thoresen, Jayashree G. Tikhe, Karen A. Maegley, Robert J. Almassy, Jianke Li, Xiao-Hong Yu, Scott E. Zook, Robert A. Kumpf, Cathy Zhang, Theodore J. Boritzki, Rena N. Mansour, Kanyin E. Zhang, Anne Ekker, Chris R. Calabrese, Nicola J. Curtin, Suzanne Kyle, Huw D. Thomas, Lan-Zhen Wang, A. Hilary Calvert, Bernard T. Golding, Roger J. Griffin, David R. Newell, Stephen E. Webber, and Zdenek Hostomsky. "Novel tricyclic poly(ADP-ribose) polymerase-1 inhibitors with potent anticancer chemopotentiating activity: design, synthesis, and X-ray cocrystal structure". In: *Journal of Medicinal Chemistry* 45.23 (2002), pp. 4961–4974 (cit. on p. 12).

[47] A. W. White, R. Almassy, A. H. Calvert, N. J. Curtin, R. J. Griffin, Z. Hostomsky, K. Maegley, D. R. Newell, S. Srinivasan, and B. T. Golding. "Resistance-modifying agents. 9. Synthesis and biological properties of benzimidazole inhibitors of the DNA repair enzyme poly(ADP-ribose) polymerase". In: *Journal of Medicinal Chemistry* 43.22 (2000), pp. 4084–4097 (cit. on p. 12).

[48] Huw D. Thomas, Christopher R. Calabrese, Michael A. Batey, Stacie Canan, Zdenek Hostomsky, Suzanne Kyle, Karen A. Maegley, David R. Newell, Donald Skalitzky, Lan-Zhen Wang, Stephen E. Webber, and Nicola J. Curtin. "Preclinical selection of a novel poly(ADP-ribose) polymerase inhibitor for clinical trial". In: *Molecular Cancer Therapeutics* 6.3 (2007), pp. 945–956. DOI: 10.1158/1535-7163.MCT-06-0552 (cit. on p. 12).

[49] Takayoshi Kinoshita, Isao Nakanishi, Masaichi Warizaya, Akinori Iwashita, Yoshiyuki Kido, Kouji Hattori, and Takashi Fujii. "Inhibitor-induced structural change of the active site of human poly(ADP-ribose) polymerase". In: *FEBS Letters* 556.1-3 (2004), pp. 43–46. DOI: 10.1016/S0014-5793(03)01362-0 (cit. on p. 13).

[50] Areum Park, Youn-Jung Kim, Eun-Mi Choi, Murray T. Brown, and Taejun Han. "A novel bioassay using root re-growth in *Lemna*". In: *Aquatic Toxicology (Amsterdam, Netherlands)* 140-141 (2013), pp. 415–424 (cit. on pp. 13, 14).

[51] David W. Bowker, Anthony N. Duffield, and Patrick Denny. "Methods for the isolation, sterilization and cultivation of Lemnaceae". In: *Freshwater Biology* 10 (1980), pp. 385–388 (cit. on p. 13).

[52] Richard A. Brain and Keith R. Solomon. "A protocol for conducting 7-day daily renewal tests with *Lemna gibba*". In: *Nature Protocols* 2.4 (2007), pp. 979–987. DOI: 10.1038/nprot.2007.146 (cit. on p. 13).

[53] G. Björndahl. *Growth performance, nutrient uptake and human utilization of duckweeds (Lemnaceae family)*. Oslo: The Agricultural Research Council of Norway, University of Oslo, 1982 (cit. on p. 13).

[54] E. Landolt. *The family Lemnaceae - a monographic study*. 1st ed. Zürich: Geobotanisches Institut ETH, Stiftung Rübel, 1986 (cit. on p. 13).

[55] Gordon D. Lemon, Usher Posluszny, and Brian C. Husband. "Potential and realized rates of vegetative reproduction in *Spirodela polyrhiza, Lemna minor,* and *Wolffia borealis*". In: *Aquatic Botany* 70.1 (2001), pp. 79–87. DOI: 10.1016/S0304-3770(00)00131-5 (cit. on pp. 13, 20, 95).

[56] *ImageJ - Image Processing and Analysis in Java*. URL: https://imagej.nih.gov/ij/ (visited on 11/18/2020) (cit. on pp. 15, 17, 105).

[57] Burlyn E. Michel and Merrill R. Kaufmann. "The Osmotic Potential of Polyethylene Glycol 6000". In: *Plant Physiology* 51 (1973), pp. 914–916 (cit. on pp. 14, 15).

[58] Nicholas P. Money. "Osmotic Pressure of Aqueous Polyethylene Glycols". In: *Plant Physiology* 91 (1989), pp. 766–769 (cit. on p. 15).

[59] Cloé Paul-Victor, Tobias Züst, Mark Rees, Daniel J. Kliebenstein, and Lindsay A. Turnbull. "A new method for measuring relative growth rate can uncover the costs of defensive compounds in *Arabidopsis thaliana*". In: *New Phytologist* 187.4 (2010), pp. 1102–1111. DOI: 10.1111/j.1469-8137.2010.03325.x (cit. on p. 17).

[60] Monya Baker. "Statisticians issue warning on P values". In: *Nature* 531 (2016), p. 151 (cit. on p. 19).

[61] Lewis G. Halsey, Douglas Curran-Everett, Sarah L. Vowler, and Gordon B. Drummond. "The fickle P value generates irreproducible results". In: *Nature Methods* 12.3 (2015), pp. 179–185 (cit. on p. 19).

[62] *'One-size-fits-all' threshold for P values under fire: Scientists hit back at a proposal to make it tougher to call findings statistically significant.* 2017. URL: https://www.nature.com/news/one-size-fits-all-threshold-for-p-values-under-fire-1.22625 (visited on 11/18/2020) (cit. on p. 19).

[63] Regina Nuzzo. "Statistical errors". In: *Nature* 506 (2014), pp. 150–152. DOI: 10.1038/506150a (cit. on p. 19).

[64] Geoff Cumming. *Understanding The New Statistics: Effect Sizes, Confidence Intervals, and Meta-Analysis*. New York: Taylor & Francis Group, 2012 (cit. on p. 19).

[65] Katherine S. Button, John P. A. Ioannidis, Claire Mokrysz, Brian A. Nosek, Jonathan Flint, Emma S. J. Robinson, and Marcus R. Munafò. "Power failure: why small sample size undermines the reliability of neuroscience". In: *Nature Reviews. Neuroscience* 14.5 (2013), pp. 365–376. DOI: 10.1038/nrn3475 (cit. on p. 19).

[66] Carl J. Huberty. "A history of effect size indices". In: *Educational and Psychological Measurement* 62.2 (2002), pp. 227–240 (cit. on p. 19).

[67] Shinichi Nakagawa and Innes C. Cuthill. "Effect size, confidence interval and statistical significance: a practical guide for biologists". In: *Biological Reviews of the Cambridge Philosophical Society* 82.4 (2007), pp. 591–605. DOI: 10.1111/j.1469-185X.2007.00027.x (cit. on p. 19).

[68] Jessica Middlemis Maher, Jonathan C. Markey, and Diane Ebert-May. "The other half of the story: effect size analysis in quantitative research". In: *CBE Life Sciences Education* 12.3 (2013), pp. 345–351. DOI: 10.1187/cbe.13-04-0082 (cit. on p. 19).

[69] Jacob Cohen. *Statistical power analysis for the behavioral sciences*. New York: Academic Press, 1969 (cit. on pp. 19, 29).

[70] Gene V. Glass. "Primary, Secondary, and Meta-Analysis of Research". In: *Educational Researcher* 5.10 (1976), pp. 3–8 (cit. on p. 19).

[71] Larry V. Hedges. "Distribution Theory of Glass's Estimator of Effect Size and Related Estimators". In: *Journal of Educational Statistics* 6.2 (1981), pp. 107–128 (cit. on p. 19).

[72] Ken Kelley. "Confidence Intervals for Standardized Effect Sizes: Theory, Application, and Implementation". In: *Journal of Statistical Software* 20.8 (2007). DOI: 10.18637/jss.v020.i08 (cit. on pp. 20, 31).

[73] E. Ashby and E. Wangermann. "Senescence and Rejuvenation in *Lemna minor*". In: *Nature* 164.4161 (1949), p. 187. DOI: 10.1038/164187a0 (cit. on p. 21).

[74] Patrick M. Barks, Robert A. Laird, and Niels Anten. "Senescence in duckweed: age–related declines in survival, reproduction and offspring quality". In: *Functional Ecology* 29.4 (2015), pp. 540–548. DOI: 10.1111/1365-2435.12359 (cit. on p. 21).

[75] Marie Laure Delignette-Muller and Christophe Dutang. "fitdistrplus: An R Package for Fitting Distributions". In: *Journal of Statistical Software* 64 (2015), pp. 1–34. DOI: 10.18637/jss.v064.i04 (cit. on p. 23).

[76] Markus Bühner and Matthias Ziegler. *Statistik für Psychologen und Sozialwissenschaftler*. 2nd ed. ps Psychologie. Pearson, 2017 (cit. on p. 29).

[77] Geoff Cumming. "The new statistics: why and how". In: *Psychological Science* 25.1 (2014), pp. 7–29. DOI: 10.1177/0956797613504966 (cit. on p. 31).

[78] Frank L. Schmidt, In-Sue Oh, and Theodore L. Hayes. "Fixed- versus random-effects models in meta-analysis: model properties and an empirical comparison of differences in results". In: *The British Journal of Mathematical and Statistical Psychology* 62.Pt 1 (2009), pp. 97–128. DOI: 10.1348/000711007X255327 (cit. on pp. 31, 32, 109).

[79] Larry V. Hedges and Jack L. Vevea. "Fixed- and random-effects models in meta-analysis". In: *Psychological Methods* 3.4 (1998), pp. 486–504. DOI: 10.1037/1082-989X.3.4.486 (cit. on pp. 31, 32, 109).

[80] Michael Borenstein, Larry V. Hedges, Julian P. T. Higgins, and Hannah R. Rothstein. "A basic introduction to fixed-effect and random-effects models for meta-analysis". In: *Research Synthesis Methods* 1.2 (2010), pp. 97–111. DOI: 10.1002/jrsm.12 (cit. on pp. 32, 109).

[81] W. Viechtbauer. "Conducting meta-analyses in R with the metafor package". In: *Journal of Statistical Software* 36.3 (2010), pp. 1–48 (cit. on p. 32).

[82] Jerry L. Hintze and Ray D. Nelson. "Violin Plots: A Box Plot-Density Trace Synergism". In: *The American Statistician* 52.2 (1998), p. 181. DOI: 10.2307/2685478 (cit. on p. 38).

[83]   B. Efron and R. Tibshirani. "Bootstrap Methods for Standard Errors, Confidence Intervals, and Other Measures of Statistical Accuracy". In: *Statistical Science* 1.1 (1986), pp. 54–75 (cit. on p. 44).

[84]   Abdul Hameed, Mariya Al-Rashida, Maliha Uroos, Arshia Syed Abid Ali, Marium Ishtiaq, and Khalid Mohammed Khan. "Quinazoline and quinazolinone as important medicinal scaffolds: a comparative patent review (2011-2016)". In: *Expert Opinion on Therapeutic Patents* 28.4 (2018), pp. 281–297. DOI: 10.1080/13543776.2018. 1432596 (cit. on p. 52).

[85]   Stefan von Niementowski. "Synthesen von Chinazolinverbindungen". In: *Journal für Praktische Chemie* 51 (1895), pp. 564–572 (cit. on p. 52).

[86]   François-René Alexandre, Amaya Berecibar, and Thierry Besson. "Microwave-assisted Niementowski reaction. Back to the roots". In: *Tetrahedron Letters* 43 (2002), pp. 3911–3913 (cit. on p. 52).

[87]   Feng Li, Yiqing Feng, Qingqing Meng, Wenhua Li, Zhiming Li, Quanrui Wang, and Fenggang Tao. "An efficient construction of quinazolin-4(3*H*)-ones under microwave irradiation". In: *ARKIVOC* i (2007), pp. 40–50 (cit. on pp. 52, 53).

[88]   Kh. S. Shikhaliev, A. S. Shestakov, S. M. Medvedeva, and N. V. Gusakova. "Cyanamides in cyclization reactions with anthranilates, 2-aminophenyl ketones, and methyl 2-(3-oxopiperazin-2-yl)acetate". In: *Russian Chemical Bulletin, International Edition* 57 (2008), pp. 170–176 (cit. on pp. 53, 54, 58, 60).

[89]   C. J. Shishoo, M. B. Devani, U. S. Pathak, S. Ananthan, V. S. Bhadti, G. V. Ullas, K. S. Jain, I. S. Rathod, D. S. Talati, and N. H. Doshi. "Reaction of Nitriles Under Acidic Conditions. Part III. A Facile Synthesis of Thienopyrimidin-4(3*H*)-ones". In: *Journal of Heterocyclic Chemistry* 21 (1984), pp. 375–380 (cit. on p. 54).

[90]   Xiaowei Liu, Hua Fu, Yuyang Jiang, and Yufen Zhao. "A simple and efficient approach to quinazolinones under mild copper-catalyzed conditions". In: *Angewandte Chemie (International ed. in English)* 48.2 (2009), pp. 348–351. DOI: 10.1002/anie. 200804675 (cit. on p. 54).

[91]   Xiaodong Zhang, Deju Ye, Haifeng Sun, Diliang Guo, Jiang Wang, He Huang, Xu Zhang, Hualiang Jiang, and Hong Liu. "Microwave-assisted synthesis of quinazolinone derivatives by efficient and rapid iron-catalyzed cyclization in water". In: *Green Chemistry* 11.11 (2009), p. 1881. DOI: 10.1039/b916124b (cit. on p. 54).

[92]   William D. Dean and Eleftherios P. Papadopoulos. "Synthesis of 4(3*H*)-Quinazolinones from Derivatives of Methyl 2-Isothiocyanatobenzoate". In: *Journal of Heterocyclic Chemistry* 19 (1982), pp. 1117–1124 (cit. on p. 54).

[93]   Jack DeRuiter, Abram N. Brubaker, Jane Millen, and Thomas N. Riley. "Design and Synthesis of 2-(Arylamino)-4(3*H*)-quinazolinones as Novel Inhibitors of Rat Lens Aldose Reductase". In: *Journal of Medicinal Chemistry* 29 (1986), pp. 627–629 (cit. on p. 55).

[94]   Bénédicte Erb, Rufine Akue, Benoît Rigo, Bernard Pirotte, and Daniel Couturier. "Synthesis of 2-Aminoquinazoline-4(3*H*)-one Derivatives as Potential Potassium Channel Openers". In: *Journal of Heterocyclic Chemistry* 37 (2000), pp. 253–260 (cit. on pp. 55, 56, 58).

[95]   Fabian Somers, Raogo Ouedraogo, Marie-Hélène Antoine, Pascal de Tullio, Bénédicte Becker, Jeanine Fontaine, Jacques Damas, Léon Dupont, Benoit Rigo, Jacques Delarge, Philippe Lebrun, and Bernard Pirotte. "Original 2-Alkylamino-6-halogenoquinazolin-4(3*H*)-ones and K_{ATP} Channel Activity". In: *Journal of Medicinal Chemistry* 44.16 (2001), pp. 2575–2585. DOI: 10.1021/jm0004648 (cit. on pp. 56, 58).

[96]   Jacob Heppell and Jasim Al-Rawi. "Functionalization of Quinazolin-4-ones Part 1: Synthesis of Novel 7-Substituted-2-thioxo Quinazolin-4-ones from 4-Substituted-2-Aminobenzoic Acids and $PPh_3(SCN)_2$". In: *Journal of Heterocyclic Chemistry* 51.1 (2014), pp. 162–174. DOI: 10.1002/jhet.1669 (cit. on pp. 56, 58).

[97]   Jacob T. Heppell and Jasim M. A. Al-Rawi. "Functionalization of Quinazolin-4-Ones Part 2: Reactivity of 2-Amino-3,4,5, or 6-Nitrobenzoic Acids with Triphenylphosphine Thiocyanate, Alkyl Isothiocyanates, and Further Derivatization Reactions". In: *Journal of Heterocyclic Chemistry* 52.5 (2015), pp. 1361–1367. DOI: 10.1002/jhet.2235 (cit. on pp. 56, 58).

[98]   Joseph A. DiMasi, Henry G. Grabowski, and Ronald W. Hansen. "Innovation in the pharmaceutical industry: New estimates of R&D costs". In: *Journal of Health Economics* 47 (2016), pp. 20–33. DOI: 10.1016/j.jhealeco.2016.01.012 (cit. on p. 56).

[99]   *The 5 most expensive drugs in the United States*. 2018-05-12. URL: https://edition.cnn.com/2018/05/11/health/most-expensive-prescription-drugs/index.html (visited on 11/18/2020) (cit. on p. 56).

[100] James N. Ayres, Kenneth B. Ling, and Louis C. Morrill. "N-Cyanation of Secondary Amines Using Trichloroacetonitrile". In: *Organic Letters* 18.21 (2016), pp. 5528–5531. DOI: 10.1021/acs.orglett.6b02775 (cit. on p. 58).

[101] Marie-Hélène Larraufie, Giovanni Maestri, Max Malacria, Cyril Ollivier, Louis Fensterbank, and Emmanuel Lacôte. "The Cyanamide Moiety, Synthesis and Reactivity". In: *Synthesis* 44.9 (2012), pp. 1279–1292. DOI: 10.1055/s-0031-1289749 (cit. on p. 58).

[102] M. R. Ranga Prabhath, Luke Williams, Shreesha V. Bhat, and Pallavi Sharma. "Recent Advances in Cyanamide Chemistry: Synthesis and Applications". In: *Molecules (Basel, Switzerland)* 22.4 (2017). DOI: 10.3390/molecules22040615 (cit. on p. 58).

[103] Kazumasa Hayasaka, Kozo Fukumoto, and Hiroshi Nakazawa. "Dehydrogenative desulfurization of thiourea derivatives to give carbodiimides, using hydrosilane and an iron complex". In: *Dalton Transactions (Cambridge, England : 2003)* 42.28 (2013), pp. 10271–10276. DOI: 10.1039/c3dt50996f (cit. on p. 58).

[104] Santosh K. Sahoo, Latonglila Jamir, Srimanta Guin, and Bhisma K. Patel. "Copper(I)-Catalyzed Cascade Synthesis of 2-Arylsulfanyl-arylcyanamides". In: *Advanced Synthesis & Catalysis* 352.14-15 (2010), pp. 2538–2548. DOI: 10.1002/adsc.201000383 (cit. on p. 58).

[105] Jayashree Nath, Bhisma K. Patel, Latonglila Jamir, Upasana Bora Sinha, and K. V. V. V. Satyanarayana. "A one-pot preparation of cyanamide from dithiocarbamate using molecular iodine". In: *Green Chemistry* 11.10 (2009), p. 1503. DOI: 10.1039/b914283p (cit. on p. 58).

[106] Abdur Rezzak Ali, Harisadhan Ghosh, and Bhisma K. Patel. "A greener synthetic protocol for the preparation of carbodiimide". In: *Tetrahedron Letters* 51.7 (2010), pp. 1019–1021. DOI: 10.1016/j.tetlet.2009.12.017 (cit. on p. 58).

[107] Michael P. Hay, Sandra Turcotte, Jack U. Flanagan, Muriel Bonnet, Denise A. Chan, Patrick D. Sutphin, Phuong Nguyen, Amato J. Giaccia, and William A. Denny. "4-Pyridylanilinothiazoles That Selectively Target von Hippel-Lindau Deficient Renal Cell Carcinoma Cells by Inducing Autophagic Cell Death". In: *Journal of Medicinal Chemistry* 53.2 (2010), pp. 787–797. DOI: 10.1021/jm901457w (cit. on pp. 58, 59).

[108] C. R. Rasmussen, F. J. Villani, L. E. Weaner, B. E. Reynolds, A. R. Hood, L. R. Hecker, S. O. Nortey, A. Hanslin, M. J. Costanzo, E. T. Powell, and A. J. Molinari. "Improved Procedures for the Preparation of Cycloalkyl-, Arylalkyl-, and Arylthioureas". In: *Synthesis* 6 (1988), pp. 456–459 (cit. on p. 58).

[109] R Core Team. *R: A Language and Environment for Statistical Computing*. Vienna, Austria, 2017 (cit. on p. 108).

List of Figures

List of Tables

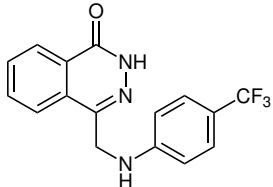| BER-C*xxx*	IPB	Structure	$d_{st}\,(CI_{0.95})$	$d_{rec}\,(CI_{0.95})$	$d_{tot}\,(CI_{0.95})$
001	574		0.123 (± 1.136)	-0.468 (± 1.138)	-0.268 (± 1.131)
002	575		-0.439 (± 1.137)	0.066 (± 1.134)	-0.444 (± 1.137)
003	576		-0.067 (± 1.130)	-0.784 (± 1.164)	-0.761 (± 1.161)
004	577		0.381 (± 1.153)	-0.430 (± 1.136)	0.060 (± 1.133)
005	578		0.989 (± 1.231)	-0.386 (± 1.135)	0.792 (± 1.200)
006	579		0.109 (± 1.135)	0.368 (± 1.152)	0.445 (± 1.159)
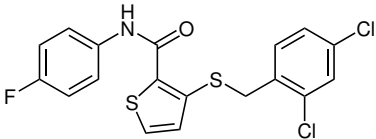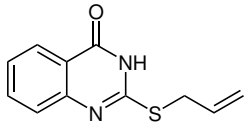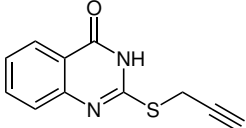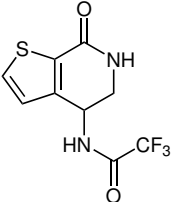
BER-C*xxx*	IPB	Structure	$d_{st}\,(CI_{0.95})$	$d_{rec}\,(CI_{0.95})$	$d_{tot}\,(CI_{0.95})$
007	580		0.017 (± 1.132)	1.227 (± 1.275)	1.090 (± 1.249)
008	581		0.146 (± 1.137)	0.860 (± 1.210)	0.917 (± 1.219)
009	582		-0.759 (± 1.161)	0.339 (± 1.149)	-0.571 (± 1.145)
010	583		0.623 (± 1.178)	0.664 (± 1.183)	1.291 (± 1.287)
011	584		1.490 (± 1.330)	0.707 (± 1.188)	2.318 (± 1.543)
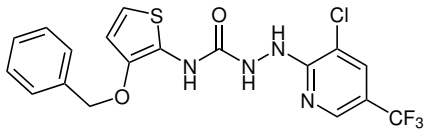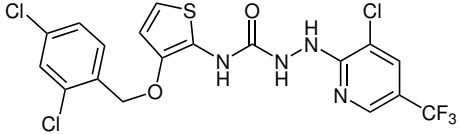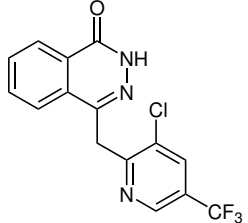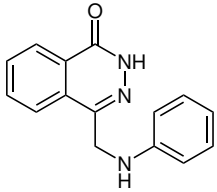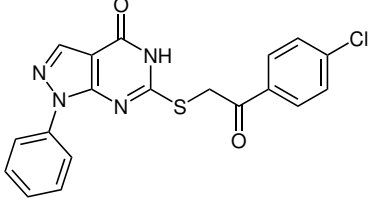
BER-C*xxx*	IPB	Structure	$d_{st}\,(CI_{0.95})$	$d_{rec}\,(CI_{0.95})$	$d_{tot}\,(CI_{0.95})$
012	585		0.944 (± 1.224)	0.498 (± 1.164)	1.512 (± 1.335)
013	586		0.266 (± 1.144)	-0.293 (± 1.132)	0.048 (± 1.133)
014	587		0.333 (± 1.149)	-0.870 (± 1.173)	-0.379 (± 1.134)
015	588		0.338 (± 1.149)	-0.682 (± 1.154)	-0.208 (± 1.130)
016	589		-1.121 (± 1.208)	-0.353 (± 1.133)	-1.588 (± 1.295)
017	590		-1.074 (± 1.201)	-0.404 (± 1.135)	-1.579 (± 1.293)
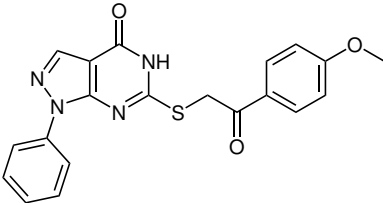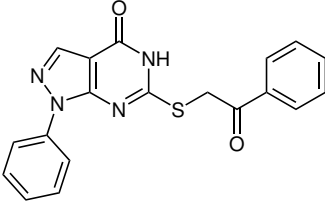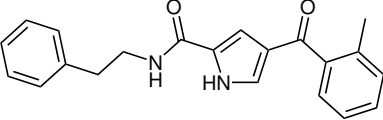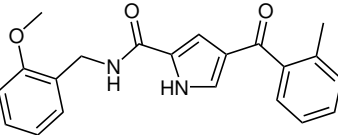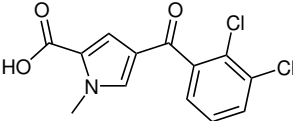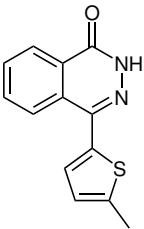
BER-C*xxx*	IPB	Structure	$d_{st}\,(CI_{0.95})$	$d_{rec}\,(CI_{0.95})$	$d_{tot}\,(CI_{0.95})$
018	591		-0.405 (± 1.135)	-0.183 (± 1.130)	-0.622 (± 1.149)
019	592		-0.107 (± 1.130)	0.256 (± 1.143)	0.101 (± 1.135)
020	593		-0.037 (± 1.131)	0.791 (± 1.200)	0.648 (± 1.181)
021	594		0.262 (± 1.144)	0.115 (± 1.136)	0.400 (± 1.154)
022	595		-0.600 (± 1.147)	1.366 (± 1.303)	0.506 (± 1.165)
023	596		-0.417 (± 1.136)	1.869 (± 1.421)	1.154 (± 1.260)
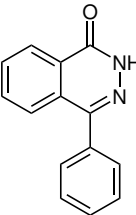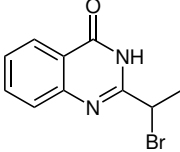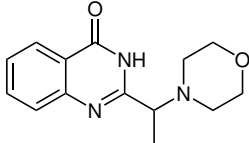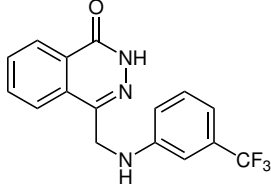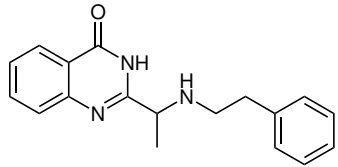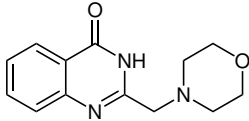
BER-C*xxx*	IPB	Structure	$d_{\text{st}}\,(CI_{0.95})$	$d_{\text{rec}}\,(CI_{0.95})$	$d_{\text{tot}}\,(CI_{0.95})$
024	597		-0.315 (± 1.132)	1.620 (± 1.360)	1.053 (± 1.242)
025	598		0.840 (± 1.207)	-0.125 (± 1.130)	0.850 (± 1.209)
026	599		-0.426 (± 1.136)	0.359 (± 1.151)	-0.174 (± 1.130)
027	600		-0.625 (± 1.149)	0.372 (± 1.152)	-0.390 (± 1.135)
028	601		-0.116 (± 1.130)	1.388 (± 1.308)	1.078 (± 1.247)
029	602		0.640 (± 1.180)	1.543 (± 1.342)	2.077 (± 1.476)
030	603		-0.653 (± 1.151)	0.679 (± 1.185)	-0.153 (± 1.130)
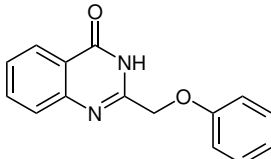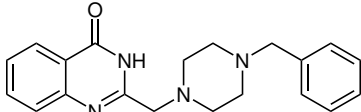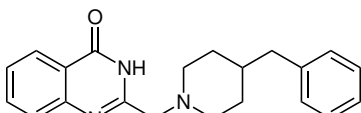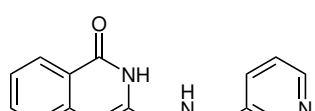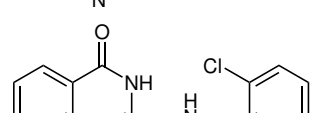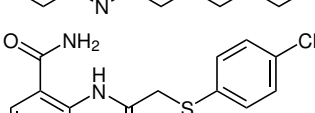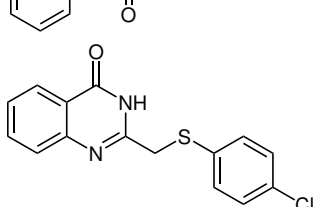
BER-C*xxx*	IPB	Structure	$d_{st}\,(CI_{0.95})$	$d_{rec}\,(CI_{0.95})$	$d_{tot}\,(CI_{0.95})$
031	604		-0.591 (± 1.146)	0.309 (± 1.147)	-0.406 (± 1.135)
032	605		0.879 (± 1.213)	2.019 (± 1.460)	2.764 (± 1.677)
033	606		-0.420 (± 1.136)	0.364 (± 1.151)	-0.161 (± 1.130)
034	607		-1.141 (± 1.211)	0.640 (± 1.180)	-0.744 (± 1.160)
035	608		-0.685 (± 1.154)	0.331 (± 1.149)	-0.494 (± 1.140)
036	609		-0.926 (± 1.180)	0.286 (± 1.145)	-0.807 (± 1.166)
037	610		-0.527 (± 1.142)	0.828 (± 1.205)	0.121 (± 1.136)

BER-Cxxx	IPB	Structure	$d_{st}\,(CI_{0.95})$	$d_{rec}\,(CI_{0.95})$	$d_{tot}\,(CI_{0.95})$
039	612		-0.167 (± 1.130)	0.559 (± 1.170)	0.297 (± 1.146)
040	613		-0.423 (± 1.136)	0.630 (± 1.179)	0.067 (± 1.134)
041	614		0.091 (± 1.135)	0.780 (± 1.198)	0.784 (± 1.199)
042	615		-0.664 (± 1.152)	0.307 (± 1.147)	-0.490 (± 1.140)
043	616		0.222 (± 1.141)	1.416 (± 1.313)	1.488 (± 1.329)
044	617		0.583 (± 1.173)	0.441 (± 1.158)	1.050 (± 1.242)
045	618		-0.017 (± 1.131)	0.624 (± 1.178)	0.524 (± 1.166)

BER-C*xxx*	IPB	Structure	$d_{st}\,(CI_{0.95})$	$d_{rec}\,(CI_{0.95})$	$d_{tot}\,(CI_{0.95})$
046	619		1.261 (± 1.281)	2.181 (± 1.504)	3.342 (± 1.864)
047	620		0.173 (± 1.138)	2.939 (± 1.732)	2.761 (± 1.676)
048	621		-0.300 (± 1.132)	1.645 (± 1.366)	1.092 (± 1.249)
049	622		-0.693 (± 1.155)	0.546 (± 1.169)	-0.316 (± 1.132)
050	623		0.346 (± 1.150)	1.543 (± 1.342)	1.741 (± 1.389)
051	624		-0.299 (± 1.132)	1.183 (± 1.266)	0.690 (± 1.186)
052	625		0.107 (± 1.135)	0.167 (± 1.138)	0.268 (± 1.144)

BER-C*xxx*	IPB	Structure	$d_{st}\,(CI_{0.95})$	$d_{rec}\,(CI_{0.95})$	$d_{tot}\,(CI_{0.95})$
053	626		0.496 (± 1.164)	0.436 (± 1.158)	0.947 (± 1.224)
054	627		0.522 (± 1.166)	0.800 (± 1.201)	1.294 (± 1.288)
055	628		-0.354 (± 1.133)	-0.474 (± 1.139)	-0.817 (± 1.167)
056	629		0.037 (± 1.133)	-0.633 (± 1.149)	-0.510 (± 1.141)
057	630		-0.627 (± 1.149)	-0.348 (± 1.133)	-1.020 (± 1.193)
058	631		-0.330 (± 1.133)	-0.050 (± 1.131)	-0.420 (± 1.136)
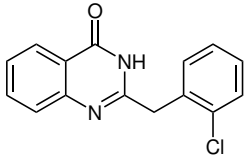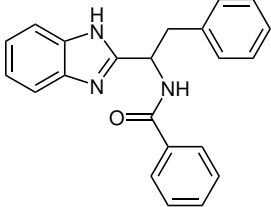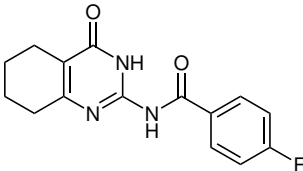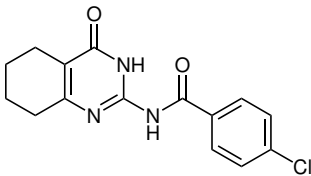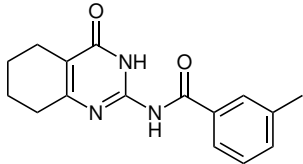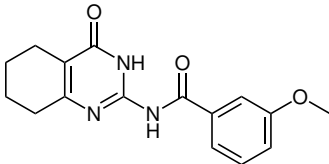
BER-C*xxx*	IPB	Structure	$d_{st}\,(CI_{0.95})$	$d_{rec}\,(CI_{0.95})$	$d_{tot}\,(CI_{0.95})$
059	632		-0.410 (± 1.136)	0.315 (± 1.147)	-0.194 (± 1.130)
060	633		0.865 (± 1.211)	0.966 (± 1.227)	1.830 (± 1.411)
061	634		1.422 (± 1.315)	0.611 (± 1.176)	2.157 (± 1.498)
062	635		0.263 (± 1.144)	-0.448 (± 1.137)	-0.091 (± 1.130)
063	636		0.302 (± 1.146)	-0.014 (± 1.131)	0.333 (± 1.149)
064	637		-0.513 (± 1.141)	1.203 (± 1.270)	0.463 (± 1.160)
065	638		0.114 (± 1.135)	1.400 (± 1.310)	1.352 (± 1.300)
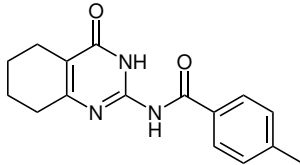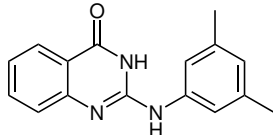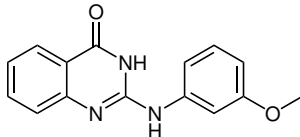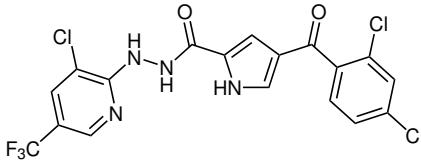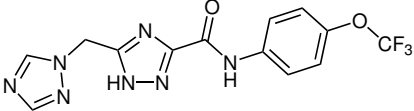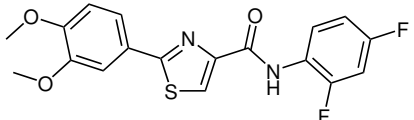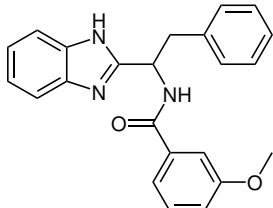
BER-C*xxx*	IPB	Structure	$d_{st}\,(CI_{0.95})$	$d_{rec}\,(CI_{0.95})$	$d_{tot}\,(CI_{0.95})$
066	639		-0.719 (± 1.157)	1.262 (± 1.282)	0.280 (± 1.145)
067	640		-0.165 (± 1.130)	0.566 (± 1.171)	0.305 (± 1.147)
068	641		-0.190 (± 1.130)	0.443 (± 1.158)	0.169 (± 1.138)
069	642		-0.659 (± 1.152)	0.053 (± 1.133)	-0.706 (± 1.156)
070	643		-0.037 (± 1.131)	-0.214 (± 1.130)	-0.229 (± 1.130)
071	644		0.922 (± 1.220)	0.694 (± 1.187)	1.658 (± 1.369)
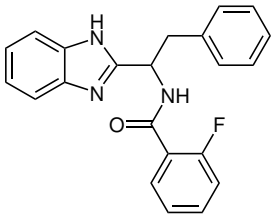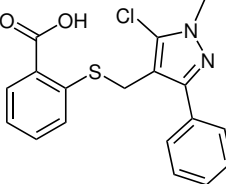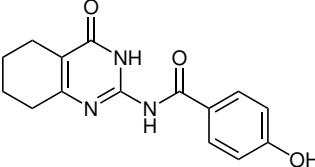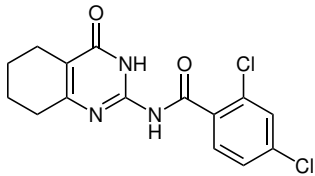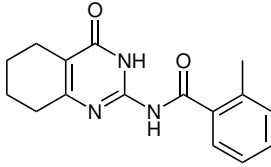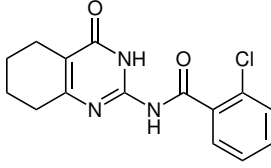
BER-C*xxx*	IPB	Structure	$d_{st}\,(CI_{0.95})$	$d_{rec}\,(CI_{0.95})$	$d_{tot}\,(CI_{0.95})$
072	645		-0.161 (± 1.130)	-0.515 (± 1.141)	-0.634 (± 1.150)
073	646		-0.006 (± 1.131)	0.227 (± 1.141)	0.191 (± 1.139)
074	647		0.277 (± 1.145)	0.618 (± 1.177)	0.856 (± 1.210)
075	648		0.681 (± 1.185)	0.940 (± 1.223)	1.597 (± 1.354)
076	649		0.963 (± 1.227)	0.200 (± 1.140)	1.273 (± 1.284)
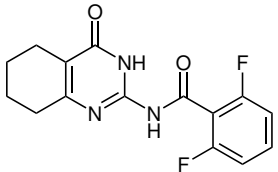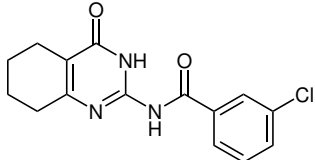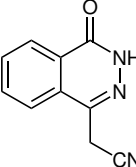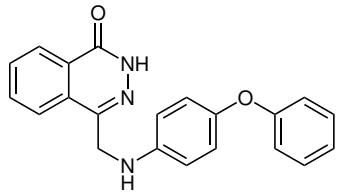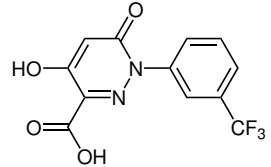
BER-C*xxx*	IPB	Structure	$d_{st}\,(CI_{0.95})$	$d_{rec}\,(CI_{0.95})$	$d_{tot}\,(CI_{0.95})$
077	650		-0.469 (± 1.138)	0.836 (± 1.207)	0.194 (± 1.139)
078	651		1.134 (± 1.257)	0.876 (± 1.213)	2.058 (± 1.471)
079	652		0.805 (± 1.202)	0.659 (± 1.182)	1.493 (± 1.331)
080	653		-0.269 (± 1.131)	0.349 (± 1.150)	-0.003 (± 1.132)
081	654		-0.262 (± 1.131)	0.602 (± 1.175)	0.227 (± 1.141)
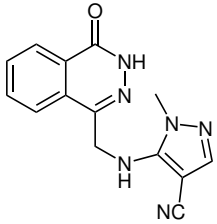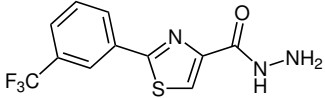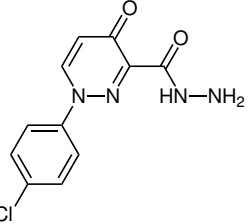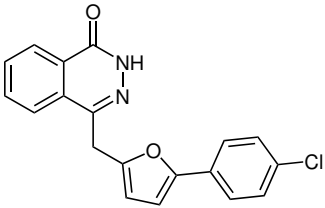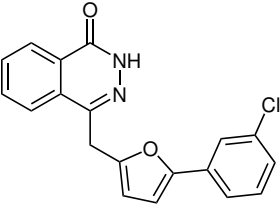
BER-C*xxx*	IPB	Structure	$d_{st}\,(CI_{0.95})$	$d_{rec}\,(CI_{0.95})$	$d_{tot}\,(CI_{0.95})$
082	655		-0.743 (± 1.159)	0.498 (± 1.164)	-0.415 (± 1.136)
083	656		-1.355 (± 1.248)	0.232 (± 1.142)	-1.344 (± 1.246)
084	657		-1.833 (± 1.351)	0.440 (± 1.158)	-1.710 (± 1.322)
085	658		0.162 (± 1.138)	0.650 (± 1.181)	0.752 (± 1.195)
086	659		0.583 (± 1.173)	0.307 (± 1.147)	0.934 (± 1.222)

BER-C*xxx*	IPB	Structure	d_{st} ($CI_{0.95}$)	d_{rec} ($CI_{0.95}$)	d_{tot} ($CI_{0.95}$)
087	660		0.062 (± 1.133)	0.106 (± 1.135)	0.164 (± 1.138)
088	661		0.778 (± 1.198)	1.356 (± 1.301)	2.071 (± 1.474)
089	662		1.069 (± 1.245)	1.262 (± 1.281)	2.321 (± 1.544)
090	663		0.401 (± 1.154)	0.655 (± 1.182)	1.029 (± 1.238)
091	664		0.646 (± 1.181)	1.232 (± 1.276)	1.813 (± 1.406)
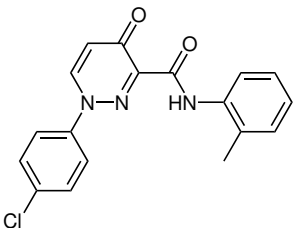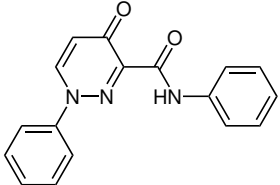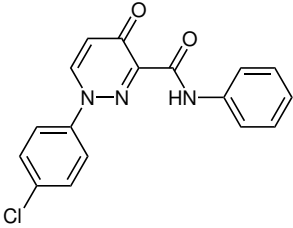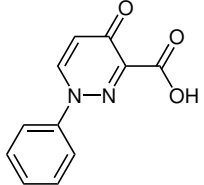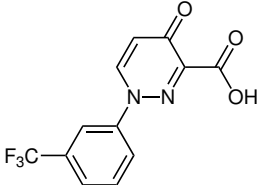
BER-C*xxx*	IPB	Structure	$d_{st}\,(CI_{0.95})$	$d_{rec}\,(CI_{0.95})$	$d_{tot}\,(CI_{0.95})$
092	665		0.390 (± 1.154)	1.658 (± 1.369)	1.892 (± 1.427)
093	666		-0.563 (± 1.144)	0.761 (± 1.196)	0.020 (± 1.132)
094	667		0.107 (± 1.135)	1.040 (± 1.240)	1.029 (± 1.238)
095	668		0.764 (± 1.196)	1.045 (± 1.241)	1.784 (± 1.399)
096	669		0.451 (± 1.159)	1.836 (± 1.412)	2.117 (± 1.487)

BER-C*xxx*	IPB	Structure	d_{st} ($CI_{0.95}$)	d_{rec} ($CI_{0.95}$)	d_{tot} ($CI_{0.95}$)
097	670		-0.121 (± 1.130)	0.868 (± 1.211)	0.619 (± 1.177)
098	671		0.219 (± 1.141)	0.158 (± 1.138)	0.388 (± 1.153)
099	672		-0.371 (± 1.134)	0.008 (± 1.132)	-0.417 (± 1.136)
100	673		-1.453 (± 1.267)	0.215 (± 1.141)	-1.472 (± 1.271)
101	674		-1.025 (± 1.193)	1.232 (± 1.276)	-0.095 (± 1.130)
102	675		-0.898 (± 1.177)	-0.068 (± 1.130)	-1.085 (± 1.202)

BER-C*xxx*	IPB	Structure	$d_{st}\,(CI_{0.95})$	$d_{rec}\,(CI_{0.95})$	$d_{tot}\,(CI_{0.95})$
103	676		-0.235 (± 1.130)	0.509 (± 1.165)	0.176 (± 1.138)
104	677		-0.258 (± 1.131)	0.858 (± 1.210)	0.454 (± 1.159)
105	678		0.004 (± 1.132)	-0.051 (± 1.131)	-0.040 (± 1.131)
106	679		-0.162 (± 1.130)	-0.334 (± 1.133)	-0.477 (± 1.139)
107	680		-0.520 (± 1.141)	0.471 (± 1.161)	-0.183 (± 1.130)
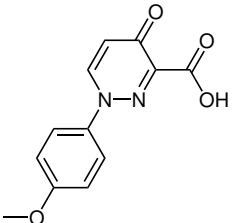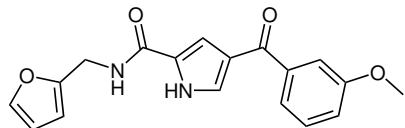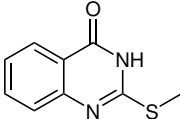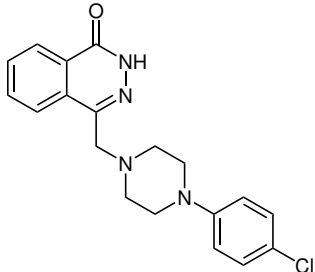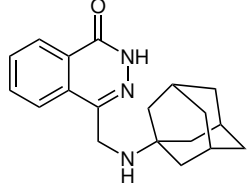
BER-C*xxx*	IPB	Structure	d_{st} ($CI_{0.95}$)	d_{rec} ($CI_{0.95}$)	d_{tot} ($CI_{0.95}$)
108	681		-0.312 (± 1.132)	0.362 (± 1.151)	-0.041 (± 1.131)
109	682		0.209 (± 1.140)	-1.074 (± 1.201)	-0.697 (± 1.155)
110	683		-0.298 (± 1.132)	-0.799 (± 1.165)	-1.036 (± 1.195)
111	684		0.623 (± 1.178)	-0.377 (± 1.134)	0.382 (± 1.153)
112	685		-0.288 (± 1.131)	1.008 (± 1.234)	0.551 (± 1.169)
113	686		-1.350 (± 1.247)	0.919 (± 1.220)	-0.739 (± 1.159)
114	687		-0.747 (± 1.160)	0.432 (± 1.157)	-0.477 (± 1.139)

BER-C*xxx*	IPB	Structure	$d_{st}\,(CI_{0.95})$	$d_{rec}\,(CI_{0.95})$	$d_{tot}\,(CI_{0.95})$
115	688		1.249 (± 1.279)	0.217 (± 1.141)	1.616 (± 1.359)
116	689		0.562 (± 1.171)	0.309 (± 1.147)	0.912 (± 1.218)
117	690		0.891 (± 1.215)	-0.087 (± 1.130)	0.942 (± 1.223)
118	691		-0.968 (± 1.186)	0.404 (± 1.155)	-0.753 (± 1.160)
119	692		-1.749 (± 1.331)	0.261 (± 1.144)	-1.770 (± 1.336)
120	693		-0.533 (± 1.142)	1.343 (± 1.298)	0.563 (± 1.171)
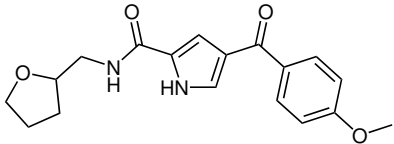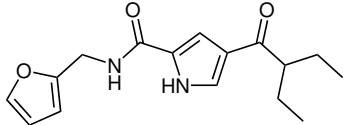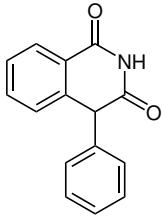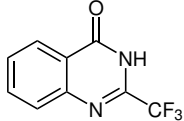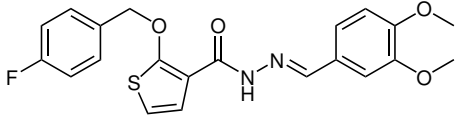
2-Amino-3-(4-Methoxyphenyl)-quinazolin-4(3H)-one

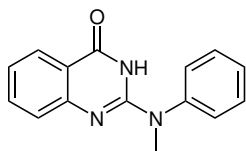**Sum formula:** $C_{15}H_{13}N_3O_2$
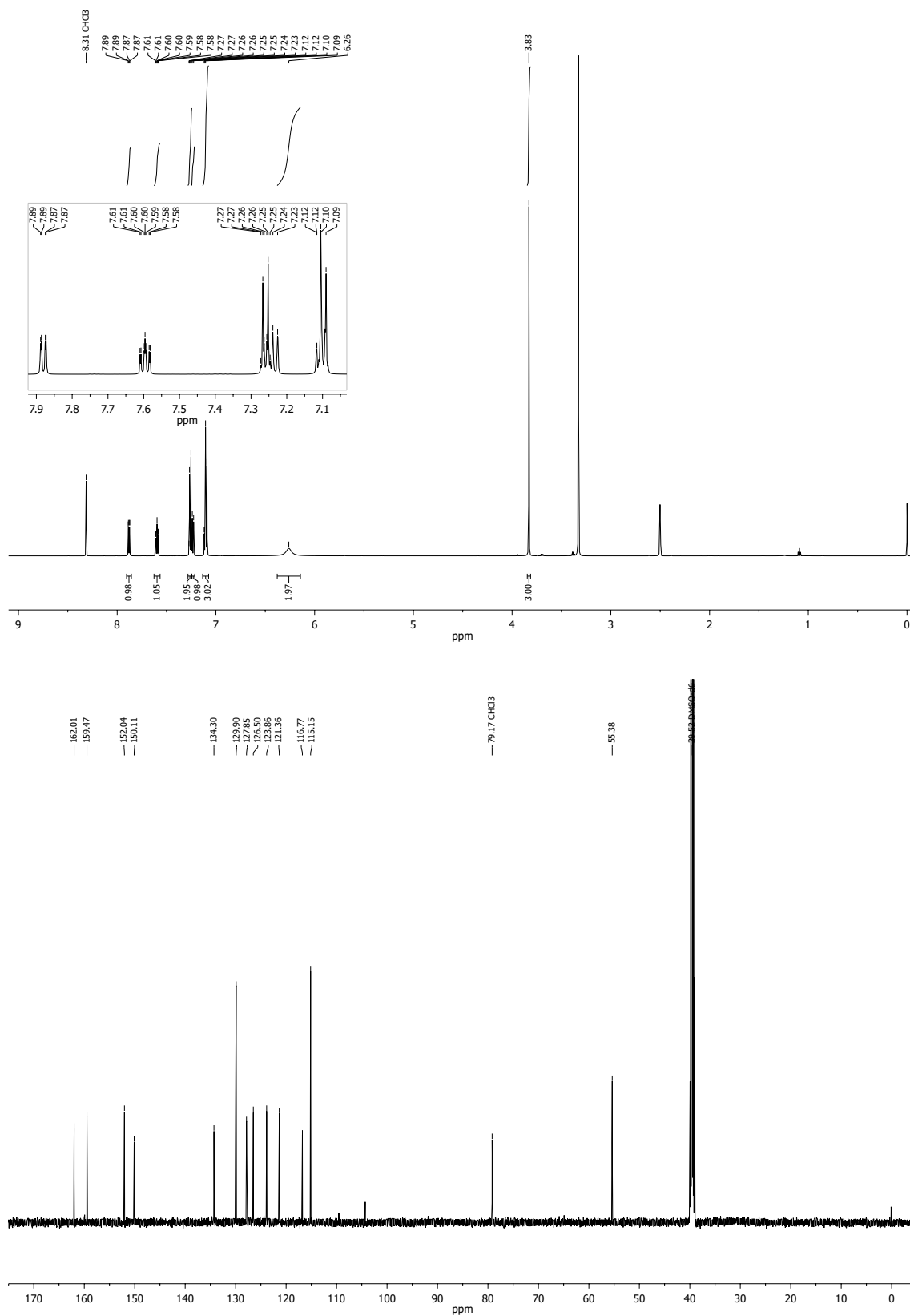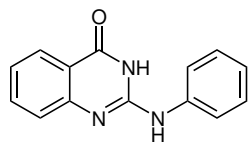
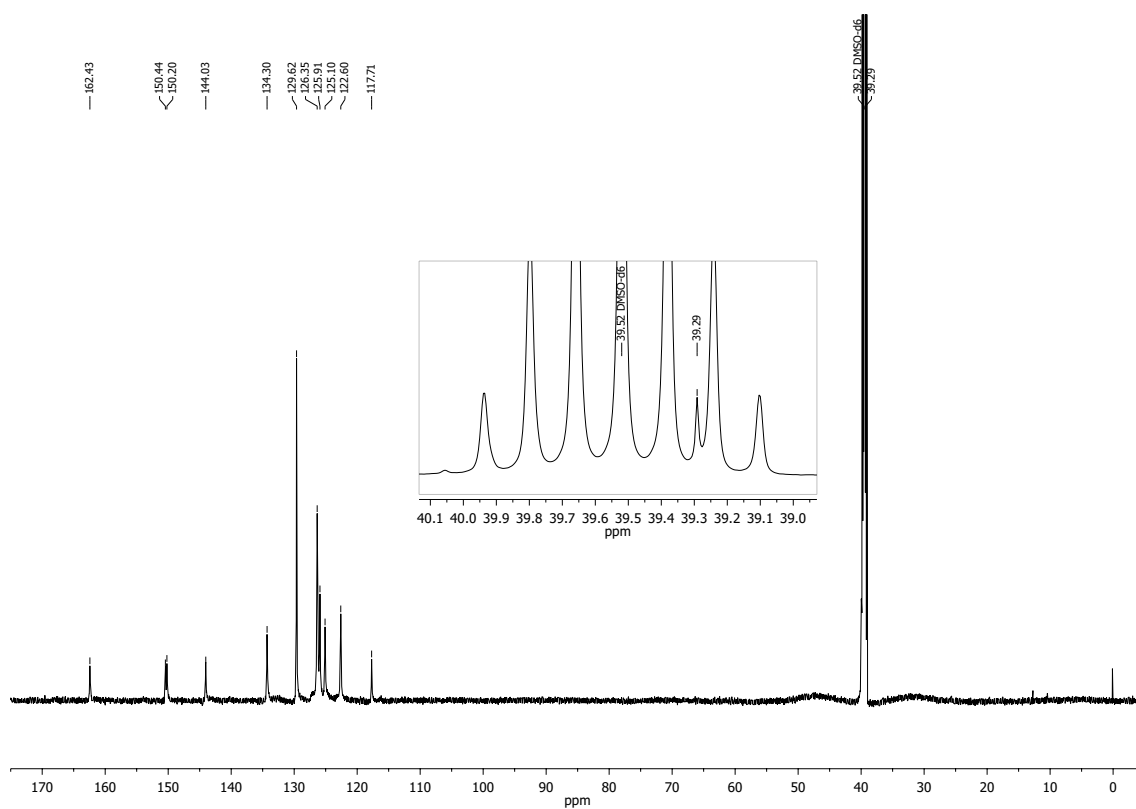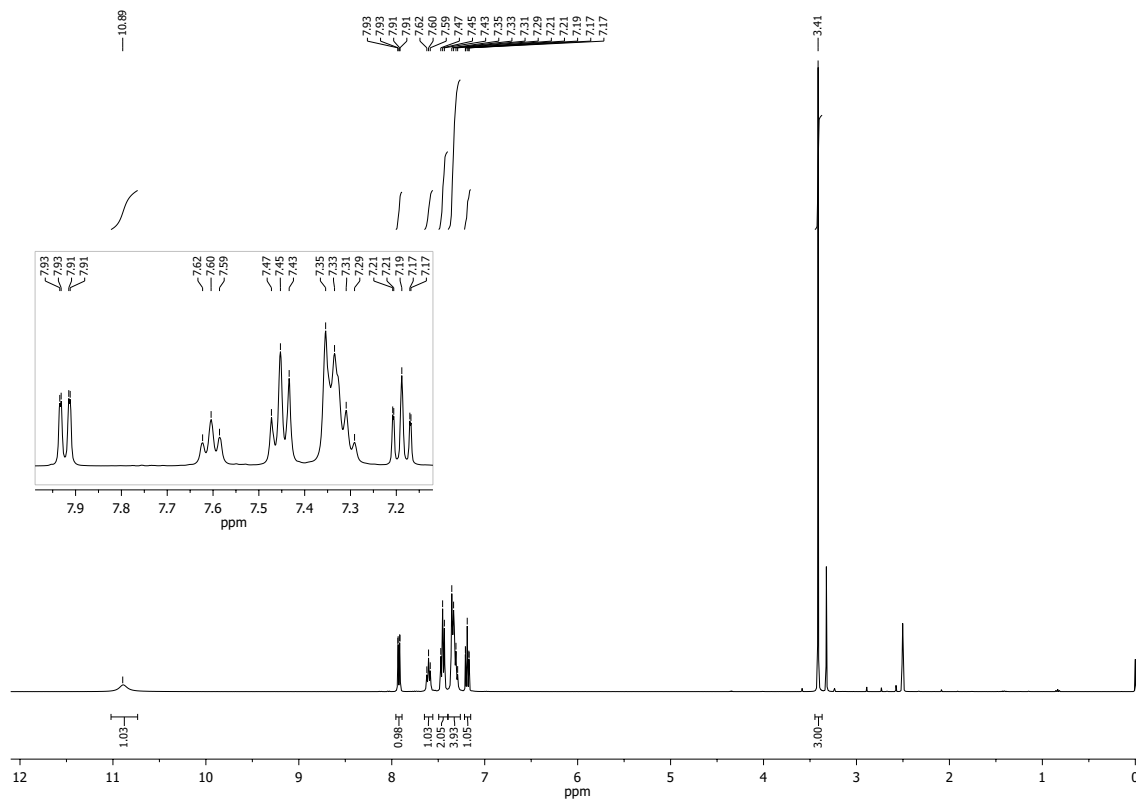2-(Phenylamino)-quinazolin-4(3*H*)-one

Sum formula: $C_{14}H_{11}N_3O$
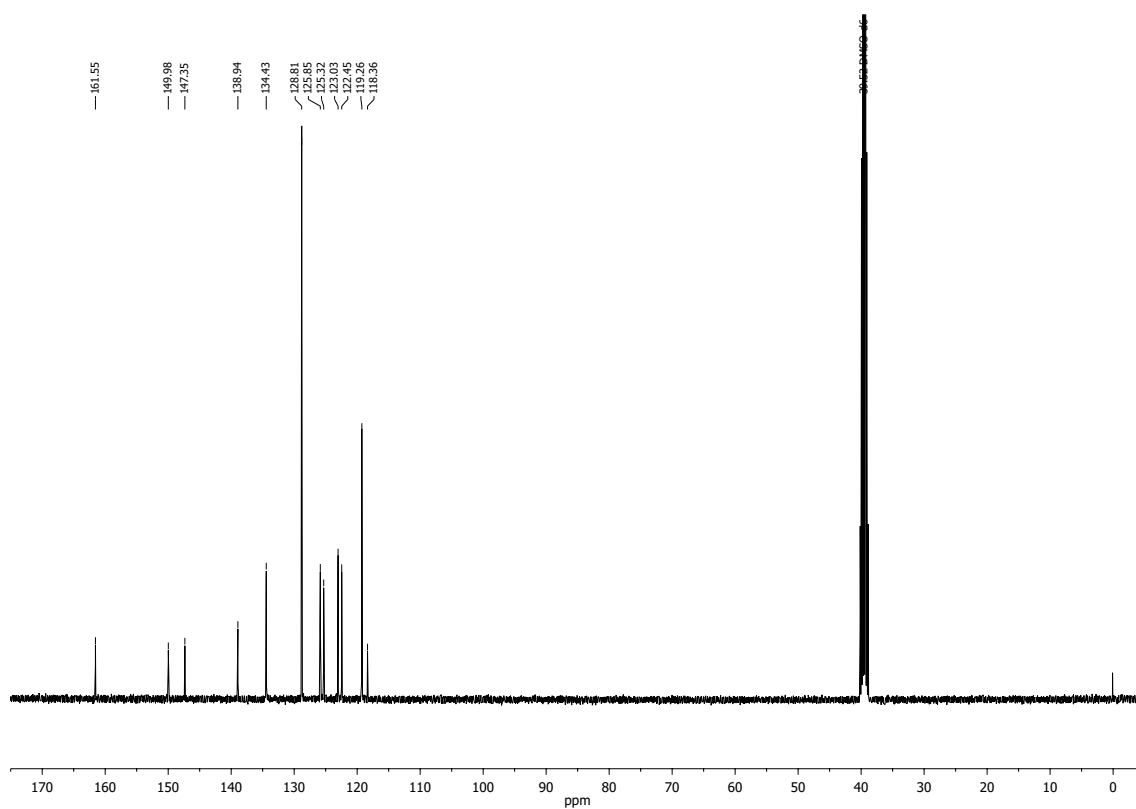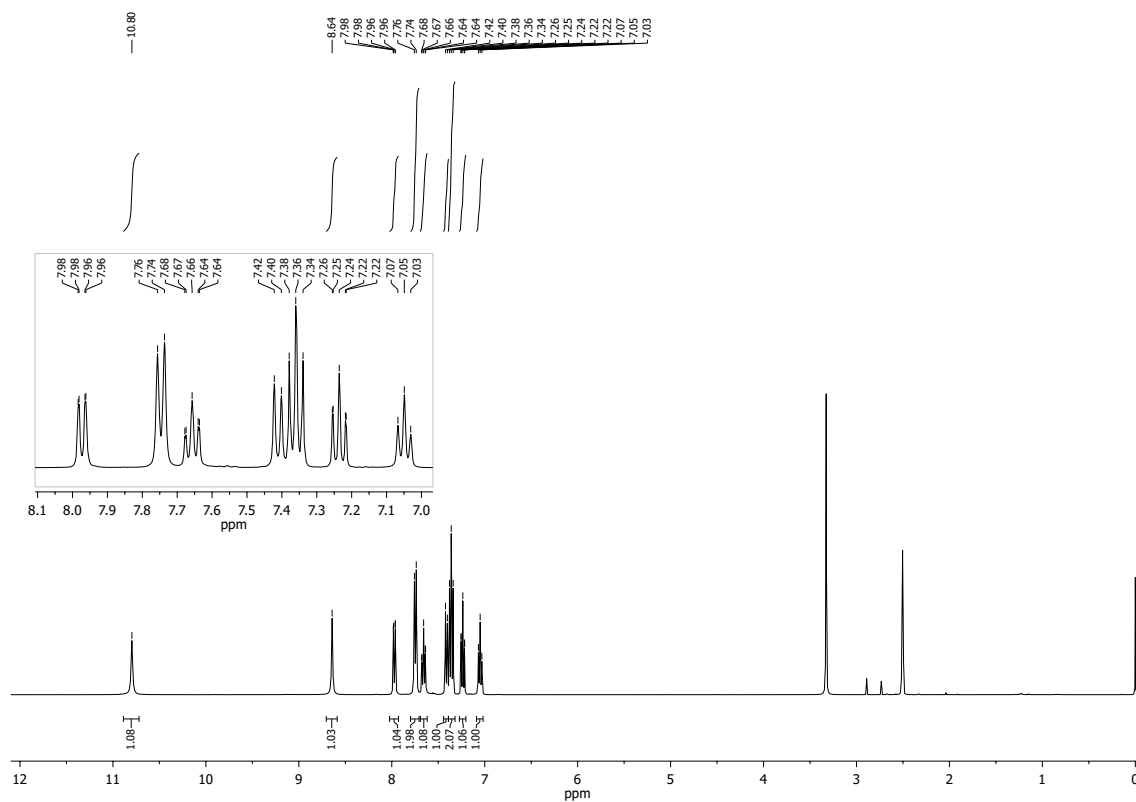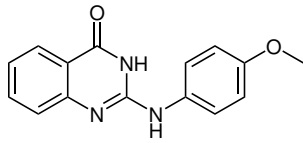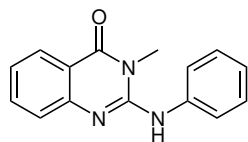
2-((4-Methoxyphenyl)amino)-quinazolin-4(3H)-one
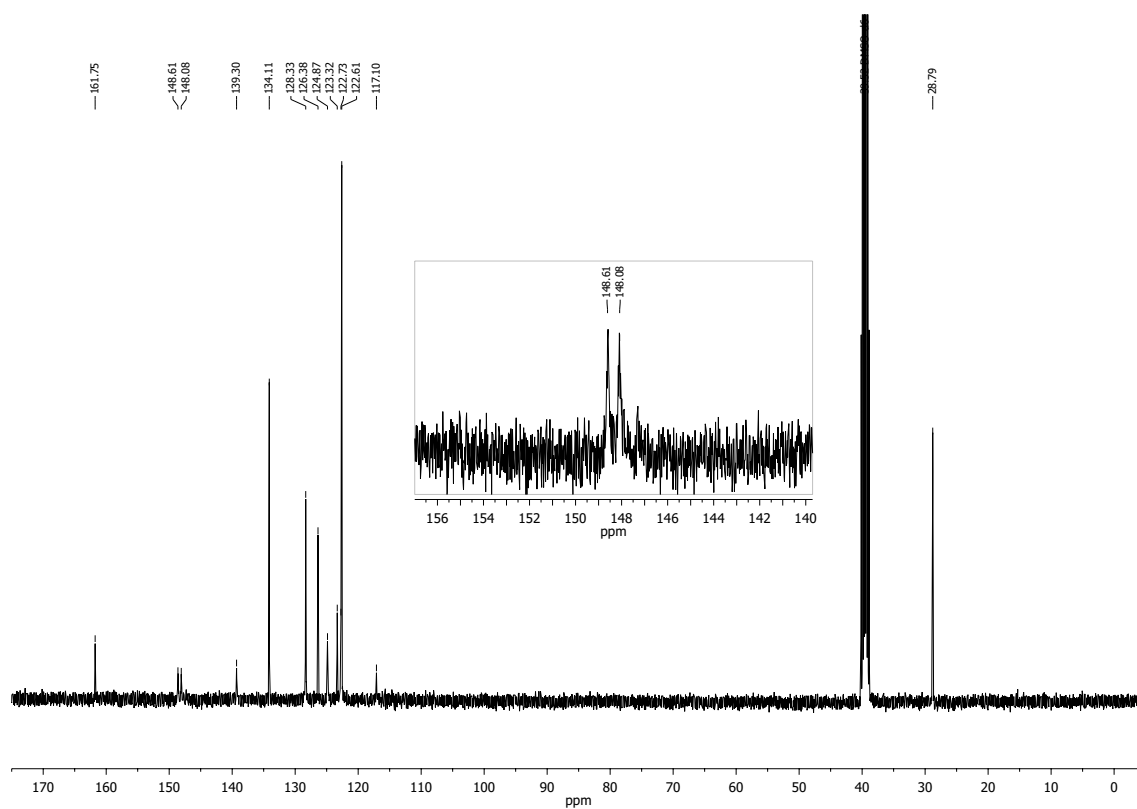
Sum formula: $C_{15}H_{13}N_3O_2$
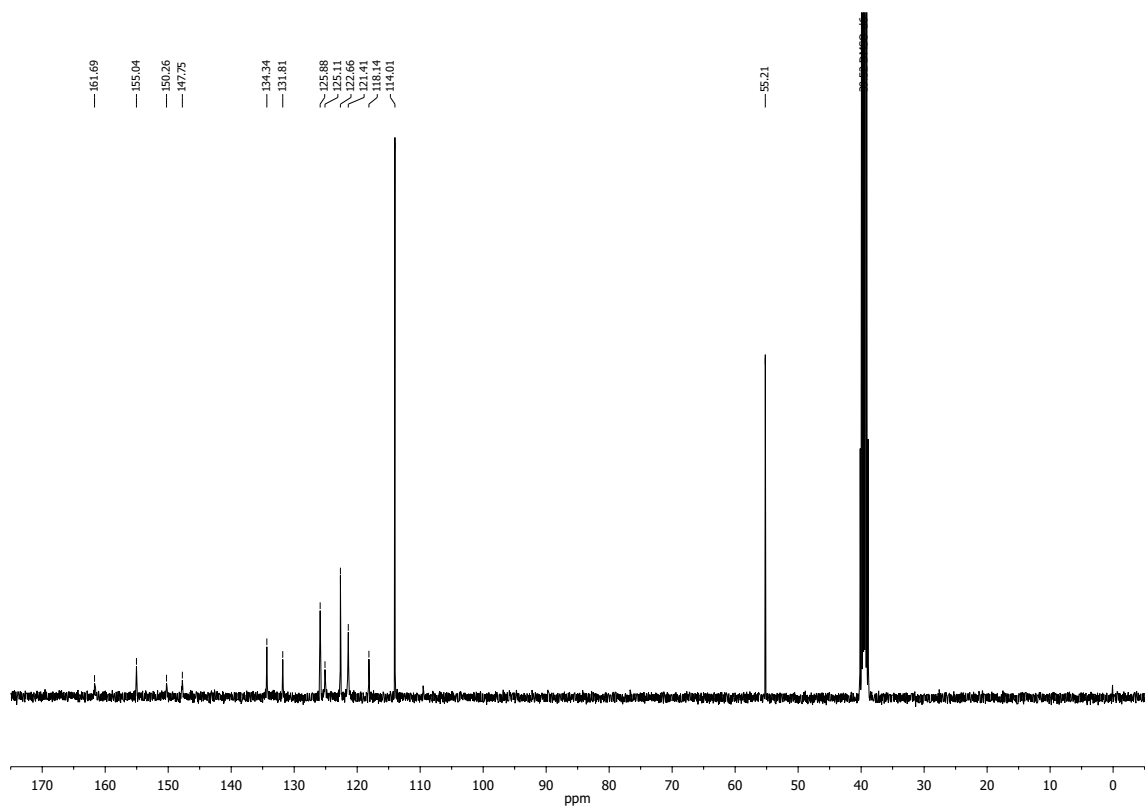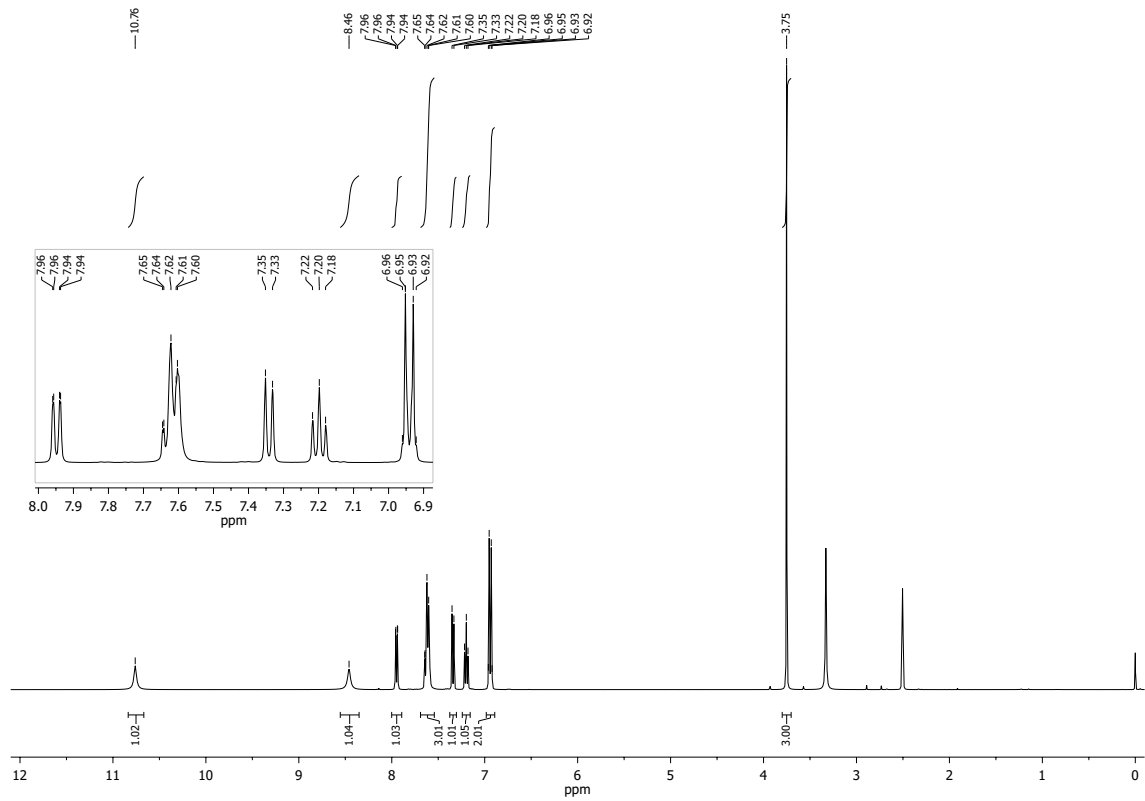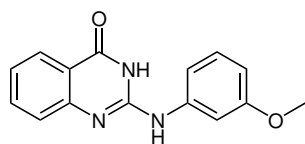
2-((3-Methoxyphenyl)amino)-quinazolin-4(3*H*)-one

Sum formula: $C_{15}H_{13}N_3O_2$
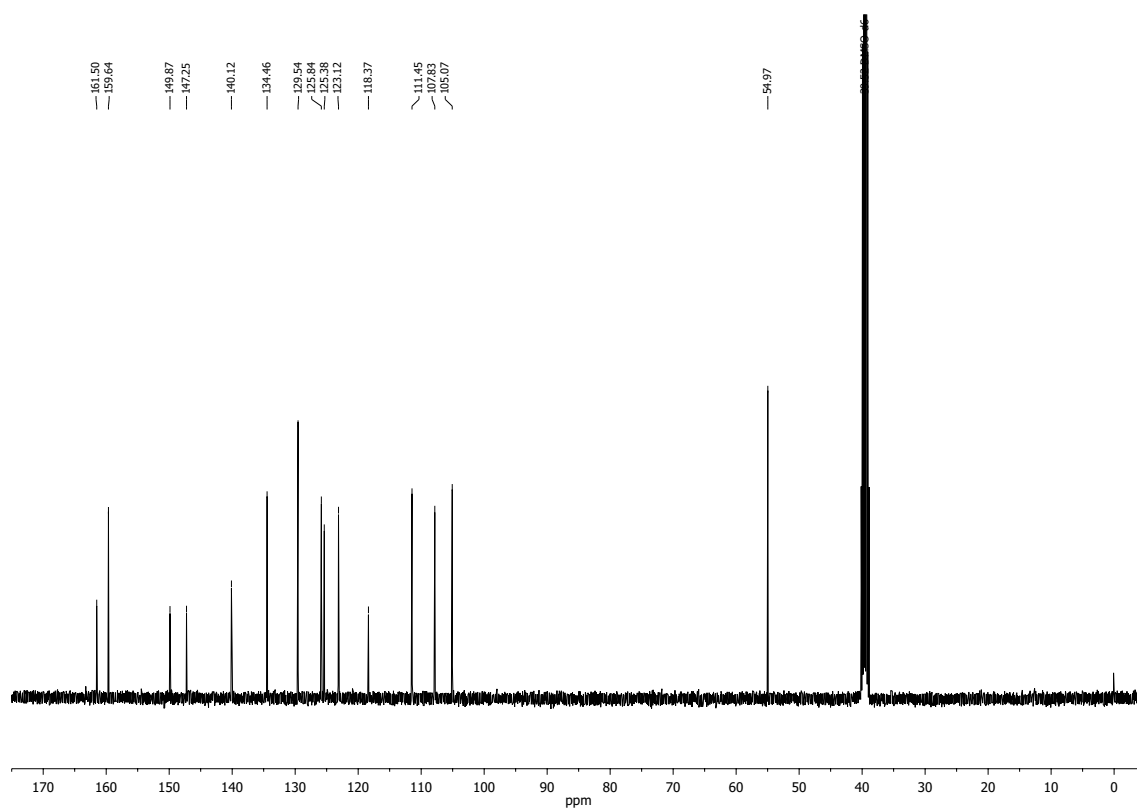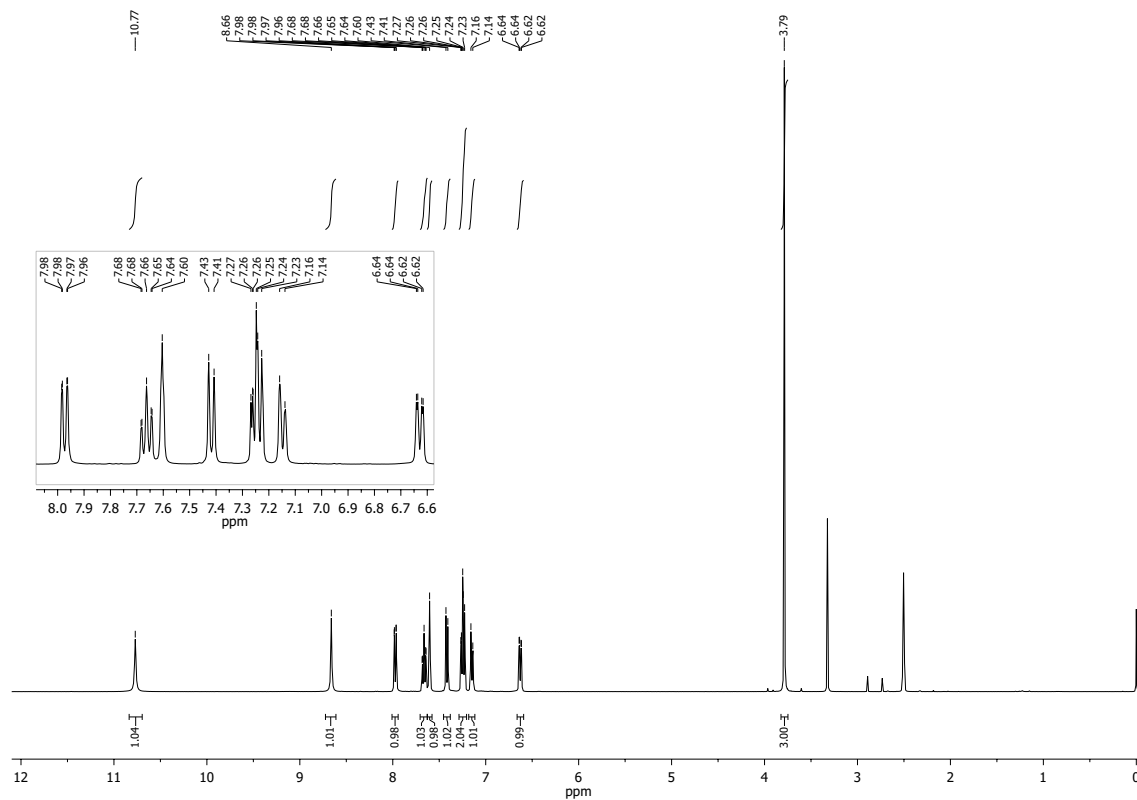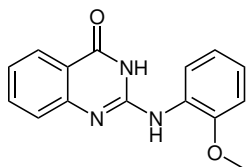
2-((2-Methoxyphenyl)amino)-quinazolin-4(3*H*)-one

Sum formula: $C_{15}H_{13}N_3O_2$
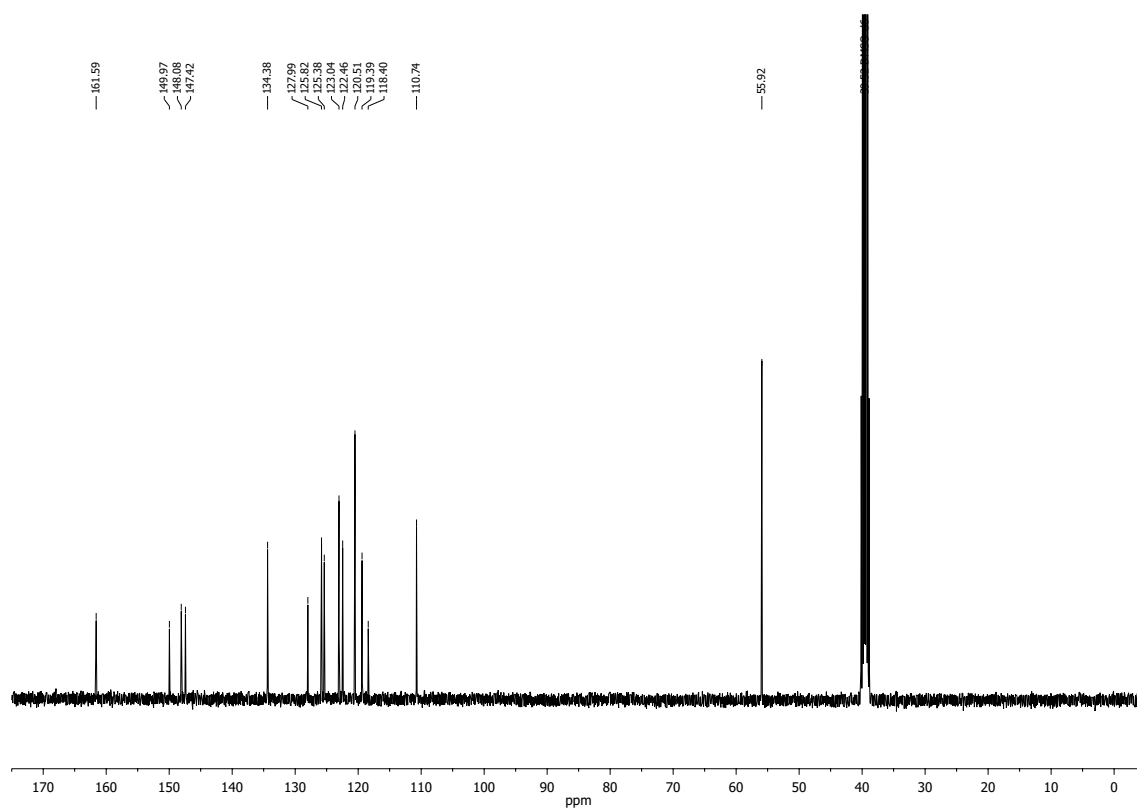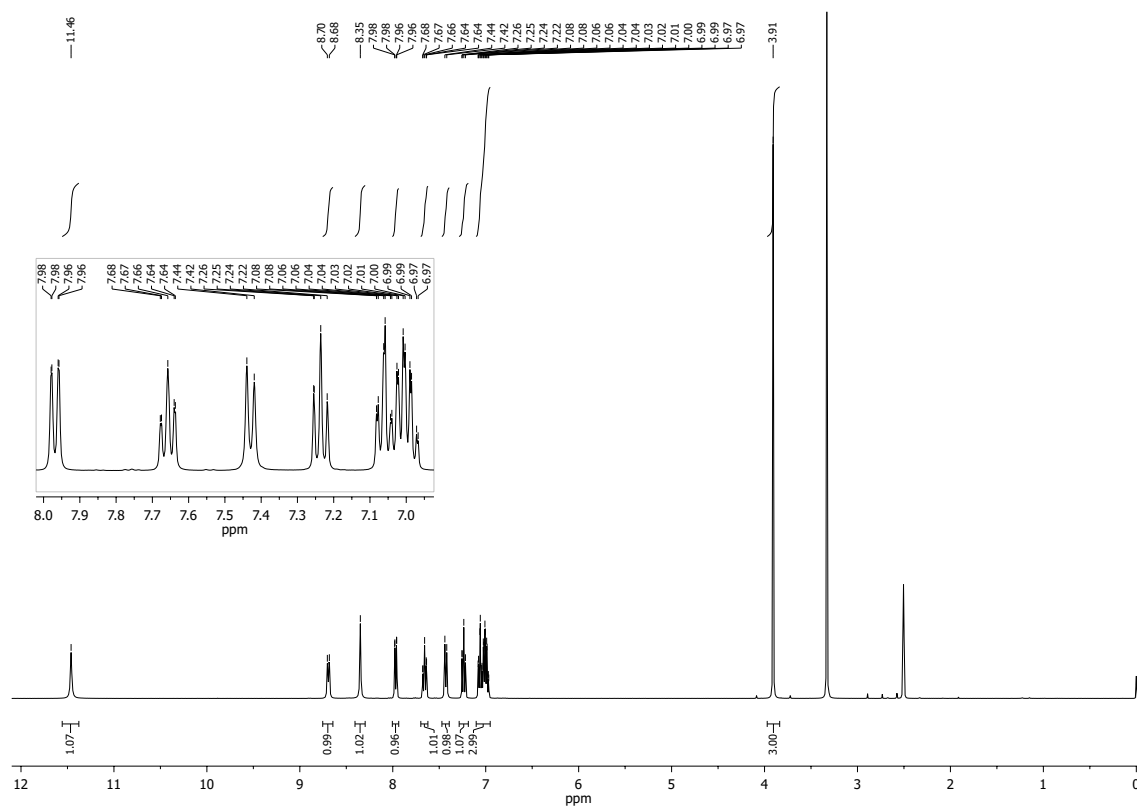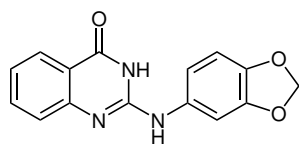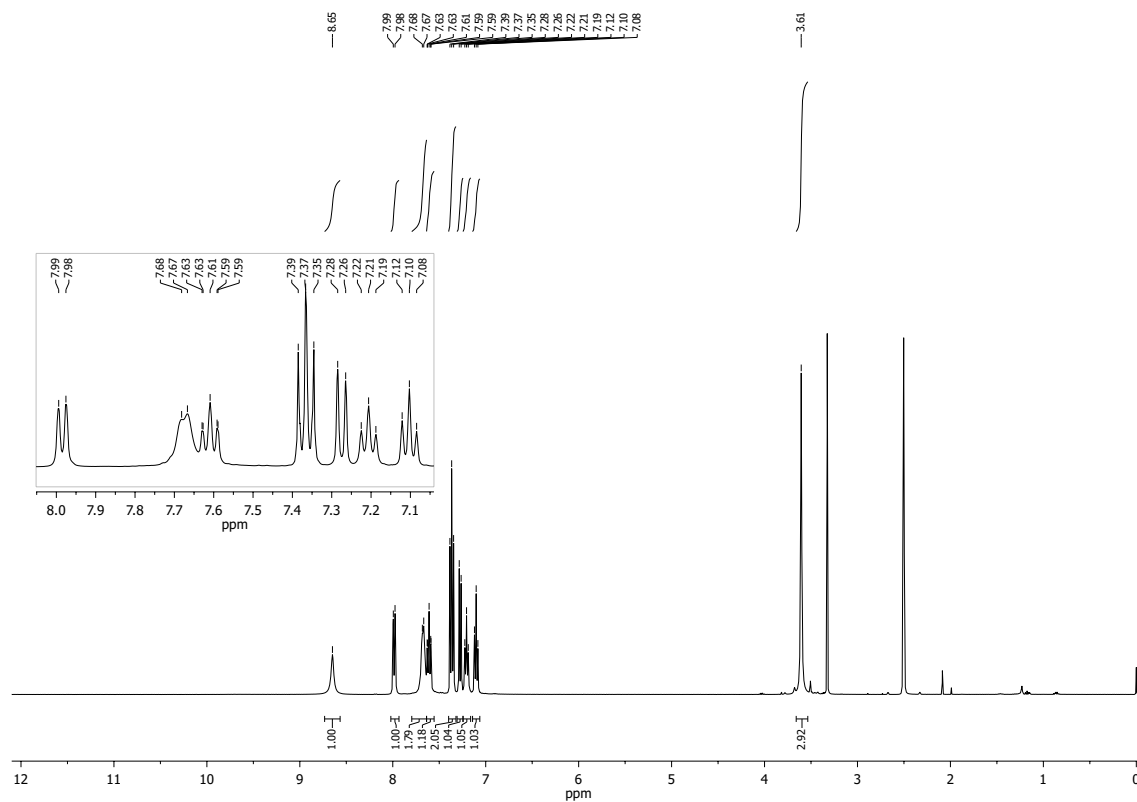
2-((3,4-Methylenedioxyphenyl)amino)-quinazolin-4(3*H*)-one

Sum formula: $C_{15}H_{11}N_3O_3$
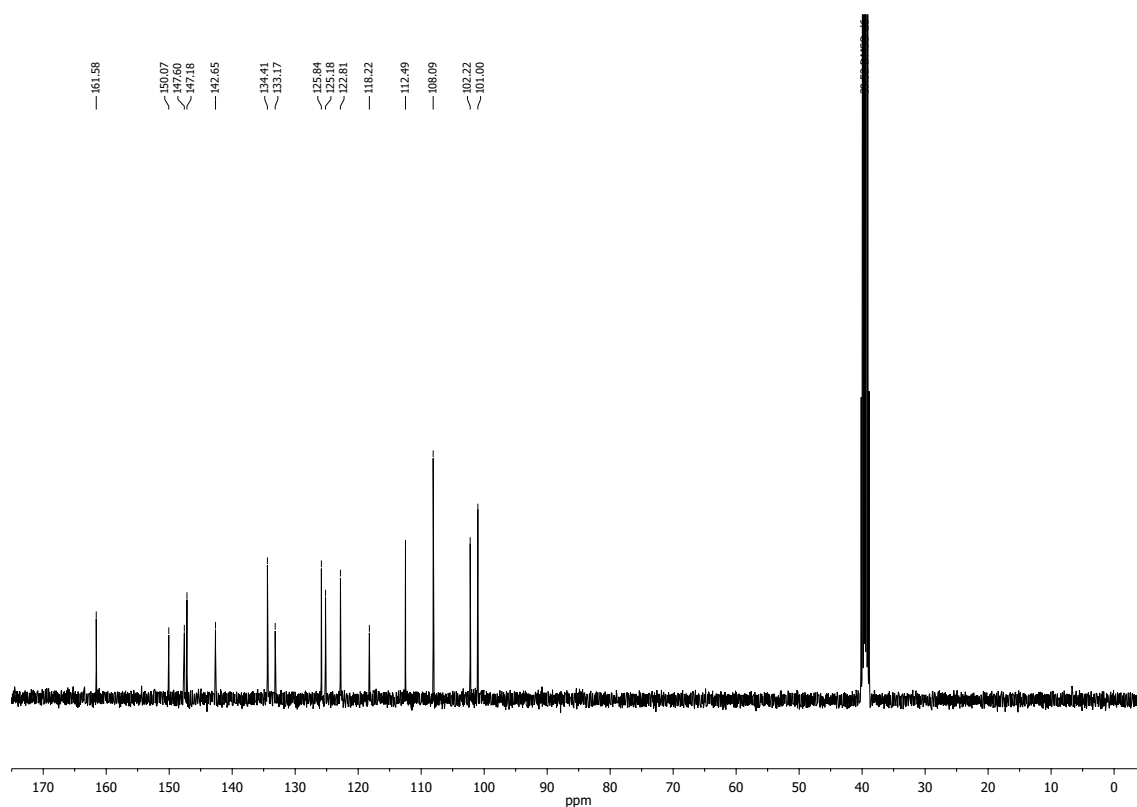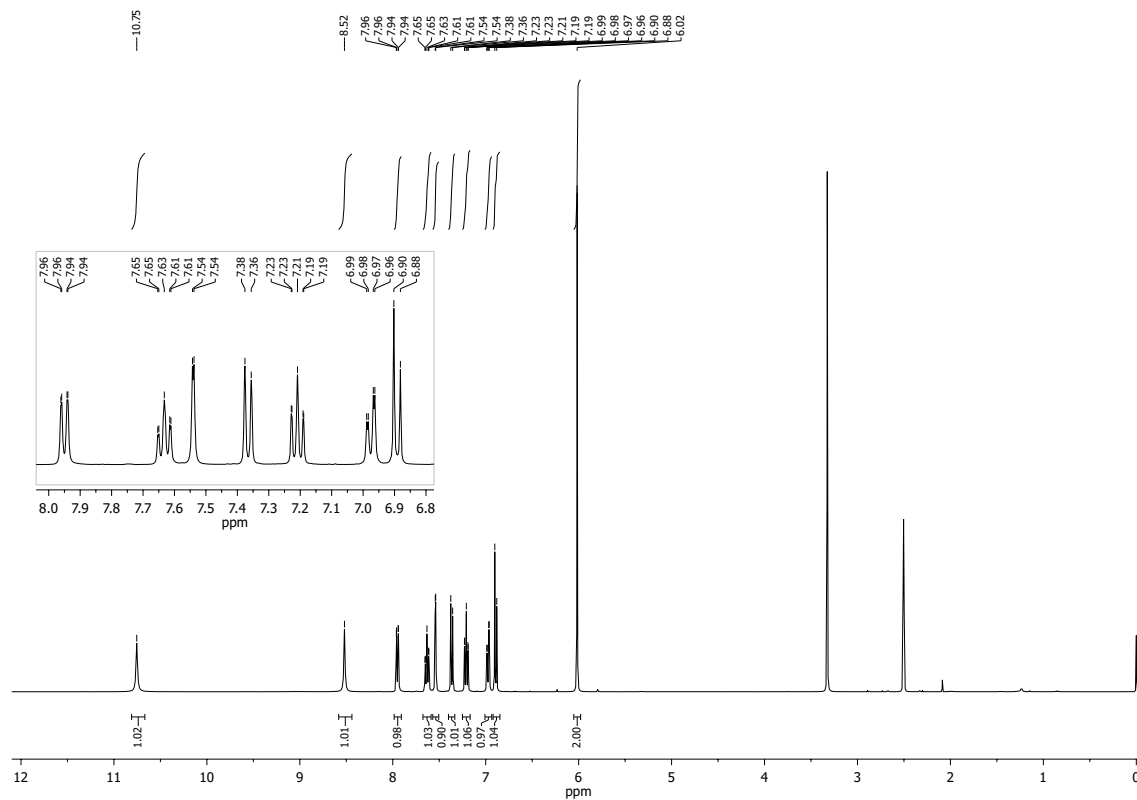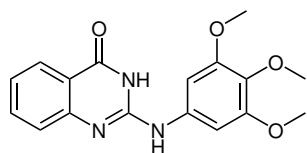
2-((3,4,5-Trimethoxyphenyl)amino)-quinazolin-4(3H)-one
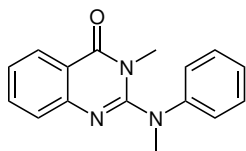
Sum formula: $C_{17}H_{17}N_3O_4$
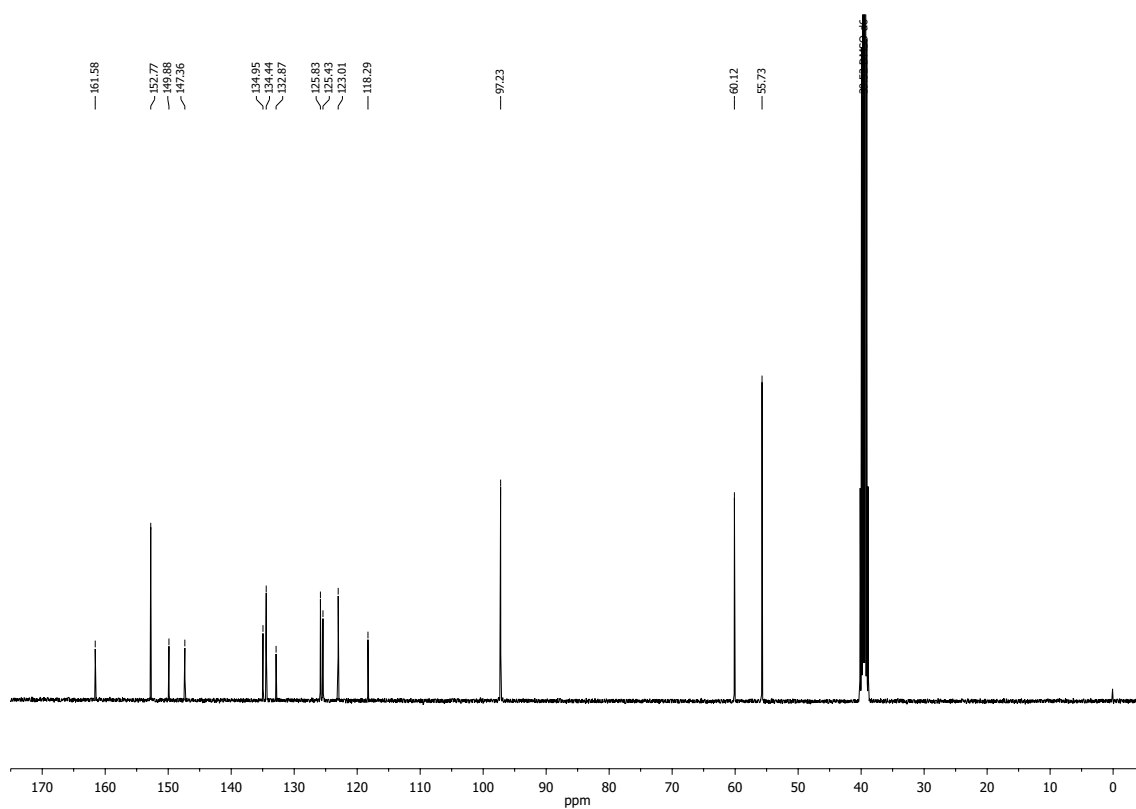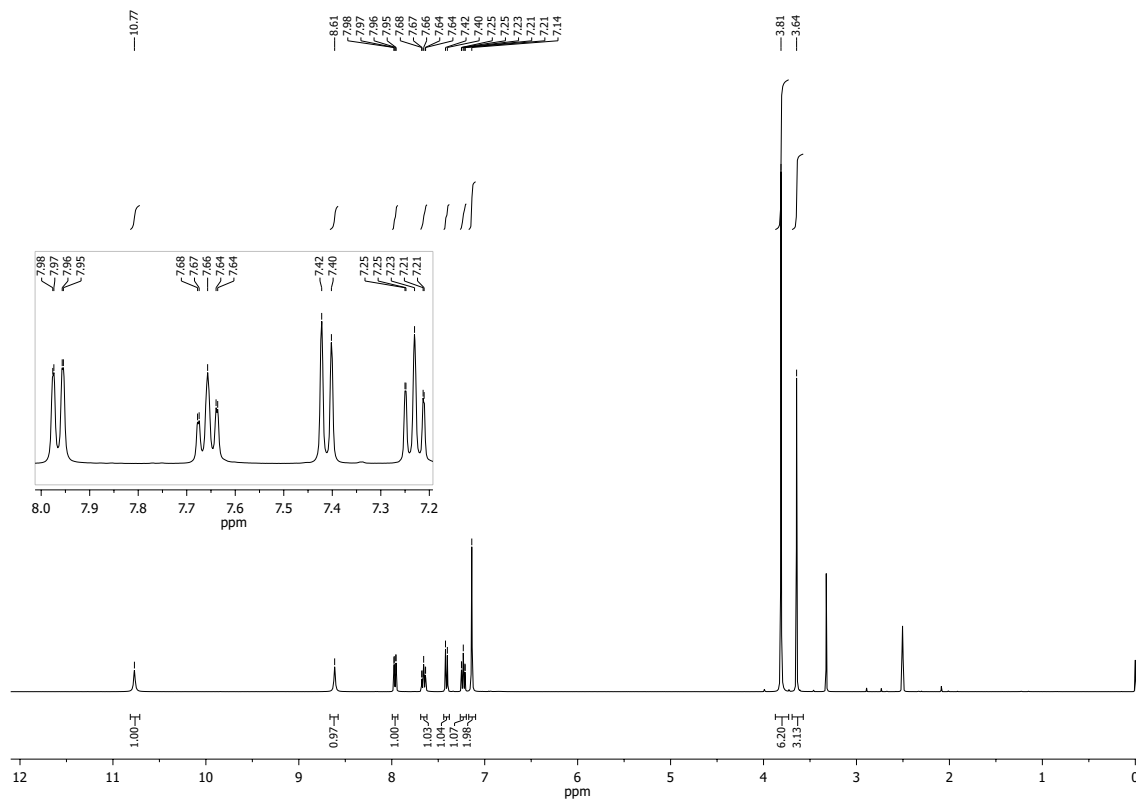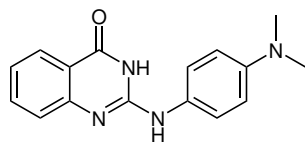
2-((4-(Dimethylamino)phenyl)amino)-quinazolin-4(3*H*)-one
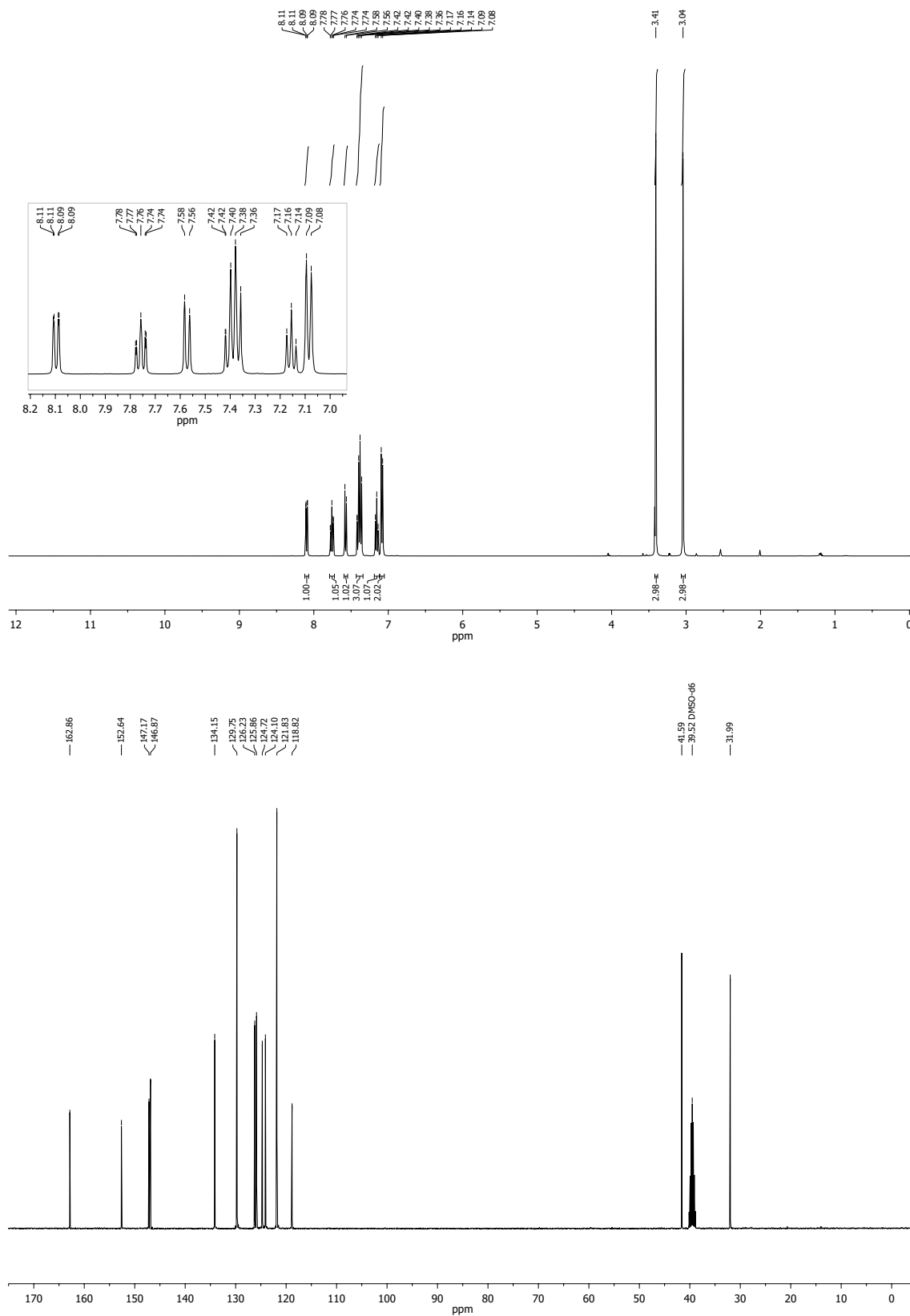
Sum formula: $C_{16}H_{16}N_4O$
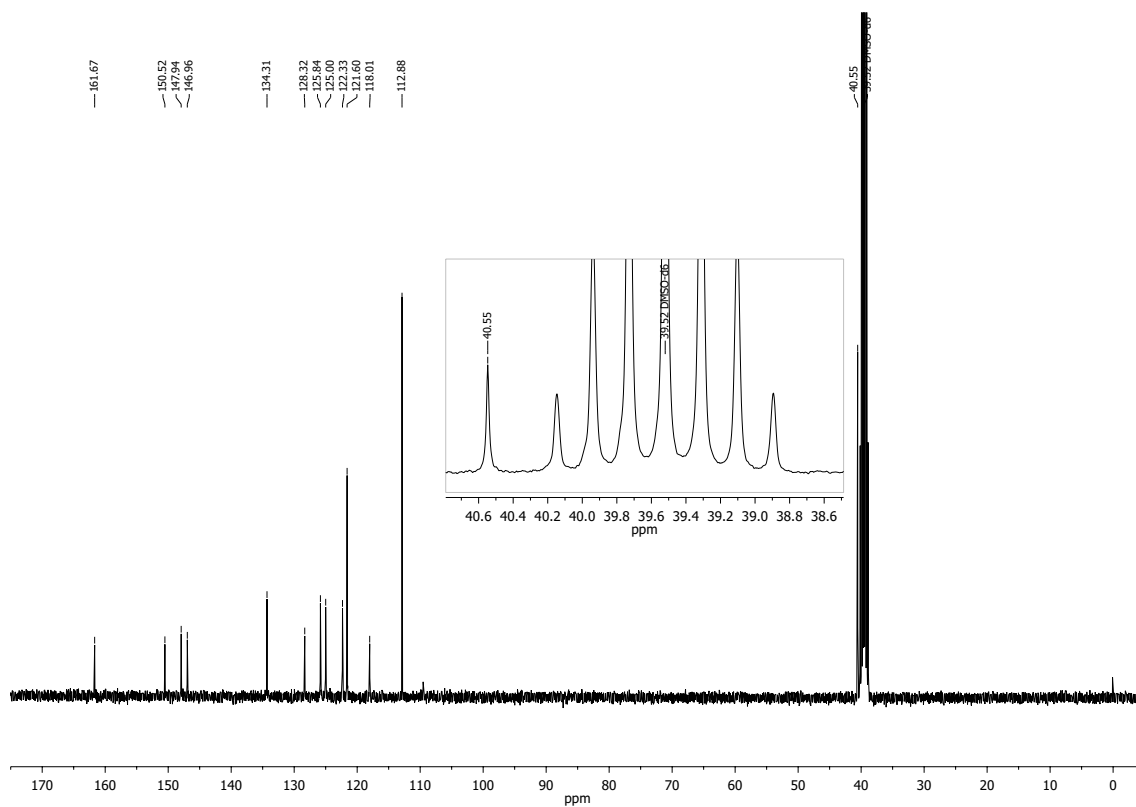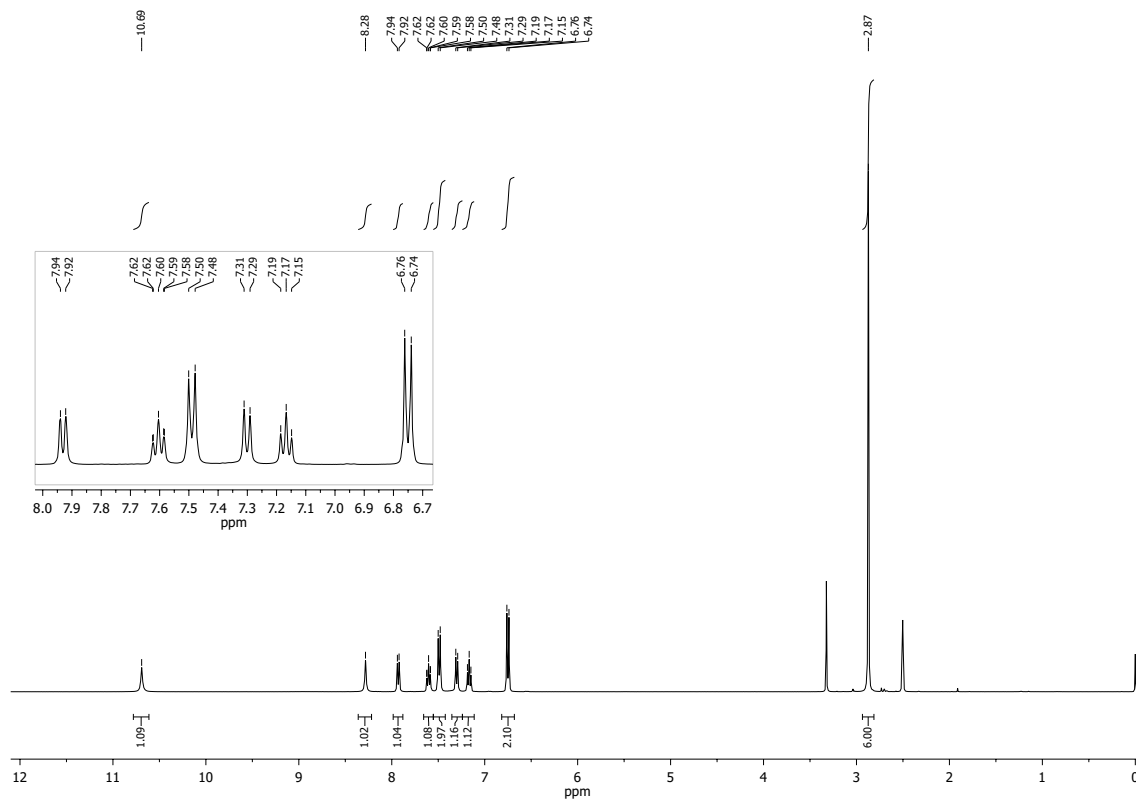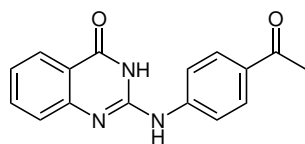
2-((4-Acetylphenyl)amino)-quinazolin-4(3H)-one

Sum formula: $C_{16}H_{13}N_3O_2$
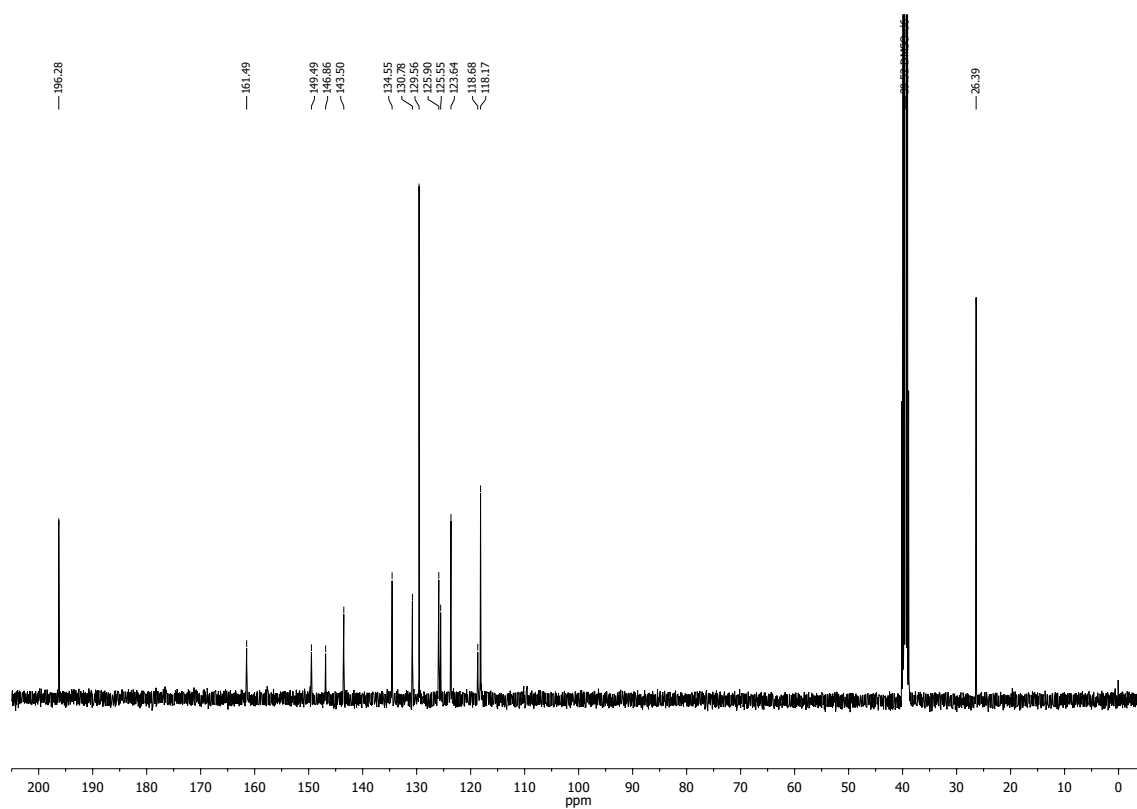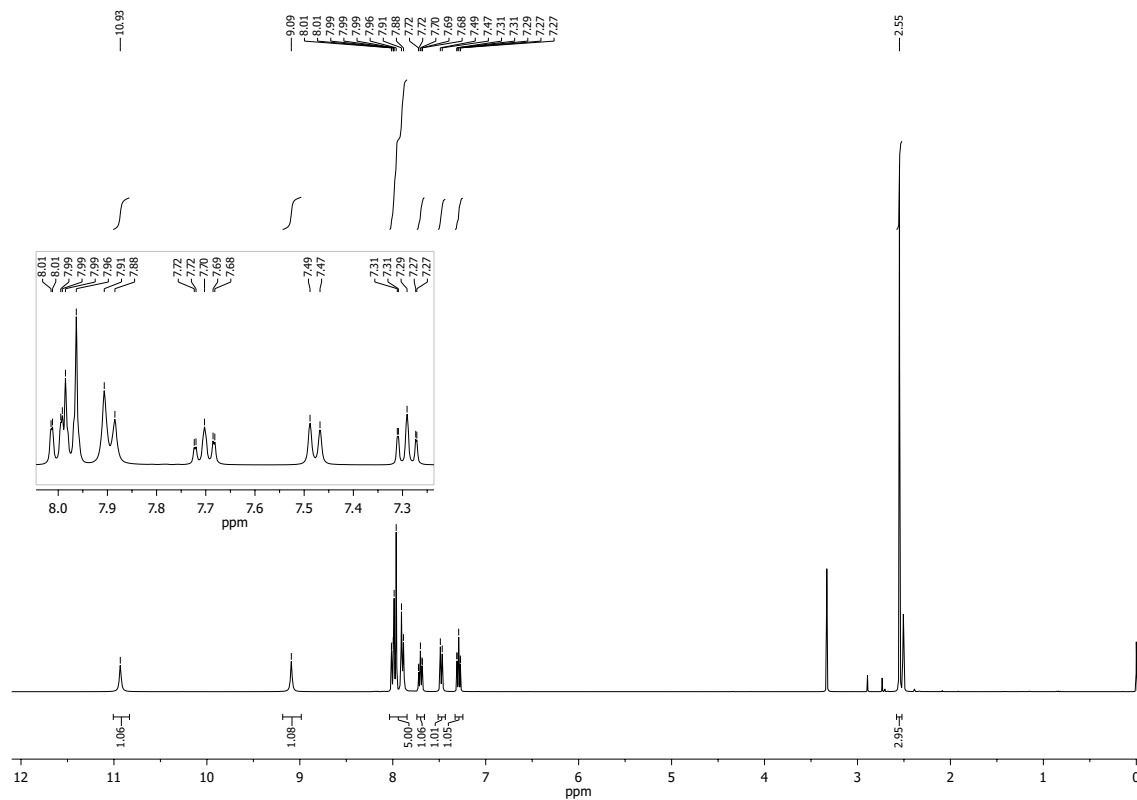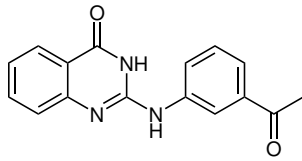
2-((3-Acetylphenyl)amino)-quinazolin-4(3*H*)-one

Sum formula: $C_{16}H_{13}N_3O_2$
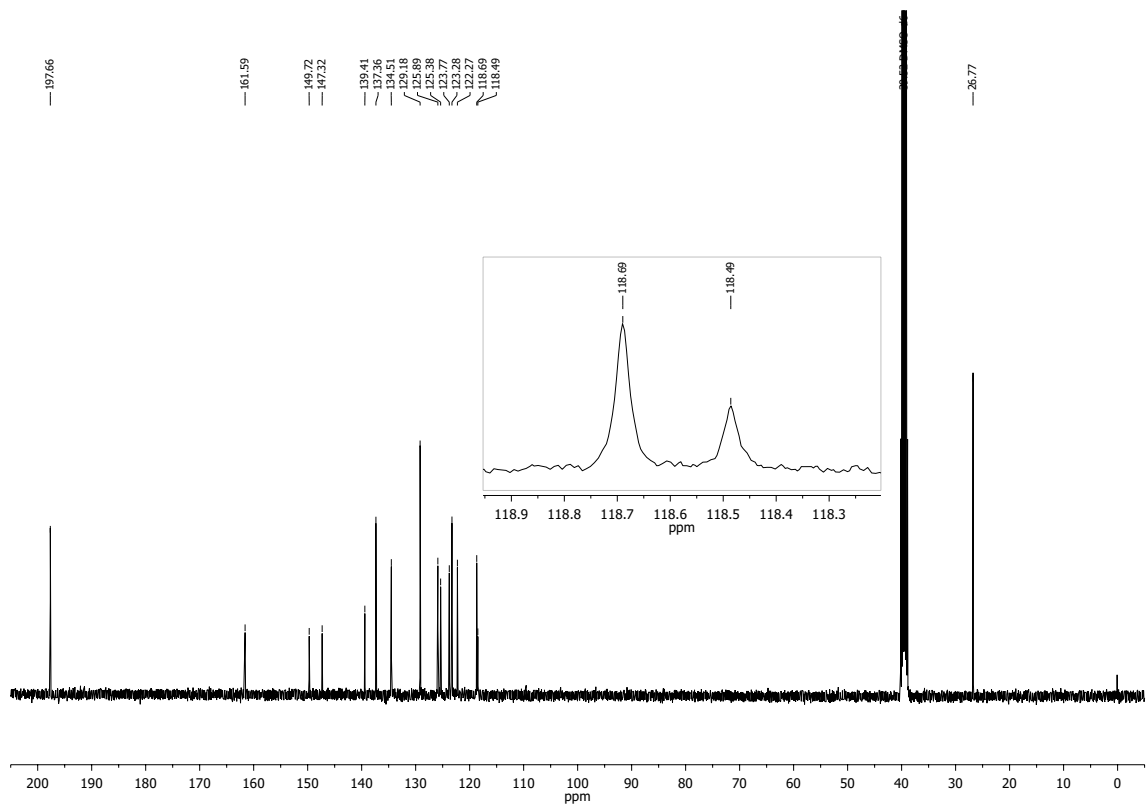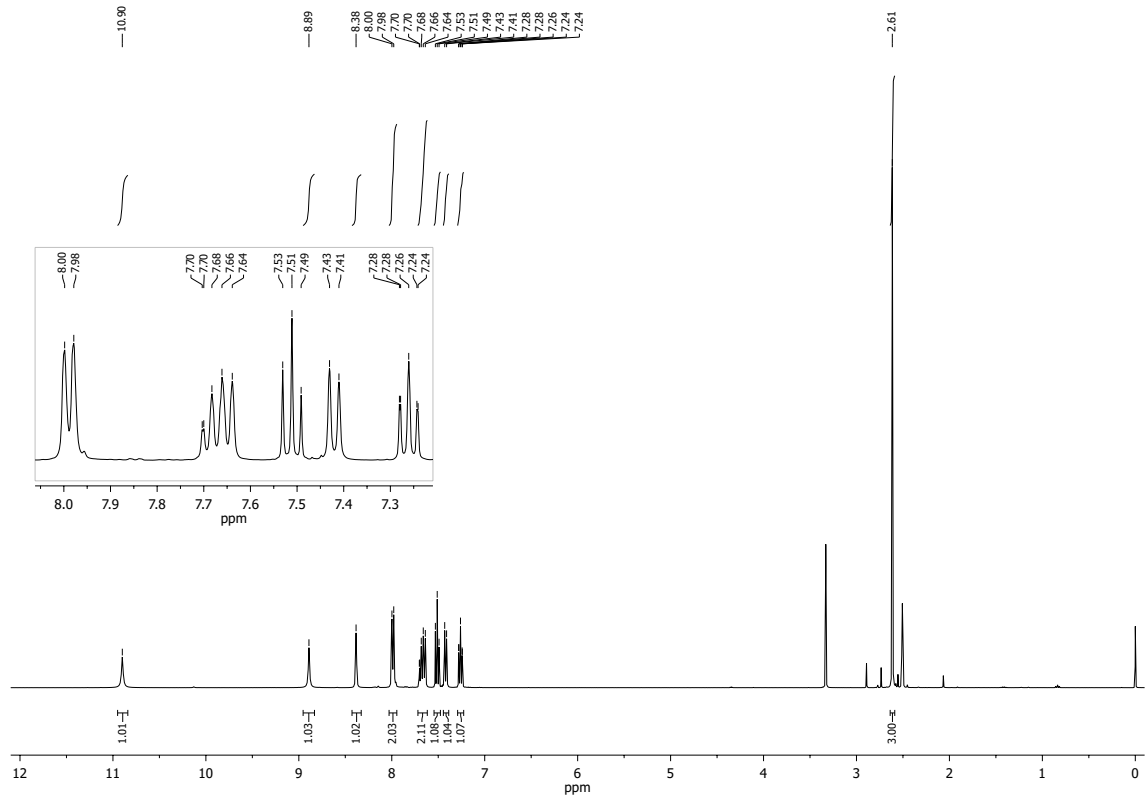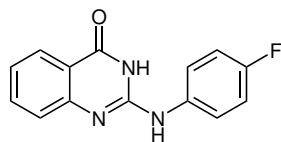
2-((4-Fluorophenyl)amino)-quinazolin-4(3*H*)-one

Sum formula: $C_{14}H_{10}FN_3O$
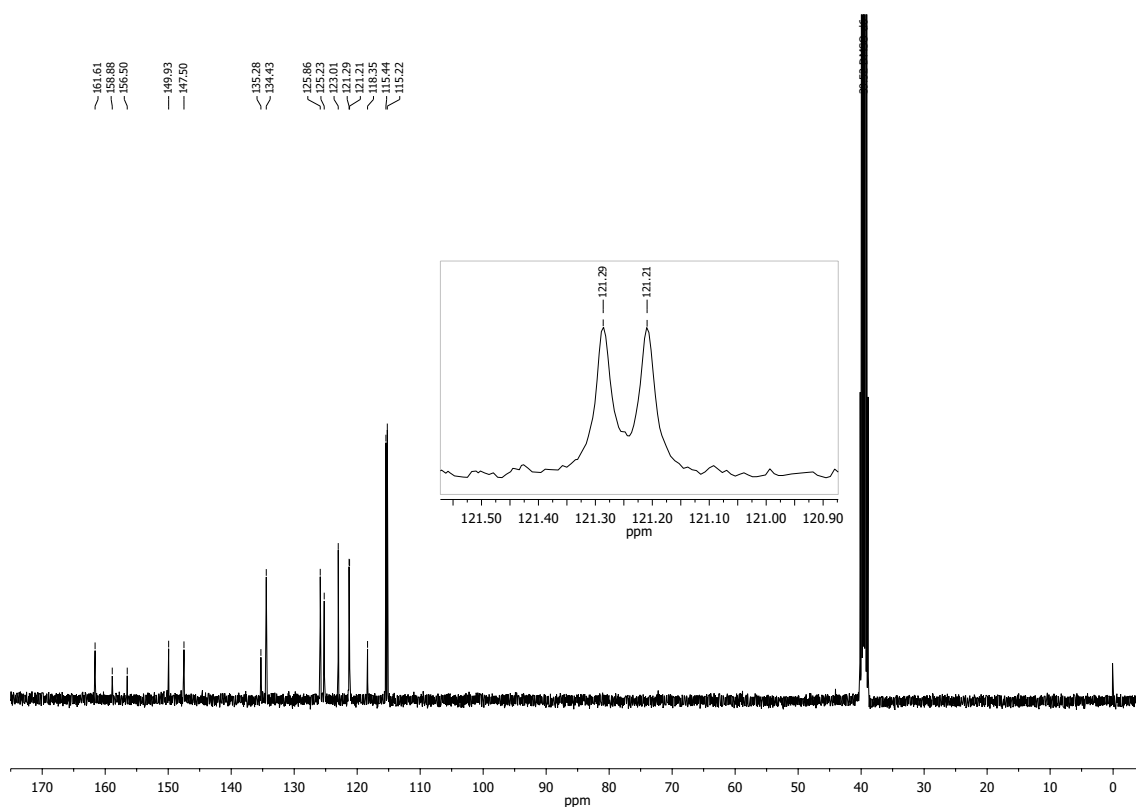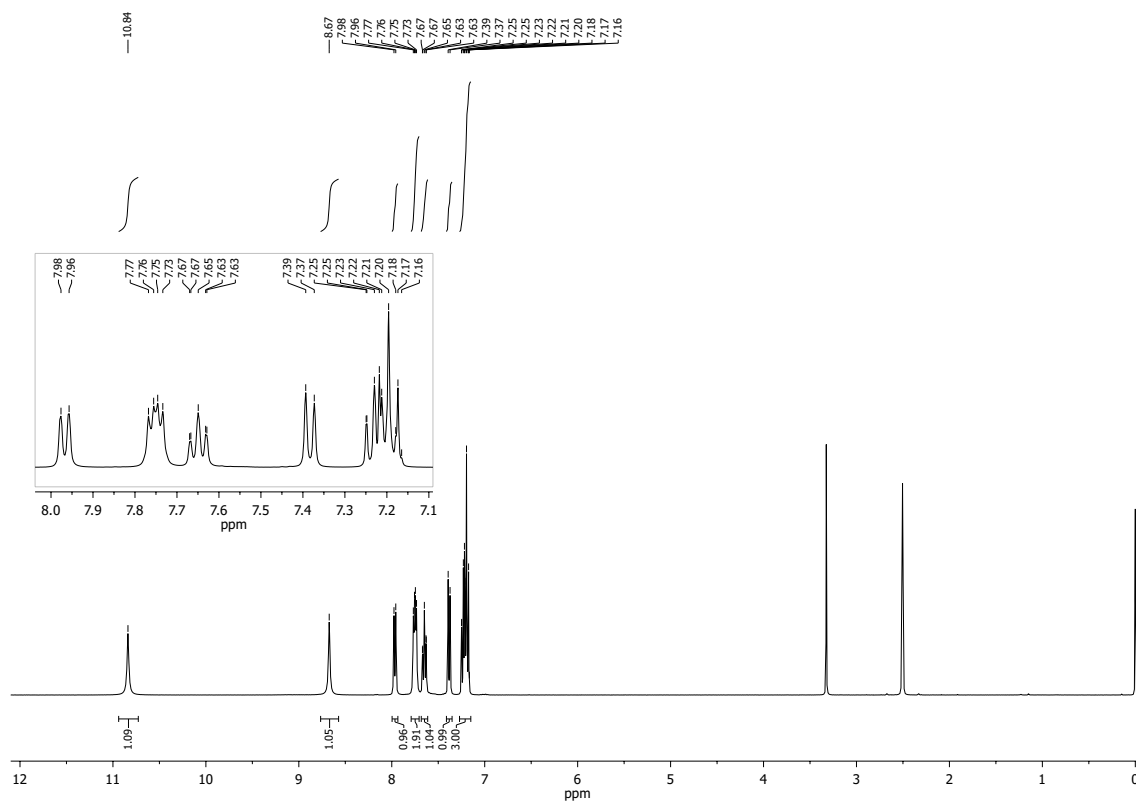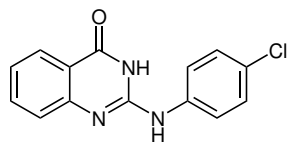
2-((4-Chlorophenyl)amino)-quinazolin-4(3*H*)-one

Sum formula: $C_{14}H_{10}ClN_3O$
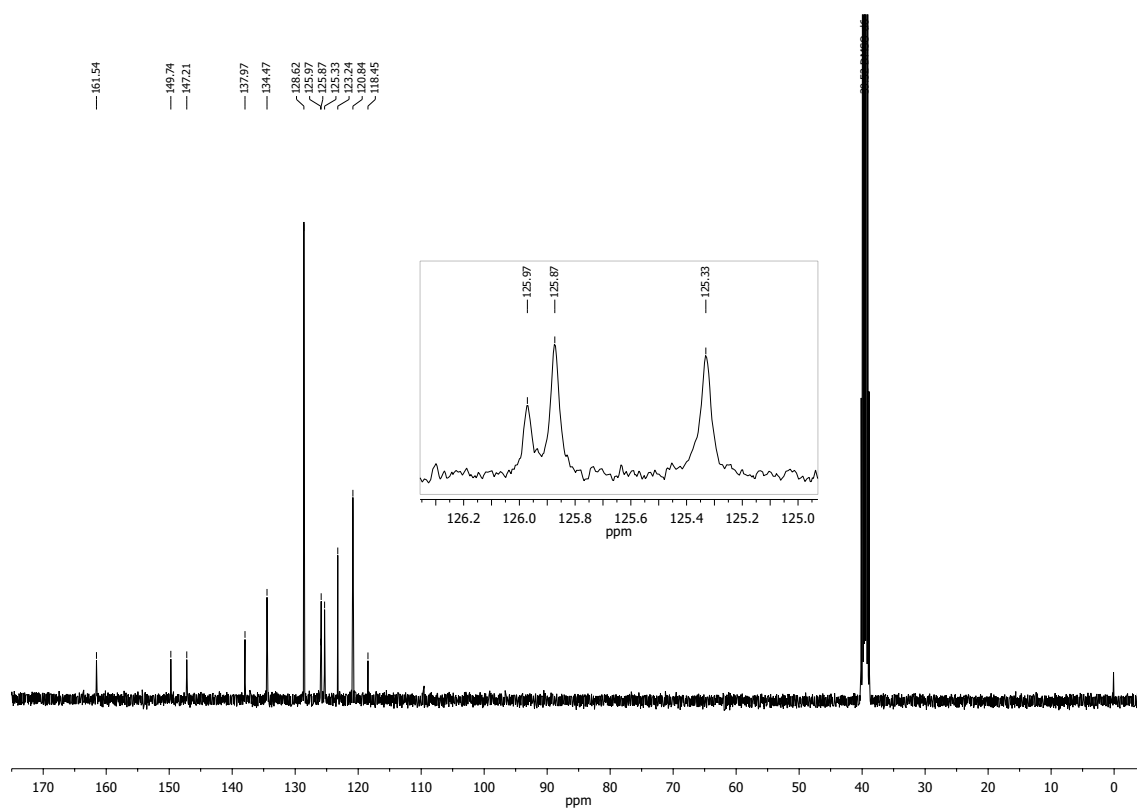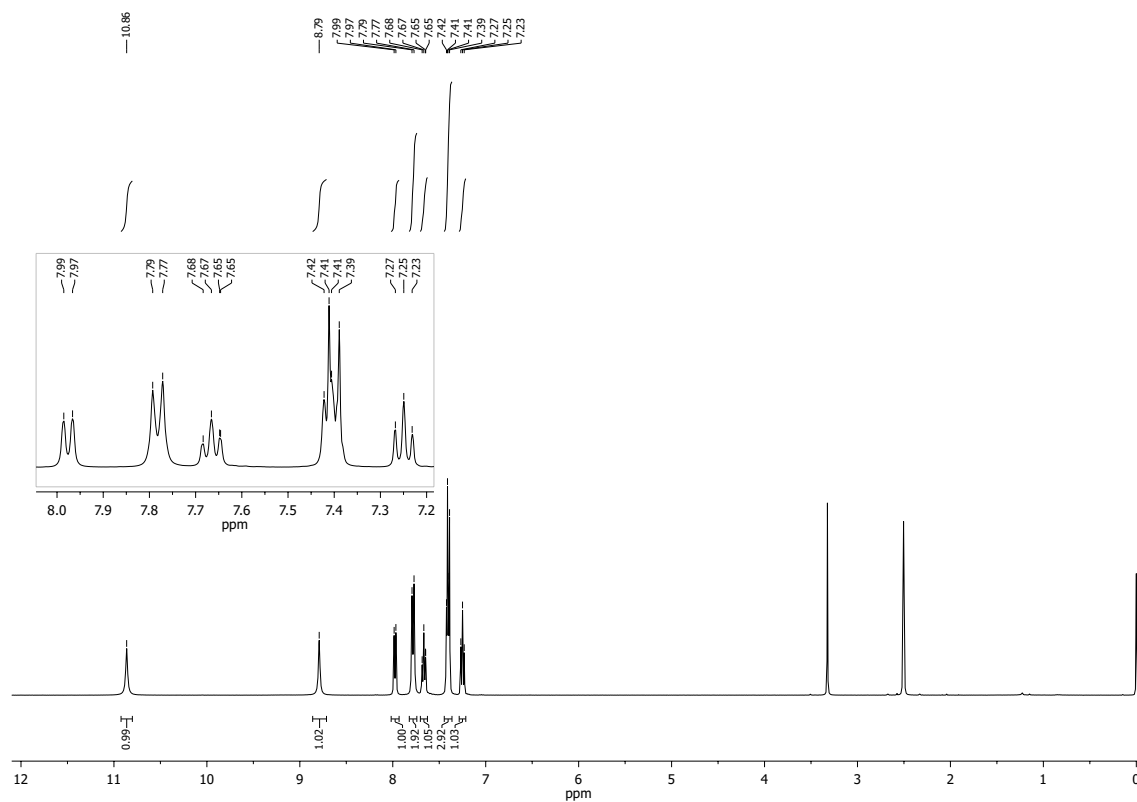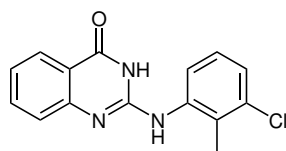
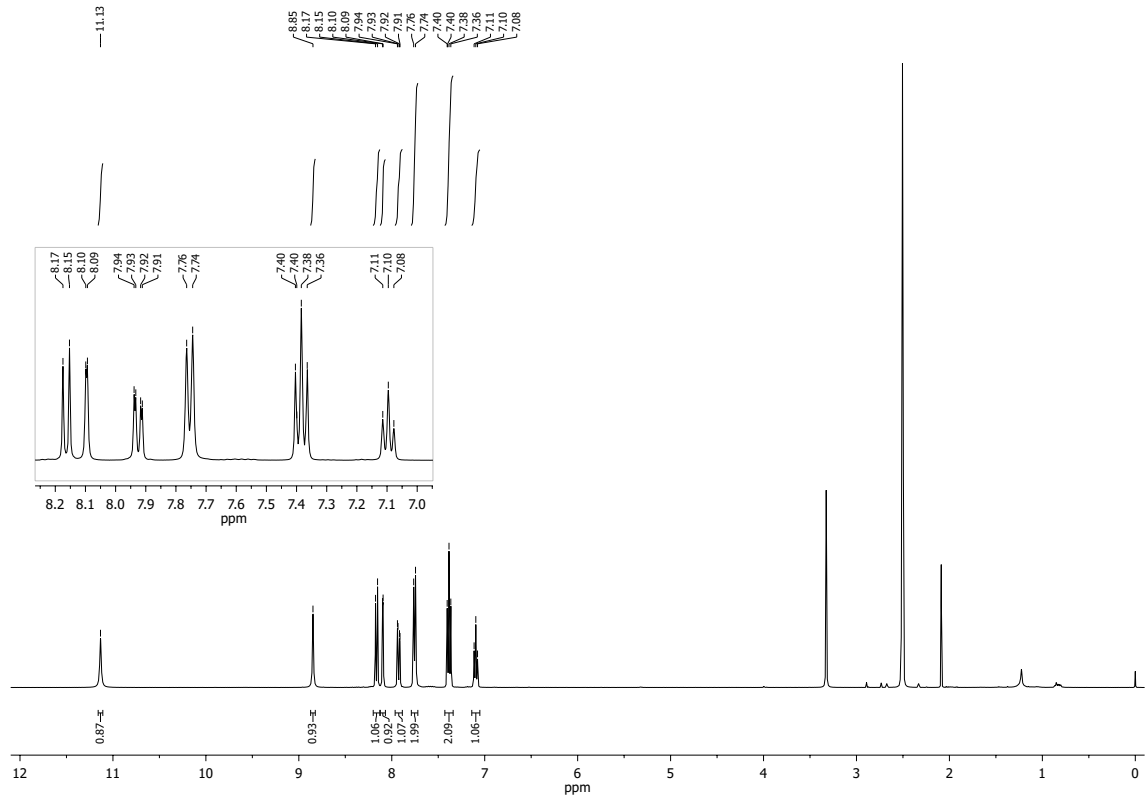2-((3-Chloro-2-methylphenyl)amino)-quinazolin-4(3*H*)-one

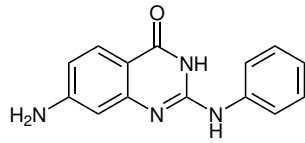**Sum formula:** $C_{15}H_{12}ClN_3O$
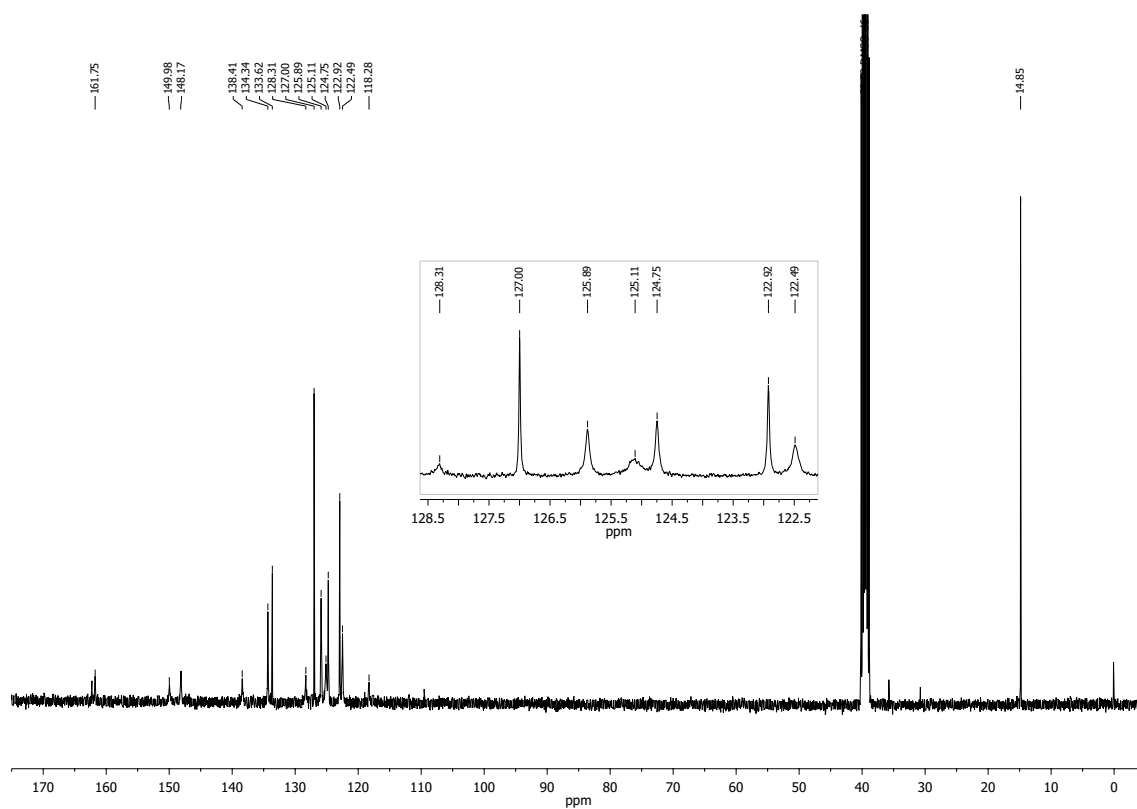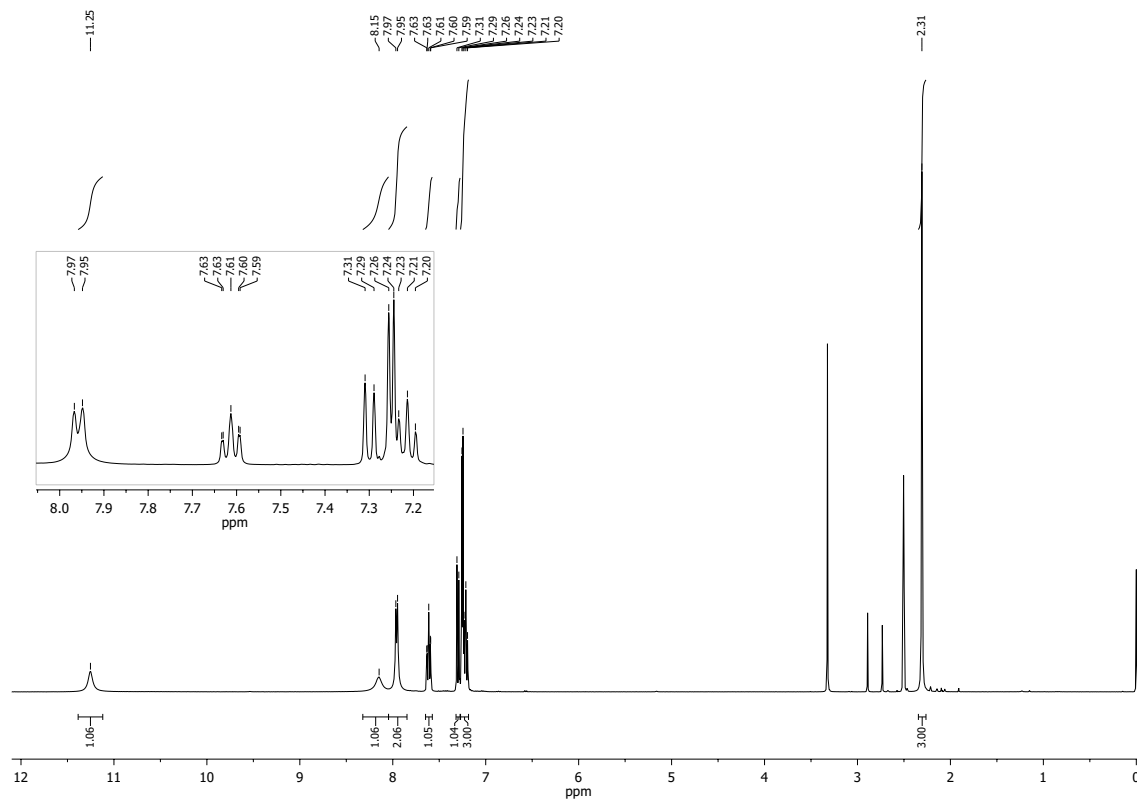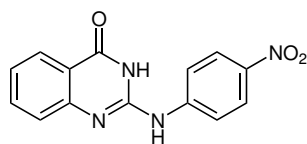
2-((4-Nitrophenyl)amino)-quinazolin-4(3H)-one
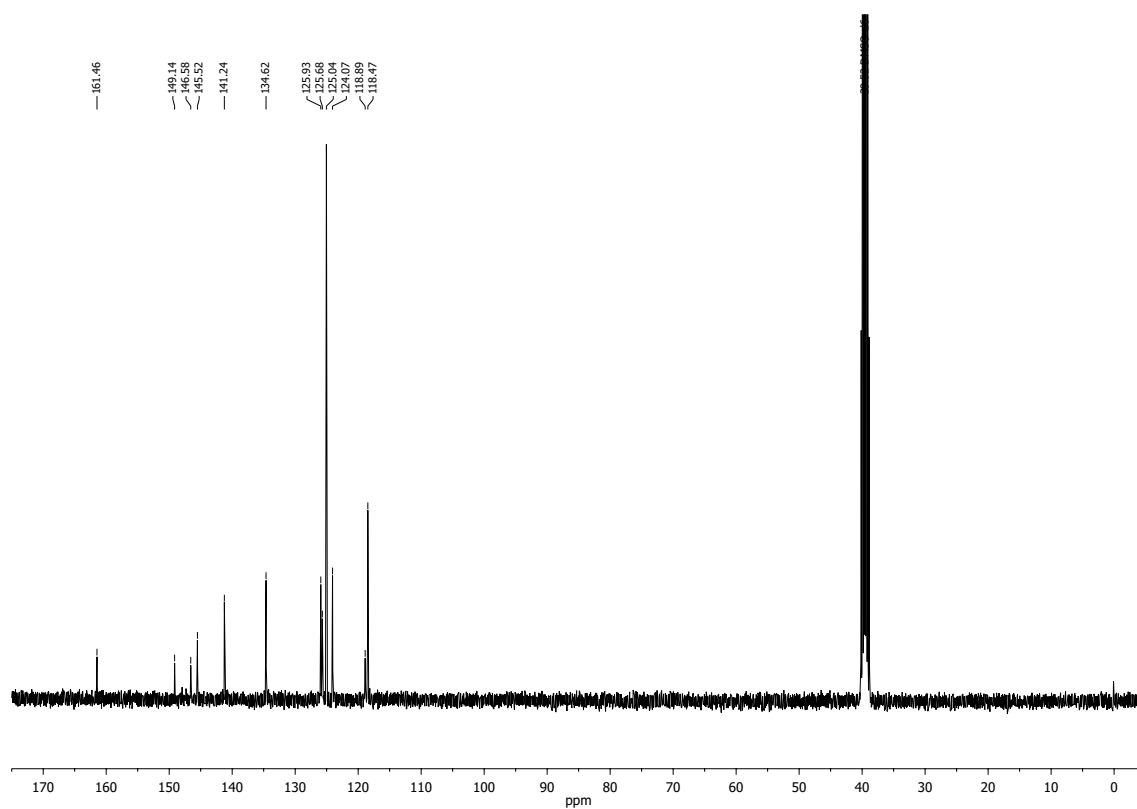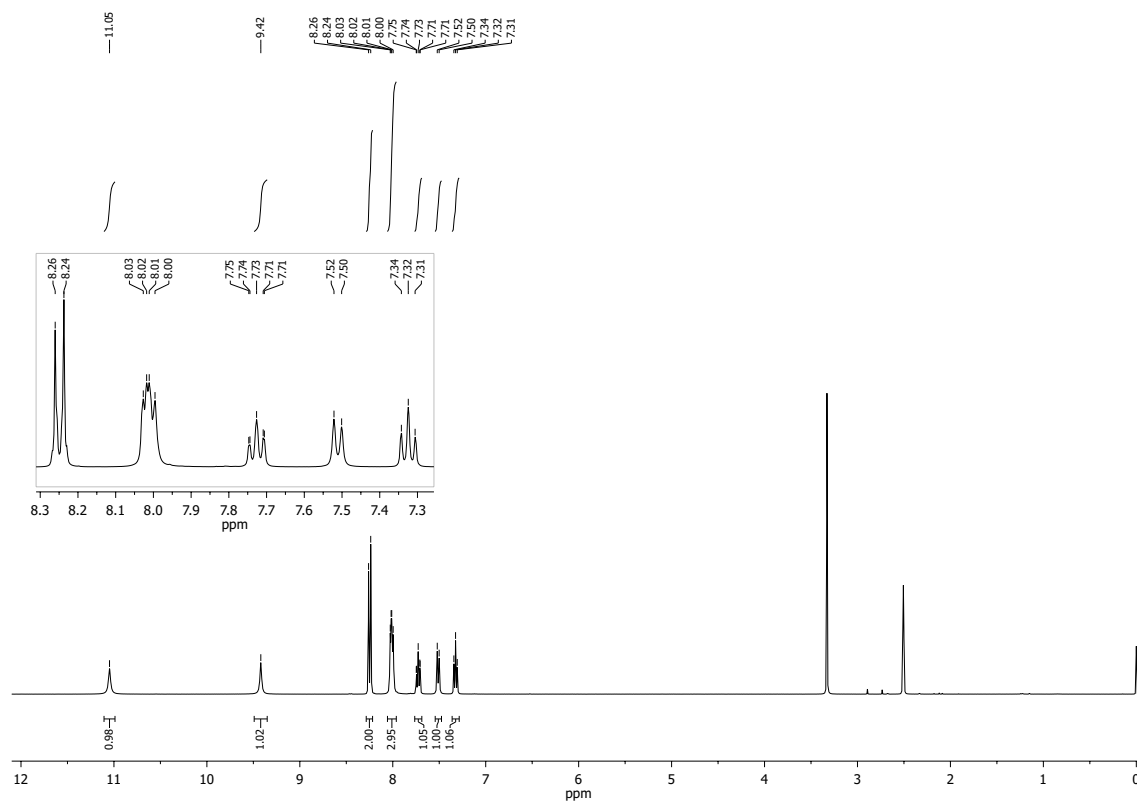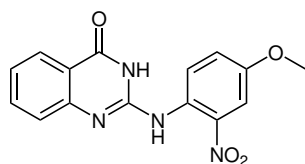
Sum formula: $C_{14}H_{10}N_4O_3$

2-((4-Methoxy-2-nitrophenyl)amino)-quinazolin-4(3*H*)-one

Sum formula: $C_{15}H_{12}N_4O_4$

2-((4-((2,4-Dinitrophenyl)amino)phenyl)amino)-

quinazolin-4(3H)-one

Sum formula: $C_{20}H_{14}N_6O_5$
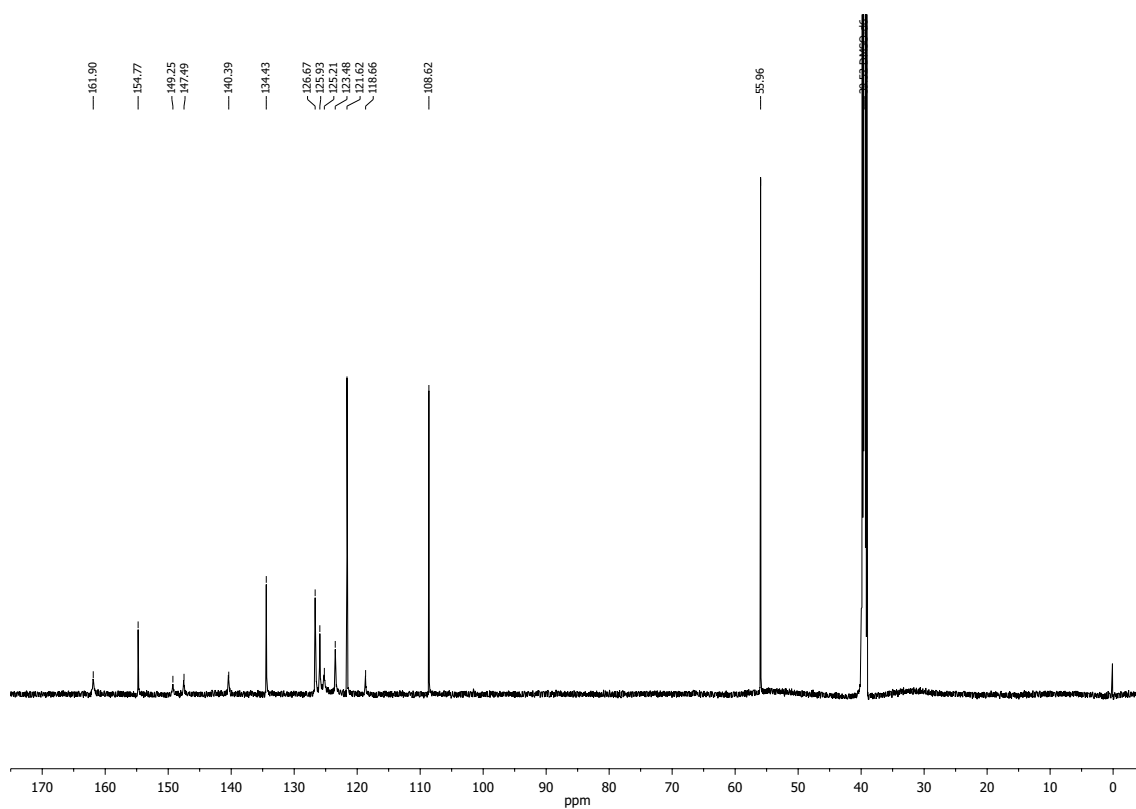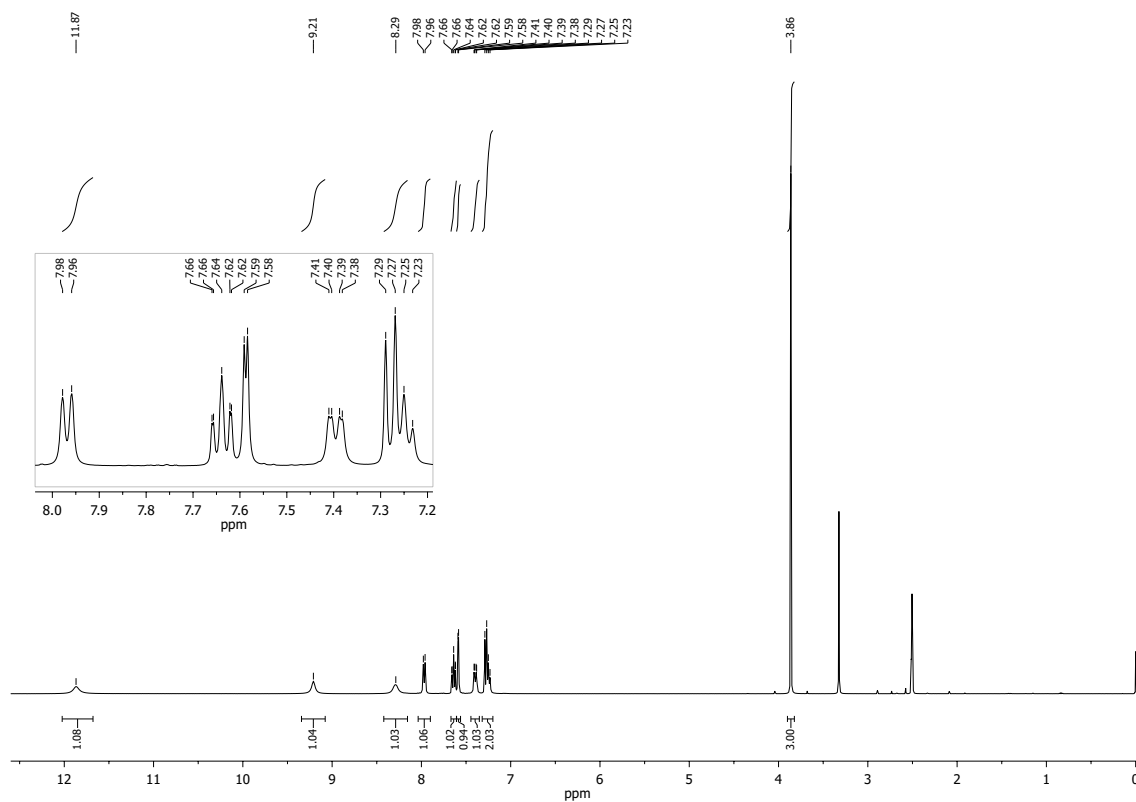
2-(*N*-Methyl-*N*-phenylamino)-quinazolin-4(3*H*)-one

Sum formula: $C_{15}H_{13}N_3O$

3-Methyl-2-(phenylamino)-quinazolin-4(3*H*)-one

Sum formula: $C_{15}H_{13}N_3O$

3-Methyl-2-(*N*-methyl-*N*-phenylamino)-quinazolin-
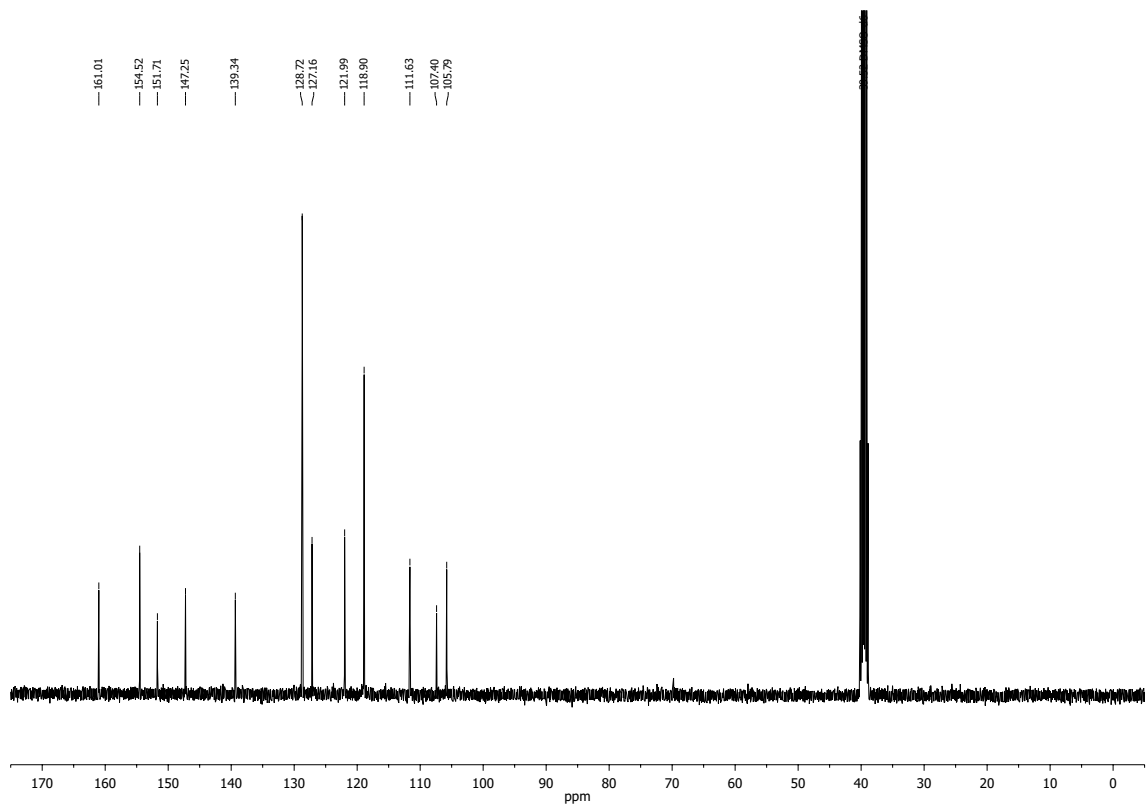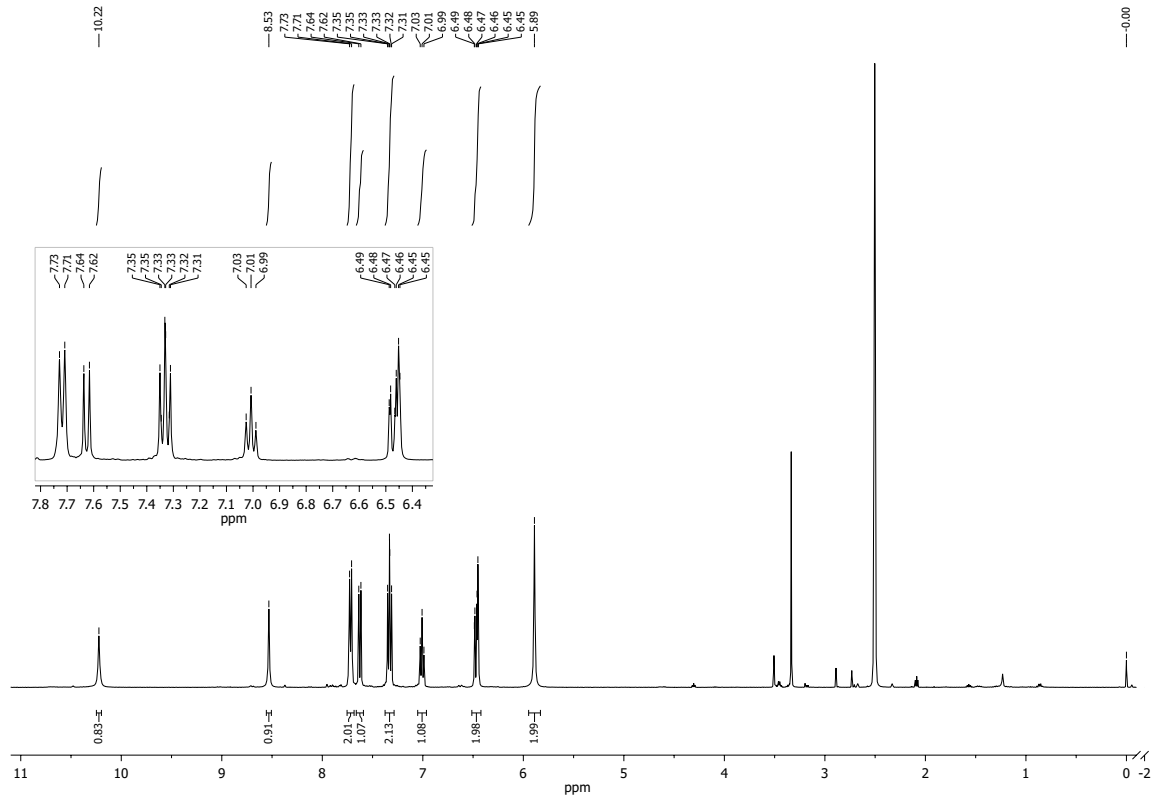
4(3*H*)-one

Sum formula: $C_{16}H_{15}N_3O$

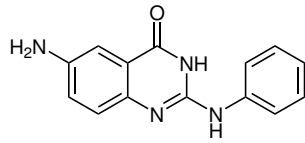7-Nitro-2-(phenylamino)-quinazolin-4(3*H*)-one

Sum formula: $C_{14}H_{10}N_4O_3$
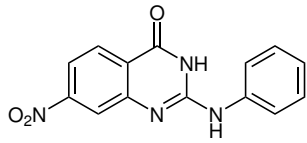
6-Nitro-2-(phenylamino)-quinazolin-4(3*H*)-one
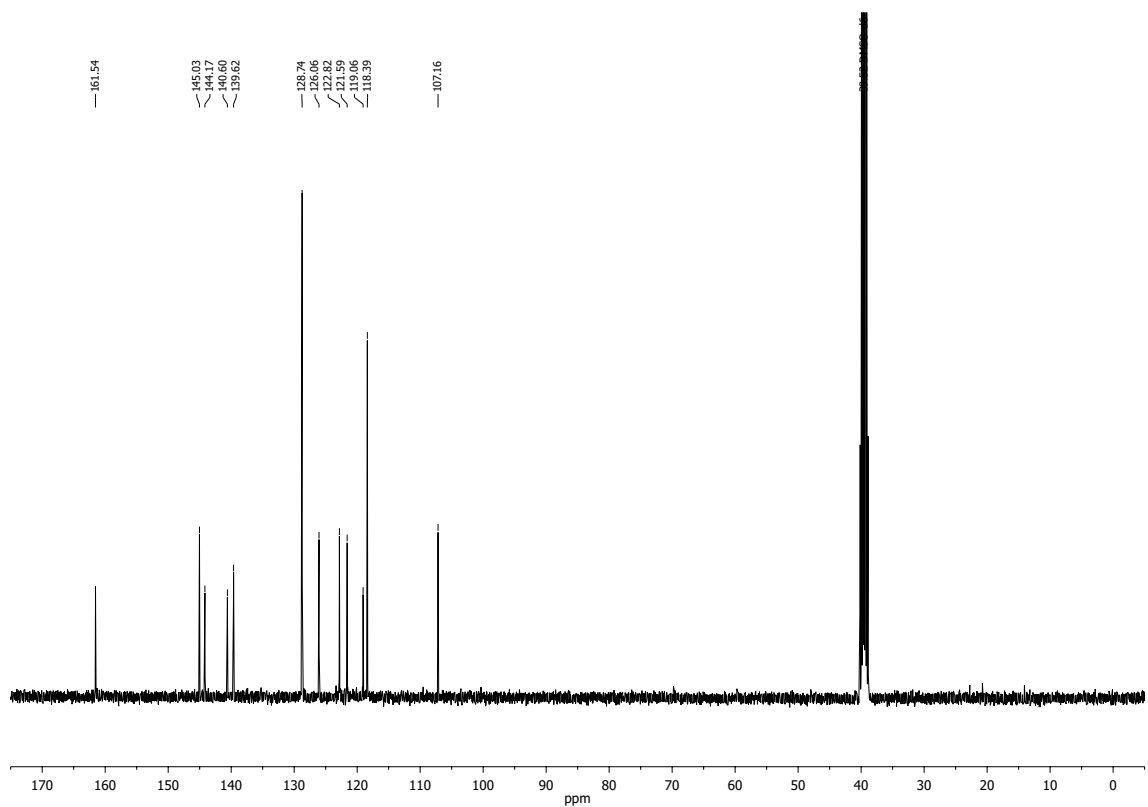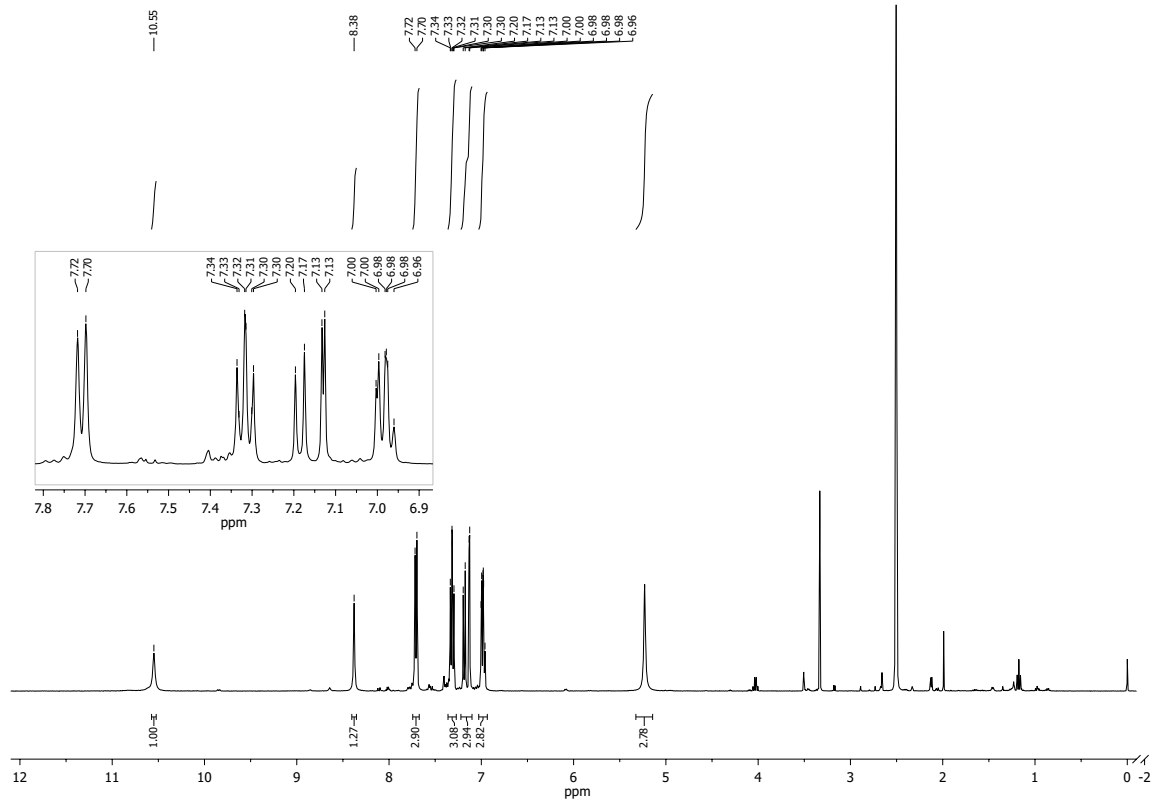
Sum formula: $C_{14}H_{10}N_4O_3$
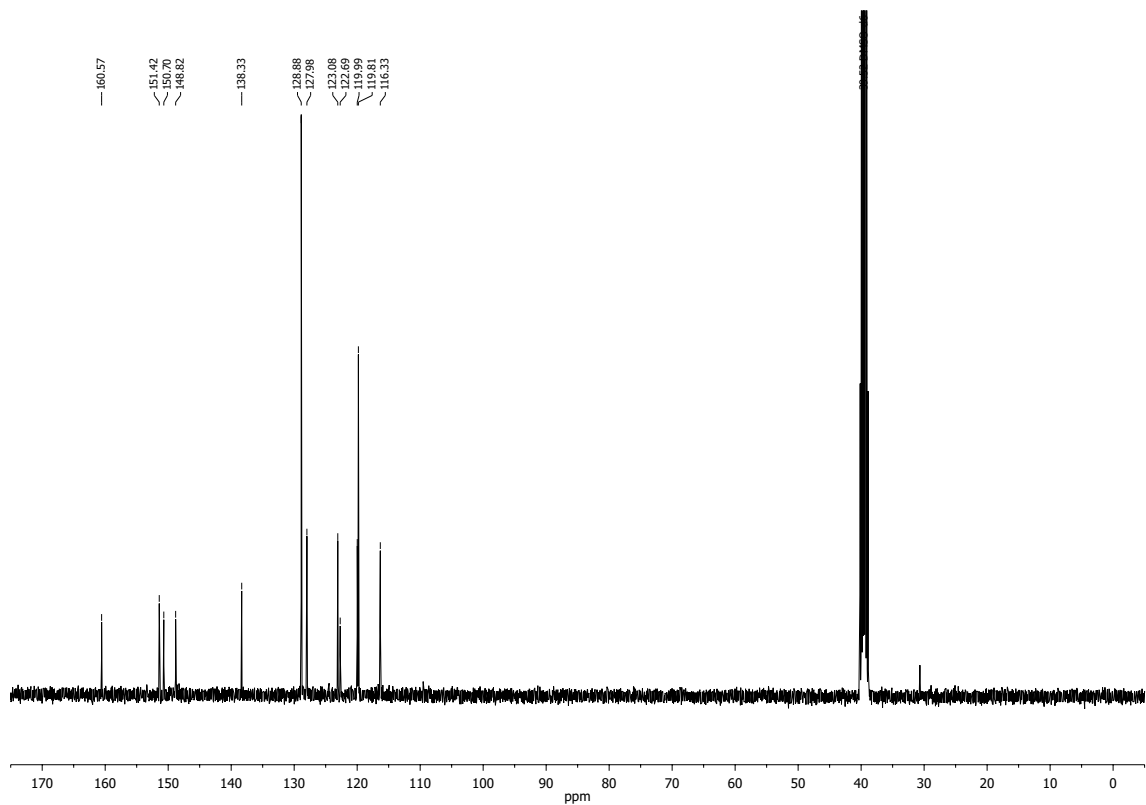
7-Amino-2-(phenylamino)-quinazolin-4(3*H*)-one

Sum formula: $C_{14}H_{12}N_4O$

6-Amino-2-(phenylamino)-quinazolin-4(3*H*)-one

Sum formula: $C_{14}H_{12}N_4O$

Curriculum vitae

Name	Robert Berger
Geburtsdatum	19. März 1988
Geburtsort	Halle (Saale)
Staatsangehörigkeit	deutsch

ab 12/21	(Senior) Manager Analytical Science and Technology, External Manufacturing, Bayer AG
06/21 – 11/21	CureVac QC Lead, Bayer AG
03/21 – 05/21	CureVac Quality and Tech Transfer, Bayer AG
03/18 – 04/19	Head of Quality Control (interim), Bayer Bitterfeld GmbH
03/17 – 05/21	Head of Quality Control Laboratory, Bayer Bitterfeld GmbH
05/13 – 02/17	Wissenschaftlicher Mitarbeiter, Leibniz-Institut für Pflanzenbiochemie Halle (Saale), Arbeitsgruppe Prof. Dr. Ludger Wessjohann (Natur- und Wirkstoffchemie) in Kooperation mit dem Agrochemischen Institut Piesteritz (AIP e. V.) und der SKW Stickstoffwerke Piesteritz GmbH
10/08 – 04/13	Studium der Lebensmittelchemie, Martin-Luther-Universität Halle-Wittenberg Abschluss: Diplom-Lebensmittelchemiker
11/12 – 04/13	Diplomarbeit, Martin-Luther-Universität Halle-Wittenberg Arbeitsgruppe Prof. Dr. Marcus Glomb (Lebensmittelchemie) Thema: "*Amininduzierter Abbau von Hopfenbittersäuren*"
09/00 – 07/07	Gymnasium im Bildungszentrum Halle (Saale) Abschluss: Allgemeine Hochschulreife

Robert Berger

Raguhn-Jeßnitz, den 01. Dezember 2023

Eidesstattliche Erklärung

Hiermit erkläre ich an Eides statt, dass ich die vorliegende Arbeit selbstständig und ohne fremde Hilfe verfasst habe. Es wurden ausschließlich die im Literaturverzeichnis angegebenen Quellen genutzt, wörtliche und / oder inhaltliche Entnahmen wurden entsprechend kenntlich gemacht. Diese Arbeit wurde bisher keiner anderen Institution zur Erlangung eines akademischen Grades vorgelegt.

Robert Berger

Raguhn-Jeßnitz, den 01. Dezember 2023